Australian Government
Geoscience Australia

Seabed Environments and Subsurface Geology of the Capel and Faust basins and Gifford Guyot, Eastern Australia

Geoscience Australia Survey TAN0713 post-survey report

Andrew D. Heap, Michael Hughes, Tara Anderson, Scott Nichol, Takehiko Hashimoto, James Daniell, Rachel Przeslawski, Danielle Payne, Lynda Radke, and Shipboard Party

Record
2009/22

GeoCat # 68630

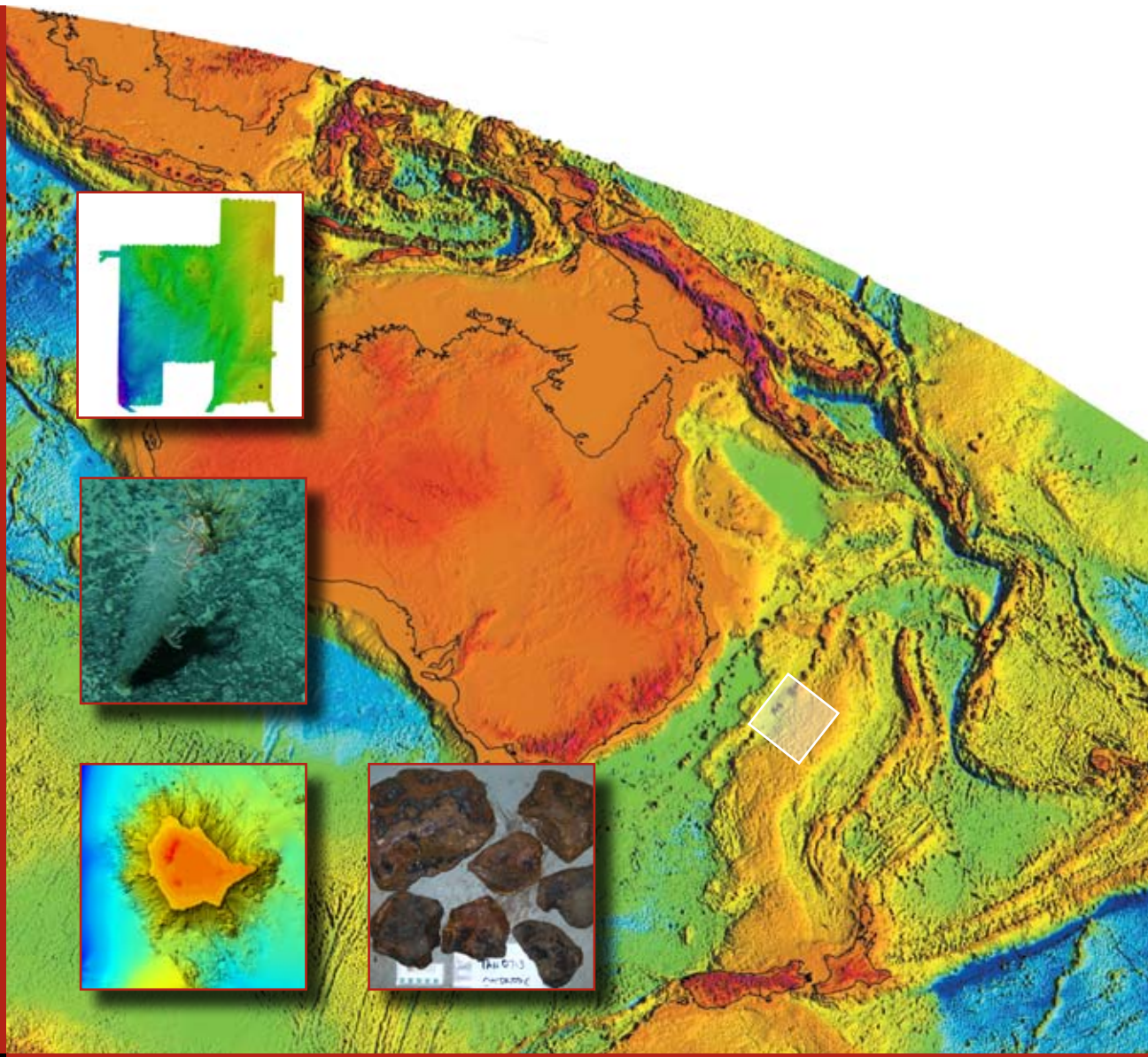

Geoscience Australia Record 2009/22

Geoscience Australia Survey TAN0713

Post-survey Report

Seabed Environments and Subsurface Geology of the Capel and Faust basins and Gifford Guyot, Eastern Australia

RV *Tangaroa*

October – November 2007

Andrew D. Heap, Michael Hughes, Tara Anderson, Scott Nichol, Takehiko Hashimoto, James Daniell, Rachel Przeslawski, Danielle Payne, Lynda Radke, and Shipboard Party

Geoscience Australia, GPO Box 378, Canberra, ACT 2601

Australian Government
Geoscience Australia

Department of Resources, Energy, and Tourism
Minister for Resources, Energy, and Tourism: The Hon. Martin Ferguson, AM MP
Secretary: Mr John Pierce

Geoscience Australia
Chief Executive Officer: Dr Neil Williams, PSM

ISSN: 1448-2177
ISBN: 978-1-921498-87-9 web
978-1-921498-86-2 CD/DVD
978-1-921498-85-5 print

GeoCat No. 68630

Bibliographic reference: Heap, A.D., Hughes, M., Anderson, T., Nichol, S., Hashimoto, T., Daniell, J., Przeslawski, R., Payne, D., Radke, L., and Shipboard Party, (2009). *Seabed Environments and Subsurface Geology of the Capel and Faust basins and Gifford Guyot, Eastern Australia – post survey report*. Geoscience Australia, Record 2009/22, 167pp.

Correspondence for feedback:
Sales Centre
Geoscience Australia
GPO Box 378
Canberra
ACT 2601

Sales@ga.gov.au

Contents

Page

List of Figures

Page

Page

List of Tables

Executive Summary

This report contains the preliminary results of Geoscience Australia marine reconnaissance survey TAN0713, offshore eastern Australia. The survey, completed as part of the Federal Government's Offshore Energy Security Program, was undertaken between 7 October and 22 November 2007 using the New Zealand Government's research vessel *Tangaroa*. Leg 1 departed Wellington on 7 October and returned to Lord Howe Island on 27 October. Leg 2 departed Lord Howe Island on 28 October and returned to Wellington on 22 November.

The survey was designed to sample key, deep-sea environments on the east Australian margin, a relatively poorly-studied region in terms of sedimentology and benthic habitats, and gather much-needed high-resolution gravity and magnetic data to better define the Capel and Faust basins, two major sedimentary basins beneath the Lord Howe Rise. Samples recovered on the survey contribute to a better understanding of the geology of the basins and assist with an appraisal of their petroleum potential. They also add to the inventory of deep-sea sediments and benthic biota to assist with surrogacy research. A major outcome stemming from the acquisition of these new data is improved resource management. This includes supporting decisions regarding the security of Australia's future energy needs. The survey also presented the first opportunity to conduct a detailed and systematic mapping study for a moderately-sized seamount. Seamounts are common on this margin and are recognised as being significant features for marine ecosystems. The principal scientific objectives of survey TAN0713 were to:

1. characterise the physical properties of the seabed associated with the Capel and Faust basins and Gifford Guyot;
2. investigate the geological history of the Capel and Faust basins from geophysical and geological data; and
3. characterise the abiotic and biotic relationships on an offshore submerged plateau, a seamount, and locations associated with fluid escape features.

The marine reconnaissance survey comprised two main components: geophysical mapping and physical sample collection. The two study regions: Capel and Faust basins and Gifford Guyot, were mapped for 100% spatial coverage. These data were then used to select areas/environments for physical sampling. A total of 39,870 km^2 (16,081 line-km) of seabed was mapped with the multi-beam sonar and 3,280 line-km of digital shallow seismic reflection data was acquired over the two study areas. In addition, the survey also resulted in 14,145 line-km of gravity and 13,843 line-km of magnetic data. A total of 46 stations were occupied throughout the survey, including 36 in the Lord Howe Rise region over the Capel and Faust basins and six on Gifford Guyot. A variety of sampling equipment was deployed, including towed-video and digital stills, grabs, boxcores, piston cores, rock dredges and benthic sleds. Different combinations of equipment were used at different stations depending on the nature of the seabed and sampling objective for each site.

Oceanographic data were also obtained from a six-month deployment of an ADCP on the shelf at Lord Howe Island and from CTD casts and associated water samples. These data gave a regional picture of the oceanography for the study areas. The oceanographic data reveal that a general anticlockwise circulation occurs in the region and that eddies from the East Australian Current influence the Lord Howe Island region.

The geomorphology of the study regions was interpreted mainly from the multi-beam (swath) sonar data. A total of five types of large-scale (10's km) features (plain, ridge, valley,

peak, and basin) and six types of small-scale features (peak, moat, hole, polygonal crack, scarp, fluid escape) were identified for the Lord Howe Rise region over the Capel and Faust basins. Ridges are the dominant geomorphic feature type, followed by sediment plains and valleys. Polygonal cracks occur mostly on the sedimented plains and ridges, and are the most numerous type of geomorphic feature. They are inferred to be formed from de-watering of the surface sediments, a process captured in the video footage. Significantly, 16 volcanic peaks were also identified over the Capel and Faust basins. Correlation with regional seismic and potential field data (gravity and magnetic) indicates that they correspond with volcanic intrusions at depth and indicate widespread post-rift volcanism. Gifford Guyot exhibits 'classic' geomorphology for a guyot, with an extensive flat summit and steep flanks. Nine geomorphic features were identified on the guyot (debris slope, plateau, spur, submarine fan, slump scar, ridge, subaqueous dune field, valley and terrace, in order of decreasing abundance). The overall geomorphology shows that seabed habitats on the guyot have a relatively complex spatial structure.

Seabed sediments of both the Capel and Faust basins and Gifford Guyot regions are very similar in texture and composition, with no significant differences between different water depths or geomorphic features. The sedimentology reflects the dominance of marine pelagic material and the remoteness from significant terrigenous sediment inputs. Despite this relatively uniform distribution in physical texture and composition, spatial differences are present in the inorganic and organic components. Specifically, the sediments contained bio-available elements in concentrations below the limits of detection (e.g. Se and Mo). The implication is that these elements could be limiting factors to benthic organisms and biogeochemical processes in the deep sea. Anomalous results for the reactivity of organic matter were also found in sediments proximal to volcanic peaks and outcrop and possibly point to fluid escape from cold seeps and/or manganese nodule formation. Core incubations show that phytoplankton was the main source of organic matter in the sediments which is consistent with the marine pelagic material composition. Bulk seabed sediment geochemistry is consistent with regions defined from global databases.

Generally, the benthic ecology is depauperate, with the sediment plains, rocky outcrops (e.g., volcanic peaks) and Gifford Guyot supporting lower numbers and densities of organisms than expected from deep sea plateaus and seamounts. Rocky substrata support surprisingly few attached or associated organisms, and almost no dense habitat-forming sessile invertebrates. It is unclear why benthic organisms are not abundant, although we infer that the lack of nutrients is a major limiting factor.

New gravity data reveal the depocentres in the Capel and Faust basins to be fault-bounded grabens and half-grabens, with the sedimentary fill affected by major faulting. Physical linkages between seabed features and sub-surface structures indicate that the depocentre-bounding faults have been active until recent and that fluid migration has occurred along fault planes and through the basin fill. No pre-rift basement or syn-rift sediments were recovered, so the existence of potential petroleum source rocks remains unresolved. Initial results of head-space gas analysis from core samples indicate that there are no direct indications of hydrocarbons within the shallow sub-bottom sediments.

Overall, data collected on the survey have improved our understanding of the nature and processes of the deep-seabed on the eastern margin of Australia and provided further insights to the geological evolution and petroleum prospectivity of the region, including better delineation of the sediment depocentres of the Capel and Faust basins.

1. Introduction

This record contains the substantive results of Geoscience Australia marine reconnaissance survey TAN0713 to the eastern margin of Australia (Fig. 1.1). The survey was completed in two legs between 7 October and 22 November 2007 using the New Zealand government's research vessel *Tangaroa*. Leg 1 departed Wellington on 7 October and returned to Lord Howe Island on 27 October. Leg 2 departed Lord Howe Island on 28 October and returned to Wellington on 22 November. The survey included scientists and technical staff from Geoscience Australia, the National Institute of Water and Atmospheric research (NIWA, NZ) and Fugro Robertson Inc., and 13 students and staff from the University of the Sea (Sydney).

The survey represents the first marine reconnaissance survey for the Offshore Energy Security Program (OESP). The OESP is a $75 M four-year program funded by the Australian Federal Government to collect fundamental scientific information to help secure Australia's future energy resources. Of this, approximately $18 M has been allocated to conduct marine reconnaissance surveys of remote offshore sedimentary basins to characterise the seabed environments and gain a better understanding of the seabed and basin architecture. The principal aim of survey TAN0713 was to explore deep-sea habitats and processes on a subsided marginal plateau and submerged guyot. The data are also used to examine the underlying geology of the Capel and Faust basins as an assessment for their petroleum potential.

1.1. BACKGROUND

The Australian margin contains 28% of the world's marginal plateaus which makes it relatively over-represented by these features compared with other continents (Heap & Harris, 2008). The abundance of marginal plateaus on the Australian margin is a result of the presence of divergent margins on three of its margins (i.e., west, south, and east). While they form topographic highs in the ocean basins, Australia's marginal plateaus are fragments of continental crust that have subsided due to the break-up of the Gondwana super-continent.

Regional seismic data and geological samples reveal that most of the marginal plateaus comprise structurally complex tectonic elements, including sedimentary basins whose sediments correlate with onshore basins. In contrast to most onshore basins, the offshore basins associated with the marginal plateaus are poorly studied and are 'frontier' in terms of their geology and petroleum potential.

A total of 158 seamounts have been mapped on the Australian margin (Heap & Harris, 2008). The global distribution of seamounts reveals that they are relatively rare in the southern hemisphere oceans and proportionately few occur around Australia (Kitchingman & Lai, 2004). Of Australia's seamounts, less than 50 have been sampled for geology and biota, and of these less than 10 have been studied in detail. Currently, only three seamounts (Cascade Seamount, Lord Howe Island, Christmas Island) have been systematically mapped using multi-beam sonar.

1.1.1. Eastern Australian Marginal Plateaus – Lord Howe Rise

The eastern margin of Australia is characterised by several deep-water (>1,000 m) sub-parallel marginal plateaus separated by narrow ridges and deeper (>3,500 m) topographic basins (Fig. 1.1). Of these, the Lord Howe Rise (LHR) is the largest. The LHR extends for 1,600 km from the Fairway Basin in the north to the Challenger Plateau (NZ) in the south.

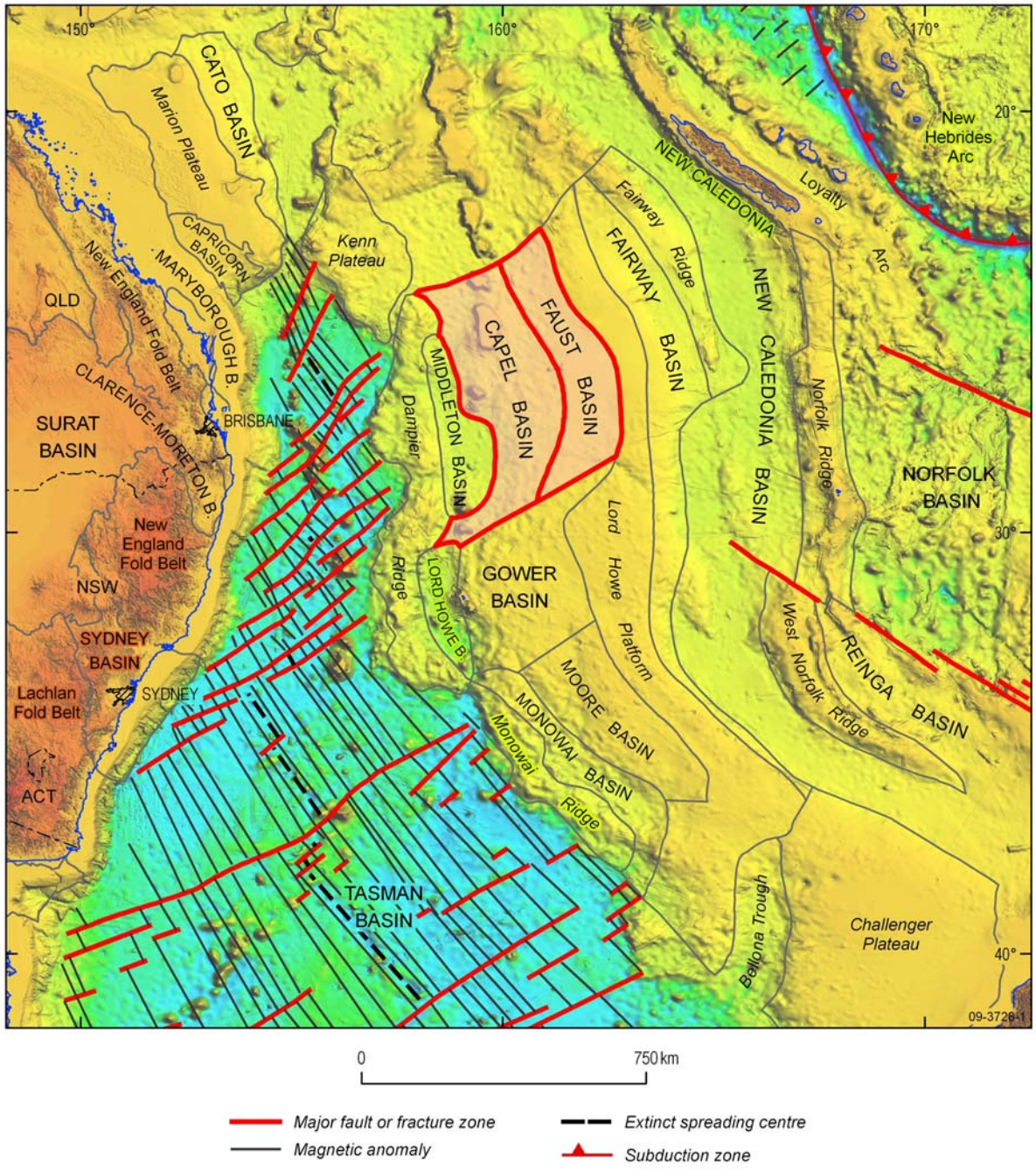

Figure 1.1. Map of eastern margin of Australia showing the main geomorphic features, including the Lord Howe Rise and the outlines of the Capel and Faust basins and location of Gifford Guyot.

Inside Australia's maritime jurisdiction, the LHR ranges in width from 450–650 km and covers an area of approximately 476,580 km^2 (Heap & Harris, 2008).

The LHR comprises a submerged piece of continental crust that separated from eastern Australia through the opening of the Tasman Sea as a result of seafloor spreading between 85–52 Ma (Stagg *et al*., 2002; Van de Beuque *et al*., 2003). Available data reveal the LHR to be a complex feature comprising several tectonic provinces divided both longitudinally and latitudinally (Fig. 1.2). Three major tectonic provinces are identified, namely: (1) the LHR Platform characterised by planated basement overlain by a thin sedimentary section. Regional seismic data suggest that the basement rocks of the LHR platform province partly comprise Palaeozoic fold belt sediments and meta-sediments, correlating with either the New England Fold Belt rocks of eastern Australia; (2) the Central Rift Province characterised by a series of shallow and relatively small half grabens; and (3) the Western Rift Province

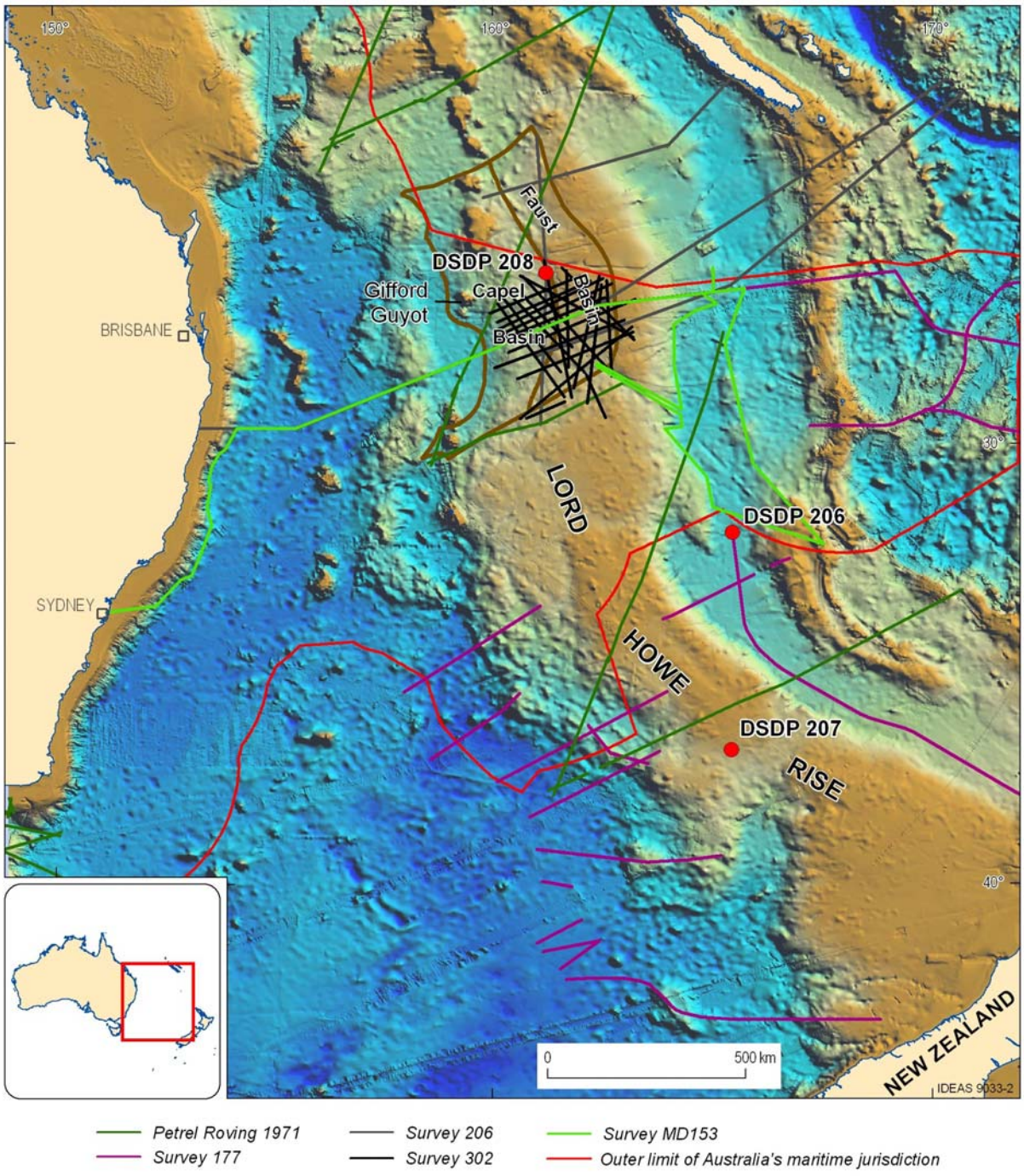

Figure 1.2. Map showing locations of previous surveys to the north-central Lord Howe Rise, including MD153 and GA302 focused on sampling sediments and rocks of the Capel and Faust basins. The location of Deep Sea Drilling Program (DSDP) holes 206, 207, and 208 are also shown as they provide the only stratigraphic control on the geology of the LHR. Note that numerous seismic surveys have been completed in the Tasman Sea region but only those seismic surveys focussed on the northern LHR relevant for this study are shown.

characterised by a deeper series of larger half grabens, down-faulted to the west. The junction between the Central and Western Rift provinces is poorly-defined, based mainly on a N-S gravity ridge that is coincident with a magnetic anomaly. Despite the regional geology of the tectonic provinces of the LHR being reasonably well established, the structure and boundaries of the sedimentary basins (including the Capel and Faust basins) that characterise these provinces are relatively poorly defined. A comprehensive account of the structure, stratigraphy and geologic evolution of the LHR and Capel and Faust basins is provided in Appendix A.

The LHR is a remote frontier province with hydrocarbon potential. Interpretation of all available regional datasets shows that potentially prospective sedimentary basins underlie it for much of its length.

Regionally, the seabed on the LHR is draped with pelagic carbonate ooze. Carbonate contents are generally >70%. Regional geological studies indicate that the seabed in the vicinity of the LHR is invariably of this type (e.g., Burns et al., 1970; Kennett et al., 1986; Colwell et al.; 2006). The pelagic ooze is very pale brown to white in colour and consists almost entirely of the skeletal remains of foraminifers, coccolithophorids, planktonic protozoans and algae. The sediments also generally contain minor amounts of silica spicules, radiolarians, silicoflagellates, diatoms and volcanic glass, and are well bioturbated.

1.1.2. Seamounts as Biological Hotspots – Gifford Guyot

Seamounts are important oceanographic features; they provide information on ocean basin formation, influence oceanographic circulation (e.g., Taylor columns) and can intersect multiple oceanic water masses. They often support distinct marine ecosystems characterised by high biodiversity and endemism. Recognition of the significance of seamounts for physical and biological systems and the increased pressure on them from extractive resource use (mainly fishing) has resulted in them being classified as vulnerable marine ecosystems (VME; UN Secretary-General, 2006).

Not only do seamounts provide different substrates to the surrounding ocean basins for marine organisms, the largest also have summits that penetrate the euphotic zone (<250 m) and develop communities that include algae and intersect zooplankton communities. In turn these organisms support a complex and rich assemblage of seamount-associated organisms.

The ecological significance of seamounts is also partly based on a presumed seabed habitat complexity. A measure of seabed habitat complexity can be derived from geomorphology (Greene *et al*., 1999; Harris *et al*.; 2008). However, our knowledge of the habitat complexity is incomplete because detailed maps of seabed habitats as represented by geomorphology are rare for seamounts.

Gifford Guyot is a flat-topped largely unexplored seamount, about halfway along the Lord Howe Rise seamount chain on the western flank of the LHR (Fig. 1.2). Seamounts in this chain, including Gifford Guyot, have formed from Miocene volcanism via a migrating magma source ("hotspot") after the opening of the Tasman Sea. Existing single-beam echo-sounder data show that Gifford Guyot rises from about 2,500 m water depth to 260 m below the sea-surface (Slater & Goodwin, 1973). Radiometric dating of basaltic rocks from the guyot suggests an age of 15.6 Ma. Samples from the guyot include alkaline olivine basalts and phosphorites overlain by Late Pliocene or Early Pleistocene fossiliferous limestones (Slater & Goodwin, 1973). No pre-existing biological data are available. No detailed mapping or sampling has been undertaken and knowledge of the seabed environments is limited.

1.2. PREVIOUS SURVEYS

The LHR marginal plateau and the sedimentary basins comprising it are considered "frontier areas" with respect to hydrocarbon exploration. The "frontier" nature of the region has been the stimulus for the acquisition of seismic reflection data to understand the geological history and setting of the LHR, as well as the architecture of the sedimentary basins. Up until the present survey a total of six major regional seismic reflection surveys had been undertaken over LHR, including 10 over the Capel and Faust basins (Fig. 1.1 & Table 1.1).

Table 1.1. Previous marine surveys to the region.

Survey	Year	Agency	Ship	Main Data Types
"Petrel" seismic	1971	Shell International	MV *Petrel*	Seismic reflection
BMR 12, 13, 15	1972	Bureau of Mineral Resources	MV *Lady Christine*	Seismic reflection
Sonne 7A	1978	BGR	RV *Sonne*	Seismic reflection, gravity, mag.
Sonne 36A	1985	BGR	RV *Sonne*	Seismic reflection
AGSO 177	1996	Australian Geological Survey Org.	RV *Rig Seismic*	Seismic reflection
AGSO 206	1998	Australian Geological Survey Org.	RV *Rig Seismic*	Seismic reflection
FR0589	1989	Australian Museum	RV *Franklin*	Biological collections
NORFANZ	2003	Multinational (NZ, Australia, France)	RV *Tangaroa*	Biological collections
MD153	2006	Geoscience Australia	RV *Marion Dufresne*	Multibeam sonar, geology
GA302	2006	Geoscience Australia	MV *Pacific Titan*	Seismic reflection

There are no existing petroleum exploration wells on the LHR. The Deep Sea Drilling Program (DSDP) hole 208 (Fig. 1.2) provides the only existing stratigraphic control in the northern LHR for the late Maastrichtian–Recent interval. Two other DSDP drill holes are situated in the New Caledonia Basin (DSDP 206) and the southern LHR (DSDP 207). The latter drill hole terminated in rhyolites of Cenomanian (c. 94 Ma) age (van der Lingen, 1973; McDougall & van der Lingen, 1974), which corresponds to the time of rift basin development within the region.

The few dredge samples from the previous regional surveys provide evidence of continental rocks in the basement of the LHR platform, Dampier Ridge, and Challenger Plateau (Roeser *et al*., 1985; McDougall *et al*., 1994; Tulloch *et al*., 1991). Younger rocks associated with Cenozoic volcanism have been recovered from the French jurisdiction over the LHR platform (Launay *et al*., 1977; Exon *et al*., 2004), and the Lord Howe and Tasmantid seamount chains (Game, 1970; Slater & Goodwin, 1973; McDougall & Duncan, 1988).

Recent marine surveys by Geoscience Australia have improved the regional data coverage. The joint French-Australian AUSFAIR MD-153 regional reconnaissance survey in February 2006 (Fig. 1.2), collected giant CALYPSO piston cores (<30 m) of the sub-bottom sediments, rock dredge samples, heat-flow measurements, multibeam bathymetry, sub-bottom profiler, gravity, and magnetic data. The Capel-Faust GA302 survey in late 2006 and early 2007, acquired approximately 6,000 line-km of 106-fold 2D seismic data along 23 lines, with a spacing of 15–30 km (Fig. 1.2). Gravity and magnetic data were also collected. Data and information from the present survey build on these previous surveys (Table 1.1), specifically on AUSFAIR MD153 and S302.

1.2.1. Local-scale Geomorphology

In a recent mapping study of the geomorphology of the Australian margin, Heap and Harris (2008) identified 11 geomorphic feature types on the eastern margin, dominated by marginal plateaus of the LHR and Dampier Ridge (Table 1.2). Basins are the next most extensive feature, followed by seamounts. Seamounts of the Tasmantid and Lord Howe chains distinguish this margin from others around Australia. The largest seamounts are emergent and form Lord Howe Island/Balls Pyramid and Elizabeth and Middleton Reefs. The east Australian margin is also characterised by a relatively narrow continental shelf and steep, incised slope. Hence, Abyssal Plain/Deep Ocean Floor is the dominant geomorphic province, comprised mostly of the Tasman Sea basin.

Table 1.2. Geomorphic provinces and features of the eastern margin of Australia (from Heap & Harris, 2008).

Code	Feature	Number	Area (km^2)
1	Shelf (unassigned)		52,970
2	Slope (unassigned)		76,190
3	Rise (unassigned)		14,310
4	Abyssal plain/deep ocean floor (unassigned)		355,320
	Total		**498,790**
5	Bank/shoal		–
6	Deep/hole/valley	5	410
7	Trench/trough		–
8	Basin	3	65,100
9	Reef	13	40
10	Canyon	33	4,500
11	Knoll/abyssal hill/hill/peak	14	2,420
12	Ridge	1	220
13	Seamount/guyot	26	28,340
14	Pinnacle	43	1,150
15	Plateau	3	422,370
16	Saddle	1	23,470
17	Apron/fan		–
18	Escarpment		–
19	Sill		–
20	Terrace	10	9,290
21	Sandwave/sand bank		–
	Total	**152**	**557,710**

1.3. SURVEY OBJECTIVES

This survey represents a valuable opportunity to sample key deep-seabed environments on the eastern Australian margin. While significant work has been completed to understand the tectonic evolution of the margin, specifically the opening of the Tasman Sea and formation of LHR and seamount chains from regional data, little information and data exist on the nature of the seabed environments and habitats. Moreover, while seamounts are common on this margin, none have been mapped in detail and few have been systematically sampled for sediments and biota. The principal scientific objectives of survey TAN0713 were to:

4. characterise the physical properties of the seabed associated with the Capel and Faust basins and Gifford Guyot;
5. investigate the geological history of the Capel and Faust basins from geophysical and geological data; and
6. characterise the abiotic and biotic relationships on an offshore submerged plateau, a seamount, and locations associated with fluid escape features.

Targeting seabed environments associated with the Capel and Faust basins and Gifford Guyot provides key data on the seabed and benthic biota for marginal plateaus and seamounts on the east Australian margin. Sampling the rocks associated with the Capel and Faust basins supports an appraisal of their petroleum potential and correlation with regional seismic data. The survey leader's log is contained in Appendix B.

1.4. SURVEY PARTICIPANTS

The vessel chartered for the survey was the New Zealand government's research vessel *Tangaroa*. The RV *Tangaroa* is 70 m long, with accommodation for 44 scientists and crew. Different crew were on board for each of the two legs.

1.4.1. Scientific Personnel

The multi-disciplinary nature of the research required the efforts of a group of scientists with a wide variety of complementary skills to make it successful. The survey personnel, representing organisation, and their substantive roles are listed in Table 1.3.

Table 1.3. Scientific survey personnel, representing organisation, and their substantive roles.

Name	Organisation	Role
Leg 1 (7-27 October)		
Peter Harris	Geoscience Australia	Chief Scientist
Scott Nichol	Geoscience Australia	Co-chief Scientist
Frederic Saint-Cast	Geoscience Australia	Physical Oceanographer
Lynda Radke	Geoscience Australia	Geochemist
Takehiko (Riko) Hashimoto	Geoscience Australia	Petroleum Geoscientist
Karen Earl	Geoscience Australia	Petroleum Geoscientist/GIS
James Daniell	Geoscience Australia	Swath Processor
Cameron Buchanan	Geoscience Australia	Swath Processor
Ian Atkinson	Geoscience Australia	Systems Analyst
Craig Wintle	Geoscience Australia	Mechanical Technician
John Jaycock	Geoscience Australia	Geological Technician
Gareth Crook	Geoscience Australia	Mechanical Technician
Stan Hancock	Geoscience Australia	Marine Technician
Kevin Mackay	NIWA	NIWA Team Leader/Swath acquisition
Niki Davey	NIWA	CTD Technician
Steve George	NIWA	DTIS/Electronics Technician
Donald Childers	Fugro Robertson Inc.	Gravity/Magnetics Technician
Kelsie Dadd	University of the Sea	Teaching Scientist
Pia Winberg	University of the Sea	Scientist
Marcelo Kitahara	University of the Sea	Scientist
Ashihiska Sharma	University of the Sea	Scientist
Maxwell Gonzalez	University of the Sea	Scientist
James Wapyer	University of the Sea	Scientist
Sonnia Asamole	University of the Sea	Scientist
Leg 2 (28 October – 22 November)		
Andrew Heap	Geoscience Australia	Chief Scientist
Michael Hughes	Geoscience Australia	Co-chief Scientist
Tara Anderson	Geoscience Australia	Benthic Marine Ecologist
Andrew Stacey	Geoscience Australia	Petroleum Geoscientist
George Bernardel	Geoscience Australia	Petroleum Geoscientist
Cameron Mitchell	Geoscience Australia	Swath Processor
Michele Spinoccia	Geoscience Australia	Swath Processor
Ray de Graaf	Geoscience Australia	Mechanical Technician
Andrew Hislop	Geoscience Australia	Mechanical Technician
John Jaycock	Geoscience Australia	Geological Technician
Franz Villagran	Geoscience Australia	Electronics Technician
Mathew Carey	Geoscience Australia	Geological Technician
Arne Pallentin	NIWA	NIWA Team Leader/Swath Acquisition
Matt Walkington	NIWA	CTD Technician
Rob Stewart	NIWA	DTIS Technician
Stephen Robbins	NIWA	IT Technician
Donald Childers	Fugro Robertson Inc.	Gravity/Magnetics Technician
Jane Jelbart	University of the Sea	Teaching Scientist
Alexander Rattray	University of the Sea	Scientist

Name	Organisation	Role
Chelsea Buckley	University of the Sea	Scientist
Alexandra Bloomfield	University of the Sea	Scientist
Hannah Power	University of the Sea	Scientist
Nishantha Kalutharage	University of the Sea	Scientist
Mary Mulcahy	University of the Sea	Scientist

1.4.2. Ship's Crew

In addition to the scientific crew, the ship's crew provided tireless support throughout the survey. The ship's crew and their substantive roles are listed in Table 1.4.

Table 1.4. Ship's crew and their substantive roles.

Name	Role
Leg 1 (7-27 October)	
Andrew Leachman	Master
Bob Graham	First Mate
Ian Popenhagen	Second Mate
John Kirkland	Chief Engineer
Lindsay Battersby	Second Engineer
Gary Wells	Third Engineer
Kim Ashby	Cook
Rohaan Dulner	Second Cook
Frances Parker	Steward
Michael Steele	Bosun
Glen Walker	Leading Hand
Eddy Fox	Deckhand
Shane Harvey	Deckhand
Andrew Williams	Deckhand
Ian Smith	Deckhand
Matt Hickman	Trainee
Leg 2 (28 October – 22 November)	
Roger Goodison	Master
Alexander Morrice	First Mate
Yoshihiro Suzuki	Second Mate
Allan Harvey	Chief Engineer
Fred De Jager	Second Engineer
Gary Wells	Third Engineer
Andrew Dickson	Cook
Rohaan Dulner	Second Cook
Sharon Henderson	Steward
Peter Healey	Bosun
Tony Reiri	Leading Hand
Russell Jones	Deckhand
Barry Fleming	Deckhand
Peter Morrison	Deckhand
Dylan Bennett	Deckhand

2. Geophysics

A comprehensive geophysical survey was conducted to determine the seabed morphology of the LHR and Gifford Guyot and subsurface geological structure of the Capel and Faust basins. Each study area was mapped for 100% spatial coverage using the multi-beam sonar, sub-bottom profiler, magnetometer and gravimeter. The geophysical survey was designed to identify priority areas for further detailed investigation and geological sampling.

2.1. DATA ACQUISITION

2.1.1. Multi-beam (Swath) Sonar

The Simrad EM300 on the RV *Tangaroa* is a 30–34 kHz multi-beam sonar system comprising 135 beams each covering a 1° arc. The system can acquire a swath width of up to 5 times the water depth in shallow water, and operate in water depths of up to 4,000 m. The performance of the multi-beam system during the survey was excellent, based on the coverage achieved and quality of the data acquired. The survey over the Capel and Faust basins was generally laid out in a N-S direction and NW-SE over Gifford Guyot, with variable line spacing designed to give maximum overall coverage. Summary statistics of the multi-beam sonar data are provided in Appendix C.

During the survey, the sea state ranged from slight to moderate, with regular swells of between 1 m and 2.0 m. Wind speeds were between 7.7 m s^{-1} and 20.6 m s^{-1} mostly from S and NE. Data was collected at a vessel speed of between 9 and 10 knots. During the survey, tidal currents were faster toward the south. Generally, noise in the data was most noticeable on the outer-most beams, particularly on the relatively smooth and hummocky seabed of the western flank of the Lord Howe Rise. Data quality was also greatly affected by the sea state, with the data being relatively noisy in sea states of >3.

Sound velocity profiles (SVP) were obtained to account for changes in the speed of sound in the water column due to changes in temperature and salinity. SVP's on the transits to and from the survey area were generated using the SVP Builder utility on board the ship. This method uses global climatology data to derive an SVP for a given set of coordinates. This method proved effective at generating accurate SVP's during deep water transits. Details of the SVP's are contained in Appendix C.

In addition, a total of 7 CTD (conductivity/temperature/depth) casts were undertaken over the two study areas. The CTD data were used to generate accurate SVP's that complimented those generated from the global climatology data. The spatial coverage of the CTD casts provided excellent results. The data were used to calculate the absorption co-efficient, which was applied to improve the backscatter returns by correcting the transducer gains for changes to the speed of sound through the water column as a result of changes in salinity and temperature.

2.1.2. Shallow Seismic Reflection

The RV *Tangaroa*'s hull-mounted Knudsen 320B 3.5 kHz sub-bottom profiler was used to record the acoustic response of surface and shallow sub-bottom sediments during the survey. The system is capable of substrate penetration of greater than a few metres in water depths of 1,000 m. The sub-bottom profiler has a linear Chirp pulse, which is a linearly swept frequency between 3–7 kHz over time. Full details of the Chirp waveform can be found in the Knudsen user documentation.

Data from the sub-bottom profiler was filtered to remove boat-induced noise, and a time-varying gain, controlled by the automatic bottom tracker, was applied to the data before output in IEEE 32 bit Seg-Y format. The raw data was also output in proprietary format. The sub-bottom profiler was operated inconjunction with the multi-beam sonar system. The two systems were synchronised to minimise interference.

2.1.3. Multi-beam (Swath) Sonar Backscatter

Backscatter or acoustic reflectance was also recorded with the Simrad multi-beam system. Acoustic reflectance (intensity) was recorded as a voltage and then returned as a value in decibels (dB). Acoustic reflectivity, which is a surrogate for substrate hardness, is recorded as a grey scale image. High acoustic reflectivity (i.e., hard seabed type) are recorded as light areas and low acoustic reflectivity (i.e., soft seabed type) are recorded as dark areas.

2.1.4. Gravity and Magnetics

Fugro Robertson Inc. was contracted by NIWA on behalf of Geoscience Australia to acquire and process marine gravity and magnetic data. For detailed descriptions of data acquisition, processing and preliminary results, see the report by Fugro Robertson Inc. (2008) in Appendices D–E.

2.1.4.1. Gravity

Gravity data was acquired using a LaCoste and Romberg marine gravity meter #S-65 fitted with a ZLS ULTRASYS™ digital control system. The system features a highly damped, zero-length spring sensor mounted on a gyro-stabilised platform and sealed in a dry nitrogen atmosphere for satisfactory operation in the marine environment. Data were sampled at 200 times per second and averaged to give 1 s values. Data were digitally recorded at 1 s intervals via a DOS operating system on a Pentium acquisition computer. For real-time data quality control, a 5 min convolution filter was applied to the raw data. Data quality was monitored during the survey via a Vertical Velocity Monitor (VMON), which measures the short-period vertical velocity of the gravity sensor as a surrogate measure of the quality of the processed data. In order to enable a tie to the global gravity network, two stationary readings were taken at Burnham Wharf in Wellington, New Zealand, at the start and end of the survey. This reference point was tied to an existing station of the New Zealand Gravity Datum (Glasgow Wharf Base #3). Details of these reference stations are given in Appendix D and Appendix 8 of the Fugro Robertson Inc. report (Appendix E).

2.1.4.2. Magnetics

Magnetic data were acquired using a SeaSpy marine magnetometer. The system featured the LCT 022 tow-fish unit that was towed 210 m astern of the vessel along the centre-line (Appendix D). An offset correction was applied to the magnetic data to align the dataset with the navigation data. Reference magnetic data were provided by Geoscience Australia from two stations on Norfolk Island and one on the New South Wales north coast, all of which were operational during the survey (Appendix D). Navigation data were recorded at 1 s intervals during the survey using two systems. A Racal Skyfix wide-angle differential GPS (WADGPS) was the primary navigation system and a shipboard Omnistar WADGPS provided a secondary navigation system. Both systems provided RTCM corrections to a Trimble 4000SE GPS receiver. The navigation data were merged with the gravity data and archived every four hours during the survey with a Unison data logger. Bathymetry data

were acquired at four-second intervals with a Simrad EA60 echo sounder. This was supplemented during post-survey data processing with the multi-beam bathymetry data.

2.2. DATA PROCESSING AND ANALYSIS

2.2.1. Multi-beam (Swath) Sonar

The multi-beam sonar data were processed using Caris HIPS/SIPS V5.4. Initially, a vessel configuration file was created to define the motion sensors and DGPS antenna offsets and record the patch test result. A new project for survey TAN0713 was then created and the vessel configuration file was attached to the project file. The raw data were then acquired in the form of "raw.all" format for each line. The motion sensor, DGPS and heading data were then cleaned using a filter that averaged adjacent data to remove artefacts. The SVP's for each of the study areas were attached to the corresponding raw multi-beam sonar data files to correct the water depths. A new blank field area was then defined that encompassed the study area and the co-ordinate system (WGS84) was specified.

Once loaded, the data were then cleaned by applying several filters that removed any remaining spikes using user defined threshold values. A visual inspection of the data for each line was then undertaken, where artefacts and noisy data not removed by the filtering process were removed manually, using the swath editor module of the Caris HIPS/SIPS software.

Parameters for the motion sensor, DGPS, ship heading, tidal height, and sound velocity profile data were then merged with the raw depth data to produce the final processed data file. A weighted grid of the processed data was then created for each of the study regions. The processed data were finally exported as grid soundings or false coloured images for presentation and reporting and as final processed data in GSF (Generic Sensor Format) format.

The acquired multi-beam bathymetry data is presented as a 30 m spatial-resolution grid. This resolution was chosen as it is close to the beam footprint (at nadir) for the average water depth of the survey area. A second, coarser grid of 100 m spatial-resolution was also created to cover data gaps. These two grids were then super-imposed on top of Geoscience Australia's 250 m spatial resolution bathymetry grid for regional context.

2.2.2. Shallow Seismic Reflection Data

The Seg-Y data from the Knudsen 3.5 kHz sub-bottom profiler were loaded into the seismic interpretation and evaluation computer program Kingdom™. Poor data quality over most of the two study areas has limited any detailed interpretations of the profiles. At the time of writing, the data were yet to be fully processed and interpreted for seabed character.

2.2.3. Multi-beam (Swath) Sonar Backscatter Data

An algorithm for processing the Simrad EM300 multi-beam backscatter data has been developed by Geoscience Australia. The algorithm calculates the backscatter coefficient corrected for transmission loss and isonification areas, and is based on the equation given in Talukdar *et al.* (1995). With these measurements, the corresponding incidence angle and coordinates on the seafloor, X-Y and depth (Z), are calculated. The full processing algorithm was developed into the computer software program Matlab®. It contains the following steps:

1. conversion from the Simrad raw ALL data format into Matlab data format;

2. calculation of the absolute X, Y, Z position and the incidence angle θ for each beam and each ping;
3. removal of the system transmission loss;
4. removal of the system model;
5. calculation of the surface backscattering strength, which involves correction for transmission loss and area; and
6. removal of the angular dependence.

The Simrad system incorporates a scattering model that makes best use of the limited dynamic range of the electronics used (Hammerstad, 2000). The model includes Lambert's law and the scattering area. In addition, the Simrad system uses different expressions in three different angular domains of the incidence angle. The first domain relates to the normal incidence angle (i.e., $\theta = 0°$); the second domain pertains to the incidence angle defined by $0° < \theta < \theta_{crossover}$; and the third domain involves the oblique incidence angle $\theta > \theta_{crossover}$, where $\theta_{crossover}$ is the crossover angle which is between 5° and 30° as selected by the operator. It is necessary to remove these models to get the true angular response of the backscatter.

The surface scattering coefficient can be determined by correcting the backscatter intensity for the actual transmission loss and normalising the values for the area under investigation. The transmission loss is the energy lost due to spherical spreading of acoustic energy and acoustic absorption in the water column. Spherical spreading loss is a function of range R and for two-way travel is equal to $40\log_{10}R$ (dB). Absorption loss is also a function of range and the acoustic absorption coefficient (a), so for two-way travel this is $2aR$ (dB). The area that controls the peak backscatter intensity is called the insonified area. The more accurate insonified area is calculated as:

$$A = \varphi R^2 \left\{ \cos(\theta) \tan\left[\cos^{-1}\left(\frac{\cos(\theta)}{1 + \frac{cT_W}{2R}} \right) \right] - \sin(\theta) \right\} \qquad (2.1)$$

A technique for removing the angular dependence developed by the Center for Marine Science and Technology (CMST) was applied to the data (*cf.*, Gavrilov *et al.*, 2005). Removing the local mean angular trend also filters out large-scale variations due to change, either sharp or gradual, in the seabed properties along the swath line. To recover this useful information and obtain absolute values of backscatter strength, the angularly equalised backscatter strength within the sampling window is increased by adding the window-mean backscatter level at a specified reference angle (in this case a moderate angle of 25° was used). The algorithm is as follows:

$$BScor(X,Y,\theta) = BS(X,Y,\theta) - \overline{BS}(X,Y,\theta) + \overline{BS}(X,Y,25°) \qquad (2.2)$$

where $BS(X,Y,\theta)$ is all the backscatter data within the sampling window (X,Y) at angle θ, $\overline{BS}(X,Y,\theta)$ is the mean backscatter strength within the sampling window (X,Y) at angle θ, and $\overline{BS}(X,Y,25°)$ is the mean backscatter strength measured within the sampling window at the reference angle of 25°.

Following the procedure described in Siwabessy *et al.* (2005), the probability distribution function (PDF) was derived from normalised backscatter values using a linear scale across a homogenous area. The backscatter values were then normalised to the maximum backscatter value of the area and a gamma distribution model fitted to the resulting distribution. This approach is based on the work of Middleton (1999) who demonstrated theoretically that the statistical distribution of the average backscatter intensity for a Gaussian scattering process should follow a gamma distribution. A nonparametric Kolmogorov-Smirnoff (KS) statistic test was used to assess the goodness-of-fit between the

theoretical and experimental distributions of the data collected in the study areas using respective cumulative distribution functions (CDF). This defines the maximum absolute difference (D_{KS}) between the theoretical and experimental CDFs. The *p*-value of D_{KS} indicates the probability of observing an absolute difference greater than D_{KS} under the null hypothesis (H_o).

2.2.4. Gravity and Magnetic Data

Data were input to Fugro Robertson's DATAPRO™ database for processing. Due to the failure of the recording system during the survey, additional navigation data were provided to Fugro Robertson by NIWA for processing. After a comparison of the echo sounder and multi-beam (swath) bathymetry data, it was decided that the multi-beam data would be used for processing over the entire survey area due to its higher spatial resolution.

2.2.4.1. Gravity Data

Gravity data were reconstructed from the primary components of spring tension, beam slope and total cross-coupling correction. A cross-correlation procedure, based on the method of Lacoste (1973), was employed to improve data quality, particularly for data acquired during heavy seas. Data were converted from counter units to milligals (mGal) using the calibration factor for the #S-65 gravity meter of 0.9909. Further corrections were applied to remove the influence of gravity drift, earth tides and Eötvös effect. Gravity anomalies were derived by subtracting a theoretical gravity value for each measurement point that was derived from:

1. a normal gravity value at the GRS80 latitude of each measurement (computed from a closed-form expression for normal gravity on the ellipsoid); and
2. free-air and 3D Bouguer corrections (simple slab correction and terrain correction using a density of 2,000 kg m^{-3}).

The complete Bouguer correction was calculated using a terrain model derived from the GEBCO Digital Atlas and the multi-beam (swath) bathymetry acquired during the survey.

2.2.4.2. Magnetic Data

The raw magnetic data acquired during the survey were first corrected for the magnetometer offset. At each sample point, the value of the earth's normal magnetic field, based on the IGRF-10, was subtracted from the corrected measured value in order to derive the magnetic anomaly. In order to remove the effects of diurnal field fluctuations, the survey data were de-correlated using the readings from base stations located on Norfolk Island. Low-pass filtering was applied to some of the data to remove high-frequency noise.

Survey network adjustment was performed to reconcile mis-ties between the survey lines. However, the survey had only one significant tie line and some lines had no intersections, so a systematic grid-based levelling technique was employed. The adjustment reduced the mean mistie value in the 3D Bouguer gravity to 0.14 mGal (RMS = 0.23) and in magnetic anomaly to 0.70 nT (RMS = 1.25). The free-air gravity, adjusted 3D Bouguer gravity, magnetic anomaly, and multi-beam bathymetry data were gridded using the minimum-curvature method with a grid-increment of 1,500 m and without any further filtering. The dataset datum is WGS 84, projected to UTM Zone 57 South.

2.3. RESULTS

In total, the geophysical survey resulted in 39,870 km^2 of multi-beam sonar data and 16,081 line-km of shallow sub-bottom profiler and high-resolution magnetics and gravity data,

Table 2.1. Summary statistics of multi-beam (swath) sonar data collected during TAN0713.

	Area (km^2)	Line-km
Study Areas		
A: Capel and Faust basins	23,400	9,788
B: Gifford Guyot	2,045	1,005
Transits	14,425	5,288
Total Survey	**39,870**	16,081

including transits (Fig. 2.1; Table 2.1). The LHR and Gifford Guyot study areas were divided into two separate survey areas for logistical reasons (Fig. 2.2). Area A covered the Capel and Faust basins study area, and area B covered the Gifford Guyot study area. The data show for the first time the details of the seabed environments on the top and western flank of the LHR (a large marginal plateau) and Gifford Guyot (a seamount). The results for Gifford Guyot represent the most detailed complete bathymetric survey of a large seamount on the Australian margin. Features revealed by the geophysical survey include: low-gradient plains characterised by polygonal faulting, volcanic cones, shallow-gradient valleys, broad domes on the LHR, and aprons, slide blocks, subaqueous dunes, plateaus, terraces and slumps on Gifford Guyot. A detailed description of the geomorphology is contained in Chapter 5.

2.3.1 Multi-beam (Swath) Sonar

The multi-beam coverage comprises 23,400 km^2 (9,788 line-km) collected in study area A, Capel and Faust basins, 2,045 km^2 (1,005 line-km) in study area B, Gifford Guyot, and 14,425 km^2 (5,288 line-km) on the transits (Table 2.1). Data coverage varied across the two study areas due to rapidly changing water depths. In study area A data coverage ranged from 0.75–2.91x water depth, which equates to 2,300–4,000 m swath width. In study area B data coverage ranged from 0.5–5.99x water depth, which equates to 1,540–1,550 m swath width. Swath widths in the order of 2–3x water depth were common for all the deep water survey areas and were slightly less than optimum for the system. The slightly reduced data coverage was caused by a loss of signal from the outermost beams caused by the low reflectivity of the seabed. Low reflectivity over most of the study area was a result of relatively high water content in the surface sediments. Data coverage was greater for study area B, over Gifford Guyot, because of the generally harder substrate producing stronger returns from the seabed. Survey line spacing was regularly reviewed and changed based on data coverage, to ensure 100% of the area was mapped. Additional lines were required in study area B to fill gaps in the coverage resulting from significant changes in water depth. Water depths for study area A range from 944–2,668 m (Fig. 2.3) and a hypsometric analysis of the data revealed peaks at 1,400 m and 1,750 m that are related to the large-scale topographic highs and lows within the survey area (Fig. 2.4). Water depths for study area B range from 256–3,090 m (Fig. 2.5) with a dominant hypsometric peak at 350 m corresponding to the extensive flat-topped summit (Fig. 2.6).

2.3.2. Shallow Seismic Reflection

A total of 3,280 line-km of digital shallow seismic reflection data (8 GB) was acquired during the survey (Fig. 2.1). Sub-bottom penetration was minimal and highly dependent on sediment character, water depth and sea state. Penetration of up to 20 m (15 ms) was attained during this survey in sediments on the western flank of the Lord Howe Rise. Digital images of the shallow seismic reflection profiles are contained in Appendix F.

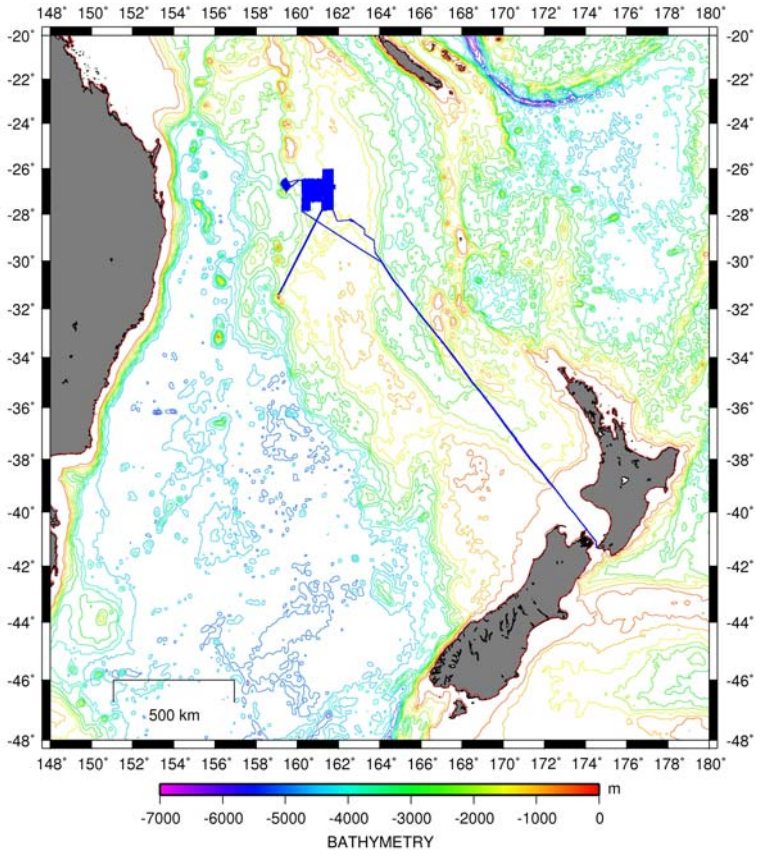

Figure 2.1. Contour map showing regional bathymetry of the Tasman Sea. The RV *Tangaroa* survey ship-track (shown in blue) over the Capel and Faust basins and Gifford Guyot, including transits to and from New Zealand and Lord Howe Island.

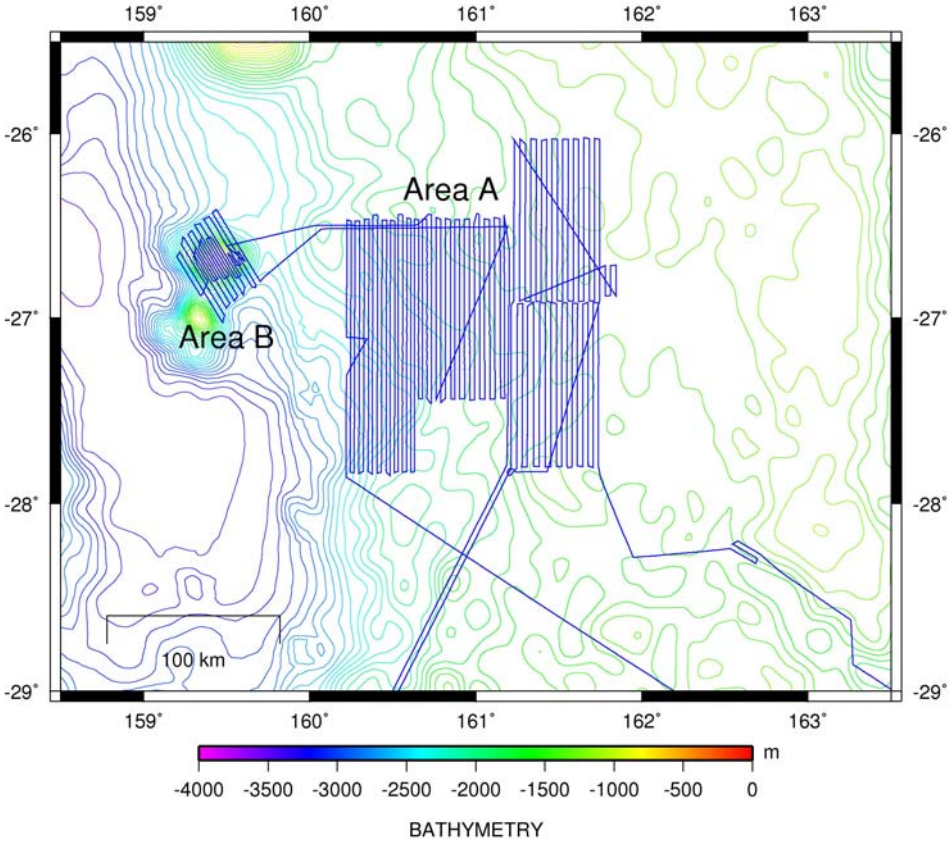

Figure 2.2. Contour map showing bathymetry of study area A (Capel and Faust basins) and study area B (Gifford Guyot), including survey ship-tracks.

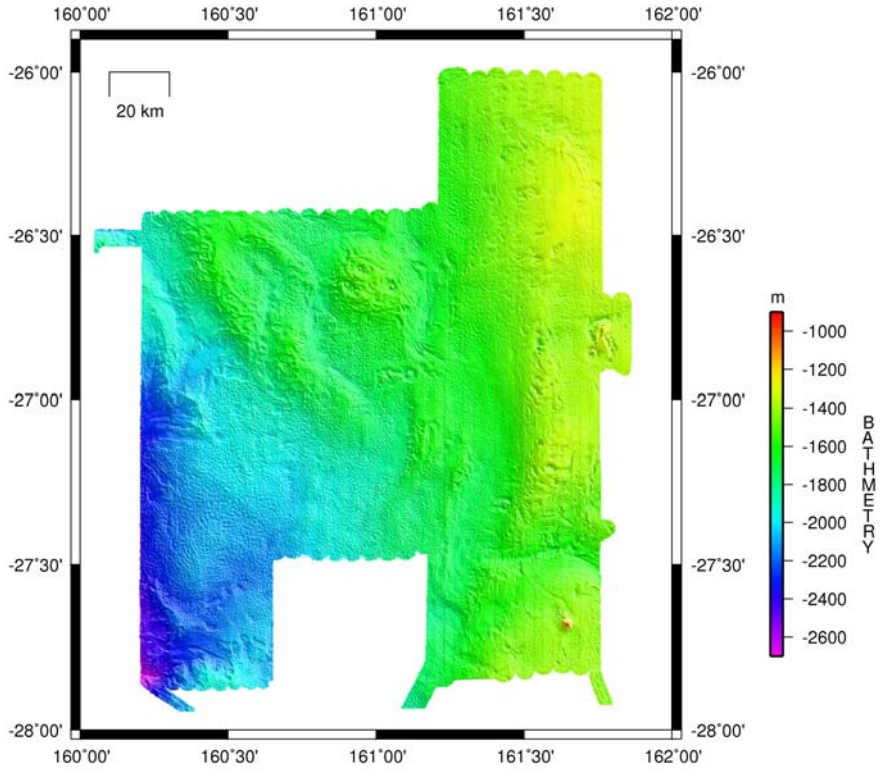

Figure 2.3. Map showing multi-beam (swath) sonar bathymetry for study area A over the Capel and Faust basins.

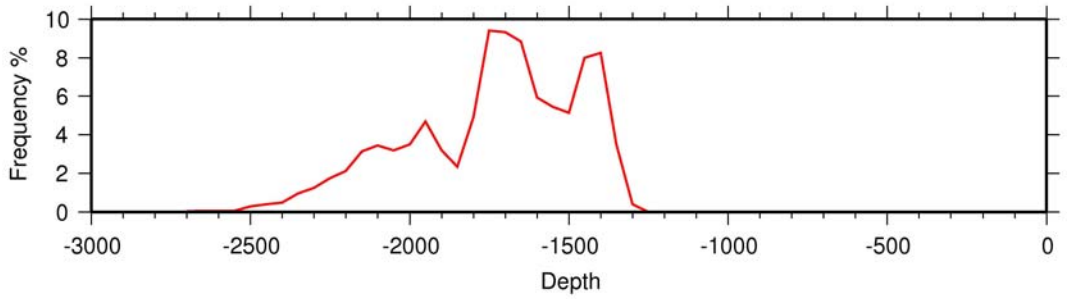

Figure 2.4. Hypsometric curve of multi-beam (swath) sonar bathymetry for study area A over the Capel and Faust basins.

2.3.3. Multi-beam (Swath) Sonar Backscatter

2.3.3.1. Study Area A: Capel and Faust basins

The processed backscatter grid of the Capel and Faust basins survey region has a relatively homogenous acoustic character (Fig. 2.7). The area is also characterised by low backscatter intensity due to the predominant presence of pelagic nannofossil ooze with a relatively high water content. The histogram of the backscatter is unimodal and peaks at -105 dB (Fig. 2.8).

High backscatter values occur in study area A over the Capel and Faust basins and are identified by the coloured squares in Figure 2.7. High values are mainly associated with relatively harder substrates of volcanic cones, mounds and ridges (Figs. 2.9 & 2.10). In the far southwest corner of the region, high backscatter values coincide with a slump feature. Histograms of the backscatter values show these features have peaks at -88 dB and -103 dB compared with the relatively low backscatter of the surrounding plains.

Representative examples of the probability distribution function (PDF) over a "homogenous" section and an area of high backscatter in study area A (Station 42 on Fig. 2.7;

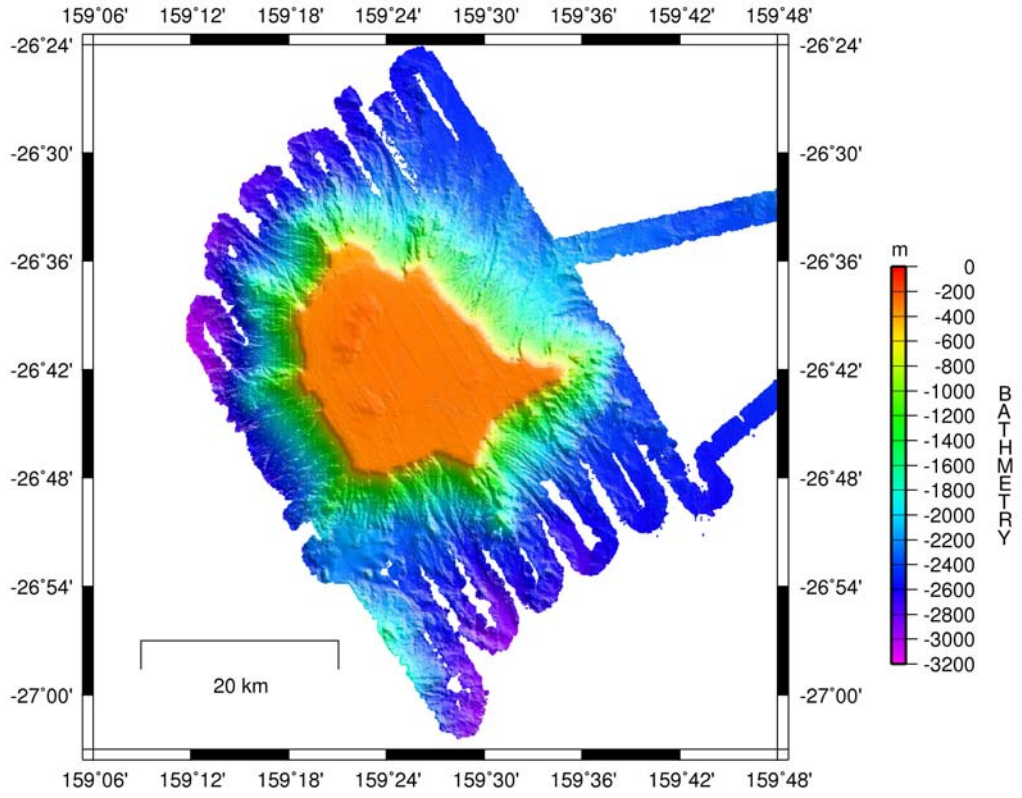

Figure 2.5. Map showing multi-beam (swath) sonar bathymetry for study area B over Gifford Guyot.

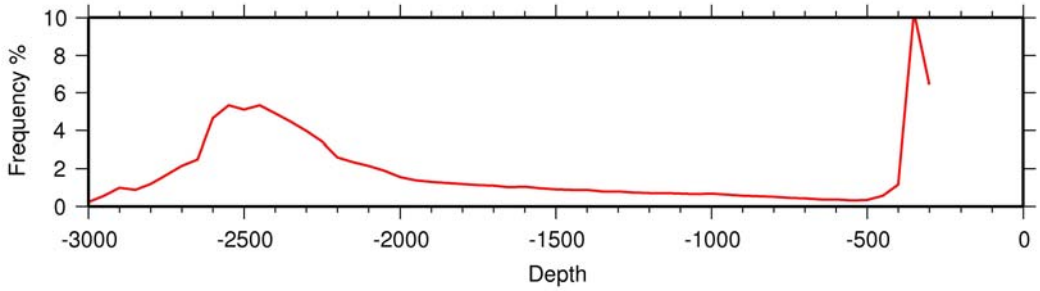

Figure 2.6. Hypsometric curve of multi-beam (swath) sonar bathymetry for study area B over Gifford Guyot. Note the prominent peak at 320-280 m corresponding to the extensive flat-topped summit of the seamount.

and Fig. 2.10a, respectively) show, in both cases, that the gamma distribution model (red dotted line in Fig. 2.11) fits the empirical distribution according to the KS statistic test (p-value = >0.05). Although not shown in Fig. 2.11, the log-normal distribution model also fits the empirical distribution (p-value = >0.05). This is expected as the gamma distribution is a 2-parameter model characterised by the scale (λ) and shape (β) parameters and it tends to the Gaussian distribution when $\beta >> 1$.

The gamma distribution model indicates that PDF's peak at -104.7 dB (Fig. 2.11a) for low backscatter and at -88.1 dB (Fig. 2.11b) for high backscatter. The seabed of the Capel and Faust basins survey region can be quantised into these two categories. Low backscatter values correspond to the soft sediment, which comprises carbonate pelagic ooze to carbonate coarse sand, all of which have similar backscatter values. High backscatter values correspond to volcanic peaks, ridges and mounds, which all exhibit similar high backscatter values, and cannot be further subdivided.

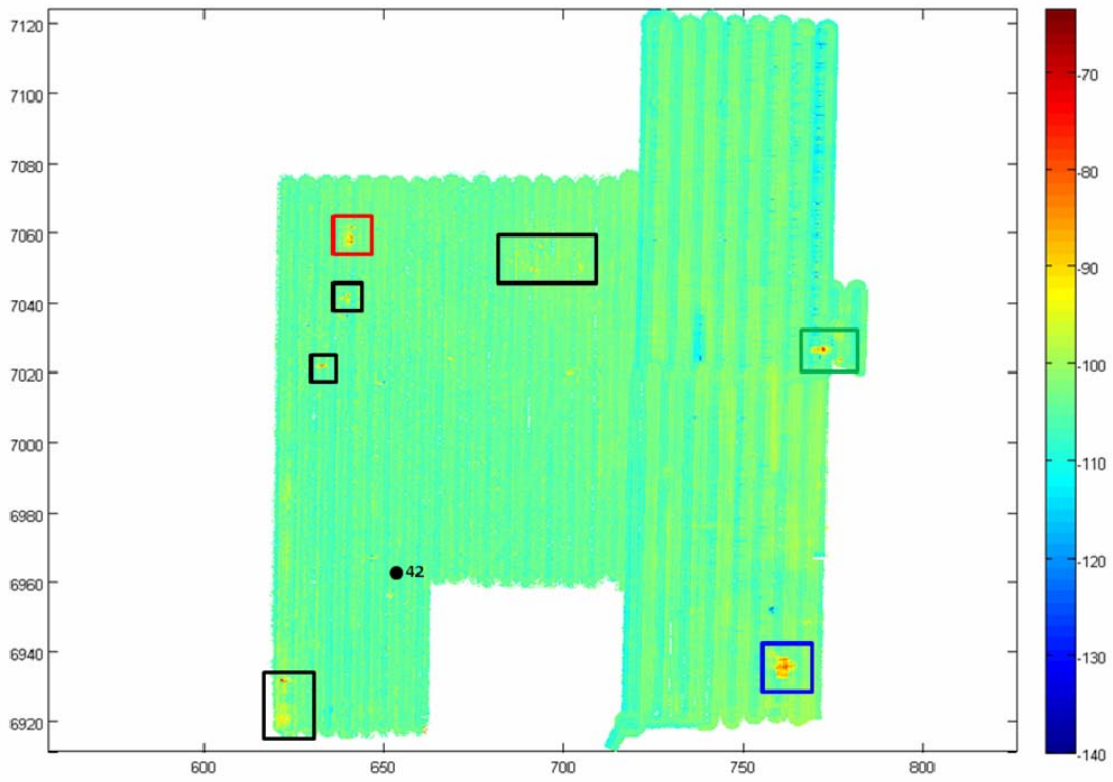

Figure 2.7. Processed multi-beam (swath) sonar backscatter grid of study area A. Rectangle indicate regions of higher backscatter values associated with outcropping volcanic cones (see Figure 5.9). Red and blue rectangles refer to areas with high backscatter values shown in Figures 2.9(a) and 2.10(a) respectively. Number refers to station where representative low backscatter distribution has been derived (see Figure 2.11(a)).

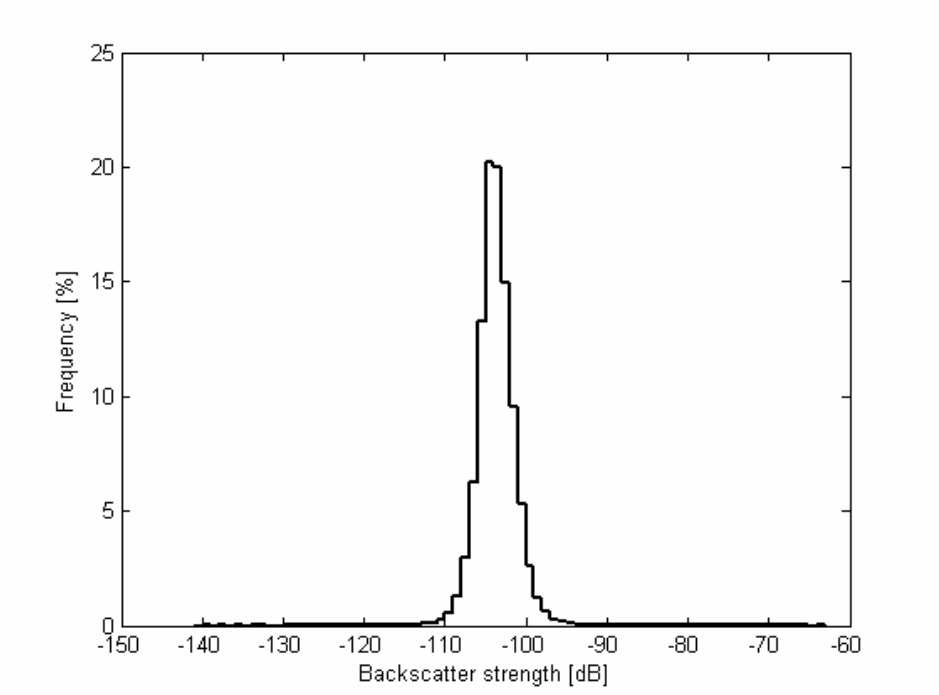

Figure 2.8. Histogram of the processed multi-beam (swath) sonar backscatter data study area A showing a prominent peak at -105 dB corresponding to volcanic cones and slump features.

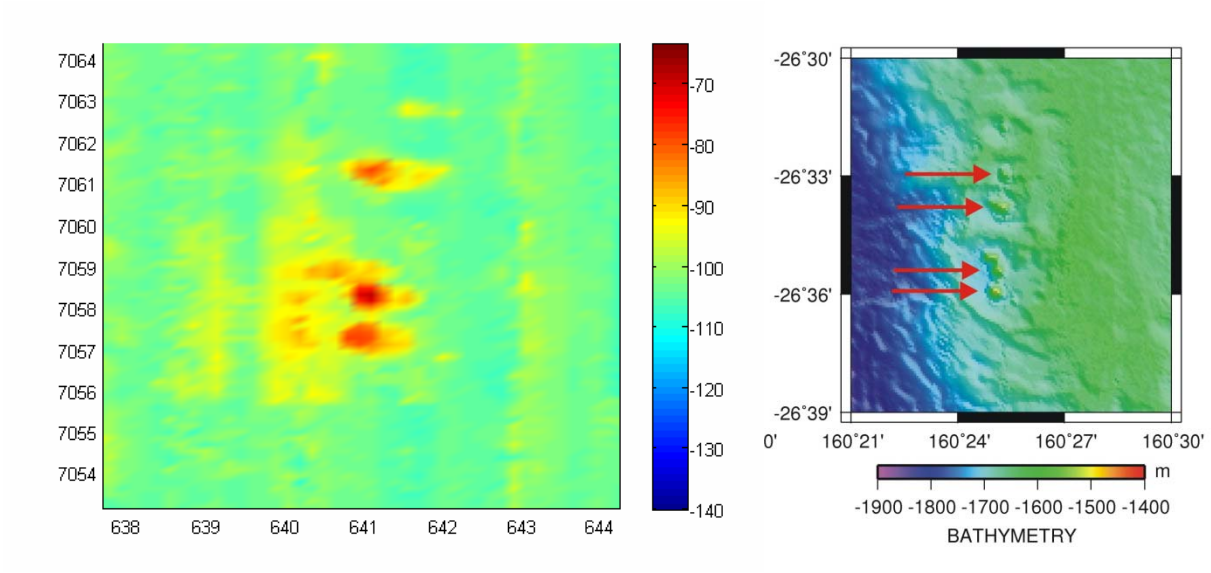

(a) (b)

Figure 2.9. Multi-beam (swath) sonar backscatter image showing: (a) high reflectivity associated within the region outlined by the red rectangle in Figure 2.7 with (b) volcanic cones outcropping at the seabed surface.

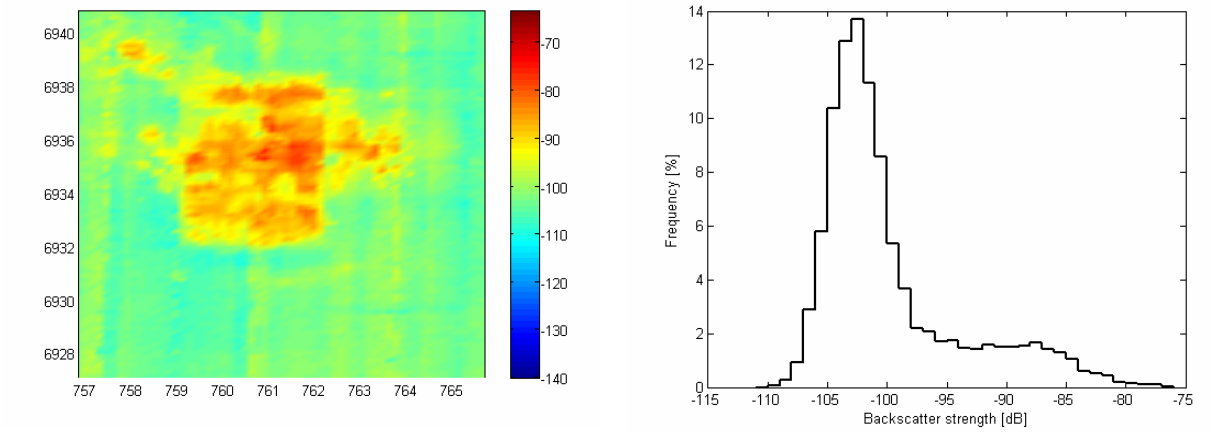

(a) (b)

Figure 2.10. Multi-beam (swath) sonar backscatter image showing: (a) high backscatter returns within the region outlined by the blue rectangle in Figure 2.7 and (b) the associated histogram of backscatter anomalies with a prominent peak at -88 dB.

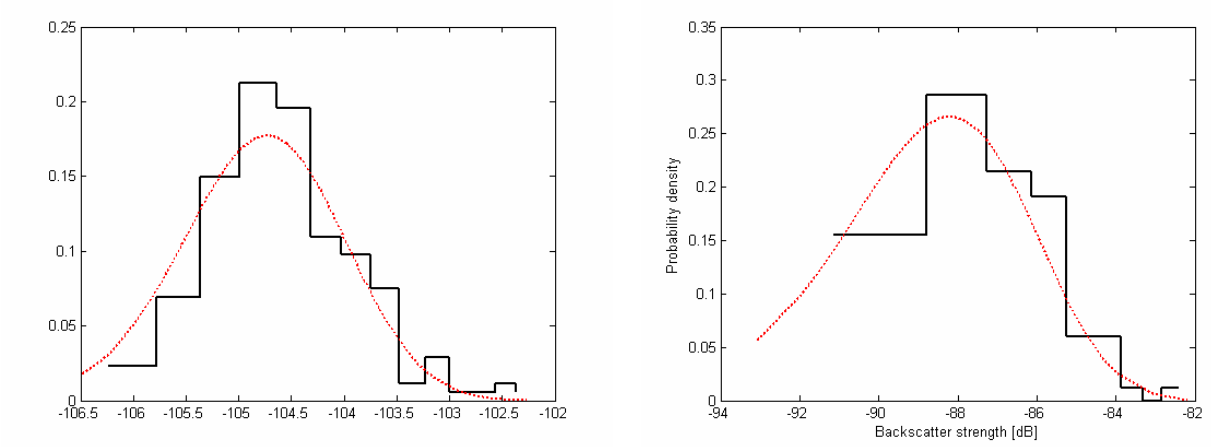

(a) (b)

Figure 2.11. Representative examples of probability distribution functions of (a) low backscatter returns with peak at -104.7 dB and (b) high backscatter returns with peak at -88.1 dB in the Capel–Faust Basins region.

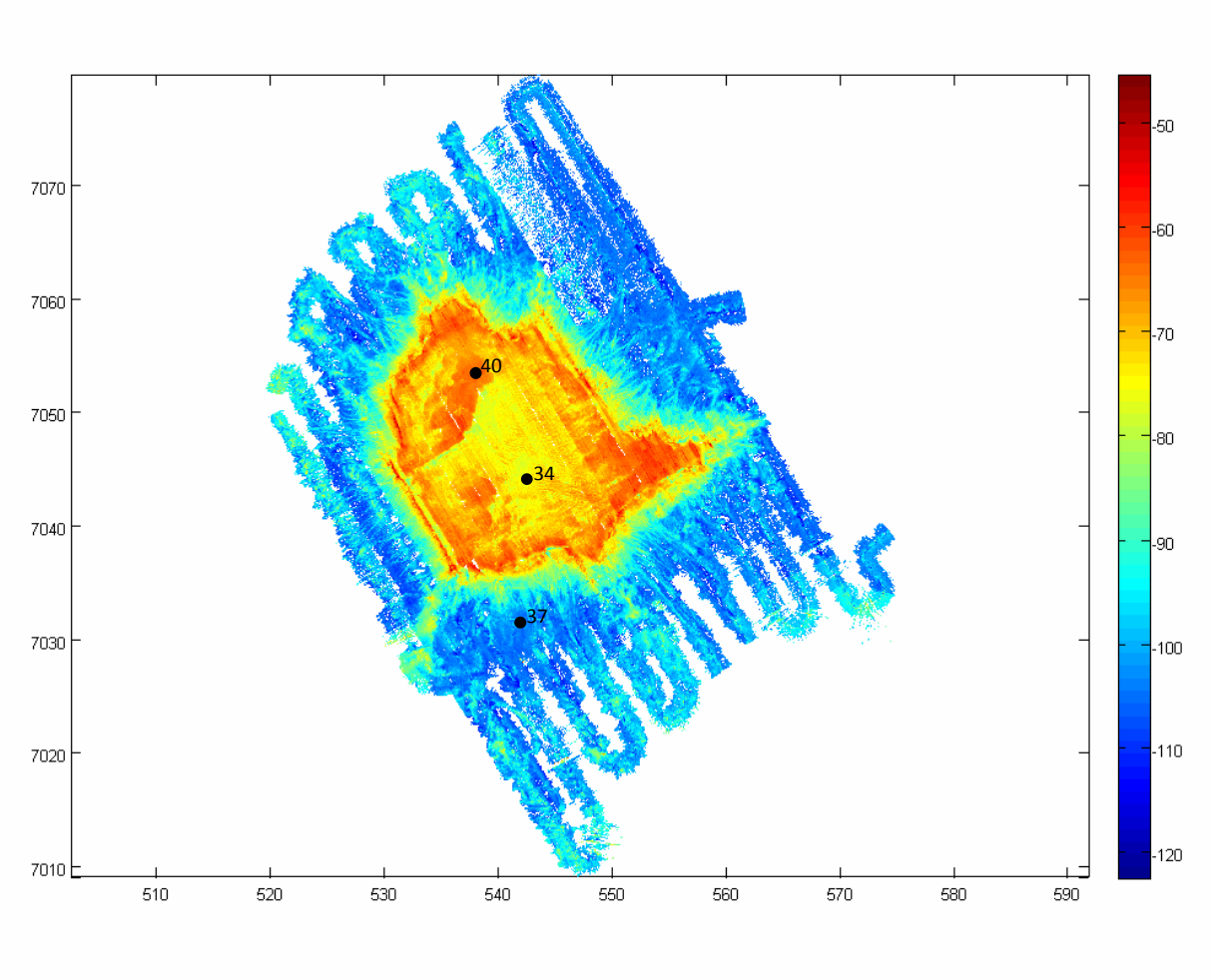

Figure 2.12. Processed multi-beam (swath) sonar backscatter grid for study area B. Numbers refer to stations where representative backscatter distributions have been derived (see Figure 2.15).

2.3.3.2. Study Area B: Gifford Guyot

The backscatter signals from study area B over Gifford Guyot are more diverse than those from study area A over the Capel and Faust basins (Fig. 2.12). The histogram of the data indicates that there are two peaks at -71 dB and -104 dB, corresponding to the highly acoustic reflective seabed of the top of the guyot and the lower acoustic backscatter of the surrounding flanks and plain, respectively (Fig. 2.13). The histogram also shows that the distribution around each of these two peaks is quite wide, approximately 20 dB, in comparison to the narrower distribution for study area A (Fig. 2.8). These patterns suggest a variable acoustic character around each peak, which is also observed in the backscatter grid (Fig. 2.12). Examples include the relatively high backscatter variation on the flat top of the seamount, and particularly, associated with the ridges and valleys on the flanks (Fig. 2.14).

PDFs were derived over three different "homogenous" regions at sampling stations 34, 37 and 40 (Fig. 2.12). Station 40 is a broad carbonate ridge on the top of the guyot and has the highest backscatter values and a peak at -64.5 dB. Station 37 is a sediment covered ridge and valley feature with relatively high backscatter values with a peak at -74.5 dB. Station 34 represents a region of partially-lithified dunes with relatively low backscatter values with a peak at -104.5 dB. The gamma distribution model (red dotted lines in Fig. 2.15) fits the empirical distribution derived from each station according to the KS statistic test (p-value = >0.05).

The backscatter returns from the flanks and base of the guyot represented by station 37 and those from most of the surveyed area in study area A show a similar acoustic character

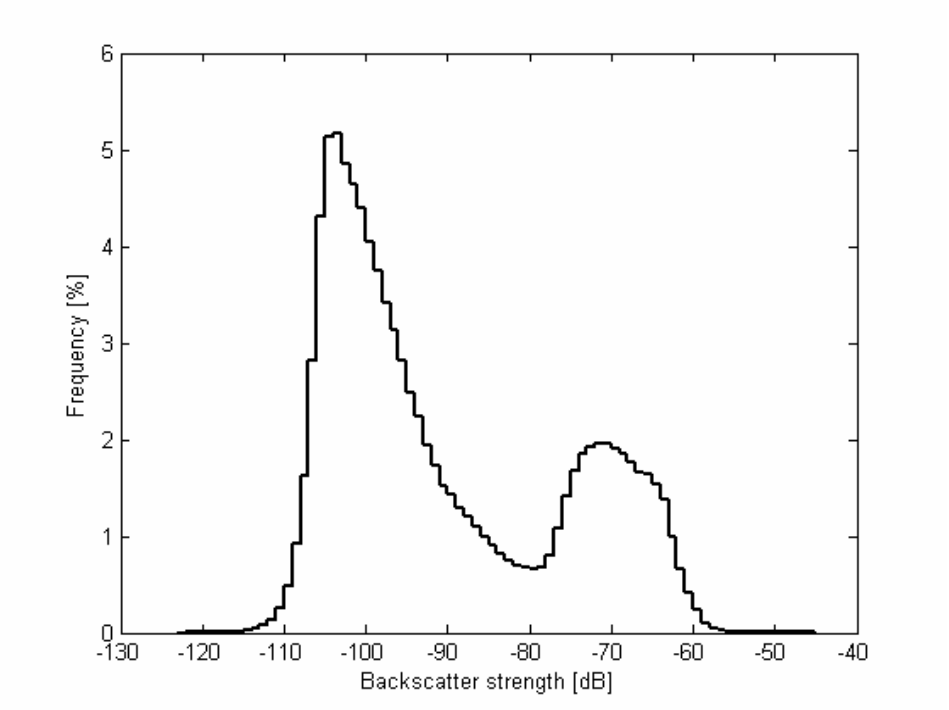

Figure 2.13. Histogram of the processed multi-beam (swath) backscatter for study area B with peaks at -104 dB and -71 dB.

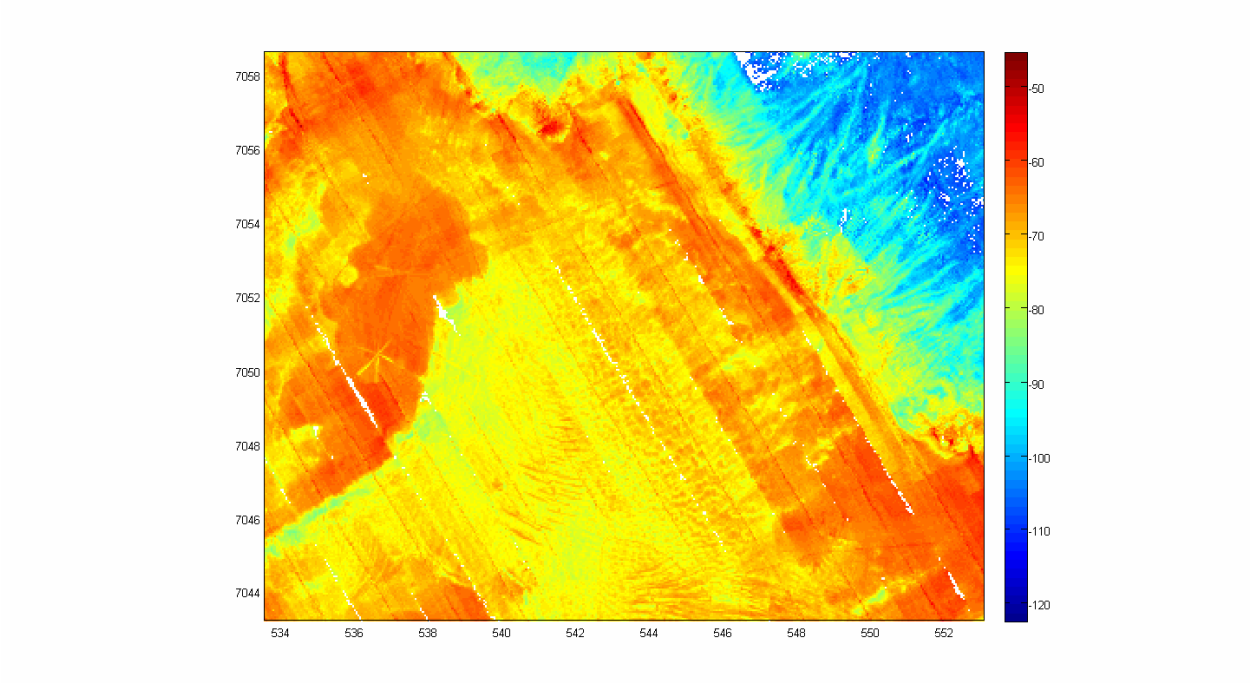

Figure 2.14. Processed multibeam sonar backscatter grid showing the variations in backscatter values around the flat topped seamount and ridges.

with a mean backscatter value of about -105 dB. The high backscatter values corresponding to the outcrops and volcanic cones, however, differ in their acoustic character to the hard, reflective seabed regions in study area B on Gifford Guyot.

2.3.4. Gravity and Magnetics

A total of 14,145 line-km of gravity and 13,843 line-km of magnetic data were acquired. The overall quality of magnetic data is good. While overall good, the quality of the gravity data was degraded in some places due to heavy seas which necessitated significant filtering of the

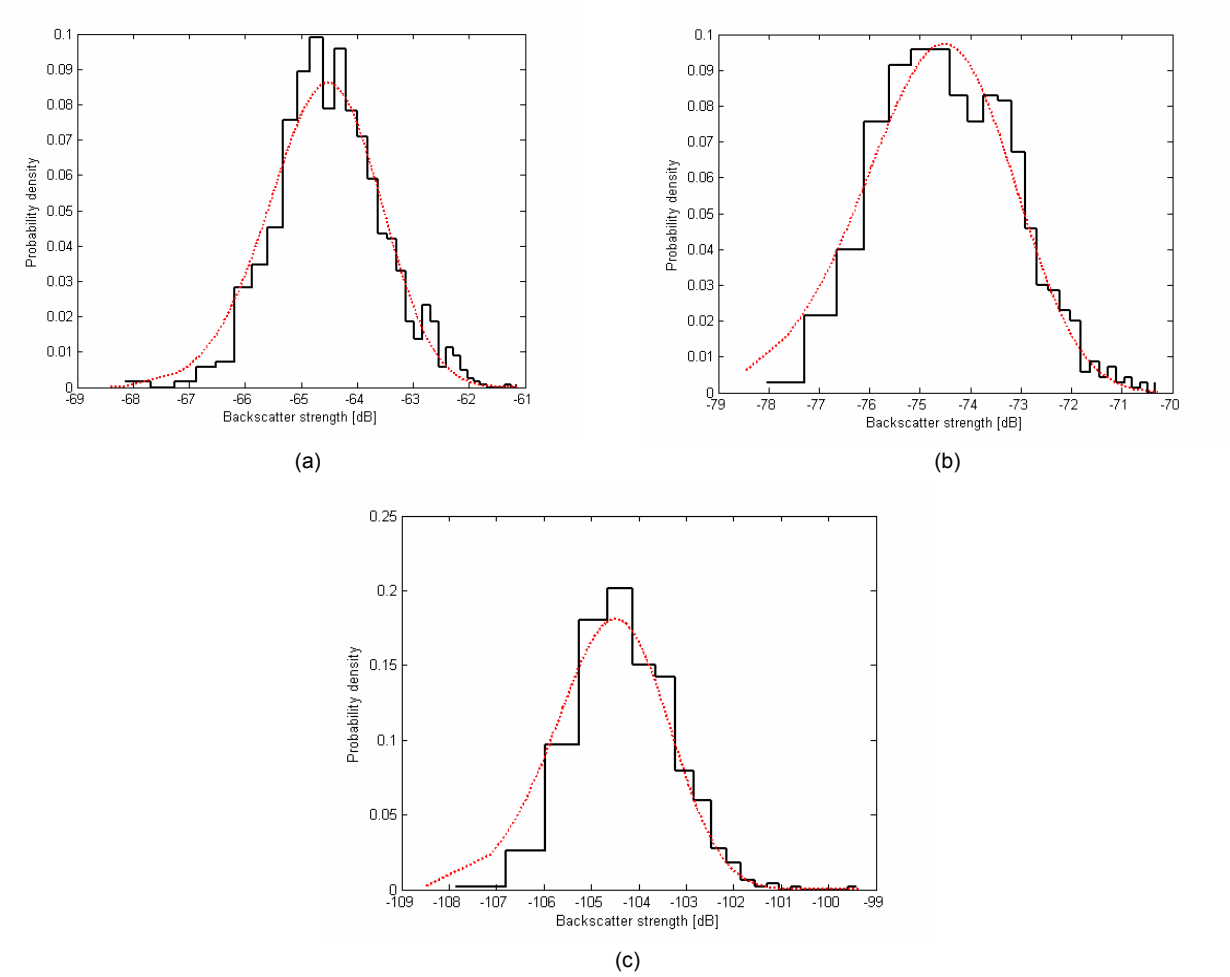

Figure 2.15. Representative examples of probability distribution functions of (a) high backscatter returns with peak at -64.5 dB, (b) medium backscatter returns with peak at -74.5 dB and (c) low backscatter returns peak at -104.5 dB from three different environments (stations 40, 34 and 37 respectively).

data. Further details on filtering are contained in Fugro Robertson's report (Appendix E). Products resulting from this work, and supplied to Geoscience Australia, include raw and reduced line-orientated data and grids of bathymetry, free-air and Bouguer gravity, and magnetic anomaly. 1:350,000-scale colour maps of these datasets were also supplied.

2.3.4.1. Gravity

In the eastern part of the 3D Bouguer gravity image (Fig. 2.16), a series of elongate highs and lows, roughly oriented north–south, extend continuously over horizontal distances of about 100 km. These anomalies have a dominant wavelength of about 50 km. Elsewhere, gravity lows are more isolated. Comparison with GA302 survey seismic reflection data shows that the gravity lows correspond to sediment depocentres. Gifford Guyot is associated with a gravity high that partly reflects the high density of the seamount, but also partly reflects the thinner crust toward the Middleton Basin.

2.3.4.2. Magnetics

The magnetic data (Fig. 2.17) do not show any obvious correlations with the gravity data. This suggests that the magnetic data reflect the distribution of magmatic rocks within the crust rather than the distribution of sediment depocentres. Two parallel, NNE-trending positive anomalies bound the most prominent gravity low in the eastern part of area (at about -27°) and may represent dykes intruded along depocentre-bounding faults. Gifford

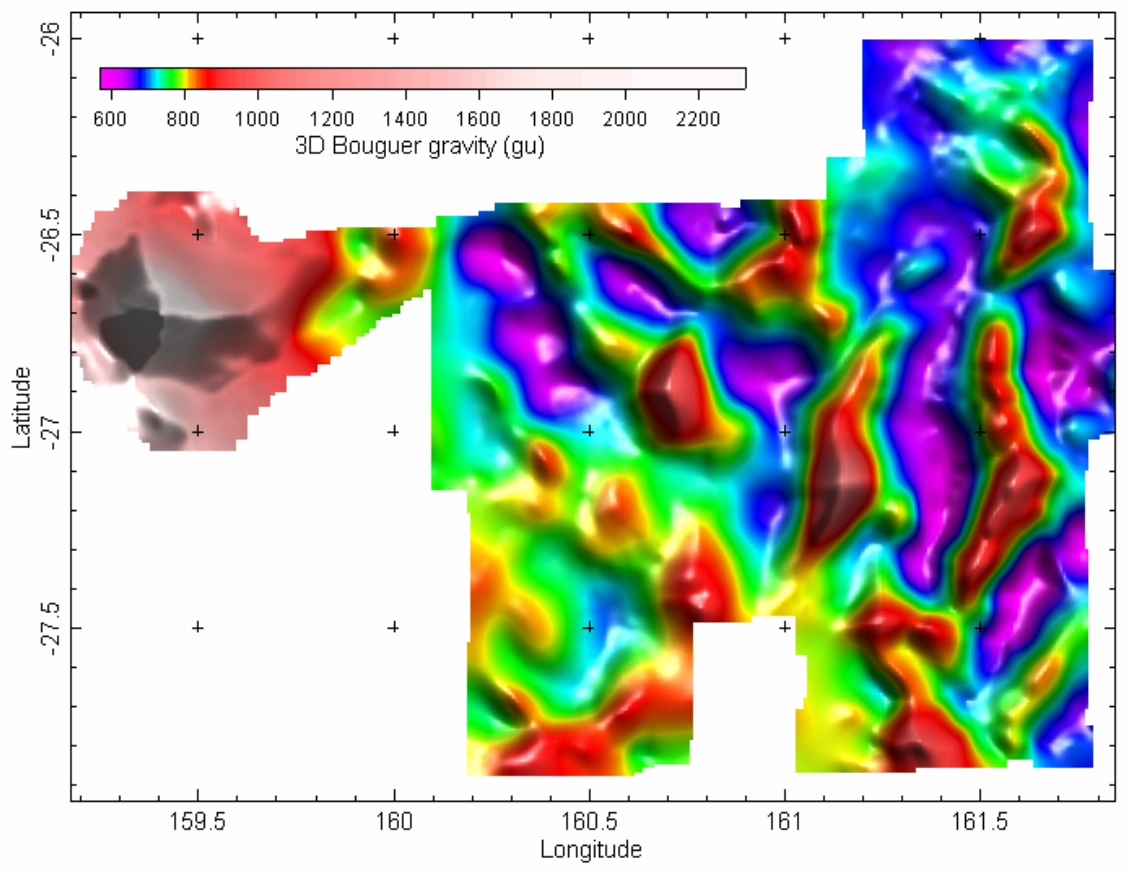

Figure 2.16. Map showing 3D Bouguer gravity data for study areas A and B.

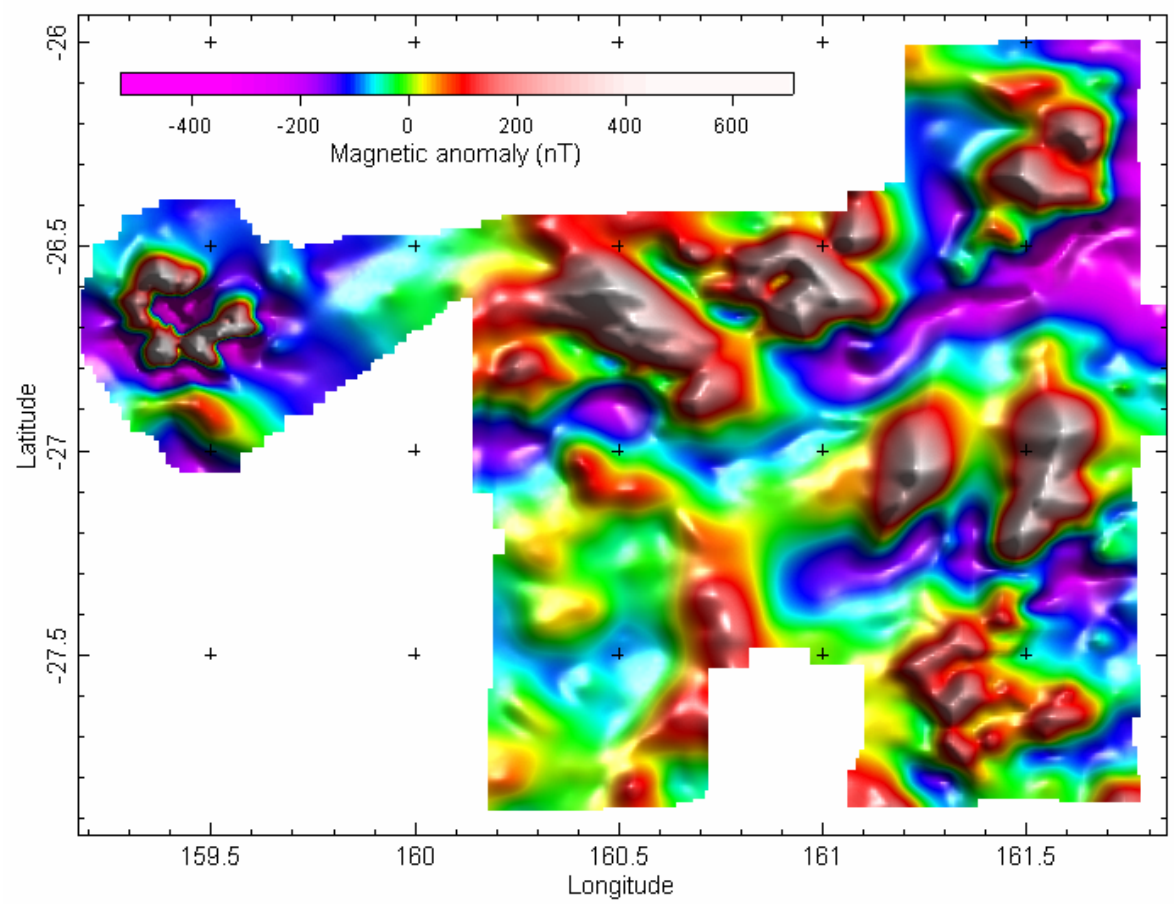

Figure 2.17. Map showing magnetic anomaly data for study areas A and B.

Guyot is associated with a negative magnetic anomaly enclosed by a near-complete ring of positive magnetic anomalies.

A more thorough interpretation of the gravity and magnetic data requires the integration of other ship-track data, further data processing (e.g., reducing the magnetic data to the pole and filtering), and interpretation in conjunction with seismic reflection and multi-beam (swath) bathymetry data.

3. Sample Acquisition

Each study area was mapped for 100% spatial coverage using the multi-beam sonar, sub-bottom profiler, magnetometer and gravimeter. The results of the geophysical survey helped identify priority areas for further detailed investigation and geological sampling. Locations for rock dredging were partly determined from pre-existing satellite altimetry-derived gravity data. Aspects of seabed sediment and rock samples are discussed in Chapters 6-9.

3.1. SAMPLE STATIONS

A total of 46 stations were occupied during the survey (Fig. 3.1; Table 3.1). Samples were collected from representative seabed environments to cover the full spectrum of sedimentary environments. Different combinations of sampling devices were used at each station depending on the sampling objectives for that seabed environment. Typically, a camera run was completed at each station to support characterisation of the physical properties and biota.

3.1.1. Towed-video and Still Images

High-resolution video footage and still images of the seabed were collected using a deep-towed imaging system (DTIS). The system comprised a high-definition Sony camcorder (model HCR-HC1E), a high resolution stills camera (Canon model 350D), depth and altimeter sensors (SeaBird SBE50 and Tritech PA200), and lights (2x 450 watt halogen lights) (Fig. 3.2). The system was hired from the National Institute of Water & Atmospheric Research (NIWA), New Zealand.

During Leg 1 of the survey the video-camera on the DTIS faced directly down. However, to enable real-time observations of the seabed to be made during Leg 2, the video-camera on the DTIS was moved into a forward facing position (45° angle) increasing the field of view.

At each of the 42 camera stations (Tables 3.1 & 3.2a-b) the DTIS towed-camera system, deployed from the starboard side of the RV *Tangaroa*, was towed 1-2 m above the seabed at a speed over ground of 0.5 to 1.5 knots for approximately 60 minutes. High-resolution video footage was recorded to a mini DV tape in real-time on the DTIS unit, while low-resolution slow-scan footage (2 frames per second) was simultaneously transmitted to the surface. The height of the towed-camera system above the seabed was controlled manually using the ship-board winch while watching one of two surface video monitors with reference to the altimeter. Concurrent to video footage, high resolution still photographs (8 megapixels) were captured every 15 s along the seabed using an automatic timer. The stills were stored on the camera memory card. Paired lasers, set 0.20 m apart, that projected onto the seabed within video and still camera view provided a reference to size objects and organisms. Upon retrieval of the towed camera system the DV mini tape was removed, backed up, and archived. The memory card was removed and the still images immediately downloaded to a ship-board computer.

As biology researchers were not present on Leg 1 of the survey, towed-video footage from Leg 1 was simply recorded for post-processing (Fig. 3.2). Video footage was recorded to mini DV tapes, backed-up to digital hard drive, and archived. Start of video recording and end of video recording were automatically logged to enable navigation and video footage to be merged during post-processing.

3.1.2. Surface Sediment and Benthic Biota Sampling

Surface sediments and benthic biota were collected using a rock dredge, Smith-McIntyre grab, boxcore, and epibenthic sled (Figs 3.3-3.6). Station locations covered all of the main seabed environments, namely: sediment plains, volcanic peaks, valleys, basins and the flanks and surface of Gifford Guyot. Details of samples and sub-samples were entered into Geoscience Australia's Marine Samples database (MARS; http://www.ga.gov.au/oracle/mars).

3.1.2.1. Rock Dredge

Lithified, partially-lithified and unconsolidated seabed sediments and benthic biota were recovered at 13 stations with a rock dredge towed behind the vessel (Tables 3.1 & 3.3; Fig. 3.3). The rock dredge comprises a 0.5 x 1 m rectangular-shaped metal collar to which is attached a 1 x 1 m chain bag. Two pipe dredges are attached to the base of the chain bag to collect finer material. Dredging was undertaken using the port trawl winch. To ensure successful recovery a weight was attached approximately 10 m in front of the dredge to a chain connected to the trawl wire. A 'weak-link' in the form of a rope attached to the dredge from the bridle on the main wire was used to allow recovery in case of hook-ups and to prevent too much strain being imparted to the wire. In all cases, the total wire paid out for dredging was twice the water depth. Dredges were typically 0.5 to several km in length depending on the extent of suitable outcrop, seabed slope, and water depth.

3.1.2.2. Grab Sampler

Seabed sediments and biota at three stations (Tables 3.1 & 3.4) were collected using a surface sediment grab deployed from the starboard A-frame (Fig. 3.4). Sediment samples were double-bagged, labelled (including an aluminium tag), and stored in a refrigerated container before being sent to Geoscience Australia for grain size and carbonate content analysis. Benthic biota were recovered, identified, catalogued, preserved, and archived in a refrigerated container before being sent back to Geoscience Australia for formal identification and distribution to relevant experts.

3.1.2.3. Boxcore

Seabed sediment and biota were collected at 15 stations using a boxcorer deployed from the starboard A-frame (Fig. 3.5; Tables 3.1 & 3.5). The boxcorer was an Oktopus standard boxcore that comprised a 0.5 x 0.5 m box fitted to the deployment mechanism. The box penetrates the seabed when triggered by the firing mechanism as the frame hits the seabed. Upon retrieval the spade swings down under the box to encase the sample for transport to the surface. Once on the surface, the front panel of the box was removed and photographs of the top 0.5 m of the sediment were taken. Sub-samples were then collected for geochemistry, biota and sedimentology, as detailed in the following sections.

3.1.2.4. Epibenthic Sled

An epibenthic sled was used at 10 stations to collect samples of epibenthic biota (Tables 3.1 & 3.6). The sled comprises a plastic net inside a 0.5 x 1 m x 1.5 m metal frame that was towed behind the ship (Fig. 3.6). Two pipe dredges (similar to those attached to the rock dredge) were also attached to the base of the net to collect surface sediments and biota that were not caught in the net. Sub-samples were taken for sediment grainsize and carbonate content, where possible, and biology. Biological sub-samples were sorted, identified, catalogued, preserved, and archived in a refrigerated container before being sent back to Geoscience Australia for formal identification and distribution to relevant experts.

Table 3.1. Physical samples collected on the survey.

Study Area	Station	Camera	Boxcore	Grab	Dredge	Sled	Cores	CTD
Area A	01	CAM01	-	-	DR01	-	-	CTD01
	02	CAM02	-	-	DR02	-	-	-
	03	-	-	-	-	-	-	CTD02
	04	CAM03	BC01	-	-	-	PC01	-
	05	CAM04	-	-	DR03	-	-	-
	06	-	-	-	DR04	-	-	-
	07	-	-	-	-	BS01	-	-
	08	CAM05	-	-	DR05	-	-	-
	09	CAM06	-	-	-	-	-	-
	10	CAM07	-	-	-	-	-	-
	11	CAM08	-	-	-	BS02	-	CTD03
	12	CAM09	-	-	-	-	PC02	-
	13	CAM10	BC02	-	-	-	-	-
	14	CAM11	-	-	-	BS03	-	-
	15	CAM12	-	-	-	BS04	-	-
	16	CAM13	BC03	-	-	-	-	-
	17	CAM14	-	-	DR06	-	-	-
	18	CAM15	BC04	-	-	-	PC03	-
	19	CAM16	-	-	DR07	-	-	-
	20	CAM17	-	-	DR08	-	-	-
	21	CAM18	BC05	-	-	-	-	-
	22	CAM19, 20	-	-	-	BS05	PC04	CTD04
	23	CAM21	BC06	-	-	-	-	-
	24	CAM22	BC07	-	-	-	-	-
	25	CAM23	-	GR01	-	-	-	-
	26	CAM24	BC08	-	-	-	PC05	-
	27	CAM25, 26	BC09	-	-	-	-	-
	28	-	-	-	-	-	-	-
	29	CAM27	BC10	-	-	-	PC06	CTD05
	30	CAM28	BC11	-	DR09	-	-	-
	31	CAM29	BC12	-	-	-	-	CTD06
	32	CAM30	-	-	DR10	-	-	-
	33	CAM31	-	-	DR11	BS06	-	-
Area B	34	CAM32	-	GR02	-	BS07	-	-
	35	CAM33	-	GR03	-	BS08	-	-
	36	CAM34	-	-	DR12	-	-	-
	37	CAM35	-	-	-	BS09	-	-
	38	CAM36	BC13	-	-	-	-	-
	39	-	BC14	-	-	-	-	CTD07
	40	CAM37	-	-	DR13	BS10	-	-
	41	-	BC15	-	-	-	-	-
Area A	42	CAM38	-	-	-	-	PC07,08	-
	43	CAM39	-	-	-	-	PC09,10	-
	44	CAM40	-	-	-	-	PC11	-
	45	CAM41	-	-	-	-	PC12,13	-
	46	CAM42	-	-	-	-	PC14	-

3.1.3. Sub-surface Sediment Sampling

Sub-surface sediments were sampled at 11 stations (Tables 3.1 & 3.7) using a piston corer that consists of a 90 mm diameter, 6 m-long steel barrel and a 1.5 tonne "bomb" (Fig. 3.7). An 84 mm diameter, 6 m long polycarbonate liner was used to contain the sediment inside the barrel and a core catcher is fitted to the base of the barrel to enhance core recovery.

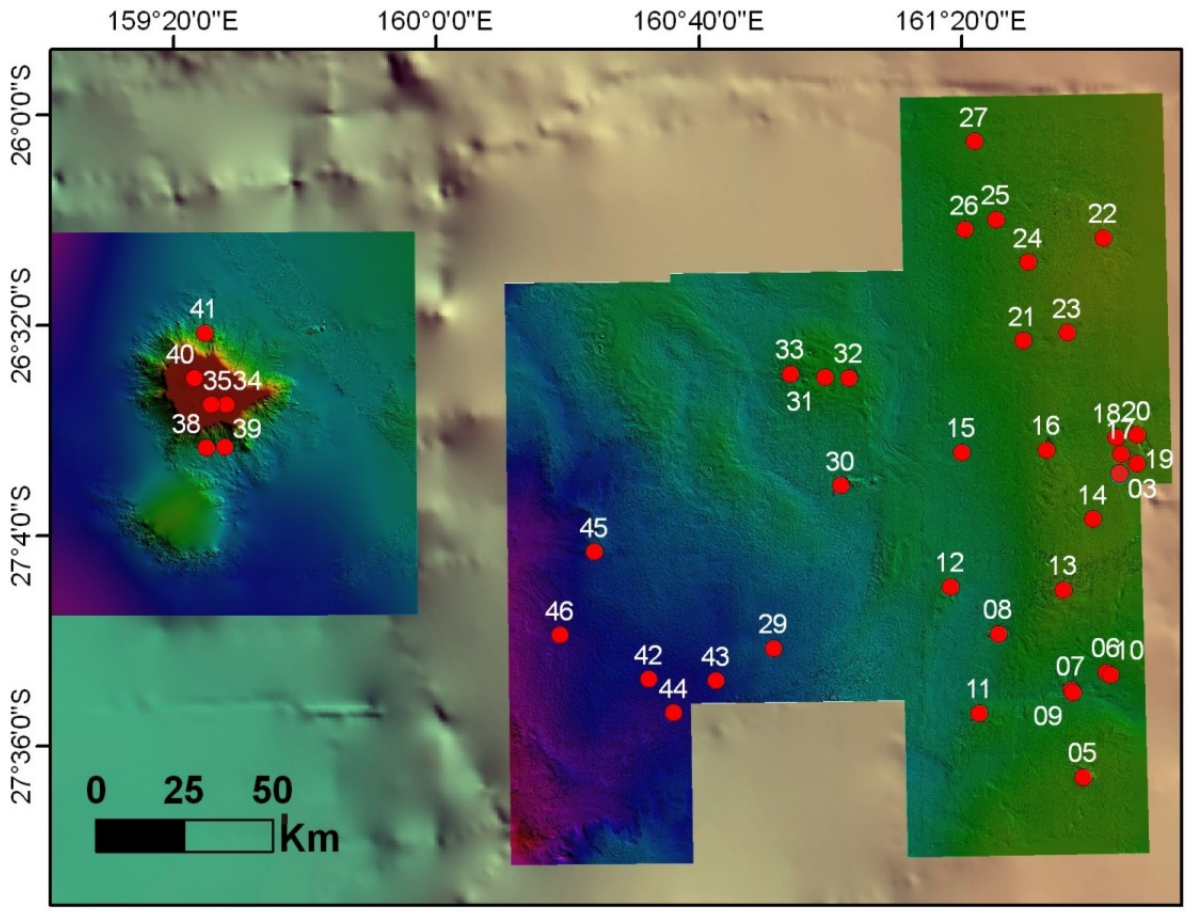

Figure 3.1. Map showing locations of sample stations for study area A over the Capel and Faust basins and study area B over Gifford Guyot.

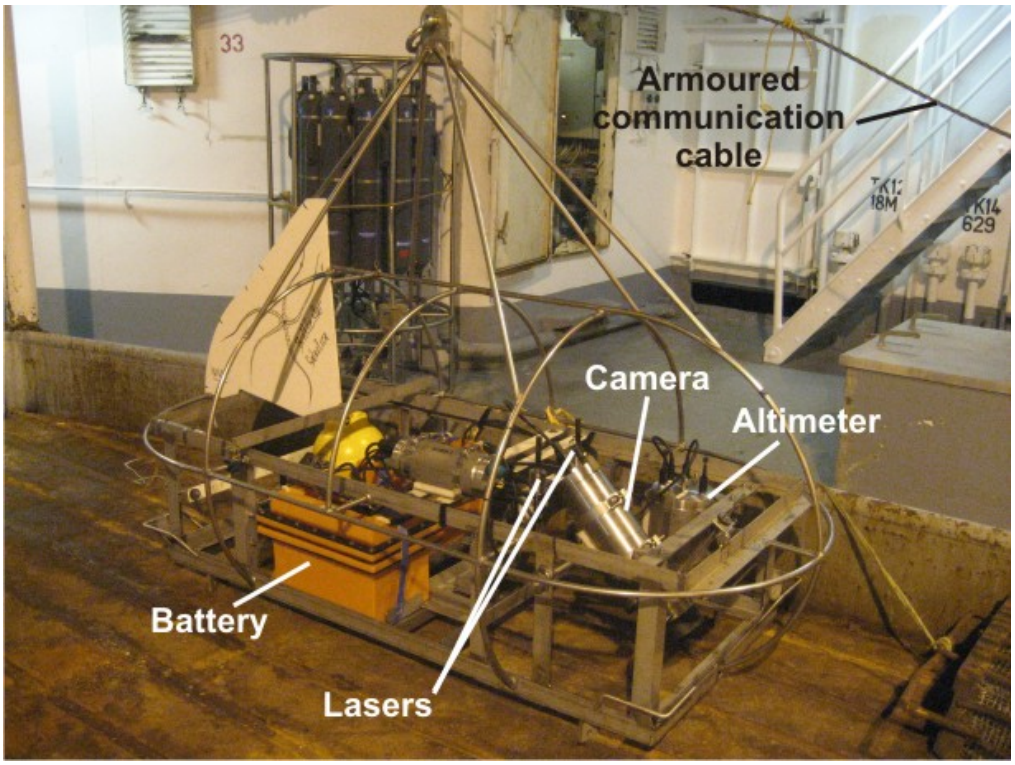

Figure 3.2. NIWA's deep-towed imaging system (DTIS) which supported seabed habitat characterisations.

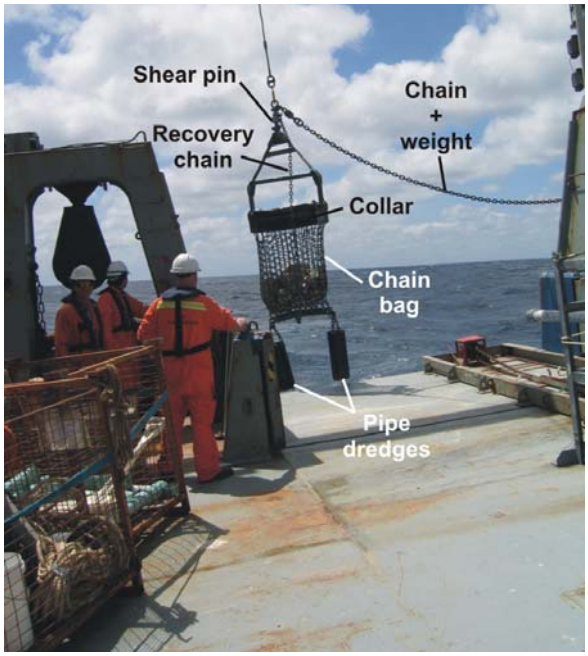

Figure 3.3. Rock dredge used to sample lithified, partially-consolidated and unconsolidated deep-sea sediments. The dredge consists of metal collar, chain bag and pipe dredges to sample all fractions. The dredge was towed behind the vessel for 500 m to several km depending on seabed slope, extent of sediment outcrop and water depth.

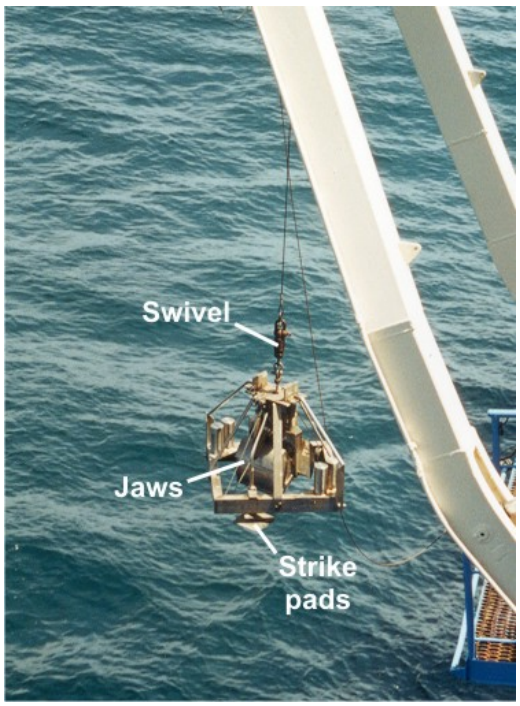

Figure 3.4. Grab sampler used on the survey. The grab collects about 0.1 m^3 of sediment in the jaws. The jaws are released when the strike pads hit the seabed releasing the trigger mechanism. The grab was deployed from the starboard A-frame.

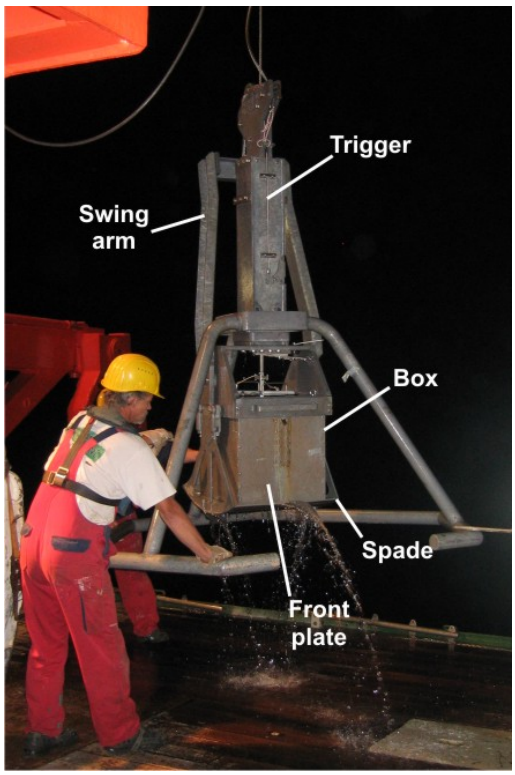

Figure 3.5. Box core used to sample unconsolidated seabed sediments. After the box has penetrated the seabed, the swing arm is triggered and seals the base of the box with the spade and the sample is returned to the surface. Upon retrieval, the front plate of the box was removed to reveal sedimentary structures in the upper 0.5 m of sediment.

Figure 3.6. Epibenthic sled used to sample seabed biota. The sled comprises a 1 m x 1 m x 0.5 m metal frame containing several mesh bags of varying mesh sizes that catch the biota. Two pipe dredges were also attached to the end of the sled to sample seabed sediments.

Table 3.2a. Leg 1 station operations for the DTIS towed-video transects where video footage and still images were collected.

Study Area	Stn	Camera	Start Lat.	Start Long.	Start Depth (m)	Duration	No. Stills	Seabed Characterisations (# p/camera)
Area A	01	CAM01	-28.2379	162.6293	1,310	00:57:31	104	*No characterisations made*
	02	CAM02	-28.2857	161.9415		00:46:00	^ 1	Post-survey characterisations
	03	-	-	-	-	-	-	-
	04	CAM03	-27.7650	161.4550	1,455	00:33:00	^ 0	Post-survey characterisations
	05	CAM04	-27.6778	161.6480	998	01:02:31	113	Post-survey characterisations
	06	-	-	-	-	-	-	-
	07	-	-	-	-	-	-	-
	08	CAM05	-27.3144	161.4339	1,546	01:00:04	183	Post-survey characterisations
	09	CAM06	-27.4639	161.6145	1,567	00:33:04	101	Post-survey characterisations
	10	CAM07	-27.4193	161.7093	1,543	01:00:31	184	Post-survey characterisations
	11	CAM08	-27.5180	161.3664	1,626	00:40:45	135	Post-survey characterisations
	12	CAM09	-27.1899	161.3064	1,650	01:02:00	191	Post-survey characterisations
	13	CAM10	-27.2016	161.5972	1,369	01:00:31	127	Post-survey characterisations
	14	CAM11	-27.0228	161.6668	1,386	00:40:31	126	Post-survey characterisations
	15	CAM12	-26.8546	161.3258	1,629	00:35:14	^ 0	Post-survey characterisations
	16	CAM13	-26.8528	161.5389	1,421	00:54:27	172	Post-survey characterisations
	17	CAM14	-25.1414	161.7347	977	00:59:58	185	Post-survey characterisations
	18	CAM15	-26.8194	161.7214	1,392	00:42:39	131	Post-survey characterisations
	19	CAM16	-26.3107	161.6950	1,380	01:02:29	191	Post-survey characterisations
	20	CAM17	-26.8084	161.7652	1,301	01:00:01	184	Post-survey characterisations
	21	CAM18	-26.5720	161.4801	1,427	00:50:00	153	Post-survey characterisations
	*(22)	(CAM19)	-26.3107	161.6950	1,296	05:47:00*	†20	*No sample, poor visibility*
	22	CAM20	-26.2904	161.6950	1,307	*05:48:00-	130	Post-survey characterisations
	23	CAM21	-26.5512	161.5996	1,368	00:44:48	166	Post-survey characterisations
	24	CAM22	-26.3771	161.4962	1,400	00:40:02	163	Post-survey characterisations
	25	CAM23	-26.2659	161.4194	1,483	00:40:02	163	Post-survey characterisations
	26	CAM24	-26.2886	161.3348	1,509	00:55:13	170	Post-survey characterisations
	27	CAM25	-26.0633	161.3642	1,446	01:00:10*	185*,	Post-survey characterisations
	*(27)	(CAM26)	-26.0644	161.3664	1,447			*Experimental camera with bait*

NB: *(#) = At stations 22 and 27 two transects were run. At station 22, CAM19 was abandoned due to turbid water that resulted in negligible visibility. As a result, a second transect, CAM20, was then selected and successfully surveyed. Both CAM19 and CAM20 were recorded on the same videotape. At station 27, CAM25 was successfully surveyed. However, as time permitted, a second experimental transect, CAM26, was run with a baited bag attached to the DTIS. ^ stills camera failed, † seabed is not visible.

The corer was deployed and retrieved over the starboard side of the vessel using a hydraulically powered cradle and the ship's main coring wire and winch. The corer was lowered to the seabed at 30 m min^{-1} to within 30 m of the seabed and then left to stabilise for up to 5 minutes. The corer was then lowered to the seabed whereby the piston was released to drive the core into the seabed. Recognition that the core had penetrated the seabed was determined by a sharp decrease in wire tension. The core was then brought to the surface at 40–45 m min^{-1}.

Once on board the ship, the polycarbonate liners were cut into 1 m-long sections, sealed with end caps (and packed with high-density foam biscuits where necessary), labelled, engraved, and stored up-right in a refrigerated container before being transported to Geoscience Australia for geophysical logging and sub-sampling for grain size distribution and carbonate content analysis (see below). All sample and sub-sample details were entered into the MARS database.

Select cores were recovered for geochemical analysis. Sub-samples of the cores were taken for head-space gas analysis and lipid biomarker extraction. Generally, two to three sub-samples were taken within each core at 1 m intervals down core for geochemical analysis. The depth of sub-samples varies between each core because sub-samples were

Table 3.2b. Tan0713 Leg 2 station operations for the DTIS towed camera-transects where video footage and still photographs were collected.

Study Area	Stn	Camera	Start Lat.	Start Long.	Start Depth	Duration	No. Stills	Seabed Characterisations (# p/camera)
Area A	28	-	-	-	-	-	-	-
	29	CAM27	-26.9382	161.0235	1,940	01:01:09	250	Real-time characterisations (145)
	30	CAM28	-26.6477	160.9963	1,566	01:01:32	264	Real-time characterisations (76)
	31	CAM29	-26.6588	161.0531	1,516	01:00:58	253	Real-time characterisations (60)
	32	CAM30	-26.6509	160.9023	1,327	01:01:32	248	Real-time characterisations (74)
	33	CAM31	-26.7250	159.4672	1,351	01:01:31	240	Real-time characterisations (87)
Area B	34	CAM32	-26.7263	159.4288	288	01:01:42	125	Real-time characterisations (86)
	35	CAM33	-26.7730	159.4520	286	01:01:32	252	Real-time characterisations (82)
	36	CAM34	-26.7947	159.4059	319	01:02:10	61	Real-time characterisations (130)
	37	CAM35	-26.8395	159.4036	414	01:01:36	251	Real-time characterisations (108)
	38	CAM36	-26.9382	161.0235	2,198	00:22:45	93	Real-time characterisations (25)
	39	-	-	-	-	-	-	-
	40	CAM37	-26.6635	159.3699	248	01:01:36	252	Real-time characterisations (77)
	41	-	-	-	-	-	-	-
Area A	42	CAM38	-27.4333	160.5386	2,104	01:01:48	^ 0	Real-time characterisations (73)
	43	CAM39	-27.4393	160.7154	2,078	01:01:55	34	Real-time characterisations (77)
	44	CAM40	-27.5174	160.6037	2,150	01:01:40	260	Real-time characterisations (86)
	45	CAM41	-27.1092	160.3990	2,025	01:02:12	252	Real-time characterisations (84)
	46	CAM42	-27.3199	160.3194	2,171	00:30:44	126	Real-time characterisations (31)

^ stills or video failed.

Table 3.3. Rock dredge (DR) locations, water depths and descriptions.

Study Area	Station	Sample	Start Latitude	Start Longitude	Start water Depth (m)	Sample description
Area A	01	DR01	-28.2385	162.6268	1,365	Nannofossil ooze/sand; pumice; manganese crust; rhyolite; basalt
	02	DR02	-28.2763	161.9491	1,590	Nannofossil ooze/sand; pumice; manganese crust
	05	DR03	-27.6794	161.6403	1,424	Basalt; pumice; breccia;
	06	DR04	-27.4136	161.7003	1,532	Nannofossil ooze/sand; basalt; manganese crust; pumice; scoria
	08	DR05	-27.3159	161.4257	1,622	Nannofossil ooze; pumice; manganese crust; iron oxides; concretions
	17	DR06	-26.8588	161.7367	1,354	Nannofossil ooze; basalt; scoria; volcaniclastic sandstone;
	19	DR07	-26.8840	161.7762	1,400	Nannofossil ooze/sand; basalt
	20	DR08	-26.8117	161.7774	1,335	Nannofossil ooze/sand; basalt; manganese crust
	30	DR09	-26.9374	161.0218	1,591	Nannofossil ooze/sand; manganese nodules; pumice
	32	DR10	-26.6660	161.0467	1,594	Nannofossil ooze/sand; basalt; pumice; manganese crust
	33	DR11	-26.6561	160.8974	1,632	Nannofossil ooze/sand; pumice; basalt; manganese crust
Area B	36	DR12	-26.7831	159.4575	638	Nannofossil ooze/sand; limestone; basalt; calcrete; manganese nodules
	40	DR13	-26.6677	159.3856	280	Nannofossil ooze/sand; calcrete

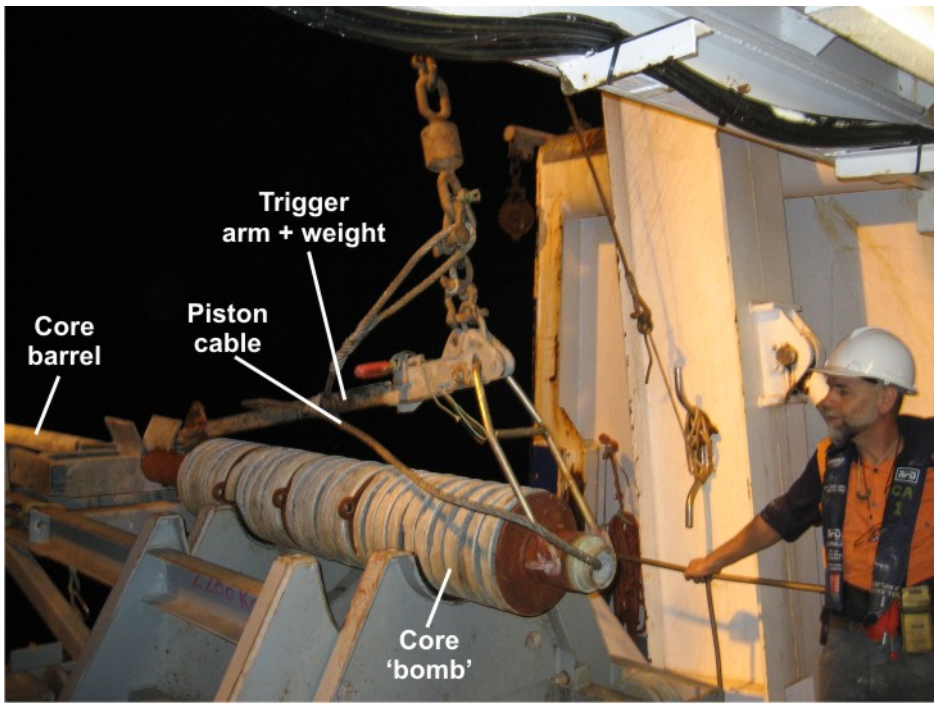

Figure 3.7. Piston corer used to sample shallow (<6 m) sub-surface seabed sediments. The corer was deployed using the starboard A-frame and comprises a 90 mm diameter, 6 m-long steel barrel connected at the top to a 1.5 tonne lead 'bomb'. An 84 mm diameter, 6 m long polycarbonate liner was used to recover the sediment inside the barrel and a core catcher was fitted to the base of the barrel to enhance core recovery.

collected from the base of each core. Sub-samples collected for pore space gas were transported frozen and analysed by TDI-Brooks, College Station, Texas, USA. Concentration data (ppm) was reported for C1-C5 hydrocarbons and CO_2 for one set of replicate tins. A second set of tins was retained at Geoscience Australia at -80° C to provide a back-up in case of shipping problems or sub-sample loss.

Table 3.4. Surface grab (GR) locations, water depths and descriptions.

Study Area	Station	Sample	Latitude	Longitude	Water Depth (m)	No. Sub-sample	Amount of Sample	Sub-sample	Sample description
Area A	25	GR01	-26.2647	161.4202	1,488	1	79 x 200 mm	Y	Sub-sample collected from a single PVC pipe
Area B	34	GR02	-26.7346	159.4662	293	1	79 x 200 mm	Y	Sub-sample collected from a single PVC pipe
	35	GR03	-26.7340	159.4279	289	1	79 x2 00 mm	Y	Sub-sample collected from a single PVC pipe

Table 3.5. Boxcore (BC) sample locations, water depths and descriptions.

Study Area	Station	Sample	Lat.	Long.	Water Depth (m)	Horizontal Sub-sample	Penetration Depth (m)	Vertical Sub-sample	Sample description
Area A	04	BC01	-26.2387	161.4664	1,455	½	0.18	All	*vertical sections combined*
	13	BC02	-27.2045	161.5910	1,360	½	0.38	All	*vertical sections combined*
	16	BC03	-26.8489	161.5479	1,492	½	0.10	Top (No btm)	negligible amount of sample returned
	18	BC04	-26.8171	161.7245	1,415	½	0.15	Top	sample displaced to side of boxcore
	21	BC05	-26.5721	161.4888	1,434	½	0.10	Top	sample displaced to side of boxcore
	23	BC06	-26.5475	161.6024	1,360	½	0.16	Top	
	24	BC07	-26.3727	161.5015	1,388	½	0.03	Top (No btm)	small amount of sample, displaced to side of boxcore
	26	BC08	-26.2889	161.3423	1,508	½	0.03	Top (No btm)	small amount of sample, displaced to side of boxcore
	27	BC09	-26.0660	161.3658	1,447	½	0.12	Top	
	29	BC10	-27.3448	160.8693	1,935	½	0.10	Top, Btm	
	30	BC11	-26.9393	161.0258	1,573	¼	0.05	Top (No btm)	small amount of sample, displaced to side of boxcore
	31	BC12	-26.6501	160.9957	1,518	¼	0.18	Top, Btm	
Area B	38	BC13	-26.8439	159.4153	2,423	¼	0.35	Top, Btm	
	39	BC14	-26.8413	159.4608	2,183	¼	0.30	Top, Btm	
	41	BC15	-26.5527	159.4122	2,040	¼	0.40	Top, Btm	

NB: ½ of the 0.50 m^3 boxcore (i.e. 0.25 m x 0.50 m x depth); ¼ of the 0.50 m^3 boxcore (i.e. 0.25 m x 0.25 m x depth); All = vertical sections combined; Top = surface sediments (≤0.05 m sediment depth); Btm = bottom sediments (>0.05 m sediment depth); (No btm) = no bottom sediments were retrieved (i.e., penetration depth was ≤0.05 m).

Table 3.6. Benthic sled (BS) locations, water depths and descriptions.

Study Area	Station	Sample	Start Lat.	Start Long.	Start water Depth (m)	Sample description
Area A	07	BS01	-27.4592	161.6113	1,570	Coral fragments
	11	BS02	-27.5167	161.3819	1,572	Nannofossil ooze; igneous rock fragments
	14	BS03	-27.0247	161.6652	1,385	Calcareous nannofossil ooze
	15	BS04	-26.8546	161.3332	1,624	Calcareous nannofossil ooze; pumice and igneous rock fragments
	22	BS05	-26.3045	161.7019	1,300	Igneous rock fragments; manganese nodules
	33	BS06	-26.6550	160.8983	1,474	Nannofossil ooze; few benthic organisms
Area B	34	BS07	-26.7338	159.4662	290	Nannofossil ooze; calcarenite; pumice
	35	BS08	-26.7355	159.4271	290	Nannofossil ooze; carbonate sand; calcarenite
	37	BS09	-26.8051	159.2003	902	Nannofossil ooze; carbonate sand; basalt rock fragments
	40	BS10	-26.6446	159.3767	253	Nannofossil ooze; carbonate sand; calcrete
	42	BS11	-27.4323	160.5376	2,110	Nannofossil ooze; pumice; manganese crust

Table 3.7.Piston core (PC) water depths and descriptions.

Study Area	Station	Sample	Lat.	Long.	Water Depth (m)	Sample description
Area A	04	PC01	-27.7639	161.4580	1,481	3.60 m; A
	12	PC02	-27.1959	161.3047	1,628	4.20 m; A
	18	PC03	-26.8174	161.7246	1,414	3.00 m; A
	22	PC04	-26.3042	161.7033	1,309	2.90 m; A
	26	PC05	-26.2895	161.3415	1,506	2.90 m; B
	29	PC06	-27.3456	160.8687	1,936	3.30 m; A
	42	PC07	-27.4282	160.5372	2,104	3.70 m; A
		PC08	-27.4302	160.5394	2,117	3.20 m; A
	43	PC09	-27.4368	160.7007	2,063	3.20 m; A
		PC10	-27.4352	160.7083	2,055	3.65 m; A
	44	PC11	-27.5162	160.6009	2,161	3.00 m; A
	45	PC12	-27.1078	160.4023	2,022	2.30 m; B
		PC13	-27.1080	160.4007	2,022	2.85 m; A
	46	PC14	-27.3186	160.3136	2,194	3.35 m; A

A = Geochemistry core; sections kept for sedimentology. B = Stratigraphic core; whole core kept for sedimentology.

4. Oceanography

Oceanographic measurements were obtained from a fixed seabed mooring deployed on the Lord Howe Island shelf for a period of six months, as well as both underway measurements and sample station measurements obtained from shipboard instruments in study area B over the Capel and Faust basins.

4.1. LORD HOWE ISLAND SHELF – MOORING

4.1.1. Mooring Description

An RD Instruments Workhorse Sentinel 600 kHz acoustic Doppler current profiler (ADCP; Serial No. 5581) was deployed on the northern side of Lord Howe Island (Fig. 1.2). The ADCP mooring (Fig. 4.1) consisted of a triangular frame supporting both the ADCP and an acoustic release, a 100 m ground line (sinkable rope) to a bottom weight, and a 90 m line (floatable rope) to a second bottom weight to enable grappling for the mooring if the acoustic release failed. The mooring was located in approximately 59 m water depth at -31° 24.000'S 159° 04.870'E. The mooring was deployed at 05:30 hrs on 28/10/2007 (GMT) and retrieved at 11:25 hrs on 26/04/2008 (GMT). On retrieval the benthic frame and instrument were reported to be heavily encrusted with bio-fouling. A van Essen conductivity-temperature-depth (CTD) probe was also attached to the mooring.

The ADCP measures the 3-dimensional current vector from the Doppler shift of sound reflected from the water column using two pairs of orthogonal acoustic beams. ADCP Serial No. 5581 contains the following feature upgrades: Mode 5, 8, and 11 high resolution modes; high ping rate mode 12; and the waves array upgrade. The instrument was programmed to obtain profiles of current velocity extending from 1.86 m above the instrument to the water surface with measurements (sample bin elevations) spaced 0.75 m apart. A total of 15 pings were averaged over 900 s to provide current velocity time series with a sampling interval of 15 minutes for each bin elevation. The instrument was not programmed to measure waves for this deployment. The instrument functioned continuously throughout the deployment, returning 6 months of current velocity data for sample bins 1 to 30 (approximately 3 to 25 m above the bed), as well as near-bed water temperature and water depth. Current velocity data from sample bins higher in the water column were adversely affected by declining acoustic penetration over the deployment period and have been excluded from analysis.

The van Essen CTD probe returned reliable records of temperature and pressure (depth), but the conductivity record displayed non-linear drift over the deployment period and thus salinity could not be calculated. The temperature and pressure records closely match those from the ADCP and so they will not be discussed separately.

4.1.2. Meteorology

Atmospheric pressure and wind speed for the deployment period, measured at the Bureau of Meteorology's Lord Howe Island meteorological station (Station 200839), are shown in Figure 4.2. The measured variations in atmospheric pressure were accounted for when converting the measured bottom water pressure to water depth. The maximum and minimum atmospheric pressure recorded over the deployment period were 995 and 1025.1 hPa, respectively. The maximum recorded wind speed was 15.83 m s^{-1}.

Figure 4.1. Benthic frame showing acoustic release system (front) and ADCP (rear).

4.1.3. Tidal Water Levels

The time series of water level relative to mean sea level obtained by the ADCP is shown in Figure 4.2. A classical harmonic analysis of this time series was performed to determine the amplitudes and phases of the tidal constituents. The method used followed Pawlowicz *et al*. (2002), which is based on a method initially proposed by Foreman (1977) and includes nodal corrections. Using this method a total of 45 astronomical and 101 shallow-water constituents can be resolved, depending on the record length. The 6 months of data available from the ADCP deployment yielded the amplitudes and phases of 35 tidal constituents, which are listed in Table 4.1 along with their 95% confidence limits. These harmonic constituents only account for 83.2% of the water level variation at the deployment site, indicating that significant non-tidal variation in sea level occurred.

The tide can be classified according to the ratio of key diurnal to semi-diurnal tidal constituents. This is represented by the form factor F (e.g. Pugh, 2004)

$$F = \frac{a_{K1} + a_{O1}}{a_{M2} + a_{S2}} \tag{4.1}$$

where a is amplitude and the subscript denotes the relevant constituent. The amplitudes listed in Table 4.1 indicate a value for F of 0.2827, which is indicative of a mixed, mainly semi-diurnal tide. The mean spring tidal range was calculated to be 1.547 m and the mean neap range was 0.806 m.

4.1.4. Currents

The current magnitude and direction for sampling bins located between 3 and 25 m above the seabed are shown Figure 4.3. The gap in the current record is due to a continuous period of erroneous data, possibly due to a movement of the mooring and/or the gimbal-mount for the ADCP that resulted in the ADCP not looking directly upwards. A time-varying current speed due to the tide was frequently measured at the deployment site. The current direction did not always reverse, however, due to other non-tidal currents that were also active. The generation of near-bed shear in the current profile is clearly evident in the magnitude record,

Table 4.1. Listing of the amplitudes, phases and errors of the harmonic tide constituents resolved from the available 178.22 day record. The errors are for a 95 % confidence interval. The Greenwich phase was computed with nodal corrections.

Tide constitu-ents	Frequency (cycles hr^{-1})	Amplitude (m)	Amplitude error	Phase (degrees)	Phase error	Signal-to-noise ratio
MM	0.001512	0.0461	0.086	154.73	104.28	0.29
MSF	0.002822	0.0225	0.065	339.24	186.11	0.12
ALP1	0.034397	0.0008	0.0070	186.76	236.15	0.013
2Q1	0.035706	0.0038	0.008	229.26	128.04	0.23
Q1	0.037219	0.0139	0.010	289.80	39.08	2
O1	0.038731	0.0747	0.010	310.22	7.65	57
NO1	0.040269	0.0050	0.009	308.21	104.97	0.34
K1	0.041781	0.1440	0.01	342.53	3.98	2.00E+02
J1	0.043293	0.0107	0.009	3.17	54.54	1.5
OO1	0.044831	0.0057	0.006	44.27	68.11	0.95
UPS1	0.046343	0.0009	0.004	90.40	215.58	0.04
EPS2	0.076177	0.0046	0.015	266.19	177.67	0.1
MU2	0.07769	0.0174	0.016	280.14	66.29	1.1
N2	0.078999	0.1192	0.019	278.98	8.56	40
M2	0.080511	0.5883	0.019	290.34	1.89	9.70E+02
L2	0.082024	0.0170	0.014	260.79	53.28	1.4
S2	0.083333	0.1853	0.017	310.71	5.55	1.20E+02
ETA2	0.085074	0.0026	0.010	342.67	183.91	0.073
MO3	0.119242	0.0003	0.001	300.81	184.01	0.13
M3	0.120767	0.0044	0.002	228.15	22.42	7.9
MK3	0.122292	0.0033	0.001	61.23	25.17	5.9
SK3	0.125114	0.0018	0.001	132.40	45.61	2
MN4	0.159511	0.0021	0.002	57.95	48.95	1.3
M4	0.161023	0.0008	0.001	334.91	132.33	0.36
SN4	0.162333	0.0008	0.001	124.83	104.08	0.32
MS4	0.163845	0.0012	0.002	50.17	80.32	0.57
S4	0.166667	0.0012	0.002	29.94	78.35	0.6
2MK5	0.202804	0.0011	0.001	302.08	67.32	0.84
2SK5	0.208447	0.0005	0.001	138.77	123.83	0.31
2MN6	0.240022	0.0005	0.001	230.69	165.66	0.098
M6	0.241534	0.0012	0.002	282.51	93.87	0.6
2MS6	0.244356	0.0013	0.002	315.19	65.20	0.73
2SM6	0.247178	0.0008	0.001	2.62	117.08	0.32
3MK7	0.283315	0.0004	0.001	133.88	146.24	0.16
M8	0.322046	0.0005	0.001	228.71	145.28	0.23

and appears to be greatest at times of largest current speed, which is expected (Fig. 4.3; top panel). At other times there is also evidence for internal shear generated higher in the water column by water masses flowing in different directions (Fig. 4.3; bottom panel).

Time series of the current magnitude and the east, north, and vertical components of current velocity are shown in Figures 4.4 and 4.5 for two elevations, 3 m and 25 m above the bed, respectively. Mean and root-mean-square near-bed (3 m above the bed) current speeds were 0.19 and 0.14 m s^{-1}, respectively. With respect to extremes, the near-bed current speeds

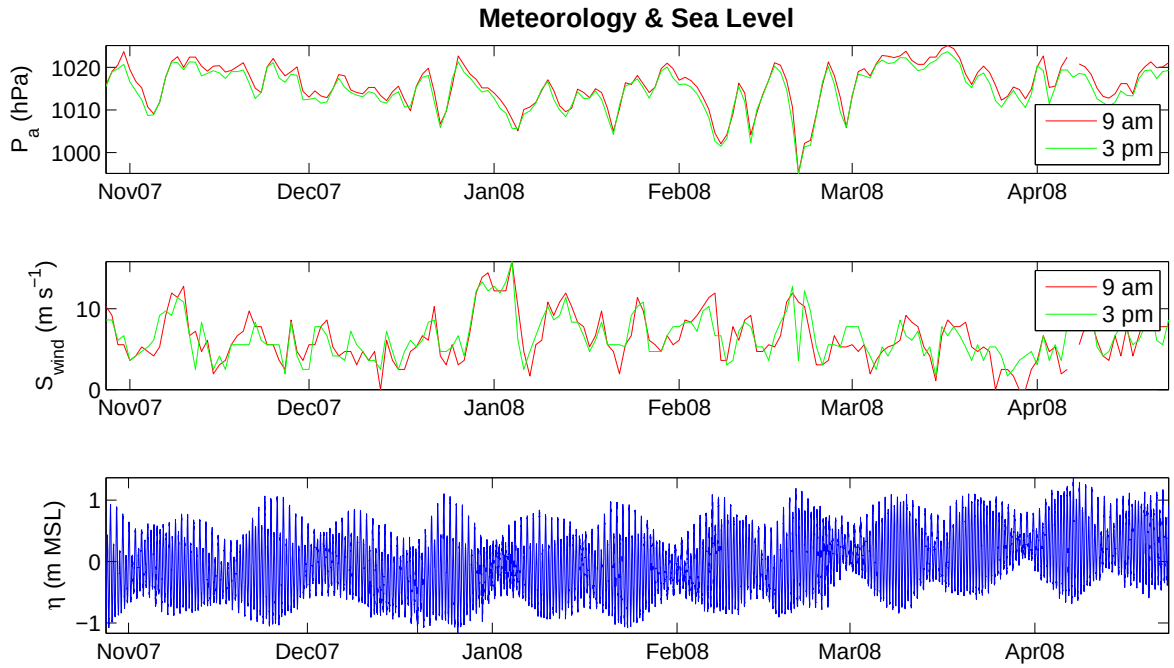

Figure 4.2. Time series of atmospheric pressure (P_a), wind speed (S_{wind}), and sea level (η) relative to mean sea level (MSL) measured over the deployment period. P_a and S_{wind} were provided by the Commonwealth Bureau of Meteorology.

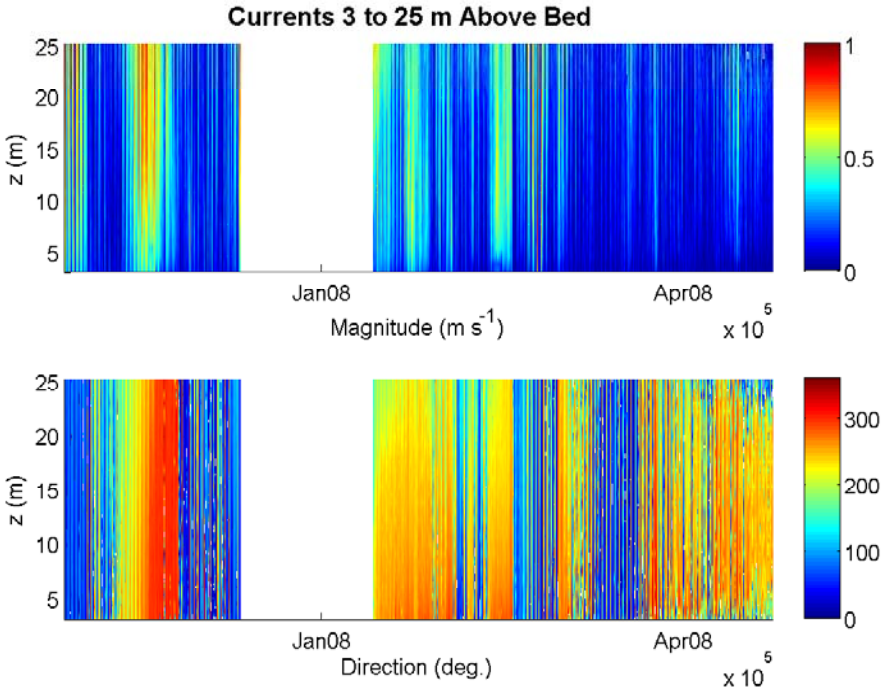

Figure 4.3. Contour plots of current magnitude and direction between 3 and 25 m above the seabed.

exceeded 0.40 m s^{-1} for 10% of the time and 0.65 m s^{-1} for 1% of the time. The maximum near-bed current speed was 0.93 m s^{-1}.

The flood and ebb of the tidal current is roughly directed to the west and east, respectively, in the absence of other current activity. This is consistent with the deployment site being located on the southern limb of a clockwise-rotating amphidrome centred further to the north or alternatively on the northern limb of an anticlockwise-rotating amphidrome

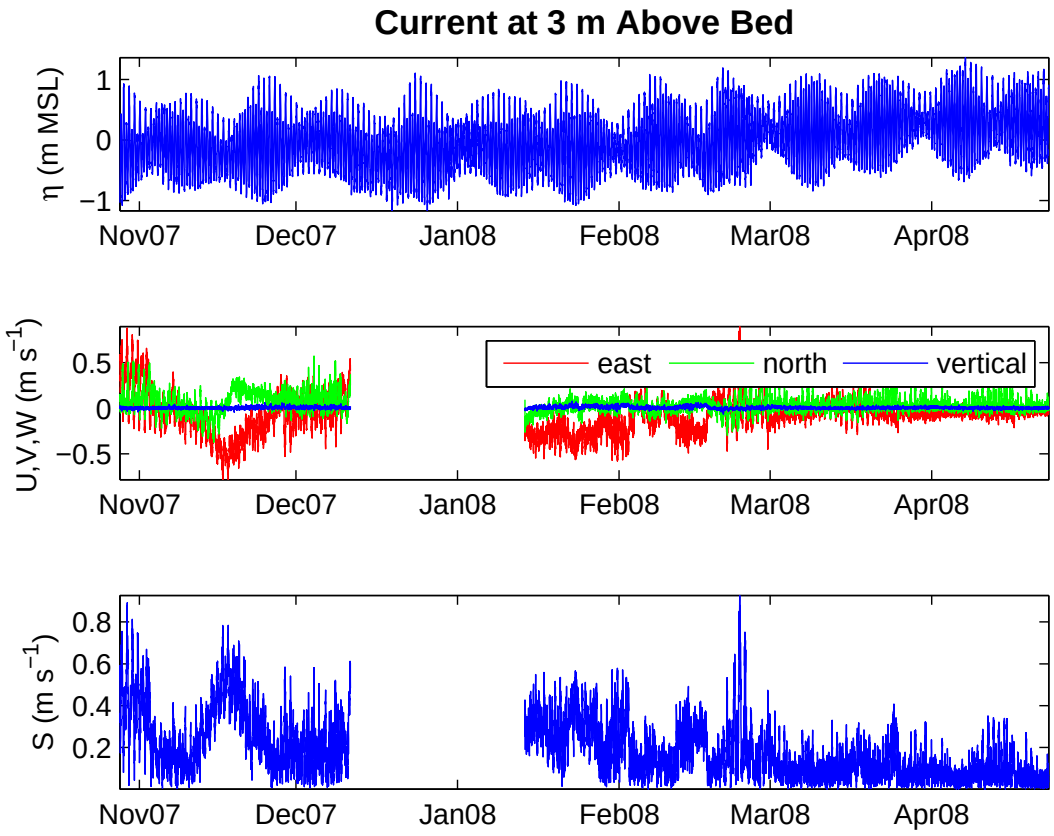

Figure 4.4. Time series of sea level (η); east, north and vertical components of the current vector, (U, V, W); and current magnitude (S) measured at 3 m above the seabed.

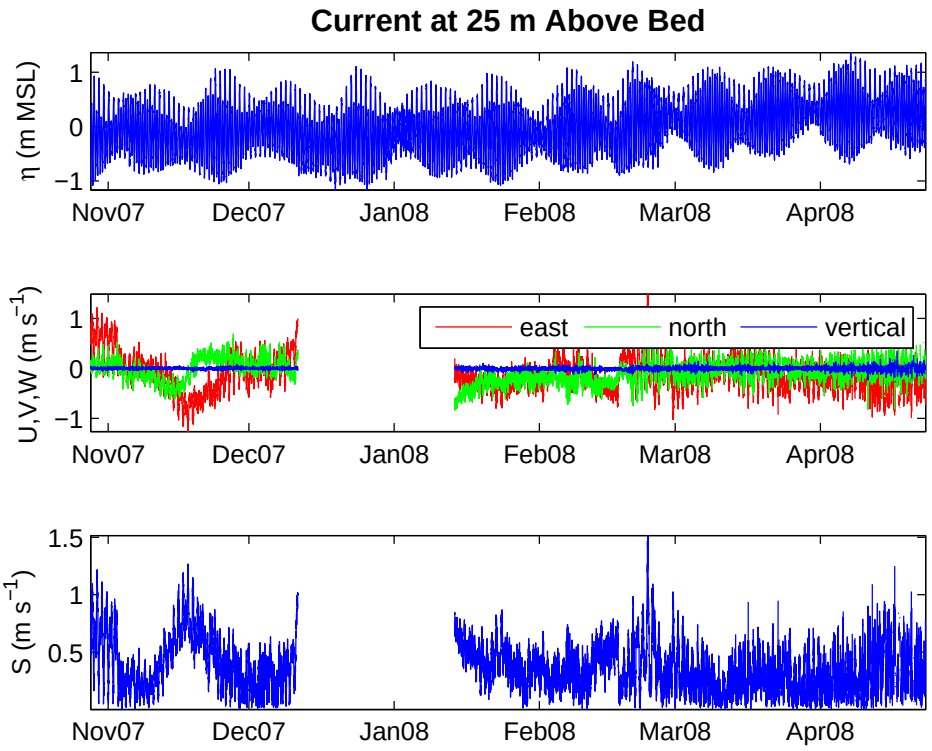

Figure 4.5. Time series of sea level (η); east, north and vertical components of the current vector, (U, V, W); and current magnitude (S) measured at 25 m above the seabed.

centred further to the south. Walters *et al*. (2001) used a barotropic tidal model driven by TOPEX/Poseidon altimetry data to demonstrate ocean tides around New Zealand, and their results show anticlockwise rotating M2 and S2 amphidromes centred on New Zealand (located to the south of Lord Howe Island). The phase difference between water level and velocity at the deployment site varied between 0° and 90°.

Contoured histograms of the east and north components of the current vector as well as rose plots of current direction show that the measured currents were predominantly directed to the western quadrants (Fig. 4.6). This is due to a quasi-steady westward directed-current apparently present to varying degree from mid-November to late-February, although, the situation from mid-December to mid-January is unknown. The directional spread of the current is considerably larger at 25 m above the seabed than it is near the bed (Fig. 4.6). Progressive vector plots for two elevations, 3 m and 25 m above the bed, both show overall displacement of water to the western quadrants, consistent with the combined effect of flooding tidal currents and a superimposed quasi-steady current. The total near-bed displacement is about 1200 km to the northwest, whereas the displacement higher in the water column is about 1600 km to the southwest (Fig. 4.6). Note that these values are for 5 months, not 6 months, due to the loss of data from mid December to mid January.

The east and north components of the current velocity vector were low-pass filtered in order to remove the tidal variation and highlight non-tidal currents. A simple zero-phase, 15-day, moving-average filter was used. The current magnitude and direction for 3 m and 25 m above the bed were then calculated from the low-pass filtered vector components and these are shown in Figure 4.7. The non-tidal currents can at times be related to regional-scale geostrophic circulation, specifically, eddies shed from the East Australian current. Figure 4.8 shows selected satellite-derived sea surface temperature images with inferred geostrophic currents superimposed. The image for the 27th October 2007 shows an easterly-directed geostrophic current at the deployment site immediately to the north of Lord Howe Island (Fig. 4.8), which is consistent with the measured current direction at the beginning of the deployment (Fig. 4.7). Similarly, the 27th January 2008 image shows a westerly-directed geostrophic current, which is consistent with that measured at the deployment site (Fig. 4.7). During March 2008 the ADCP measured very weak non-tidal currents (<0.1 m s^{-1}; Fig. 4.7), which is again consistent with the satellite-derived data during this period (e.g. 6th April 2008; Fig. 4.8). The measured non-tidal currents were not always consistent with the inferred regional currents however. For example, the satellite-derived data for the 29th November 2007 suggests a weak easterly-directed geostrophic current, but the ADCP measured a weak north-westerly-directed current that was possibly wind-driven.

4.1.5. Non-tidal Water Levels

It was mentioned previously that the predicted tide, based on 6 months of data, only accounted for 83 % of the sea level variation measured at the deployment site (Section 4.2.3). The residual sea level, after removing the predicted tidal variation, is plotted in Figure 4.9 together with the atmospheric pressure and seabed (59 m depth) temperature records. From mid-December to the end of April there is a steady rise in the mean sea level at the deployment site, which is unrelated to atmospheric pressure (since the measured sea level was corrected for atmospheric effects). The rise in mean sea level over this period does correspond with a rise in water temperature and suggests that a warm core eddy and associated positive sea level anomaly passed over the deployment site. This is confirmed by satellite altimetry data.

The 24th November 2007 and 1st December 2007 satellite images show a switch from a

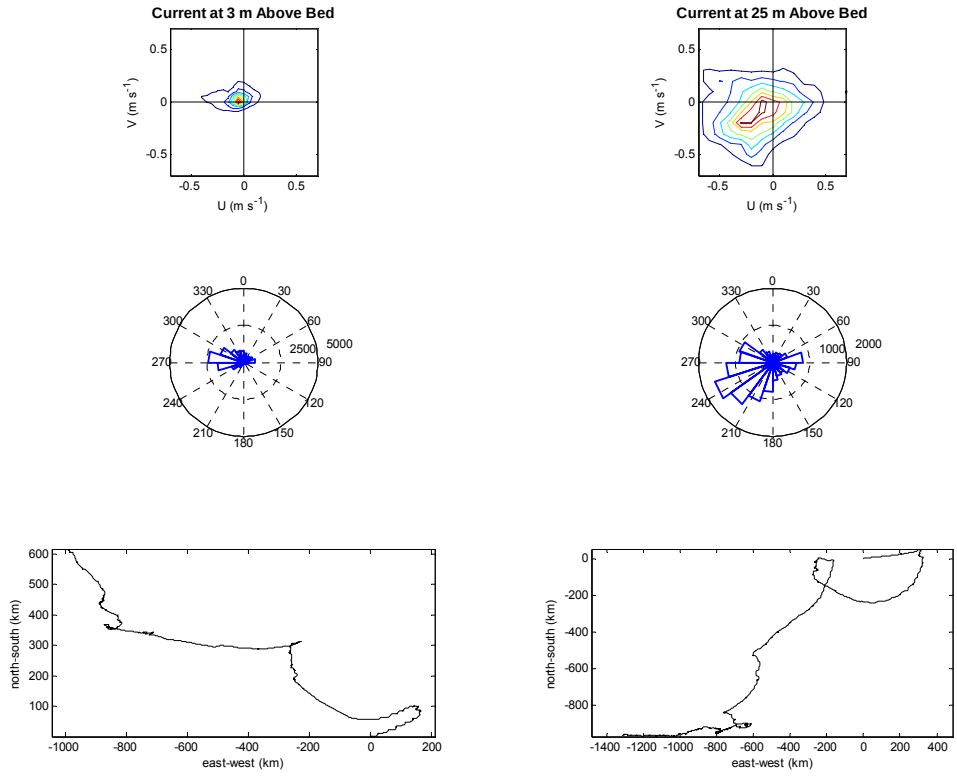

Figure 4.6. Histograms of the east and north (U and V) components of the measured current vectors at 3 m and 25 m above the seabed (top panel). Rose plots of the current direction (middle panel). Progressive vector plots (bottom panel).

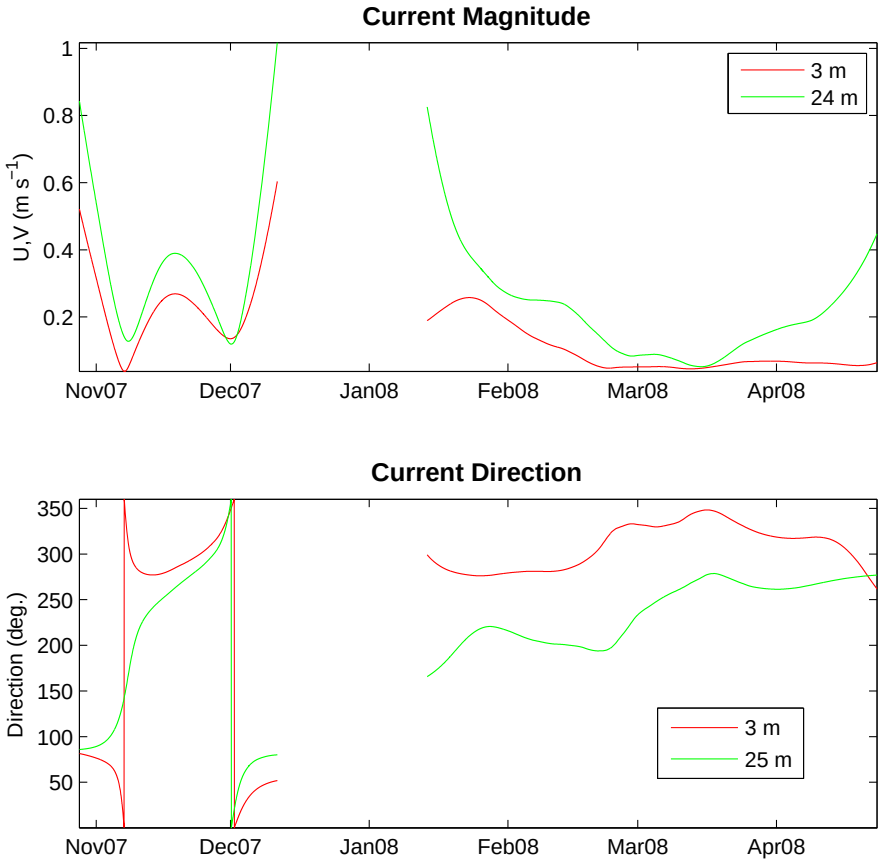

Figure 4.7. Time series of low-pass filtered current magnitude and direction measured at 3 m and 25 m above the seabed.

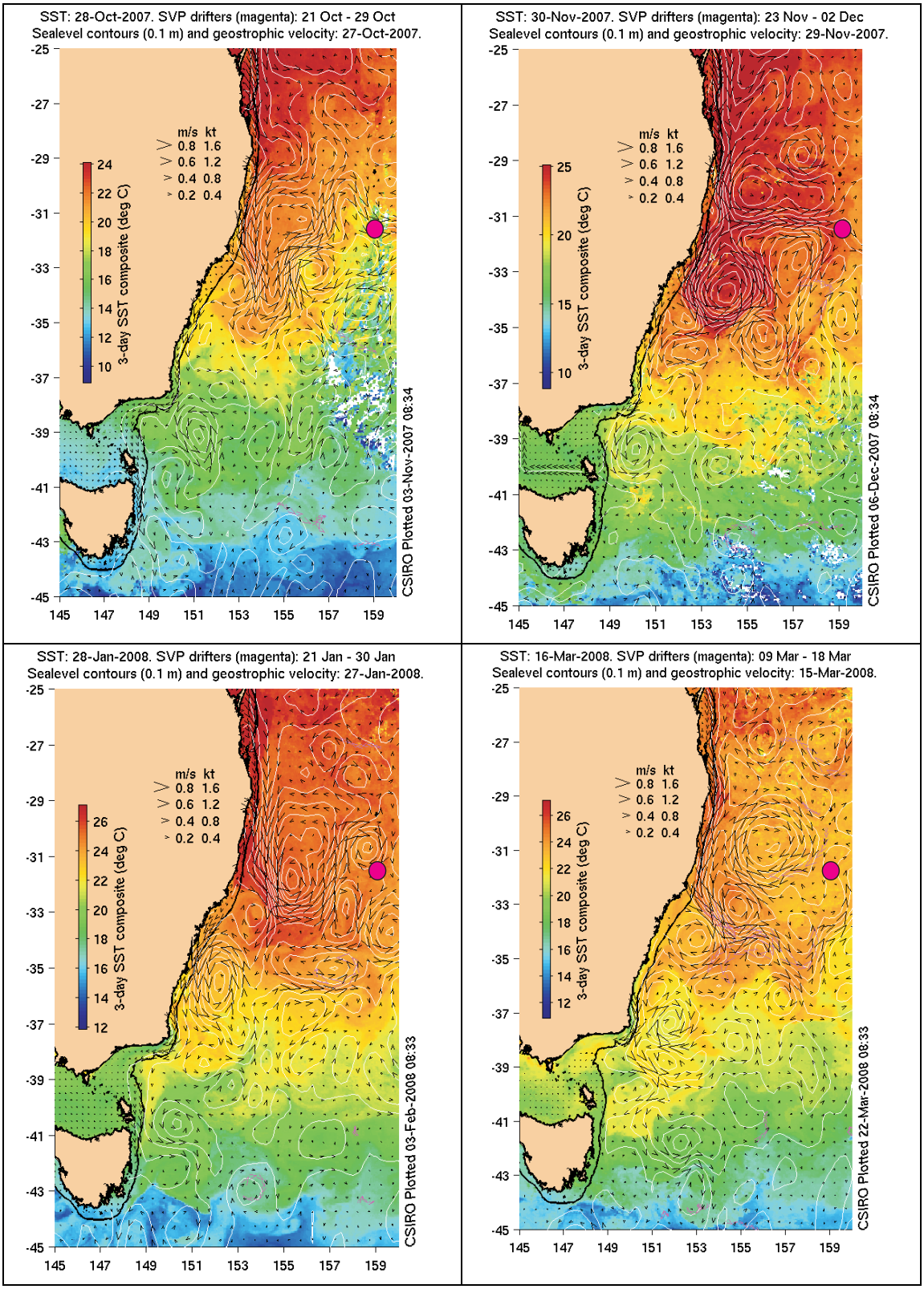

Figure 4.8. Satellite-derived sea surface temperature images with super-imposed (inferred) geostrophic circulation. The position of Lord Howe Island is marked with a magenta circle. Images provided by CSIRO Marine and Atmospheric Research.

negative to a near-zero anomaly at the deployment site, immediately to the north of Lord Howe Island (Fig. 4.10), which is consistent with the residual sea level record shown in Figure 4.9. Similarly, the 27th March 2008 and 22nd April 2008 images show a positive sea level anomaly that corresponds to the positive residual sea level recorded at the deployment site (Fig. 4.9).

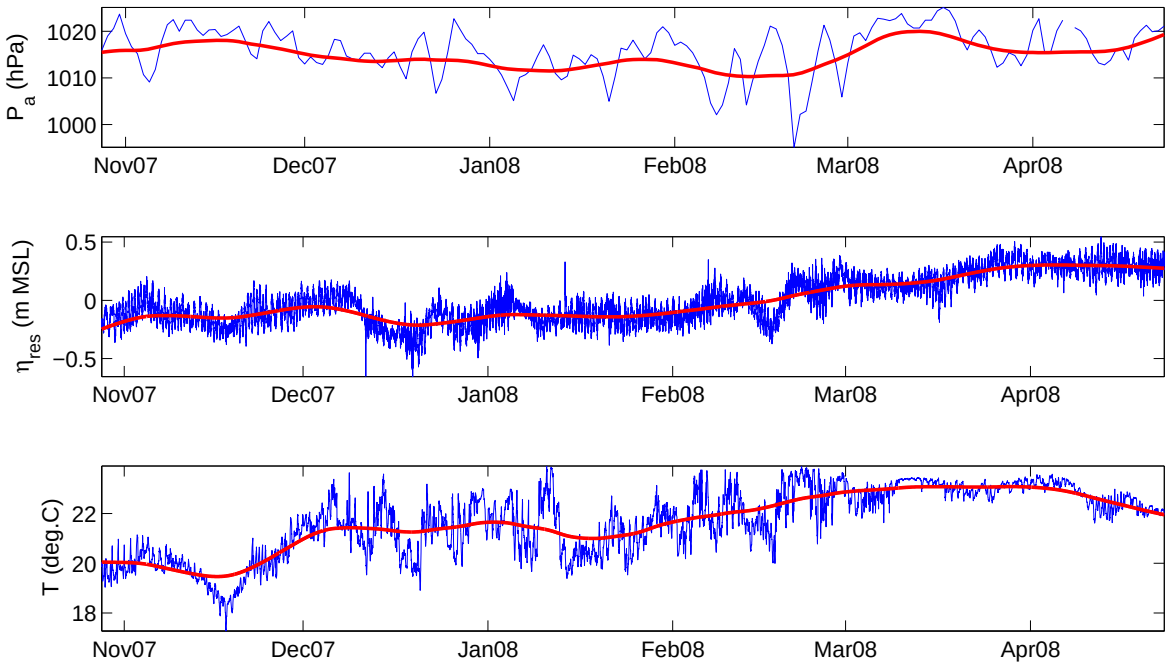

Figure 4.9. Time series of atmospheric pressure (P_a), residual sea level (η_{res}), and seabed temperature (T) at the deployment site. The red line is the low-pass filtered record.

4.2. UNDERWAY / STATION DATA

A summary of the oceanographic data acquired during the survey is given in Table 4.2. It shows what types of measurements were carried out at given locations. The surface current data recorded from the shipboard ADCP cover the whole period of the survey (between 7/10/2007 and 22/11/2007) from Wellington (New Zealand) and back, with most of the data being concentrated on the study area. CTD data were acquired at seven locations between 12/10/2008 and 08/10/2008, with the most distant casts about 3.4° (~350 km) apart, in water depths ranging from 1,320 m to 2,250 m. Water samples were acquired at each of the CTD locations.

4.2.1. Shipboard Equipment

An RD Instruments 150 kHz downward-facing ADCP that is permanently hull-mounted on the RV *Tangaroa* was used to acquire current profiles in the ocean's upper layer, down to about 250 m, with measurements (sample bin elevations) spaced 8.33 m apart. A Seabird™ SBE911 CTD was deployed at seven different stations to measure profiles of pressure, temperature, conductivity, oxygen, fluorescence and turbidity. Data were recorded during both the descent and ascent of the instrument. The CTD frame also included a SBE 32 Carousel water sampler fitted with 24 external-spring Niskin-type water sampling bottles of 10 litres each (Fig. 4.11). Samples were taken throughout the water column at each of the CTD sites.

4.2.2. Data Processing and Analysis

The current time series data were processed with the RDI software, in order to subtract the navigation speed. At the time of writing, the current measurements from the shipboard ADCP had not been fully analysed. The pressure record was converted to water depth using the UNESCO formula by Perkin and Lewis (1980). The standard ocean depth formula is:

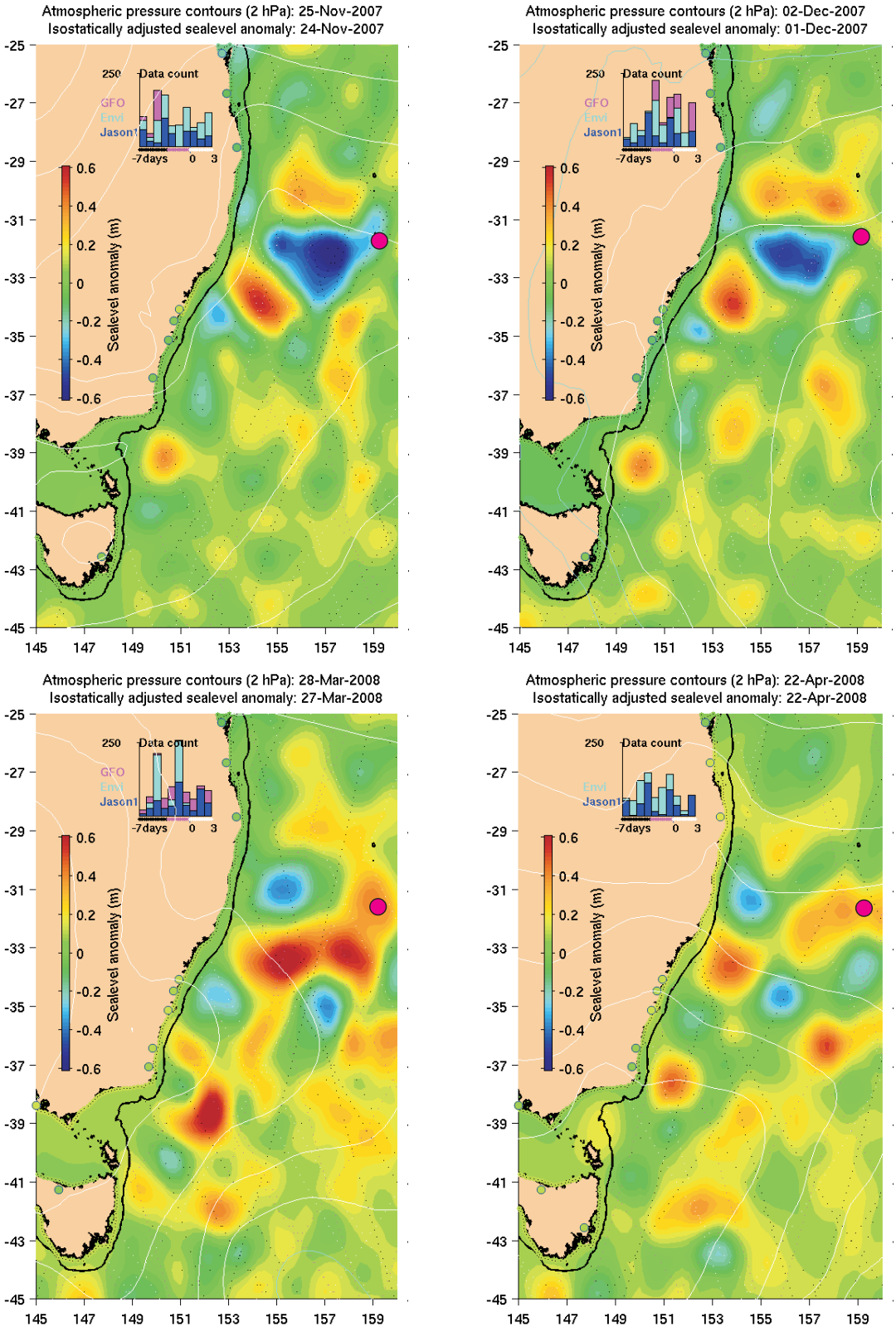

Figure 4.10. Satellite-derived sea surface elevation anomaly. The position of Lord Howe Island is marked with a magenta circle. Images provided by CSIRO Marine and Atmospheric Research.

$$z(S_0, T_0, \theta, P[db]) = \frac{9.72659\ P - 2.2512e^{-5}\ P^2 + 2.279e^{-10}\ P^3 - 1.82e^{-15}\ P^4}{9.780318\ (1 + 5.2788e^{-3}\ \sin^2\theta + 2.36e^{-5}\ \sin^4\theta) + 1.092e^{-6}\ P} \qquad (4.2)$$

Figure 4.11. Photograph of CTD rosette deployed from starboard A-frame. Niskin bottles were attached to the rosette to collect water samples from the water column.

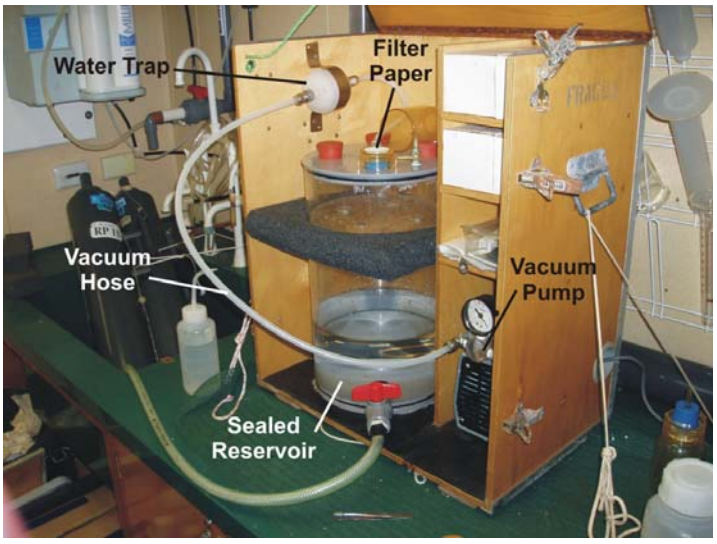

Figure 4.12. Photograph showing Geoscience Australia's purpose-built water filtering system. A total of 1 litre of seawater is filtered through 45 μm mesh filters. The filter papers are then weighed in the laboratory to determine total suspended solids (sediments).

The standard ocean depth is given in meters [m] and derived using a water density profile at a salinity S_0 = 35[PSU], a temperature T_0 = 0 [° C], a latitude θ and a compressibility correction of second order. The data acquired at seven distinct stations have been plotted against the standard ocean depth on one graph per variable to enable a spatial comparison between stations. Each profile displays some "noise" due to the superposition of the data from the downward and upward acquisition.

One litre of water was filtered through pre-weighed 0.45 μm glass filter papers using a vacuum system on board the vessel (Fig. 4.12). The filters were then stored in a dry freezer, and oven dried at 60° C and re-weighed to ±0.0001 g upon return to the laboratory to obtain the concentration of suspended sediments.

Table 4.2. Summary of the underway and station data acquisition.

	CTD Cast	01CTD1	03CTD2	11CTD3	22CTD4	29CTD5	31CTD6	39CTD7	Ship board
	Date	12/10/2007	12/10/2007	18/10/2007	24/10/2007	03/11/2007	04/11/2007	08/11/2007	07/11/2007 -
	Time (UTC)	15:45	23:05	13:20	18:54	15:39	16:06	16:53	19/11/2007
CTD instrument	Temperature (°C)	Y	Y	Y	y	Y	Y	y	N
CTD instrument	Conductivity (S m^{-1})	Y	Y	Y	Y	Y	Y	Y	N
CTD instrument	Pressure (bar)	Y	Y	Y	Y	Y	Y	Y	N
CTD instrument	Fluorescence (volts)*	Y	Y	Y	Y	Y	Y	Y	N
CTD instrument	Turbidity (FTU)	Y	Y	Y	Y	Y	Y	Y	N
CTD instrument	Potential Temperature (^{o}C)**	Y	Y	Y	Y	Y	Y	Y	N
CTD instrument	Salinity (PSU)	Y	Y	Y	Y	Y	Y	Y	N
CTD instrument	Oxygen Concentration (µmol kg^{-1})	Y	Y	Y	Y	Y	Y	Y	N
CTD instrument	Water sample	Y	Y	Y	Y	Y	y	Y	N
ADCP	Current (m s^{-1})	N	N	N	N	N	N	N	Sub-surface current #

(*) The fluorescence is commonly related to the Chlorophyll-a concentration by a power law (i.e., Chlo-a ~ 10^{Fluo}).

(**) *Potential temperature* is defined as the temperature of a parcel of water at the sea surface after it has been raised adiabatically from some depth in the ocean, i.e. to remove the influence of compressibility from measurements of the *in situ* temperature.

(#) Corrupted record. Data discarded.

Table 4.3. Summary details of CTD casts collected on the survey.

Study Area	Station	Sample	Lat.	Long.	Start water Depth (m)	No. of water samples
Area A	01	CTD01	-28.2278	162.6396	1,320	2
	03	CTD02	-26.9100	161.7332	1,376	2
	11	CTD03	-27.5162	161.3760	1,584	2
	22	CTD04	-26.3113	161.6912	1,304	6
	29	CTD05	-27.3494	161.8568	1,932	10
	31	CTD06	-26.6661	161.9853	1,515	9
Area B	39	CTD07	-26.8408	159.4626	2,245	10

4.2.3. Results

4.2.3.1. Shipboard ADCP

As a result of poor data quality, the data from the shipboard ADCP are not presented.

4.2.3.2. CTD Profiler

A total of seven CTD casts were completed during the survey, ranging in water depths from 1,304 m to 2,245 m (Table 4.3). Six of the casts were collected in study area A, over the Capel and Faust basins, and one cast in deep water in study area B over Gifford Guyot. Water samples were collected for suspended sediments during each of the casts.

Temperature and Potential Temperature:— The seven local temperature profiles show similar trends (Fig. 4.13a). From a high around 22° C at the surface, the temperature decreases to around 18° C at about 400 m. It then rapidly decreases to around 6° C at about 800 m before slowly decreasing again to around 2° C at about 2,250 m depth. The maximum deviation of temperature between locations at a similar depth is less than 3° C. Cast 39CTD7 and 01CTD01 display the smoothest temperature profile across the whole water column. Casts 31CTD06, 11CTD03 and 03CTD02 display a slow change in temperature at about 200 m water depth. Cast 29CTD04 shows a slow change in temperature in the upper 100 m water depth and a sharp drop in temperature at about 100 m. The potential temperature behaves in a very similar fashion to the local temperature (Fig. 4.13b. The effect of pressure on temperature accounts for less than 10% of the variation in the profile (Fig. 4.13c).

Conductivity:— The conductivity profiles behave in a very similar fashion to the local temperature profiles (Fig. 4.14). From a high of 5 S m^{-1} at the surface conductivity slowly decreases to 4.5 S m^{-1} at 400 m. It then rapidly decreases to 3.5 S m^{-1} at 800 m before slowly decreasing again to 3.2 S m^{-1} at 2,300 m depth.

Salinity:— The seven salinity profiles display the typical inverted "S" shape (Fig. 4.15; Pickard and Emery, 1982). In the subsurface layer, the salinity sharply increases from about 35.2 PSU at the surface to 35.7 PSU at about 10 m. Between around 10 m and 200 m, all but one salinity profile are fairly stable, while cast 01CTD01 shows a steady linear decline from a about 35.7 PSU in the subsurface layer to about 35.5 at 300 m. Between around 200 m (300 m for cast 01CTD01) and 800 m, salinity rapidly decreases to its minimum of about 34.3 PSU where it stabilises before slowly increasing again from 1,000 m onward.

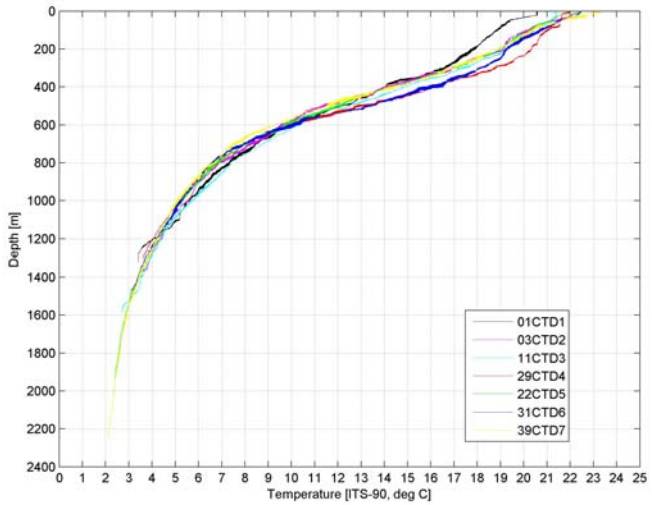

(a)

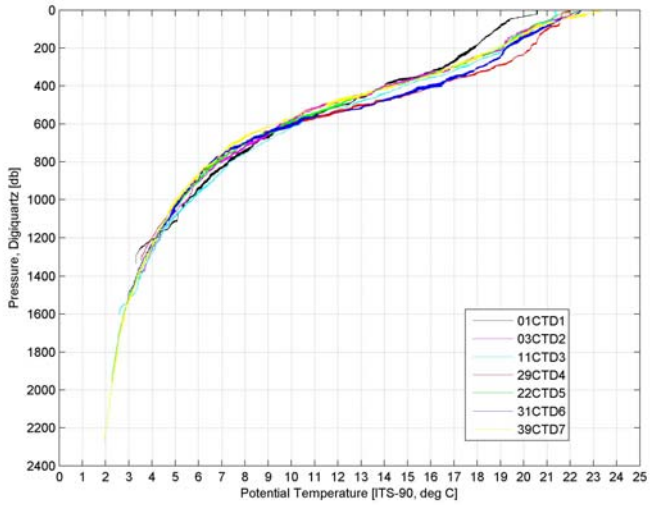

(b)

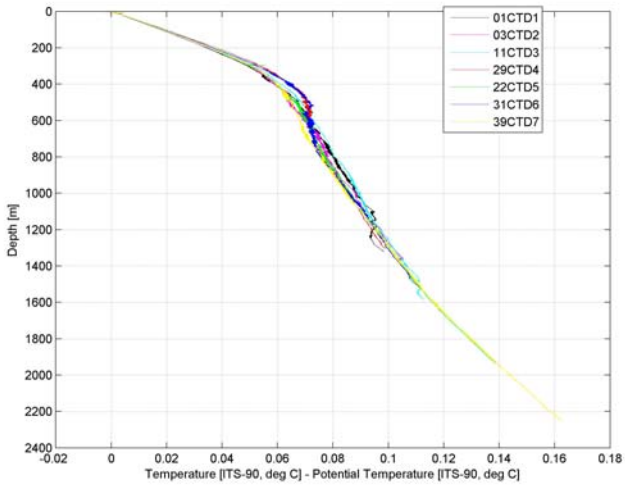

(c)

Figure 4.13. Temperature profiles: (a) local temperature, (b) potential temperature, and (c) difference between local temperature and potential temperature.

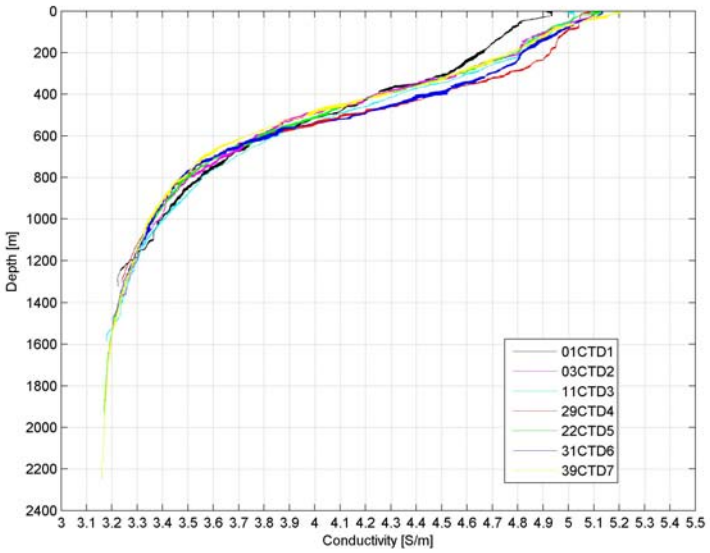

Figure 4.14. Conductivity profiles.

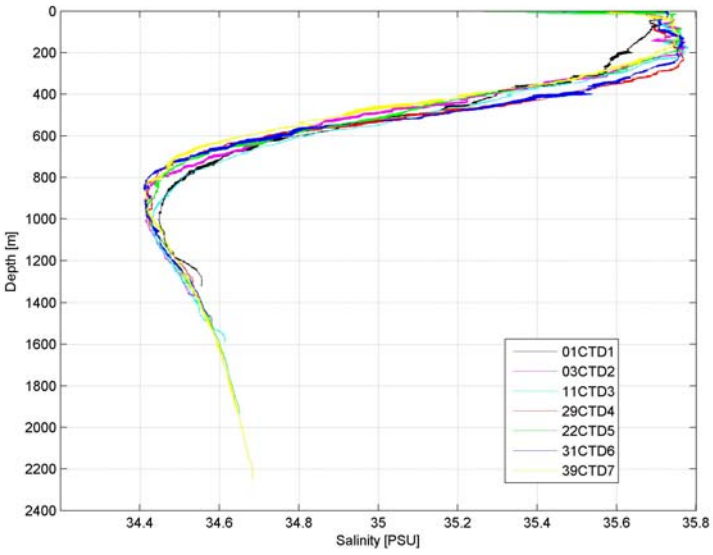

Figure 4.15. Salinity profiles.

Oxygen concentration:— The seven oxygen concentration profiles follow broadly the same trend, although some variability between the casts appears in the top 600 m (Fig. 4.16). The oxygen concentration sharply increases in the subsurface layer, peaking around 50 m at about 205 μmol kg^{-1}. From around 50 m to 400 m (200 m for cast 01CTD01), the oxygen concentration rapidly deceases to reach an intermediate minimum of about 170 μmol kg^{-1} before increasing again to about 185 μmol kg^{-1} at about 800 m (500 m for cast 01CTD01). From around 800 m to 1,600 m, the oxygen concentration rapidly deceases to reach a secondary minimum of about 125 μmol kg^{-1}, before increasing slowly again to 140 μmol kg^{-1} at about 2,250 m.

Turbidity:— The seven turbidity profiles display a similar trend (Fig. 4.17). The turbidity rapidly increases in the subsurface layer, peaking at 50 m before rapidly decreasing to its minimum at 200 m. Despite some local spikes along the profile, the majority of

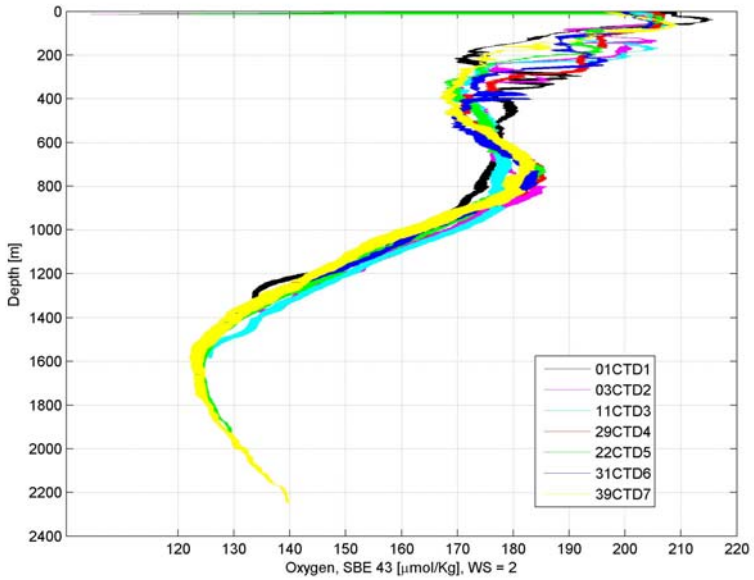

Figure 4.16. Oxygen concentration profiles.

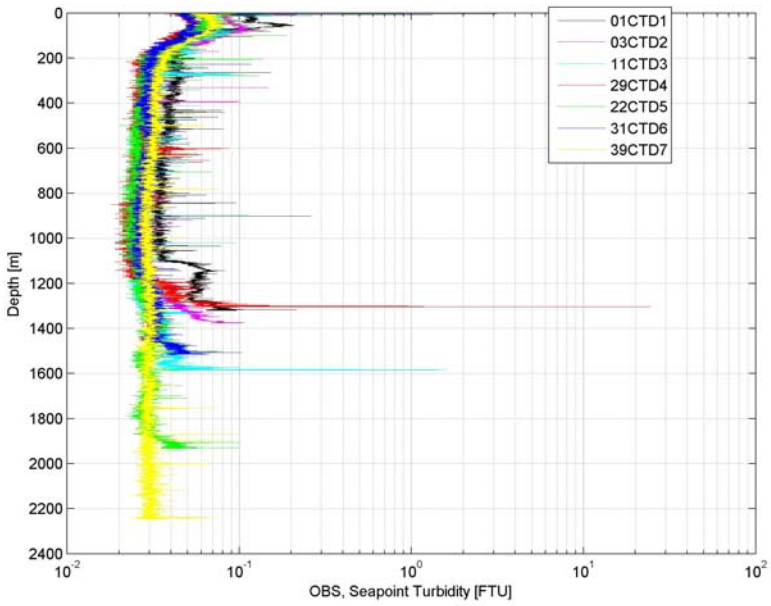

Figure 4.17. Turbidity profiles.

measurements show that the turbidity remains very low throughout most of the water column. In the bottom layer, 200 m from the seafloor, turbidity increases to levels comparable to the subsurface peak value. Cast 01CTD01 displays a turbidity increase sharper than the other stations, with the presence of a plateau of elevated turbidity.

Fluorescence:— The seven local fluorescence profiles show similar trends (Fig. 4.18). The fluorescence sharply increases from the surface to about 100 m (50 m for cast 01CTD01), before dropping sharply to its lowest level at about 200 m (100 m for cast 01CTD01). Fluorescence remains very low throughout the rest of the water column, albeit with a small increase with depth. Spikes along the profile are attributed to external noise during the acquisition, with no significant physical meaning.

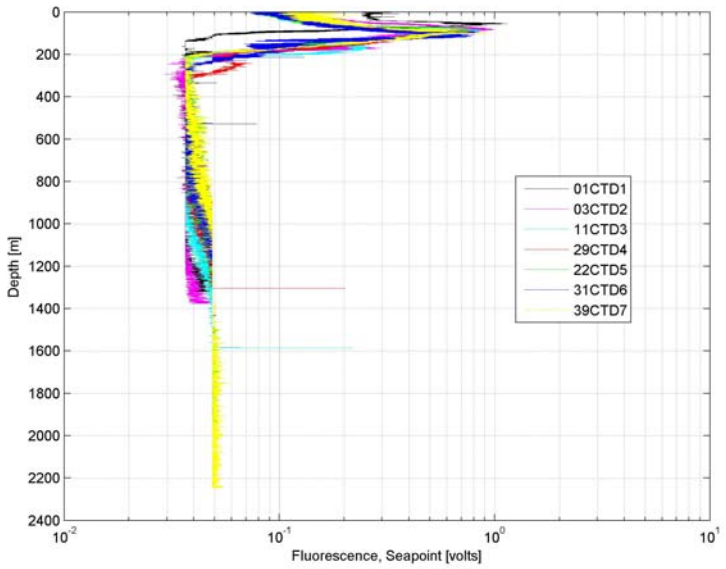

Figure 4.18: Fluorescence profiles.

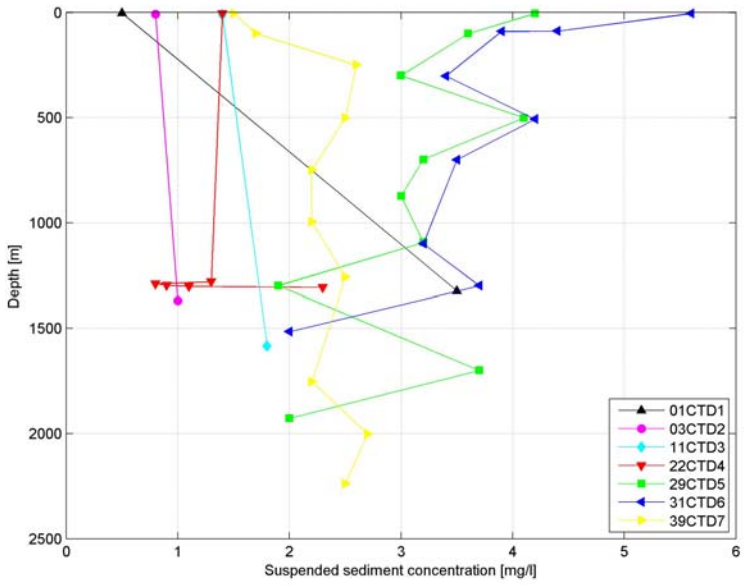

Figure 4.19. Suspended sediment concentrations.

4.2.3.3. Water Samples

The seven local suspended sediment concentration profiles show similar trends, with a fairly uniform distribution throughout the water column (Fig. 4.19; Table 4.4). Stations 29CTD05, 31CTD06 and 39CTD07 show the highest suspended sediment concentrations, ranging from 2 mg l^{-1} to 5.5 mg l^{-1}, with an average of 3 mg l^{-1}. Stations 03CTD02, 11CTD03 and 22CTD04 show the least suspended sediment concentration, ranging from 1 mg l^{-1} to 2.5 mg l^{-1}, with an average of 1.5 mg l^{-1}. Station 01CTD01 shows the widest spread of values, ranging from 0.5 mg l^{-1} at the surface to 3.5 mg l^{-1} near the bed. It should be noted that the suspended sediment concentration profiles at these latter four stations are only based on surface and bottom samples; trends and patterns throughout the water column are not captured at these sites.

Table 4.4. Summary information of the water samples collected from the CTD casts.

Study Area	Station	CTD Cast	Sample Id.	Pre-survey mass (g)	Post-survey mass (g)	Suspended sediment (g)	Water depth (m)
Area A	01	CTD01	V1383_3_Top	0.1171	0.1176	0.0005	3
			V1384_1324_Bot	0.1162	0.1197	0.0035	1324
			V1385_blank	0.1177	0.1179	0.0002	-
	03	CTD02	V1386_8_Top	0.1172	0.1180	0.0008	8
			V1387_1368_Bot	0.1159	0.1169	0.0010	1368
			V1388_Blank	0.1149	0.1153	0.0004	-
	11	CTD03	V1389_9	0.1175	0.1189	0.0014	9
			V1390_1583	0.1160	0.1178	0.0018	1583
			V1391_blank	0.1164	0.1166	0.0002	-
	22	CTD04	V1392_1302	0.1171	0.1182	0.0011	1302
			V1393_1307	0.1144	0.1167	0.0023	1307
			V1394_1297	0.1156	0.1165	0.0009	1297
			V1395_1290	0.1169	0.1177	0.0008	1290
			V1396_1279	0.1167	0.1180	0.0013	1279
			V1397_5	0.1176	0.1190	0.0014	5
			V1398_blank	0.1166	0.1174	0.0008	-
	29	CTD05	V1407_100	0.1165	0.1201	0.0036	100
			V1402_1093	0.1158	0.1190	0.0032	1093
			V1401_1298	0.1172	0.1191	0.0019	1298
			V1400_1699	0.1167	0.1204	0.0037	1699
			V1399_1927	0.1172	0.1192	0.0020	1927
			V1406_299	0.1179	0.1209	0.0030	299
			V1508_4	0.1156	0.1198	0.0042	4
			V1405_501	0.1168	0.1209	0.0041	501
			V1404_699	0.1177	0.1209	0.0032	699
			V1403_872	0.1166	0.1196	0.0030	872
			V1509_Blank	0.1157	0.1167	0.0010	-
	31	CTD06	V1512_1100	0.1163	0.1195	0.0032	1100
			V1510_1299	0.1169	0.1206	0.0037	1299
			V1511_1515	0.1176	0.1196	0.0020	1515
			V1515_302	0.1153	0.1187	0.0034	302
			V1518_4	0.1161	0.1217	0.0056	4
			V1513_507	0.1172	0.1214	0.0042	507
			V1514_700	0.1175	0.1210	0.0035	700
			V1516_88	0.1166	0.1210	0.0044	88
			V1517_89	0.1147	0.1186	0.0039	89
			V1519_Blank	0.1160	0.1160	0.0000	-
Area B	39	CTD07	V1528_100	0.1159	0.1176	0.0017	100
			V1523_1257	0.1157	0.1182	0.0025	1257
			V1522_1753	0.1169	0.1191	0.0022	1753
			V1521_2002	0.1164	0.1191	0.0027	2002
			V1520_2239	0.1151	0.1176	0.0025	2239

Study Area	Station	CTD Cast	Sample Id.	Pre-survey mass (g)	Post-survey mass (g)	Suspended sediment (g)	Water depth (m)
			V1527_250	0.1146	0.1172	0.0026	250
			V1529_4	0.1175	0.1190	0.0015	4
			V1526_501	0.1186	0.1211	0.0025	501
			V1525_749	0.1158	0.1180	0.0022	749
			V1524_996	0.1159	0.1181	0.0022	996
			V1530_Blank	0.1154	0.1161	0.0007	-

4.3. SUMMARY

Six months of data from an oceanographic mooring deployed on the outer shelf of Lord Howe Island indicate that the shelf is influenced by both tidal and non-tidal currents. Peak near-bed tidal currents are of the order 0.3–0.4 m s^{-1}, whereas non-tidal currents can exceed 0.6 m s^{-1} near the bed. It appears that the tidal currents are related to a progressive Kelvin wave propagating anticlockwise around an amphidrome that is centred to the south of Lord Howe Island. The non-tidal near-bed currents appear to be related to eddies shed from the East Australian Current (EAC), and possibly locally generated, wind-driven currents. One mechanism for generating EAC eddies at this latitude is the propagation of Rossby waves from east to west along the Tasman Front (Nilsson & Cresswell, 1981). EAC eddy activity on the Lord Howe Island shelf may therefore be seasonal, and restricted to periods when the Tasman Front is suitably located. Swell and locally generated wind waves will also influence the Lord Howe Island shelf, but are beyond the scope of this report.

The seven CTD casts display similar trends, reflecting the fairly uniform nature of the ocean properties within the 350 km radius sampled area over about a period of one month. Cast 39CTD07 would qualify as the smoothest median profile among all the casts, while cast 01CTD01 displays the most significant deviation from this median profile. Among the various water properties measured, the oxygen concentration displays the most variable vertical profile between the seven casts, with most of the variability concentrated in the upper water column above 500 m.

5. Geomorphology

This chapter describes the seabed geomorphology of the study areas. Geomorphic mapping is based on a 50 m horizontal resolution grid derived from the multi-beam (swath) sonar data. Definition and classification of seabed geomorphic features is based on those of the International Hydrographic Organisation (IHO, 2001) (Table 5.1).

5.1. AREA A: LORD HOWE RISE – MARGINAL PLATEAU

5.1.1. General Characteristics

The seabed across the survey area is characterised by a trend of increasing water depth toward the southwest (Fig. 5.1). Thus, across a distance of approximately 250 km the average water depth increases from ~1,300 m in the northeast sector (-26° 18'S, 155° 39'E) to 2,600 m in the southwest (-27° 50'S, 154° 13'E), equating to a gradient of approximately 0.3°. Within this area, large scale geomorphic features are broadly oriented north-south, tending to a northwest-southeast alignment across the western third of the survey area. Overall, the relief is subdued. Where local bathymetric anomalies occur (e.g., peaks, valleys and scarps) they introduce tens to hundreds of metres of vertical relief.

5.1.2. Large-scale Features

The geomorphology of the survey area is mapped using two categories of geomorphic feature, large scale and small scale (Fig. 5.2). Large scale geomorphic features are those that have length and width dimensions of tens of kilometres and include plains, ridges, valleys and basins.

5.1.2.1. Plains

Low gradient plains cover 9,835 km^2 of the survey area in water depths ranging from 1,700 m to 2,200 m (Fig. 5.3; Table 5.2). The most extensive plain occupies 8,365 km^2 in the southwest sector of the mapped area. Here the seabed slopes to the southwest at approximately 0.2° between 1,900 m and 2,100 m water depth, with maximum relief of 20 m over 1 km. The central north sector is also occupied by low relief plains, but here they are smaller in area (<600 km^2) and part of a more complex geomorphology that includes valleys, ridges and peaks. The boundaries between plains and ridges are gradual and typically extend several kilometres across a gently steepening surface. In contrast, where a plain borders a scarp or valley headwall the boundary is sharp.

5.1.2.2. Ridges

Ridges are the most extensive geomorphic feature in the survey area, covering 12,725 km^2 (Fig. 5.3; Table 5.2). The largest ridge in the survey area is located to the east of longitude 160.8°E, covers 9,795 km^2 and extends approximately 150 km north to south (Fig. 5.4). The ridge widens from 30 km at its southern end, to 55 km at the northern boundary of the survey area. The longitudinal profile of the ridgeline maintains a bathymetric range of 1,300 m to 1,450 m, with an overall slope of 0.03° to the south. Locally, holes and broad depressions introduce topographic variability of 50–100 m to the ridge crest across distances of 10–60 km (Fig. 5.4). In contrast, the western flank to the ridge has a relatively smooth surface with a slope of ~1° that grades onto the adjacent plain. The southern boundary of the ridge is defined by a south-facing slope that descends to a valley at 1,600 m water depth on a gradient of ~0.5°. This valley separates the ridge from another, partially-mapped, ridge that

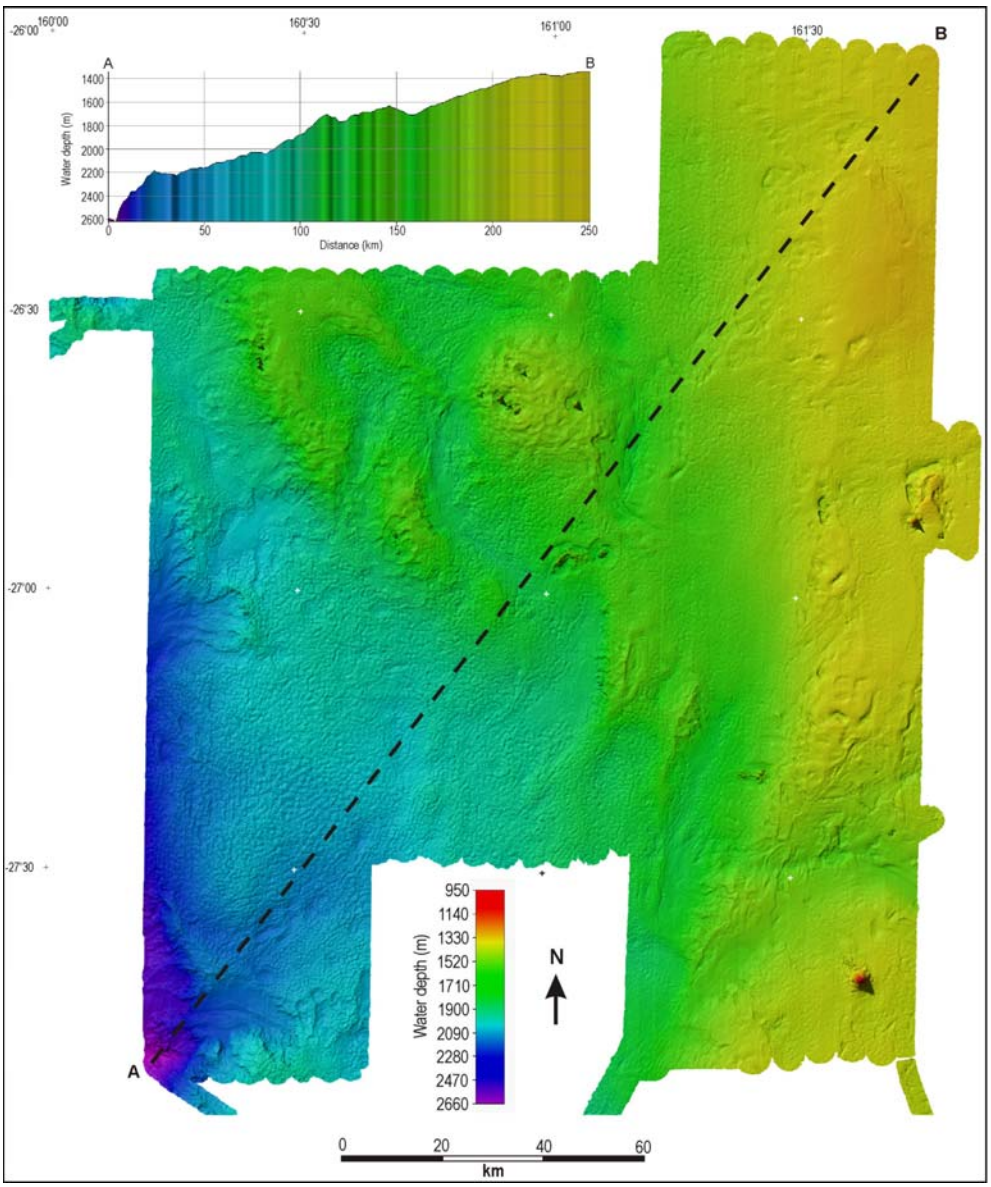

Figure 5.1. Multi-beam (swath) sonar bathymetric map and cross-section of study area A over the Capel and Faust basins, showing increased water depth to the southwest.

Table 5.1. Definitions for large-scale geomorphic features mapped in the survey area, as specified by the International Hydrographic Organisation (2001).

Geomorphic feature	Definition
Basin	A depression in the sea floor, more or less equi-dimensional in plan and of variable extent.
Escarpment (scarp)	An elongated, characteristically linear, steep slope separating horizontal or gently sloping sectors of the sea floor in non-shelf areas.
Hole	A small local depression, often steep sided, in the sea floor.
Moat	An annular depression that may not be continuous, located at the base of many seamounts, oceanic islands and other isolated elevations.
Peak	A prominent elevation either pointed or of a very limited extent across the summit.
Ridge	An elongated narrow elevation of varying complexity having steep sides.
Seamount	A discrete large isolated elevation, greater than 1,000 m in relief above the sea floor, characteristically of conical form.
Valley	A relatively shallow, wide depression, the bottom of which usually has a continuous gradient.

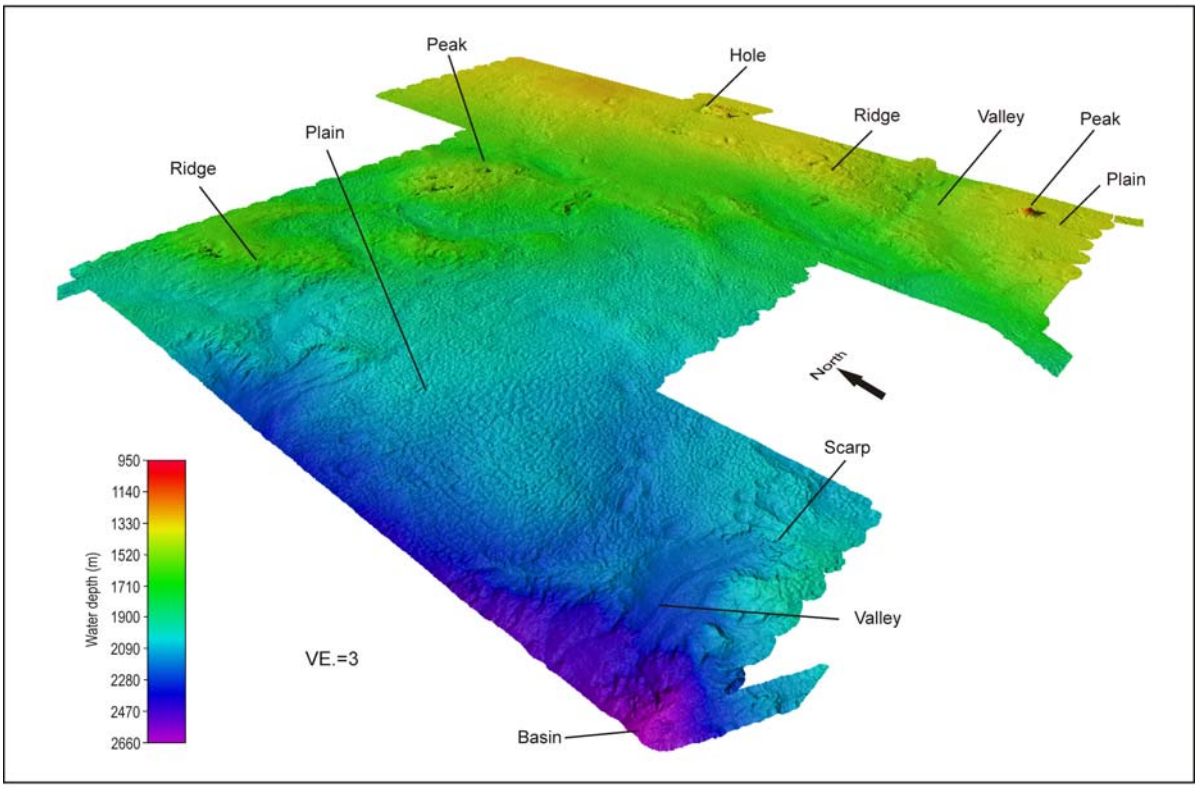

Figure 5.2. Perspective view of study area A over the Capel and Faust basins looking to the northeast, with examples of large-scale geomorphic features indicated.

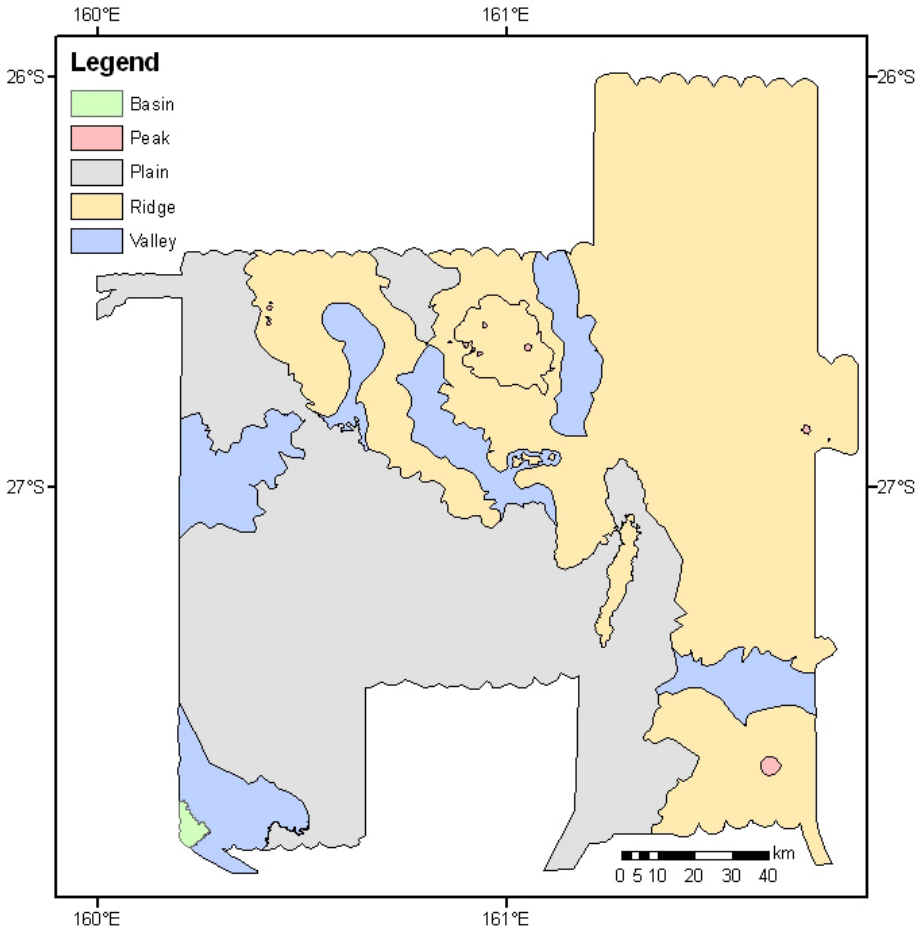

Figure 5.3. Map of large-scale geomorphic features in study area A over the Capel and Faust basins.

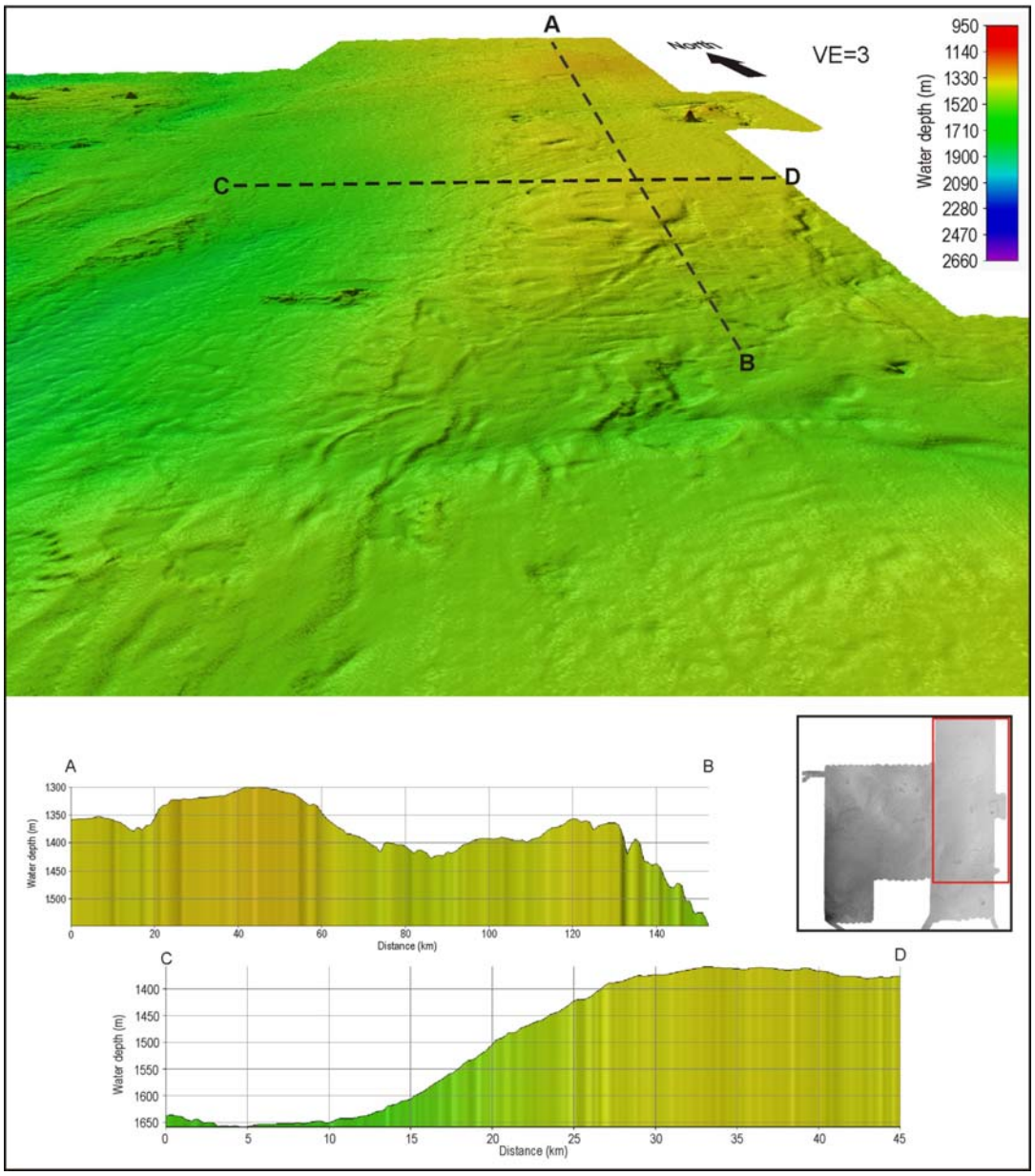

Figure 5.4. Perspective view of the ridge along the eastern boundary of study area A over the Capel and Faust basins, looking north. Bathymetric profiles A-B and C-D show representative longitudinal- and cross-sections. Inset map shows location shown in larger map.

Table 5.2. Surface area and slope gradients (range) for large-scale geomorphic features in Area A. (Note: Gradients were measured along representative cross-sections oriented perpendicular to contour lines).

Geomorphic feature	Surface area (km^2)	Surface area (%)	Slope gradient (°)
Plain	9,835	38.5	0.02–0.30
Ridge	12,725	49.8	0.01–1.20
Valley	2,900	11.4	0.70–2.00
Peak	30	0.1	5.00–30.00
Basin	50	0.2	2.30–3.00
Total	25,540	100	-

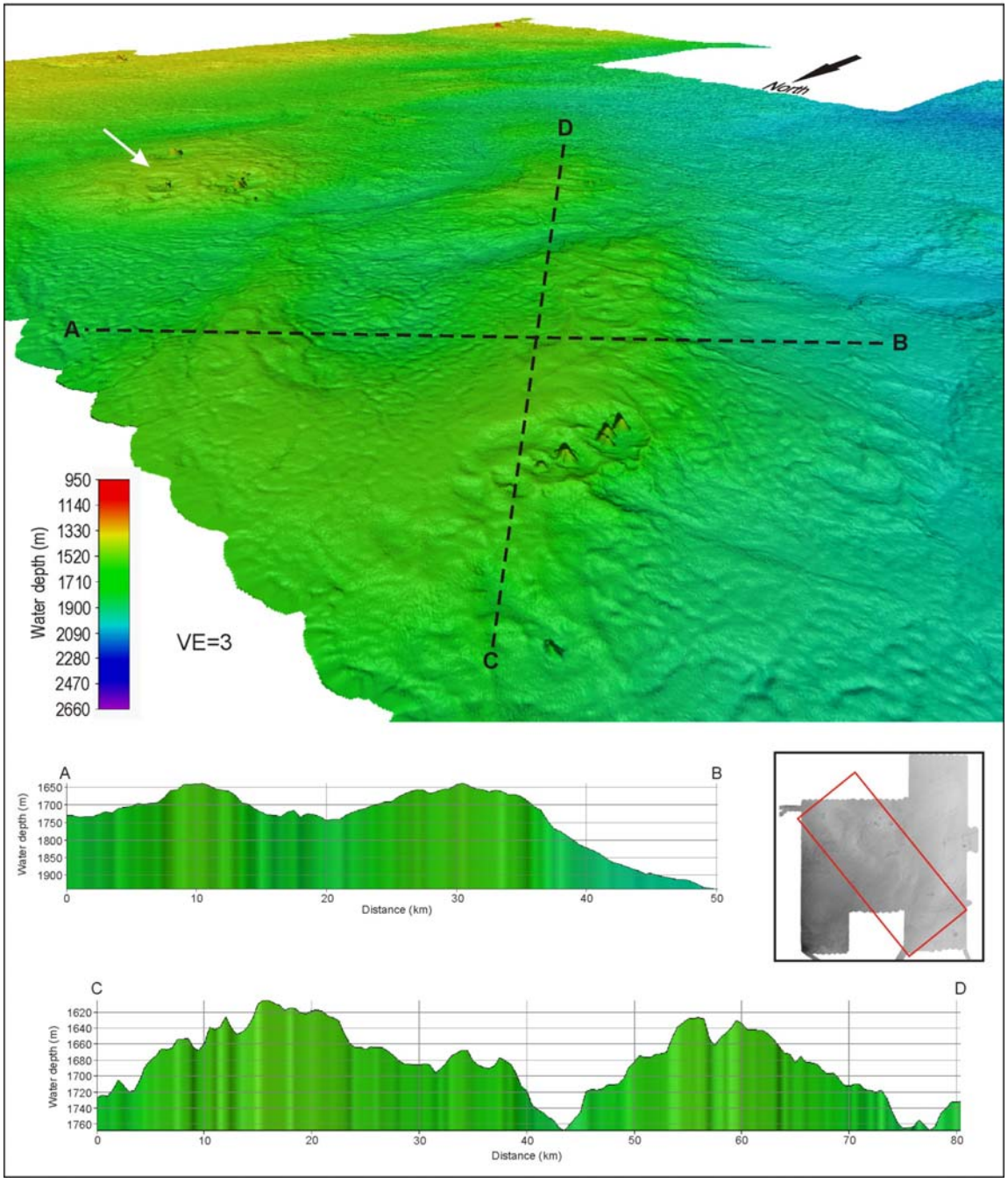

Figure 5.5. Perspective view of the linear ridge and domed ridge (white arrow) in the central north sector of study area A over the Capel and Faust basins, looking southeast. Bathymetric profiles A-B and C-D show representative cross-sections and long sections, respectively. Inset map shows location shown in larger map.

covers 1,248 km^2 in the southeast corner of the survey area, and presumably extends further south and east. The top of this ridge sits in 1,400 m water depth and forms the base for the largest volcanic peak in the survey area.

North of latitude -27.1° S and within the central to western part of the survey area, the seafloor is characterised by a relatively complex terrain of a multiple valleys and ridges, including a linear ridge and a domed ridge (Fig. 5.5). The linear ridge is 15–30 km wide and extends 80 km to the southeast from the northern boundary of the survey area. In cross-section and plan view, the ridge is irregular with valleys up to 160 m deep that cut obliquely across the main ridge line. The bathymetric range of this ridge is from 1,600 m to 1,750 m, but the feature also includes five peaks that rise to 1,500 m water depth. The domed ridge has a diameter of 30–35 km and rises from 1,650 m to 1,500 m water depth. This ridge is also

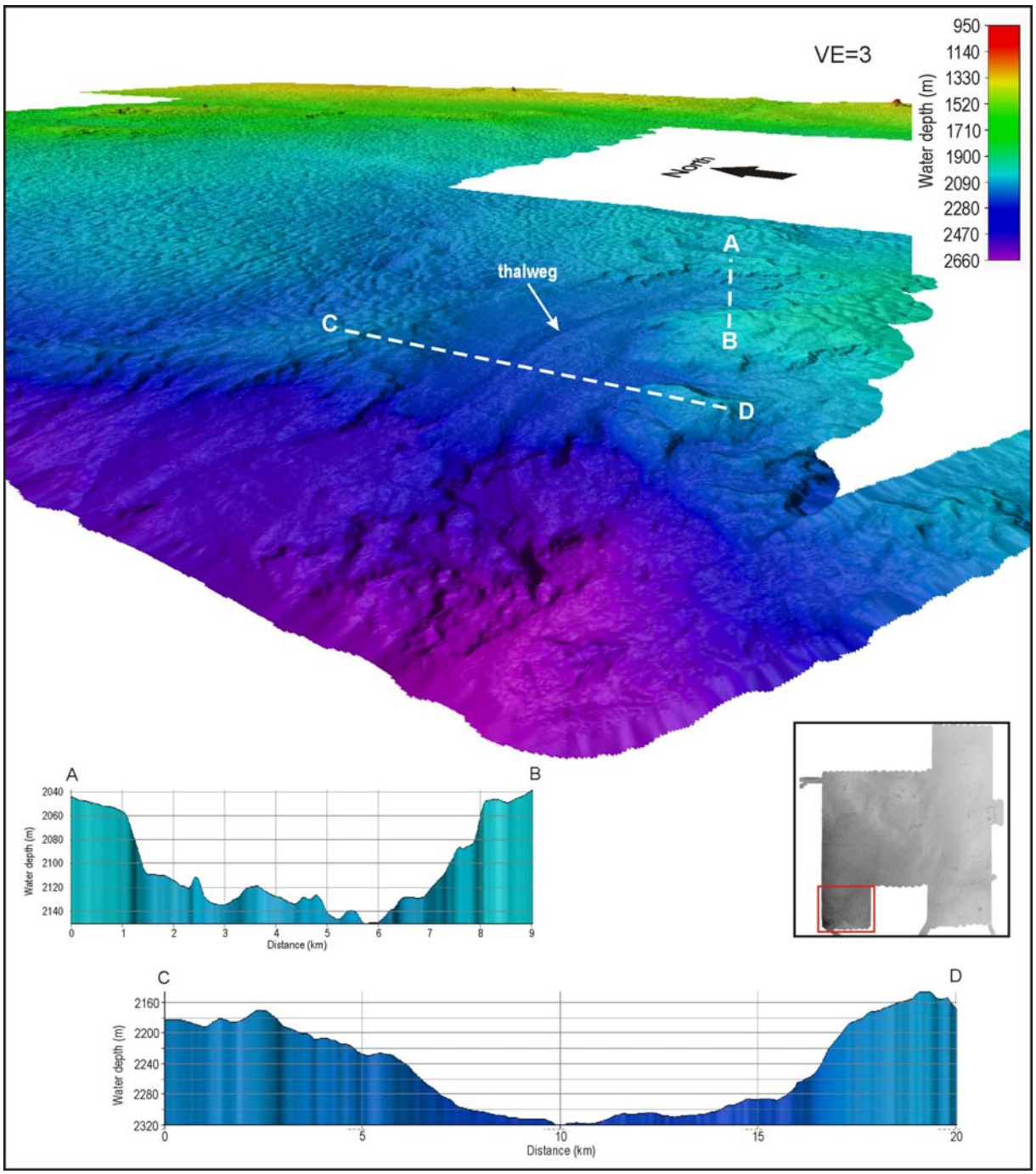

Figure 5.6. Perspective view of the deepest valley in study area A over the Capel and Faust basins, looking northeast. Bathymetric profiles A-B and C-D show representative cross-sections of the upper and lower reaches of the valley, respectively. Inset map shows location shown in larger map.

associated with six volcanic peaks that sit on the mid- to lower slopes at approximately 1,600 m water depth. Apart from these peaks, the seabed across the linear and domed ridge is relatively smooth.

5.1.2.3. Valleys

Valleys have formed across water depths ranging from 1,600 m in the east to 2,200 m in the west of the survey area and cover 2,900 km² (Fig. 5.3; Table 5.2). The deepest valley in the survey area is located in the far southwest in 2,000 m to 2,400 m water depth (Fig. 5.6). The valley extends approximately 30 km in an east-west direction, widening from 6 km at the headwall to 16 km at the mouth. Along this path, the depth of the valley below surrounding seafloor increases from 100 m to 160 m. In cross section, the valley floor is characterised by a

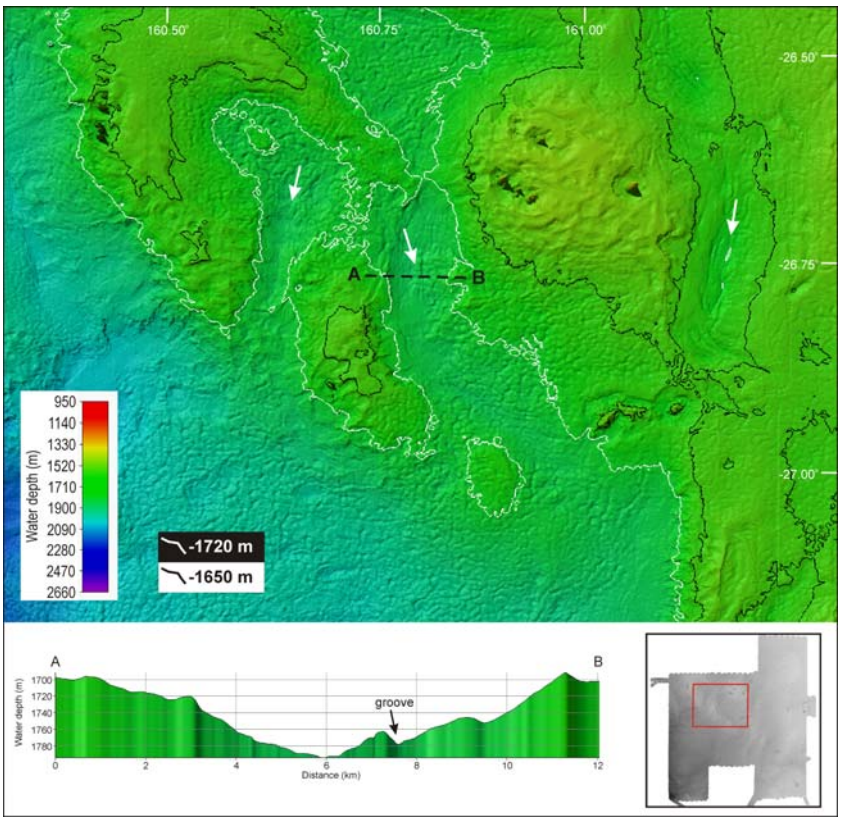

Figure 5.7. Multi-beam (swath) sonar bathymetric map of three valleys (white arrows) in the central northern part of study area A over the Capel and Faust basins, with a representative cross-section. The bathymetric contours (1,650 m & 1,720 m) define the break in slope between the valleys and flanks of adjacent ridges. Inset map shows location shown in larger map.

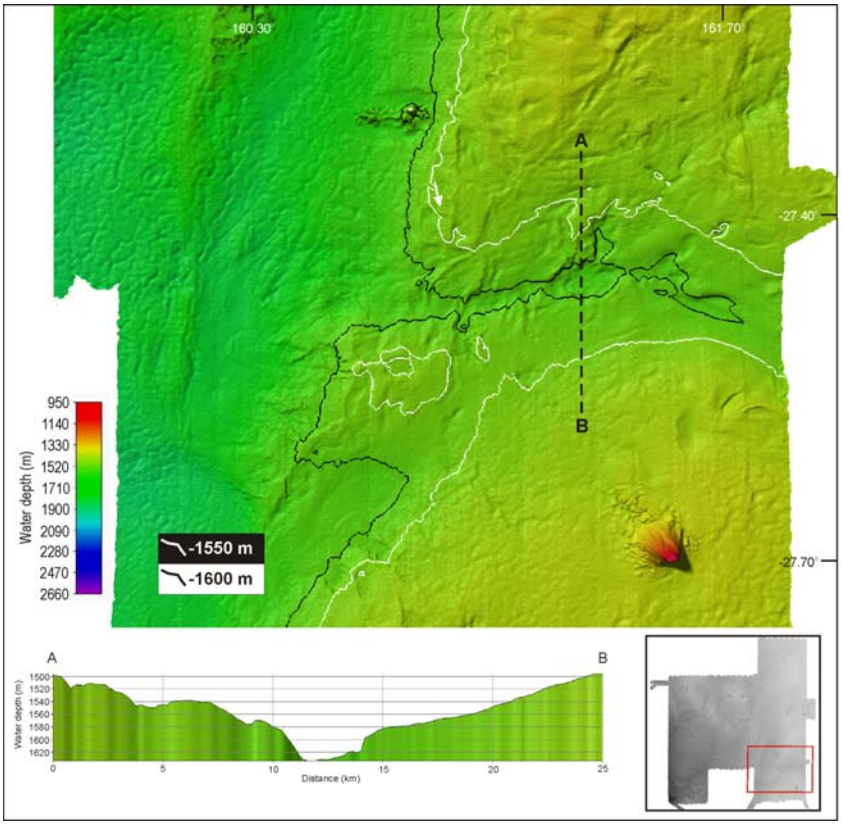

Figure 5.8. Multi-beam (swath) sonar bathymetric map of the valley in the southeast corner of study area A over the Capel and Faust basins, with representative cross-section. The 1,550 m bathymetric contour defines the break in slope between the valley and flanks of the adjacent ridges. Inset map shows location shown in larger map.

generally flat and smooth profile with a thalweg that is 20 m deep and follows a slight meandering path down-valley. In contrast, the upper reaches of the valley floor display a more rugose topography, with local relief of up to 60 m associated with small channels and interfluves that terminate at the 70 m high valley headwall. The slope of the seafloor in the valley decreases from 20° at the headwall to ~1.5° along the upper reaches and ~0.5° along the lower reaches and thalweg. To the southwest of the valley mouth, the seafloor forms a series of broad steps down to 2,600 m water depth, at the edge of the mapped area.

The central northern part of the survey area includes two narrow, shallow valleys with smooth floors located adjacent to the linear ridges described above. The boundary between ridge and valley in this area is defined by the 1,720 m bathymetric contour, across which a break in slope is identified (Fig. 5.7). On this basis, the dimensions of these valleys range from 3.5–14 km in width and 30–45 km in length, with longitudinal gradients of 0.01–0.03°. Maximum depth of valleys below the bounding contour is 60 m, but 40 m is more common. In contrast to the larger valleys in the survey area, these valleys do not have scarped headwalls. Rather, their upper reaches grade onto the flanks of adjacent ridges. Similarly, the lower reaches of these valleys grade onto the plain to the south. The floor of these valleys is generally smooth, with the exception of linear grooves that are up to 10 m deep, 150 m wide and extend along the valley for a distance of 2–8 km (Fig. 5.7).

A valley with similar dimensions and characteristics to those described above is located to the east of the domed ridge in the central north area (Fig. 5.7). This valley is oriented north to south and is defined by the 1,650 m bathymetric contour. Below this contour, maximum relief of the valley is 60 m, with the deepest points located within the narrow, linear grooves that extend along the valley. Along the southern half of the valley these grooves are up to 10 km long and sub-parallel, but less than 5 km long in the northern half. The full extent of this valley is not covered by the mapped area, with the northern boundary of the survey area crossing the valley.

The southeast corner of the survey area includes an east-west oriented valley that extends 32 km across the large ridges in the east (Fig. 5.8). The side of this valley is mapped from the 1,550 m bathymetric contour, which defines the valley width to be approximately 13 km. In cross section, the valley profile is characterised by a 3.5 km wide thalweg defined by the 1,600 m bathymetric contour, with a local maximum depth of 1,630 m. To the west, the thalweg widens to 7 km and the valley grades onto a submarine plain. In contrast to the valleys in the central north sector, the floor of this valley is smooth with no evidence of linear grooves.

5.1.2.4. Volcanic Peaks

A total of 16 volcanic peaks are mapped within the survey area, covering 30 km^2 (Fig. 5.9, Table 5.2). Thirteen of the peaks form three clusters located on ridges and are informally named the ‘western field’, ‘central field’ and ‘eastern field’ (Fig. 5.10). The western field comprises five peaks on a linear ridge that are aligned north-south over a distance of 6 km in 1,660 m to 1,700 m water depth (Table 5.3). The central field includes six peaks spread approximately 20 km across a domed ridge in 1,580 m to 1,660 m water depth. The ‘eastern field’ comprises two peaks located on the ridge at the eastern margin of the mapped area in 1,400 m water depth. The remaining three peaks are isolated features, located in the northwest, central west and southeast (Fig. 5.9).

The height of volcanic peaks ranges from 65 m to 450 m, with the two largest peaks located in the shallowest water depth (Table 5.3). Thus, peaks #14 and #16 sit in 1,400 m water depth near the eastern margin of the survey area and rise to 950 m and 1,020 m water

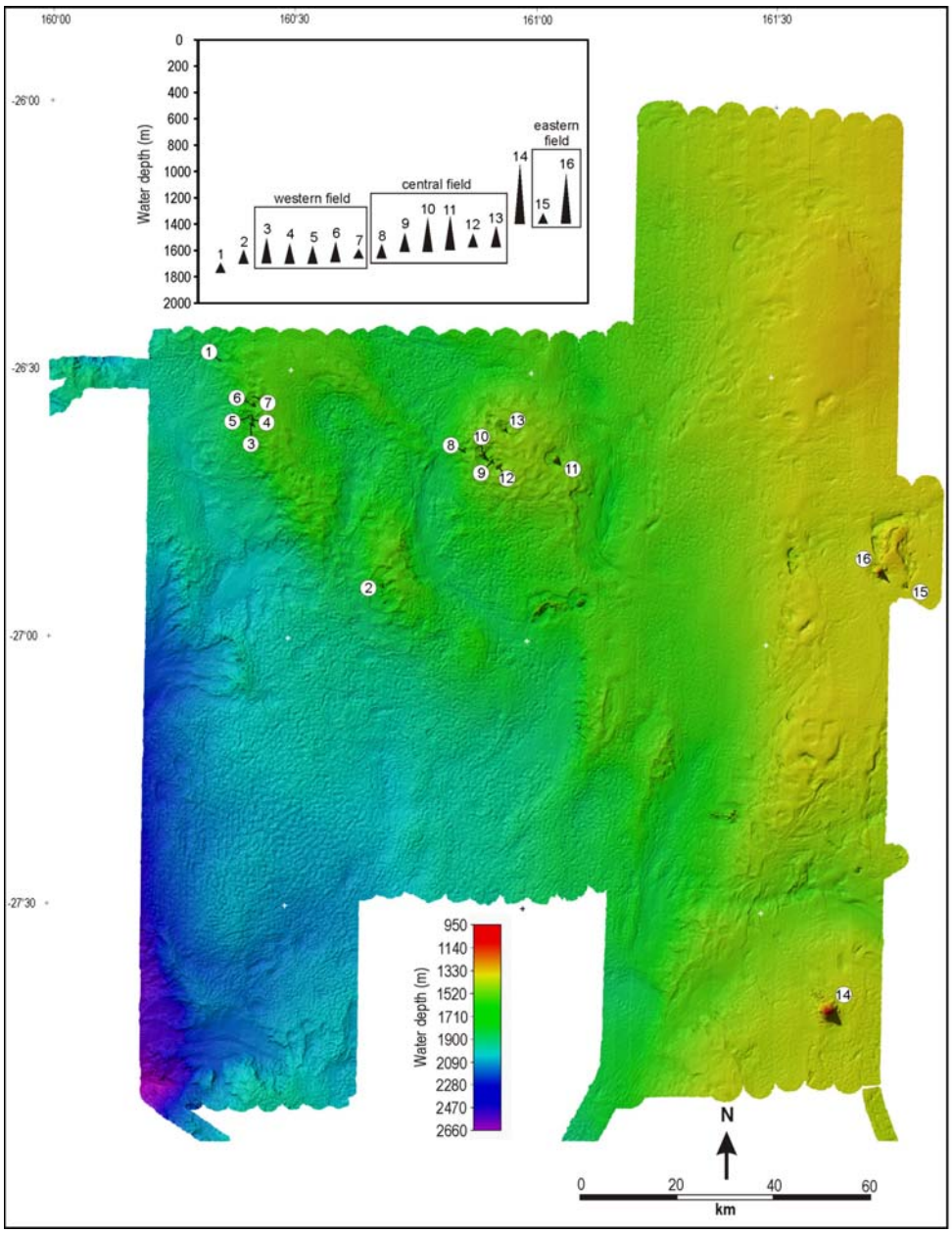

Figure 5.9. Multi-beam (swath) sonar bathymetric map of study area A over the Capel and Faust basins with the 16 volcanic peaks labelled. Inset plot shows each peak drawn to scale against water depth.

depth, respectively. Overall, there is a general trend of smaller peaks with increased water depth to the west (Fig. 5.9 inset).

All of the volcanic peaks have a near-symmetrical conical shape, with slopes ranging from 10° to 30°. The only evidence for side collapse is on the largest peak (14) which has a slump scar on its northern side and blocky material that extends 4 km from the base that is likely to be slump debris (Fig. 5.11). Most peaks have a moat that encircles the cone. For the larger peaks, these moats are up to 50 m deep and 1–2 km wide (Fig. 5.10).

5.1.2.5. Basins

The southwest corner of the survey area captures a small section of steepening seabed that extends from 2,400 m to 2,600 m water depth. Covering 50 km^2 (Table 5.2) and incorporating what appears to be the upper end of a valley, this area is mapped as the edge of a basin on the grounds that in the regional context the Middleton basin extends westward of this point (Stagg *et al.*, 2002).

Table 5.3. Location and dimensions of volcanic peaks in the survey area. Peaks are numbered in order of decreasing water depth at their base and are plotted on Fig. 5.9

Peak	Lat.	Long.	Height (m)	Water depth at summit (m)	Water depth at base (m)
1	-26.4824	160.3534	70	1,700	1,770
2	-26.8979	160.6948	100	1,600	1,700
3	-26.5995	160.4183	190	1,510	1,700
4	-26.5903	160.4196	150	1,550	1,700
5	-26.5847	160.4157	130	1,570	1,700
6	-26.5633	160.4206	150	1,540	1,690
7	-26.5498	160.4229	65	1,595	1,660
8	-26.6452	160.8609	110	1,550	1,660
9	-26.6641	160.9193	140	1,470	1,610
10	-26.6518	160.9006	250	1,360	1,610
11	-26.6593	161.0552	260	1,340	1,600
12	-26.6736	160.9350	100	1,480	1,580
13	-26.6052	160.9466	160	1,420	1,580
14	-27.6799	161.6463	450	950	1,400
15	-26.8836	161.7891	80	1,320	1,400
16	-26.8574	161.7346	380	1,020	1,400

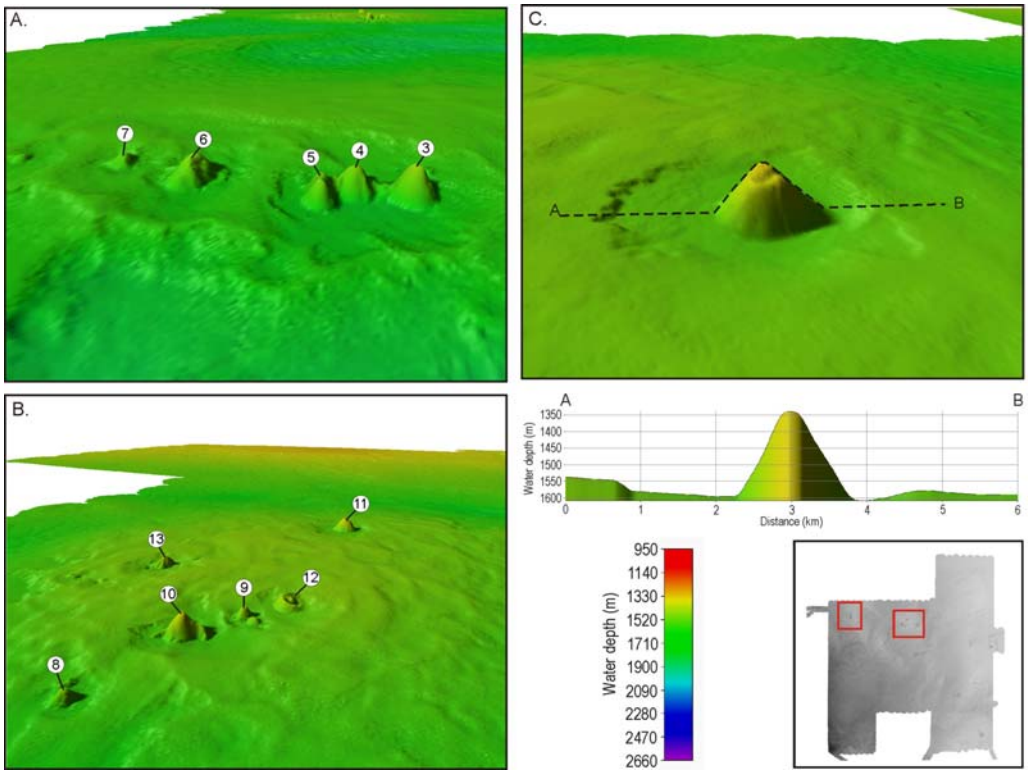

Figure 5.10. (a) Perspective view of volcanic peaks in the western field looking to the east. (b) Perspective view of volcanic peaks in the central field looking to the east. (c) Perspective view of peak #11 in the central field. Note the moat around the base of the cone. Profile shows cross section across peak #11. Inset map shows location of perspective views in (a) and (b).

5.1.3. Small-scale Features

Small-scale features are superimposed upon large-scale features, have dimensions of hundreds of metres to kilometres and include peaks, moats, holes, (polygonal) cracks, scarps and (potential) fluid escape features.

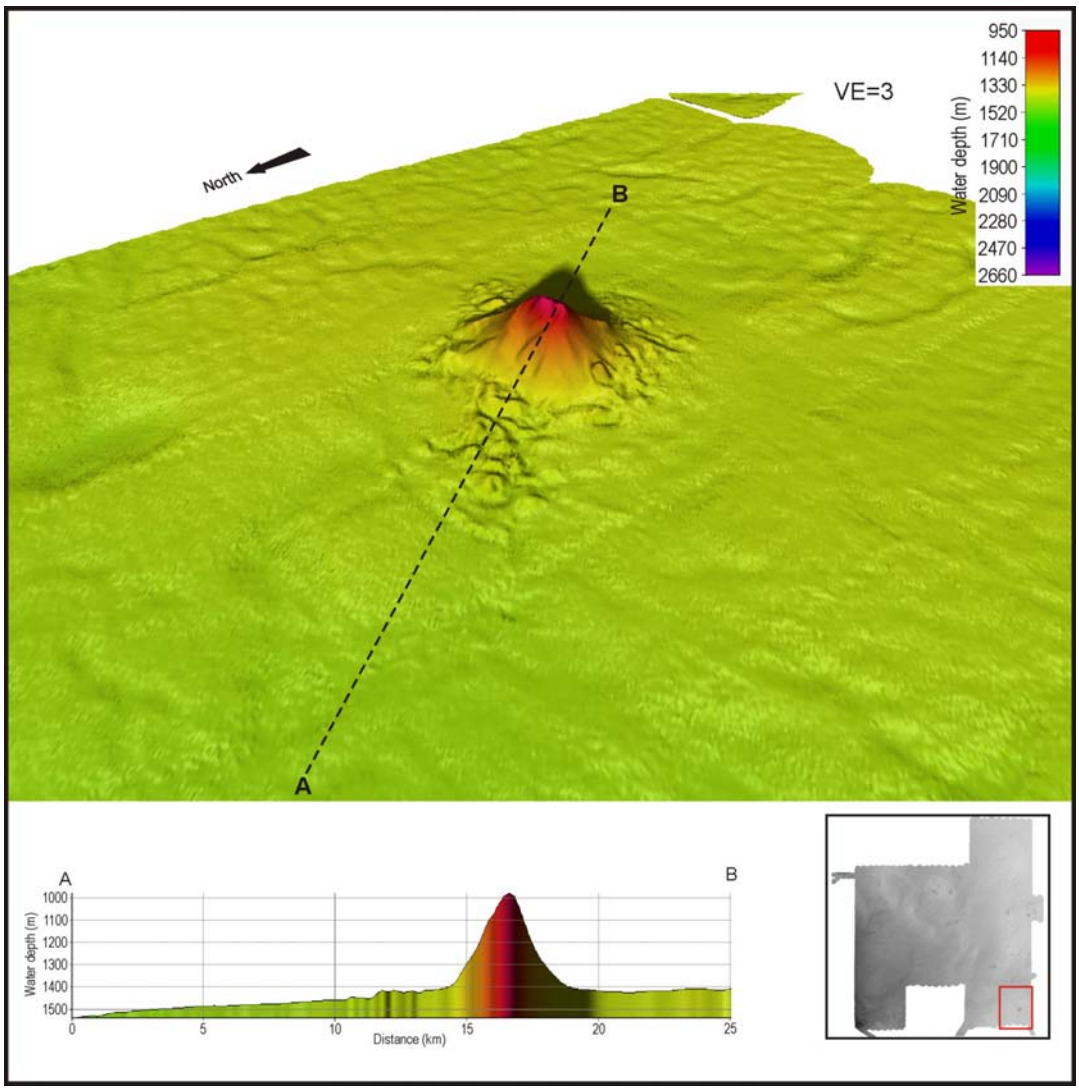

Figure 5.11. Perspective view and bathymetric cross-section of the largest volcanic peak in study area A over the Capel and Faust basins, looking southeast. Note mounds at the base of the cone. Inset map shows location within the survey area.

5.1.3.1. Holes

These geomorphic features are most clearly defined on the large ridge that extends along the eastern margin of the study area (Fig. 5.12). Holes in this area are concentrated immediately to the north of a volcanic peak on the ridge crest and on the lower flanks of the ridge. In plan view, holes range in shape from elongate forms up to 9 km long and 4 km wide, to nearly circular with a diameter of up to 1 km. Depth below the adjacent sea floor ranges from 20 m to 80 m. In cross-section, the deeper holes have asymmetric profiles with the steeper sidewall sloping at 5–7°, a nearly flat and smooth floor and an opposite wall gradient of 3–6°.

The large plain in the southwest of the survey area also has shallow holes in the seafloor. Here the holes are isolated features with a diameter of 2.5 km to 4 km and depths of up to 35 m. The location of these holes appears unrelated to water depth, as examples occur across the bathymetric extent of the plain.

5.1.3.2. Polygonal Cracks

In addition to holes, an extensive network of shallow cracks dissects the surface of the submarine plain within the southwest sector of the survey area (Fig. 5.13). These cracks are up to 10 m deep, 0.5 to 1 km wide and can be traced along the seafloor for several kilometres. In plan view, the network has developed a polygonal pattern across the seafloor with no

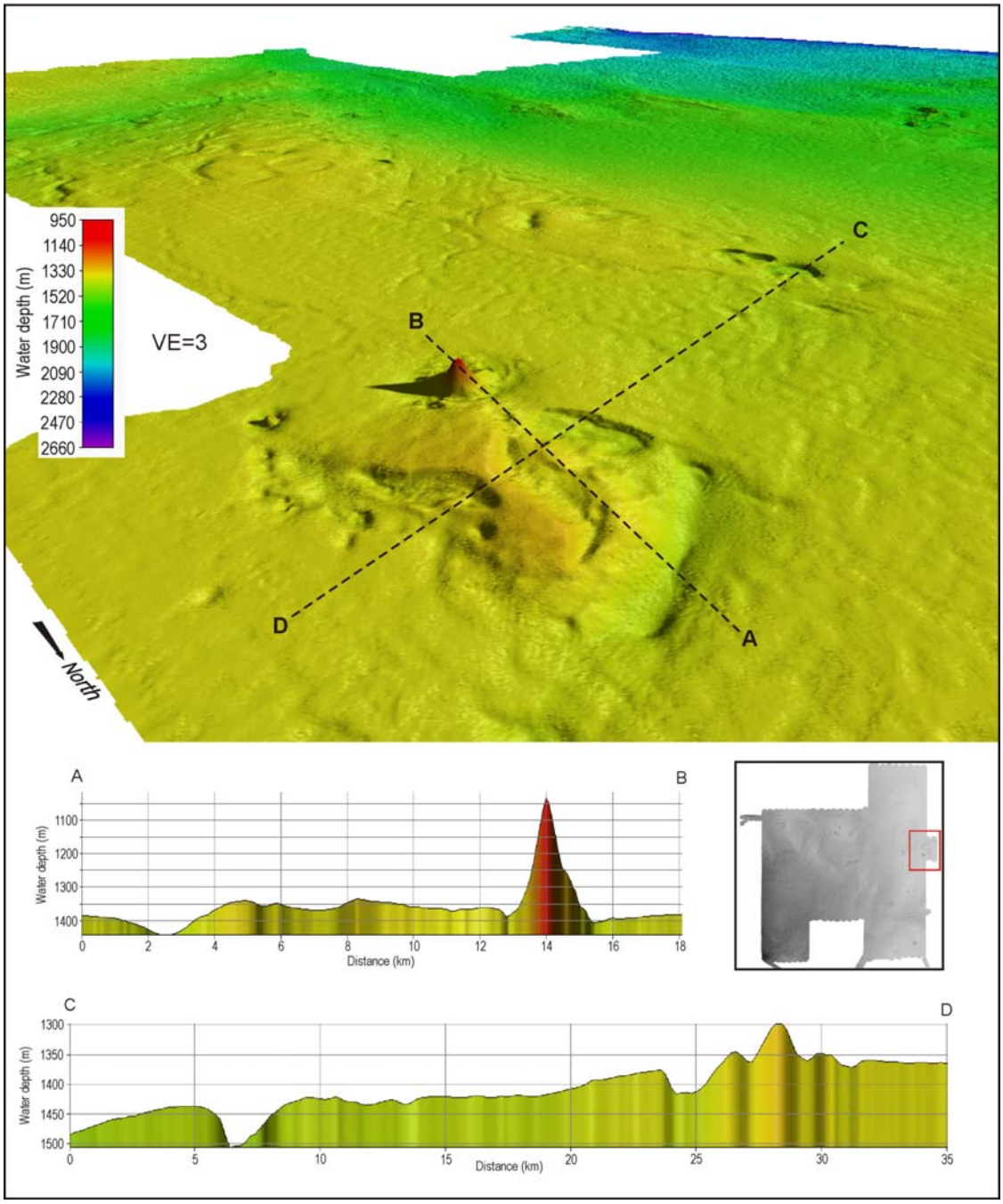

Figure 5.12. Perspective view and representative cross-sections across holes in the vicinity of volcanic peaks on the eastern ridge of study area A over the Capel and Faust basins. Inset map shows location shown in larger map.

preferred orientation and is only interrupted by small holes (2–4 km diameter), which have a smooth floor. The density of polygonal cracks appears uniform across the submarine plain, as shown by a count of cracks along a representative 90 km transect that recorded 57 cracks at an average density of six for every 10 km. Toward the western boundary of the survey area, polygonal patterning extends to the edge of the valleys that have their headwalls in the submarine plain, but does not continue onto the valley walls or floor. Within the north-western sector of the survey area polygonal patterning is discontinuous, formed only on low gradient slopes (~0.2°) (Fig. 5.7). Polygonal patterning is poorly developed within the eastern third of the study area. Here, cracks less than 5 m deep have formed on the lower slopes of the large ridge to the east. In summary, the distribution of polygonal cracks in the mapped area appears to be related to bathymetry and large scale geomorphic features, with the most extensive network on the expansive submarine plain in 1,800 m to 2,200 m water depth.

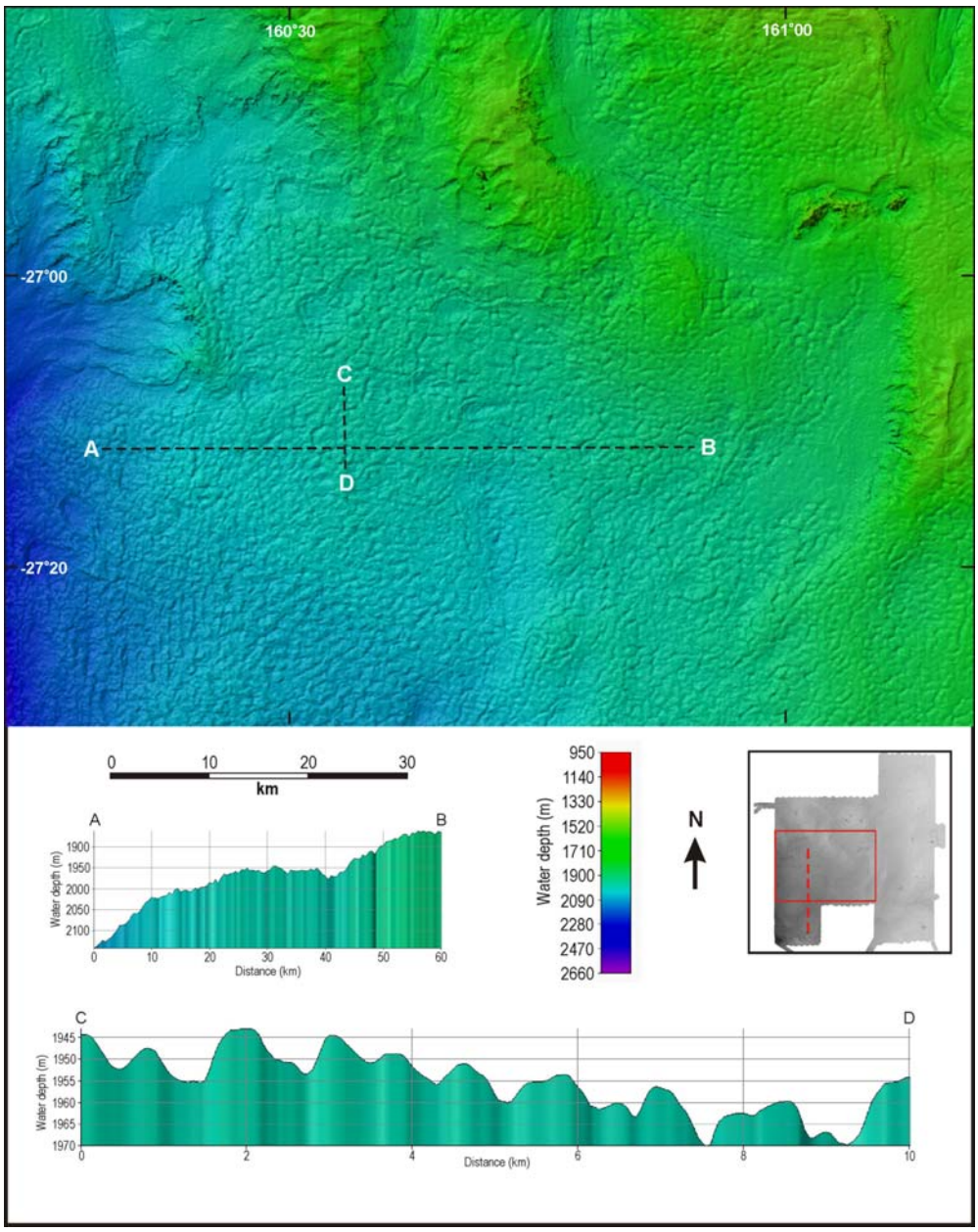

Figure 5.13: Multi-beam (swath) sonar bathymetric map and representative profiles of the submarine plain in the western sector of study area A over the Capel and Faust basins, showing the polygonal crack network. Inset map shows location shown in larger map (dashed red line shows the 90 km transect used to measure the density of cracks).

5.1.3.3. Small Ridges

Small ridges are present in four locations on the shallower part of the main submarine plain, in approximately 1,700 m water depth (Fig. 5.14). These ridges are isolated features with lengths of 7 km to 15 km, widths of 3–6 km and heights of 50–120 m. Two of these ridges are aligned broadly north-south, and the other two roughly east-west. These latter two are also surrounded by moats that are 20 m deep and up to 1 km wide.

5.1.3.4. Scarps

Scarps are highly localised features within the survey area, and are restricted to the slopes of small ridges, headwalls of some valleys, and the edge of moats and holes. Examples of ridge-associated scarping occurs along the steeper flanks of the two small north-trending ridges located on the submarine plain (centred on -27.14°S, 161.12°E and -27.20° S, 161.29°E). Scarps on these ridges are discontinuous, locally up to 40 m high with slopes of approximately 15° that extend 1–1.5 km along the ridge. In most cases, the scarp is oriented perpendicular to the

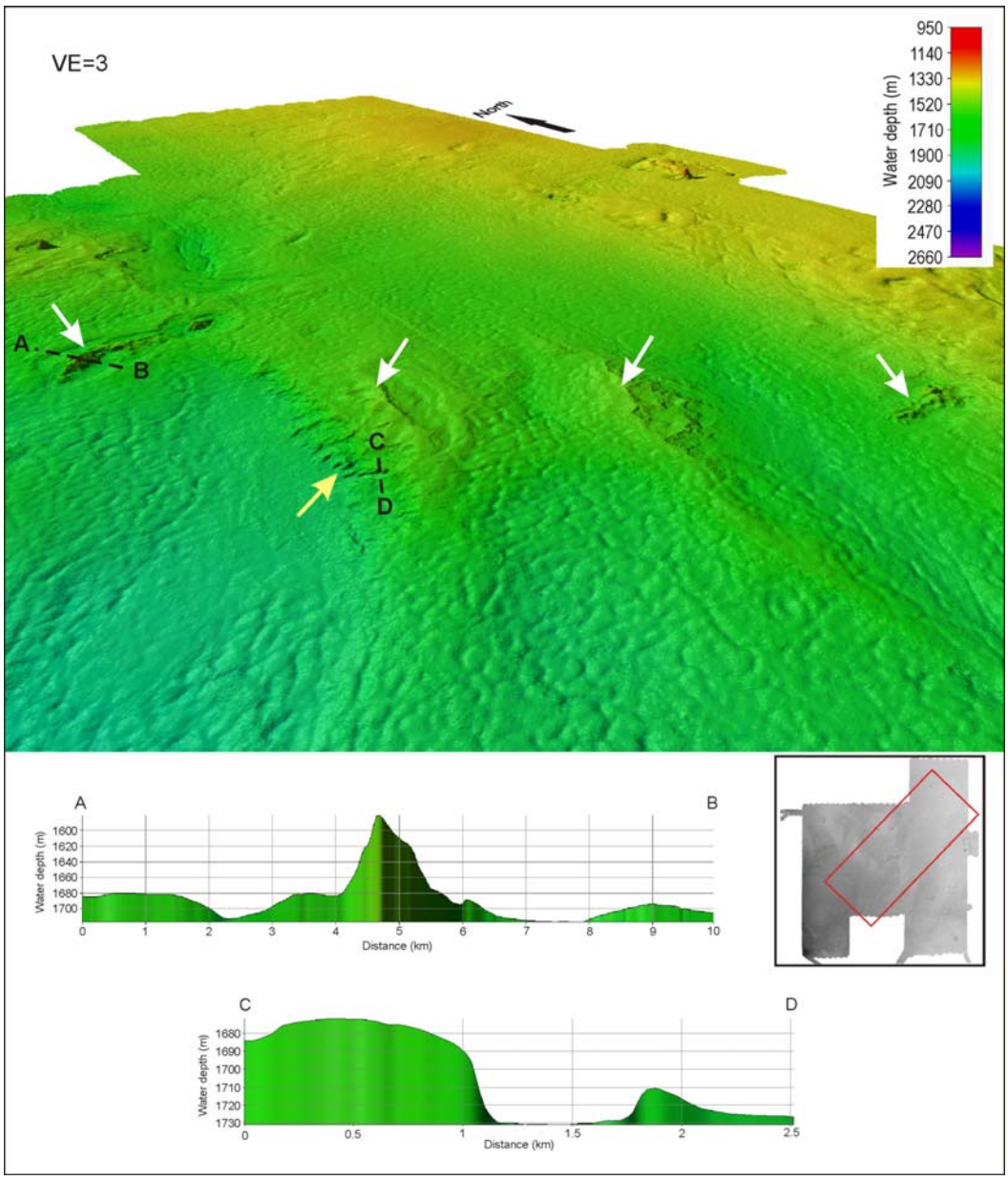

Figure 5.14. Perspective view showing four small ridges (white arrows) and a scarp (yellow arrow) in approximately 1,600 m water depth, looking northeast. Cross-section A-B shows the profile across the highest of these ridges, and section C-D shows the highest scarp. Inset map shows location shown in larger map.

ridgeline, thereby producing small side valleys incised into the lower flanks of the ridge (Fig. 5.14). A similar style of scarping, but on a smaller scale, is mapped in the southeast corner of the survey area. Here scarps are up to 20 m high and range in length from 2 km to 6.5 km (Fig. 5.15).

Scarping of valley headwalls is best developed in the deeper western part of the survey area, where two valleys are mapped (Fig. 5.16). The headwall to the larger valley in the far southwest is defined by a discontinuous scarp that extends ~20 km along the seafloor and ranges in height from 40 m to 100 m, with a gradient of 10° to 20°. In the central west of the survey area, a scarp of similar dimensions forms part of the valley headwall. This example is also discontinuous, with steep sections (~20°) interspersed with intermediate slopes of 8–10°.

Scarps on the edges of moats and holes are of a comparable scale to scarps on ridge flanks, but are relatively rare. The clearest example occurs on the western edge of the moat that surrounds the large volcanic peak (11) in the central volcanic field. This scarp is 30 m high, extends as a continuous feature for 3 km and appears to have a deposit of slump material at its base. However, this deposit is difficult to resolve in detail. Scarps on the other

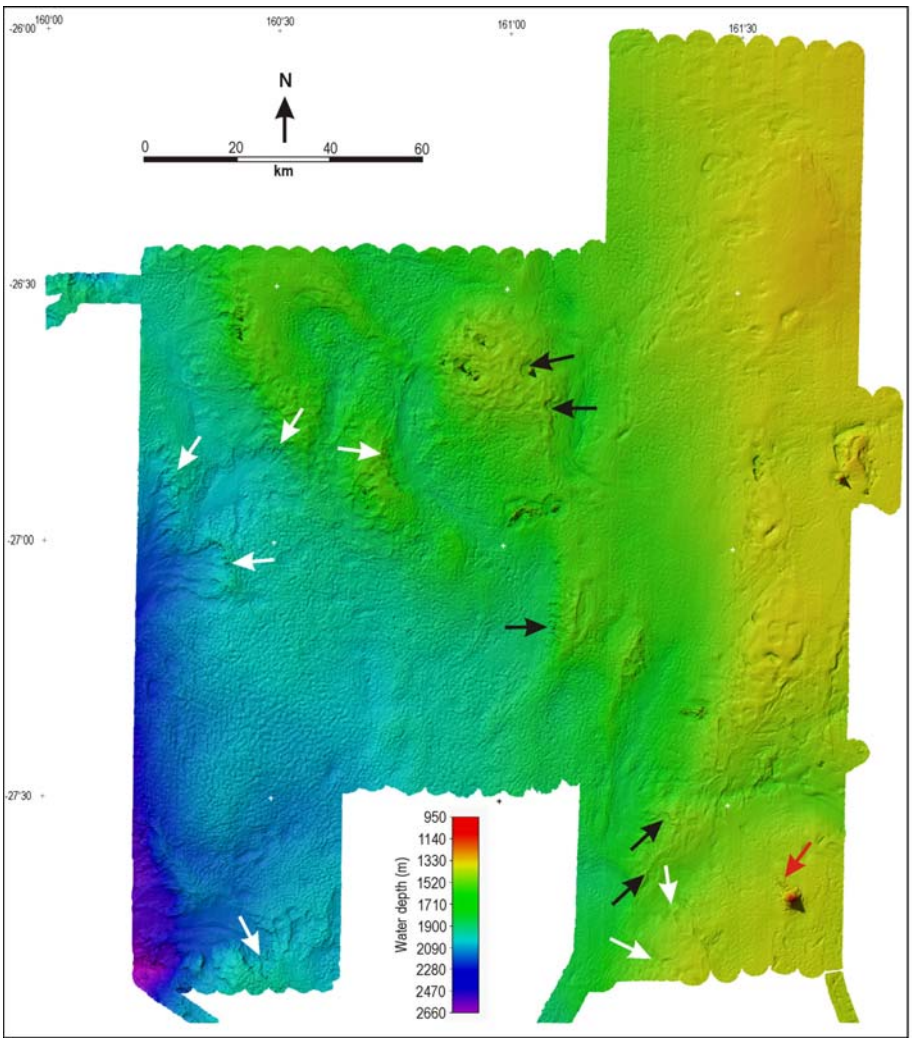

Figure 5.15. Multi-beam (swath) sonar bathymetric map of study area A over the Capel and Faust basins, indicating scarps (black arrows), potential fluid escape scours (white arrows) and slump mound at the base of a volcanic peak (red arrow).

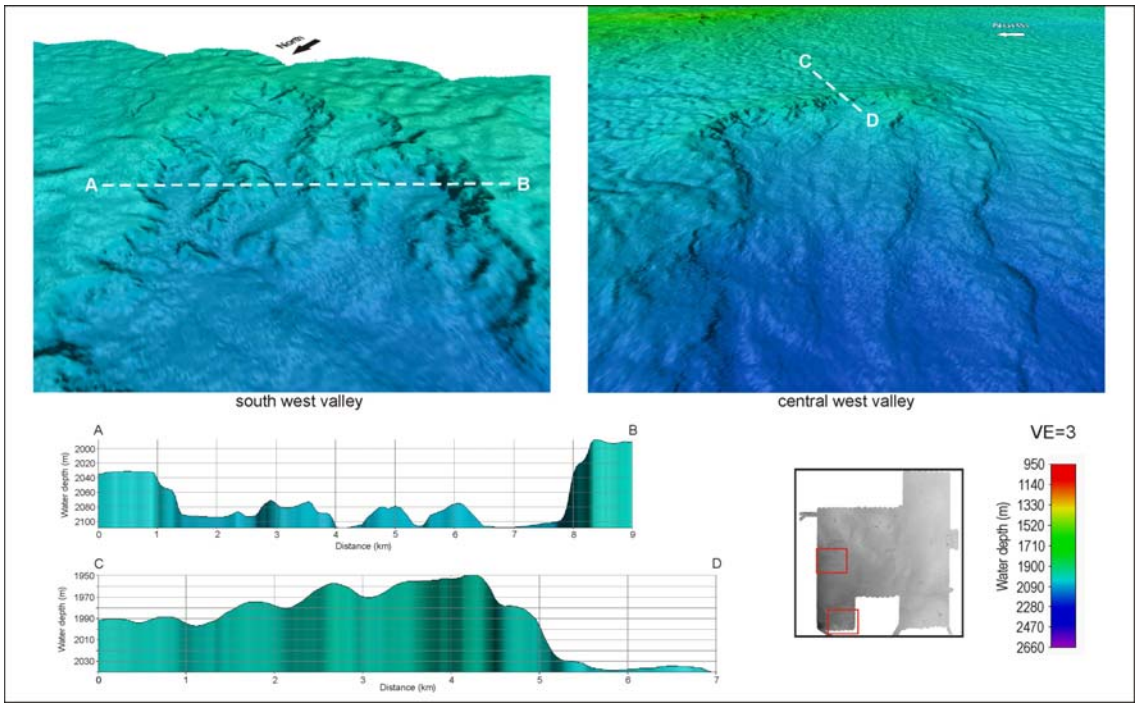

Figure 5.16. Perspective views and cross-sections of valley headwalls and scarps in the southwest and central west of the survey area. Inset map shows location within study area A.

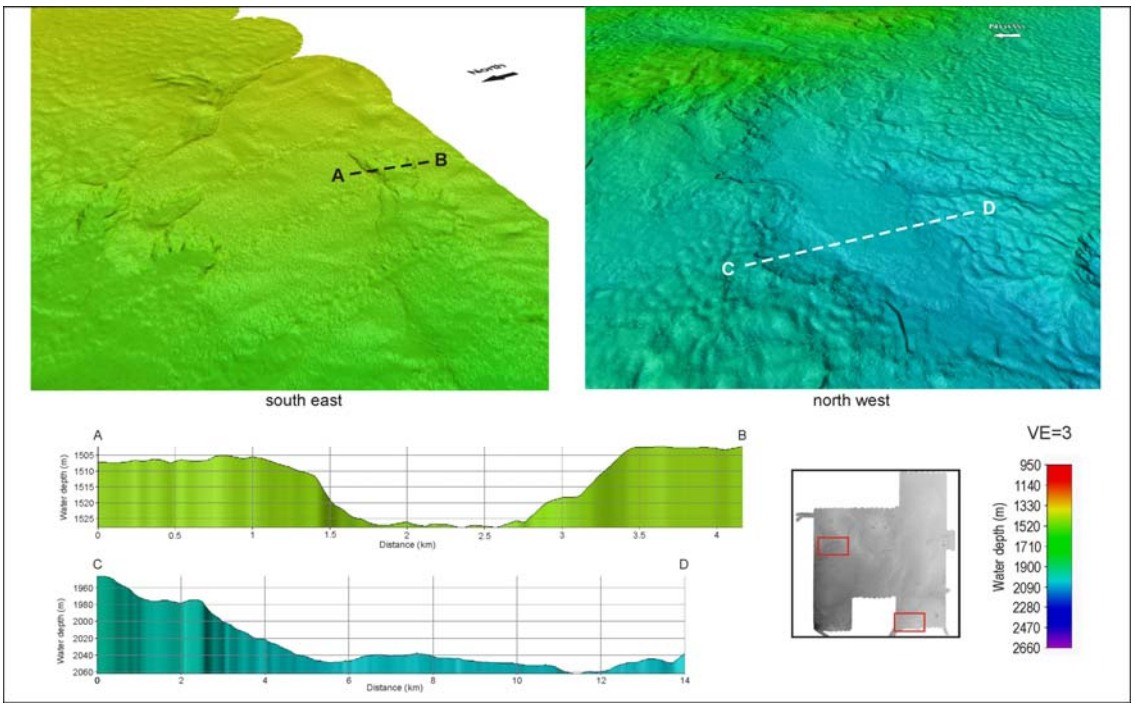

Figure 5.17. Perspective views and cross-section profiles of potential fluid escape features (eroded areas of seabed and sediment lobes) in the southeast and northwest of study area A over the Capel and Faust basins. Inset map shows locations in larger survey area.

moats in the survey area are discontinuous and less than 1 km in length. Examples of holes with steep sides occur among the larger holes located on the eastern ridge of the survey area. In all cases, the western side of these holes has a slope of approximately 10° that descend up to 50 m from the top of the hole. None of these holes show evidence of slumping of their sidewalls, with their floors characteristically smooth.

5.1.3.5. Potential Fluid Escape Features

Modification of the seabed morphology by fluid flow is potentially evident across tracts of seafloor that extend below scarps formed at valley headwalls (Fig. 5.15). These areas are characterised by a smooth surface that dips basinward at gradients of 0.5° to 1.5° and is distinct from adjacent areas that preserve polygonal networks of cracks. Some of these gently sloping surfaces are incised by channels up to 10–15 m deep. One of the larger examples of potential fluid modification is located in the northwest sector of the survey area (centred on -26.87°S, 160.42°E). This site is characterised by a downslope progression from a 50 m high scarp formed in a ridge at 1,800 m water depth to a smooth lobe that extends 20 km to the southwest (Fig. 5.17). The boundary between this lobe and adjacent areas of polygon-patterned seafloor is very well defined and is associated with a slight bathymetric rise of 10–20 m. As such, this bathymetric setting likely provides the necessary conditions for shaping the seabed to a smooth and/or channelised form. The mechanism that has driven this modification of the seafloor presumably involves fluid flow, either across the bed and/or through the saturated sub-bottom sediments.

5.2. AREA B: GIFFORD GUYOT – SEAMOUNT

5.2.1. Geomorphic Features

Gifford Guyot has the 'classic' geomorphology for a guyot, containing an extensive flat top and steep flanks (Fig. 5.18). The newly acquired multi-beam sonar data reveal that the flat

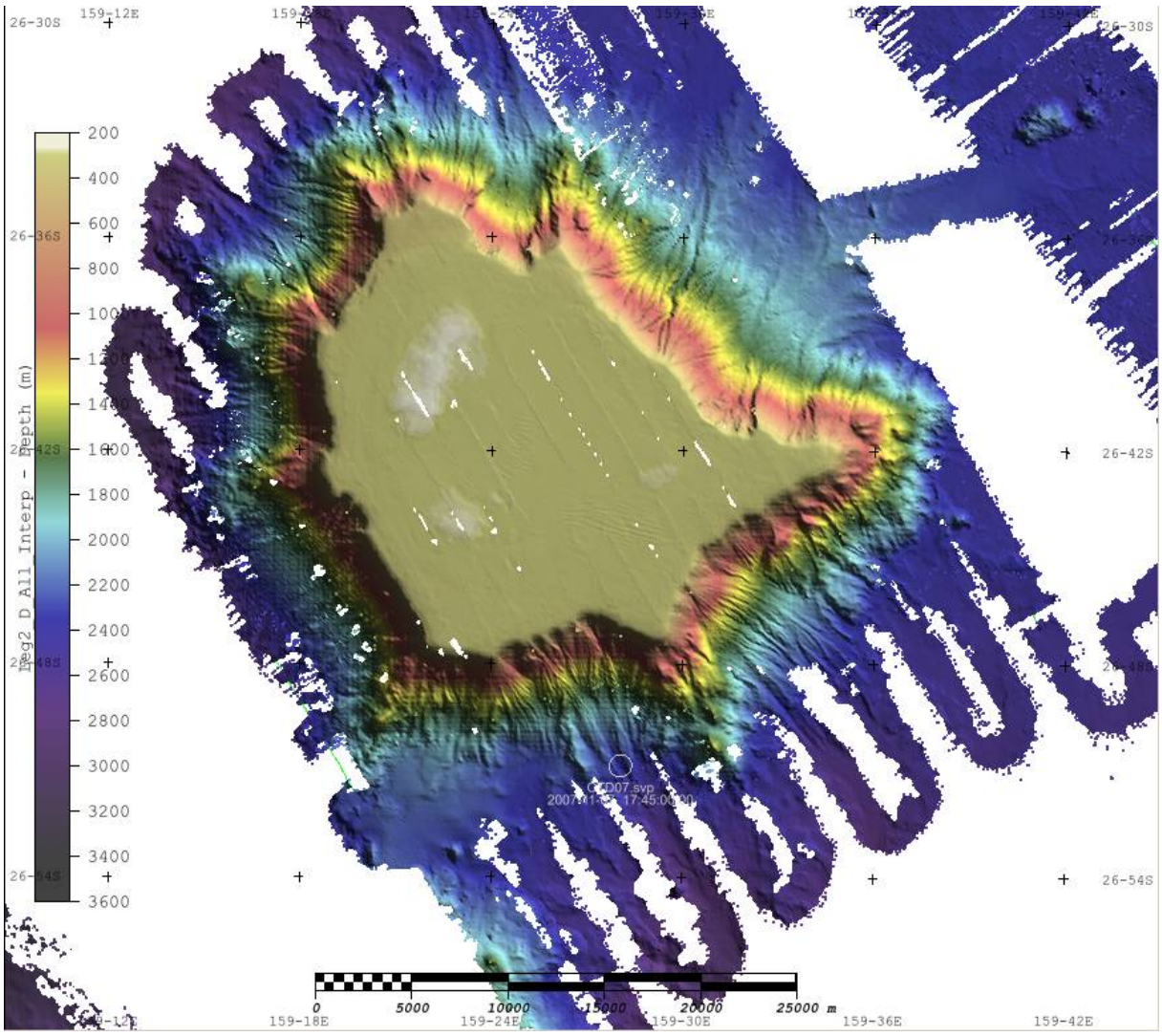

Figure 5.18. Multi-beam (swath) sonar map of study area B over Gifford Guyot. The flat-topped summit of the guyot is in water depths of 280-320 m. The steep flanks of the seamount rise 2,400 m from the surrounding flat seabed.

top of the guyot is located between 260 and 320 m water depth and has a relief of up to 30 m. This relief is characterised by a semi-continuous broad ridge in the north and northwest and a field of sinuous-crested, subaqueous dunes in the central and southern sectors. The flanks of the guyot are replete with small-scale features evident of significant mass-wasting, including: slumps, slide blocks, debris slopes and steep-sided valleys. The gradient of the flanks decreases below 1,000 m water depth. Overall, the geomorphology and steepness of the flanks differ between the N-S and E-W profiles, with the E-W profile not showing as distinct change in slope (Fig. 5.19a).

A total of nine main geomorphic features are identified on Gifford Guyot (Fig. 5.20; Table 5.4). Ridge, subaqueous dunes, plateau and terrace features occur on the top of the guyot while slump scar, debris slope, spur, and valley features occur on the flanks. Outwash fan features occur at the base of the guyot.

5.2.1.1. Debris Slope

Debris slope features cover the largest area on Gifford Guyot (Table 5.4, Fig. 5.20). They occur on all of the guyot flanks and cover an area of 418 km^2 or 35% of the total area. Debris slopes are characterised by steep, heavily channelised, fan-shaped surfaces (Fig. 5.21). They generally extend from the margins of the plateau down to the base of the guyot. They range

Table 5.4. Summary attributes of geomorphic features on Gifford Guyot. Dimensions of features are measured by length (L) and width (W).

Feature	Description	Dimensions (km)	Area (km^2) Area (%)	Relief (m)	Slope (°)
Debris slope	Multiple steep fan with downslope channel	L: 3.0-7.0 W: 1.1-4.0	418 35.0	Downslope: 1,000 Cross-slope: 200 Channels: 20	14.0-19.0
Plateau	Extensive sub-horizontal surface	L: 25.8 W:17.6	332 27.8	<1 m	0.1-0.9
Spur	Blocky ridge extending from plateau	L: 4.5-7.0 W: 3.0-12.0	238 20.0	600-800	9.0-18.0
Submarine fan	Gently sloping inter-fingering or coalescing fan	L: 5.0-6.0 W:3.0-6.0	95 8.0	80-200	1.0-3.0
Slump scar	Steep concave incision on flanks	L: 3.1-10.9 W: 2.2-4.2	46 3.8	350-1,000	9.0-60.0
Ridge	Low and elongated prominence with irregular, steep sides	L: 2.0-8.0 W: 1.0-3.0	24 2.0	10-30	1.0-2.5
Subaqueous dune field	Parallel 2D, symmetrical dunes	L: 1.7-3.8 W: 1.0-5.6	18 1.5	H: 0.3-5.0 Wavelength: 90-350	1.0-5.0
Valley	Broad and flat-bottomed incision on flanks	L: 5.0-9.0 W:1.0-1.5	13.5 1.1	150-250	Head: 24.0-27.0 Base: 5.0-12.0
Terrace	Sub-horizontal surface with steeper bounding slopes	L: 2.5-10.0 W: 0.2-1.5	9.8 0.8	<1 m	1.0-3.0

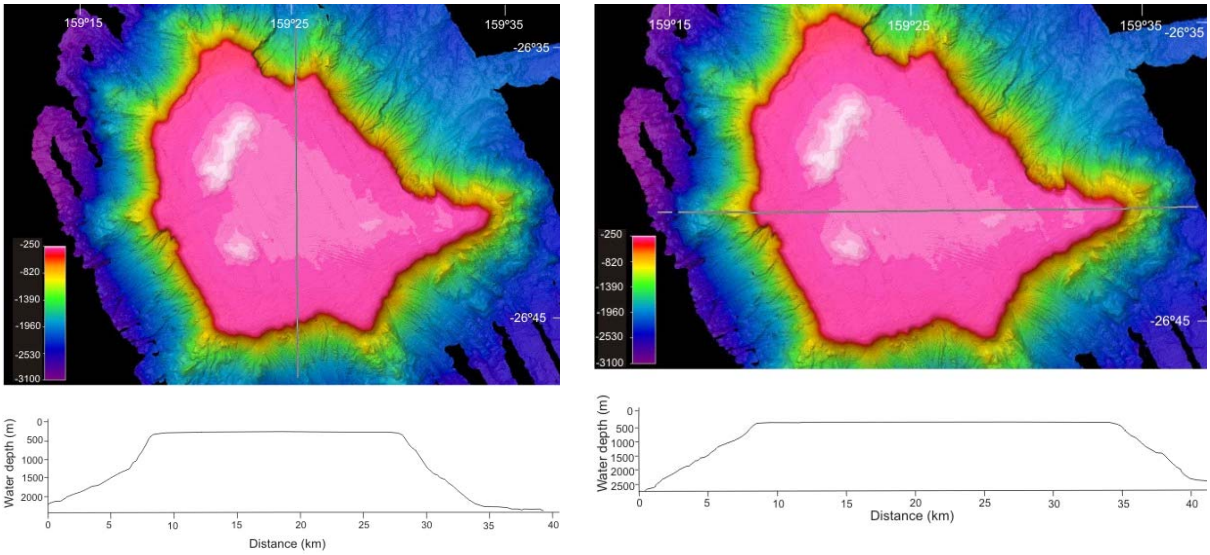

Figure 5.19. (a) N-S and (b) E-W cross-sections across Gifford Guyot showing the steeply-sided flanks and extensive flat-topped summit. The guyot is asymmetrical in shape with the E-W profile not showing as a distinct change in slope as the N-S profile.

considerably in width and length (Table 5.4). The largest debris slope is approximately 7 km long, 1.8 km wide at the top, 4 km wide at the base with an overall slope of 14-15°. The smallest debris slope is 3 km long, 0.2 km wide at the top and 1.1 km wide at the base, with an overall slope of 18-19°. Generally, the profiles of the debris slopes show a decrease in overall slope with depth. Boulders are evident on their surfaces. Available data does not reveal whether these features are loose sediment deposits or lava flow runnels.

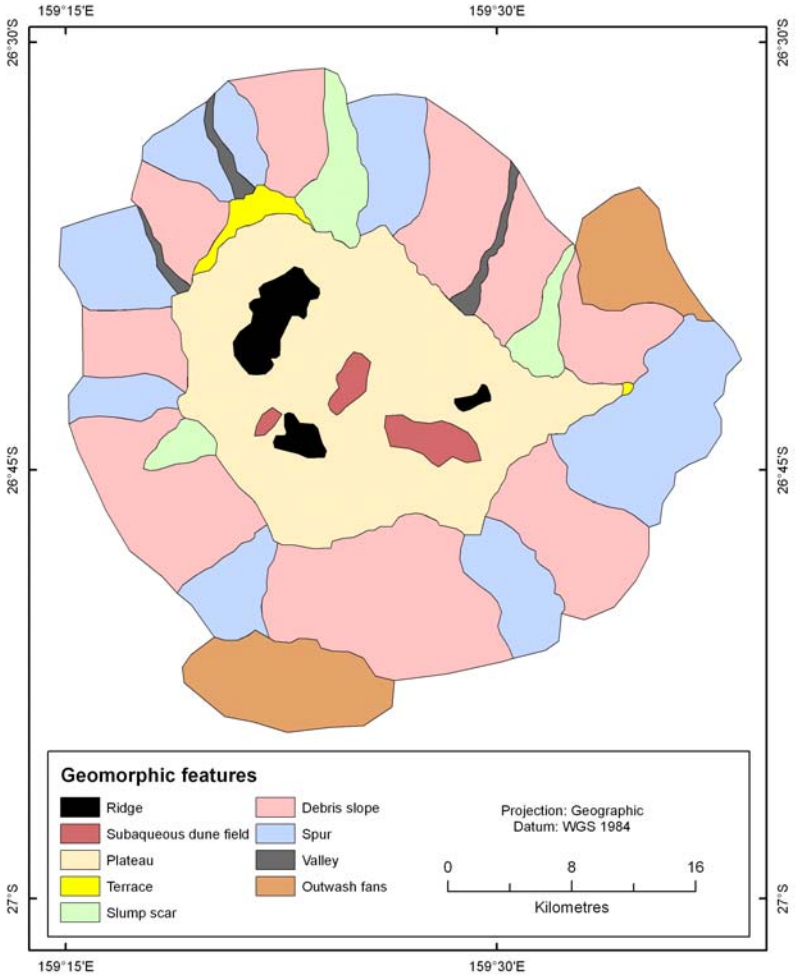

Figure 5.20. Geomorphic features identified in study area B over Gifford Guyot.

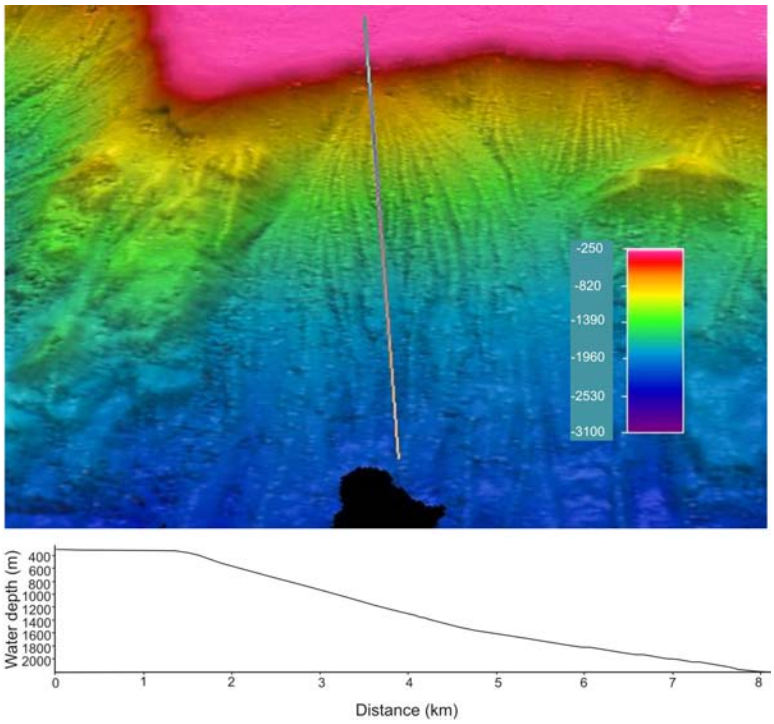

Figure 5.21. Oblique multi-beam (swath) sonar bathymetry map showing an example of a debris slope on the southeast flank of Gifford Guyot. They are the most abundant geomorphic feature, occurring on all flanks and characterised by steep, heavily channelised, fan-shaped surfaces (vertical exaggeration 1x).

5.2.1.2. Plateau

Plateau features cover the second largest area on Gifford Guyot (Table 5.4). This feature forms the 25 km long by 17 km wide sub-horizontal surface on the top of the guyot that covers an area of 332 km² or 27.8% of the total area. The plateau can be divided into two morphologically different regions: an inner region characterised by a relatively low-gradient, and a steeper-gradient outer region (Fig. 5.22). The broad ridges separate the two plateau regions. The margins of the plateau occur in water depths of between 300 and 380 m. The margin of the plateau is scalloped and has a slope of 16-18° and a width of 430-530 m before transitioning into the very steep guyot flanks.

5.2.1.3. Spur

Spur features cover the third largest area on Gifford Guyot (Table 5.4). They occur on all of the guyot flanks (Fig. 5.20). They cover an area of 238 km² or 20% of the total area (Table 5.4). They extend outwards from the protuberances of the plateau, and they separate segments containing debris slopes and valleys on the flanks (Fig. 5.23). The largest spur occurs on the eastern flank and is 12 km wide, 4.5 km long with slopes of 13-18° (Fig. 5.23).

5.2.1.4. Submarine Fan

Submarine fan features cover the fourth largest area on Gifford Guyot (Table 5.4). They occur at the base of the slump scars on the south and northeast flanks of the guyot (Fig. 5.20). They cover an area of 95 km² or 8.0% of the total area. The morphology of the submarine fans reveals them to be relatively smooth gently sloping features comprising interfingering or coalescing fans (Fig. 5.24). The largest fan occurs on the south margin and is 12 km wide and 6 km long, with an average surface slope of 1.3° (Fig. 5.24). By comparison, the fan on the northeast margin is 8.7 km wide and 5.9 km long, with an average slope of 2.2°.

5.2.1.5. Slump Scar

Slump scar features cover the fifth largest area on Gifford Guyot (Table 5.4). They occur on the north, northeast and southeast flanks and cover an area of 46 km² or 3.8% of the total area (Fig. 5.20; Table 5.4). Slump scars are erosional features that are recessed into the guyot flanks by up to 2 km and generally extend from the margins of the plateau down to the base of the guyot. They are characterised by a sharp rim with steeper slopes than other features on the guyot flanks (Fig. 5.25). The largest slump is 4.2 km wide and 10.9 km long, with an average slope of 10°, although slopes can locally attain >60° at the top (Fig. 5.25). The smallest slump is 2.2 km wide and 3.1 km long, with an average slope of 20° and maximum slopes of up to 28° locally near the top.

5.2.1.6. Ridge

Ridge features cover the fourth smallest area on Gifford Guyot (Table 5.4). Three distinct ridges form a semi-continuous chain on the west and north margins of the top of the guyot and cover a combined area of 24 km² or 2.0% of the total area (Fig. 5.20; Table 5.4). All three ridges form a broad rise with irregular sides and top. The largest ridge is 8.9 km long and 3.1. km wide and attains 30 m in height (Fig. 5.26). The flanks of this ridge have slopes ranging between 1° and 2.5° with an average of 1.7°. The next biggest ridge is 3.3 km long and 2.8 km wide and attains a height of 25 m, with slopes ranging from 0.6° to 2.5° and an average of 1.6° (Fig. 5.26). The third and smallest ridge is 2.6 km long, 1.3 km wide and

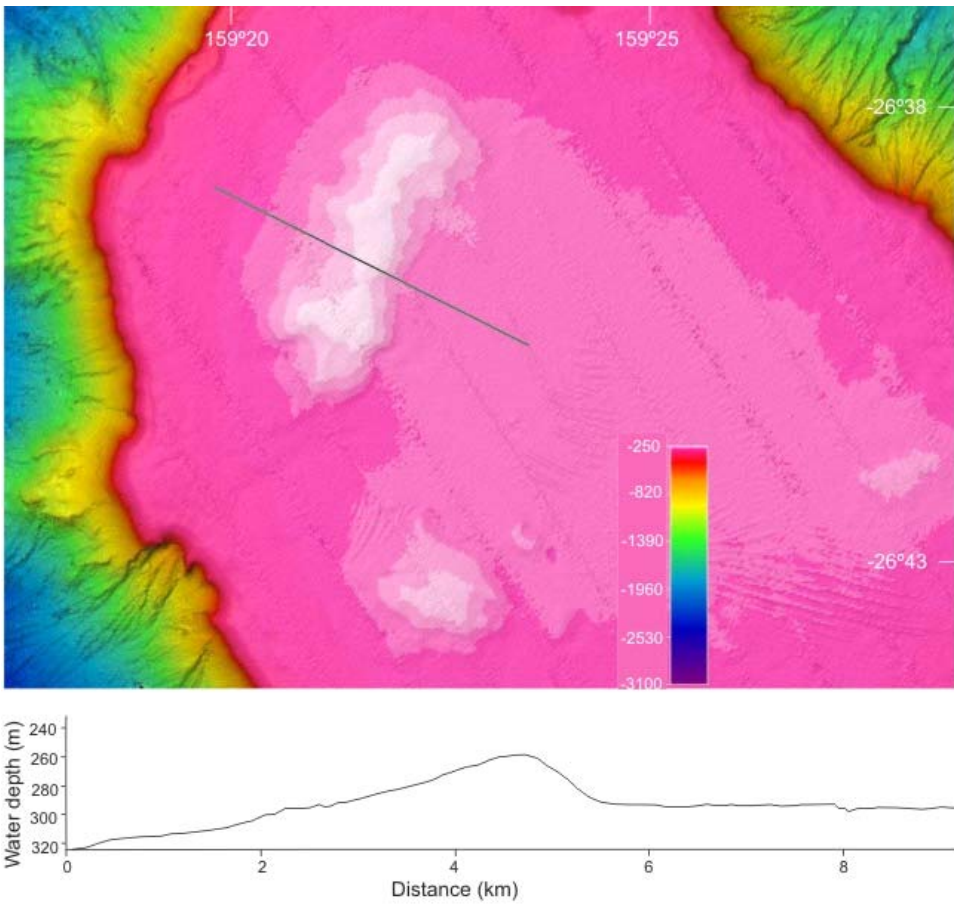

Figure 5.22. Multi-beam (swath) sonar bathymetry image showing an example of an extensive plateau surface. The plateau can be divided into two morphologically different regions: an inner region characterised by a relatively low-gradient, and a steeper-gradient outer region. The margin of the plateau is scalloped showing extensive erosion.

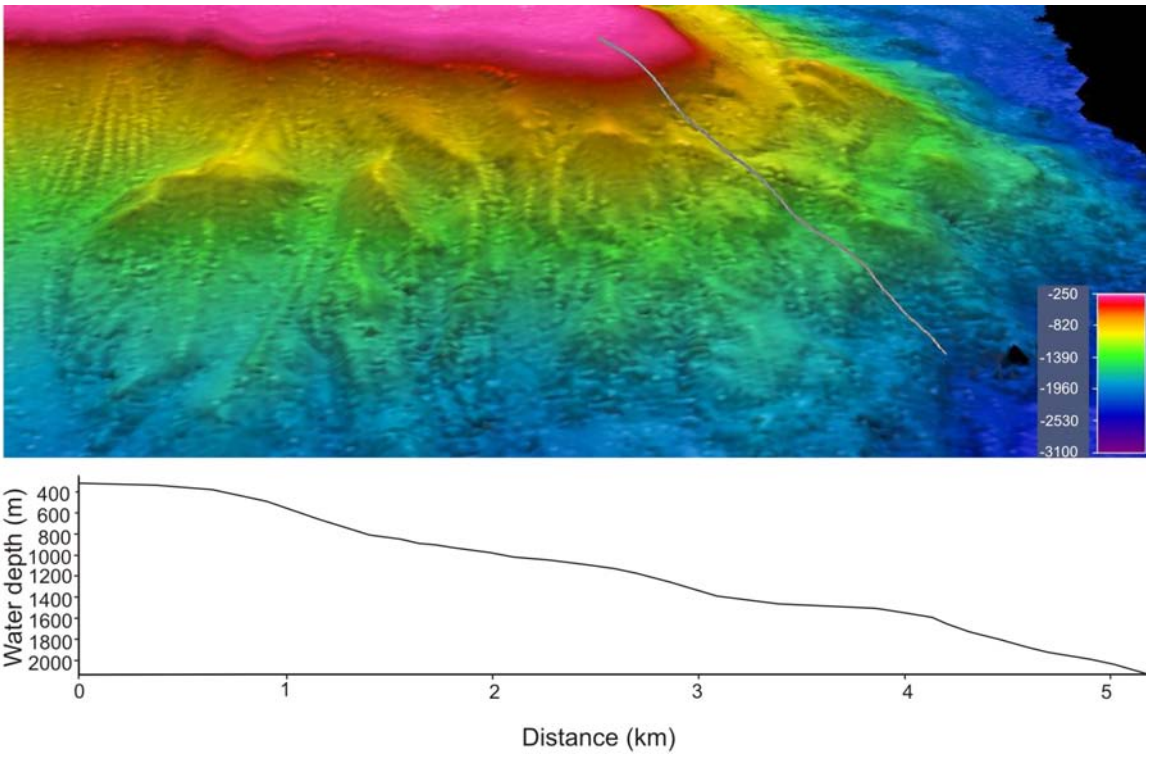

Figure 5.23. Oblique multi-beam (swath) sonar bathymetry image showing an example of a spur on the eastern flank of Gifford Guyot. Spur features separate the debris slopes and occur on all of the guyot flanks (vertical exaggeration 1x).

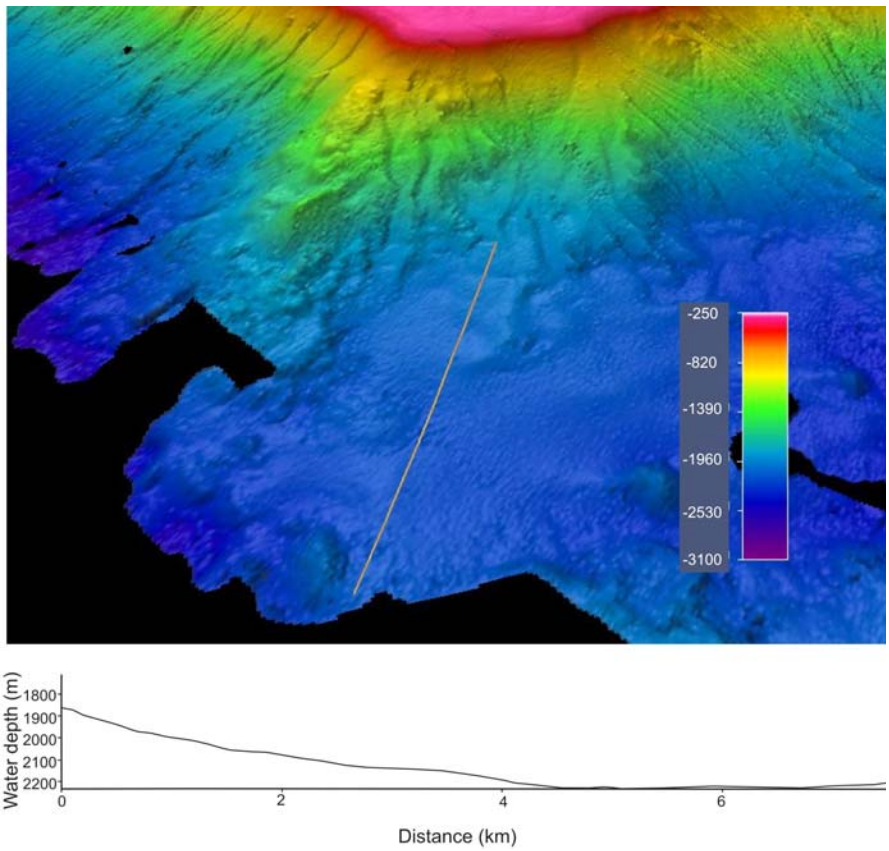

Figure 5.24. Oblique multi-beam (swath) sonar bathymetry image showing an example of a submarine fan feature on the southwest flank of Gifford Guyot. The submarine fans are relatively smooth gently sloping features comprising inter-fingering or coalescing fans (vertical exaggeration 1x).

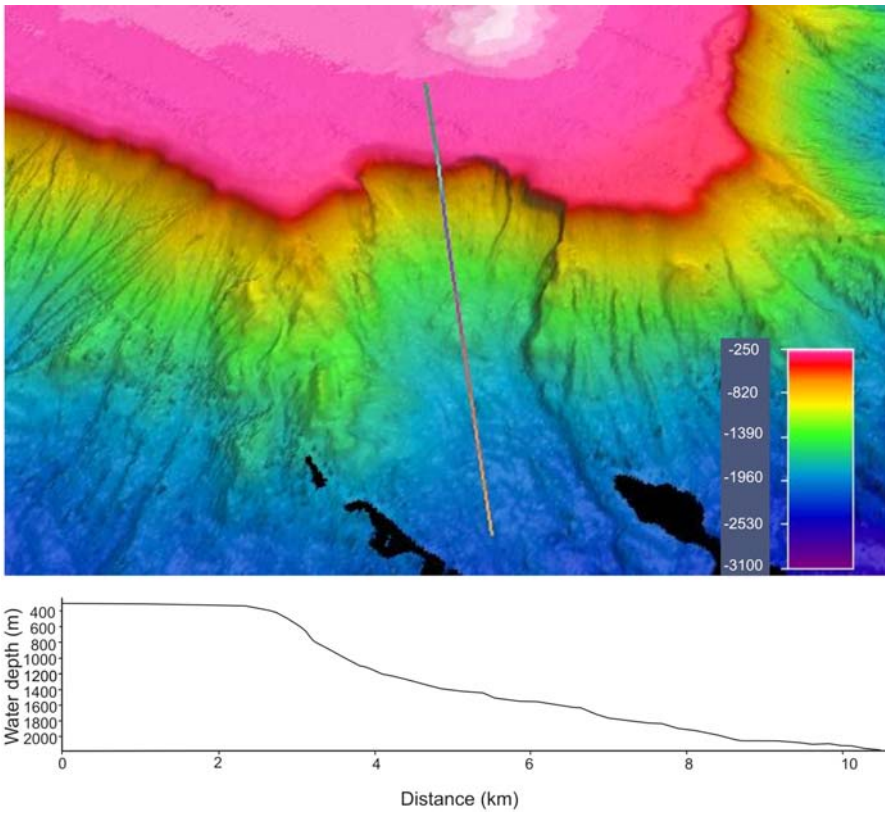

Figure 5.25. Oblique multi-beam (swath) sonar bathymetry image showing an example of a slump scar feature on the northern side of Gifford Guyot. Slump scars are erosional features that are recessed into the guyot flanks by up to 2 km and generally extend from the margins of the plateau down to the base of the guyot (vertical exaggeration 1x).

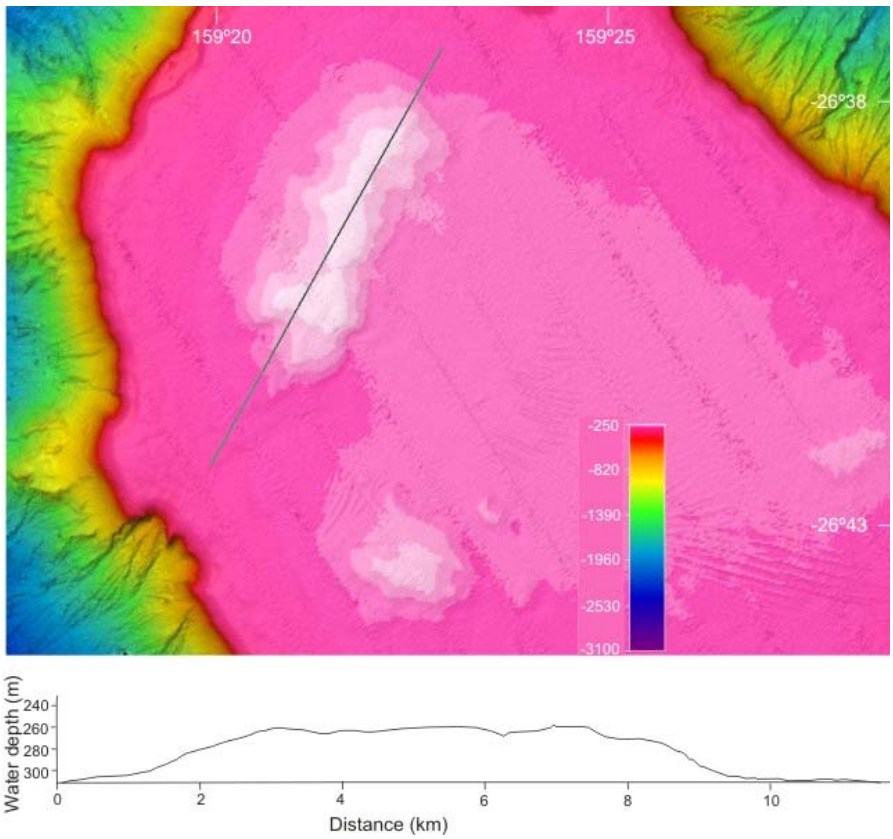

Figure 5.26. Oblique multi-beam (swath) sonar bathymetry image showing an example of a ridge feature on Gifford Guyot. Each of the three ridges on the summit of Gifford Guyot forms a broad rise with irregular sides and top.

attains 10 m in height. The flanks of this ridge have slopes of between 0.8° and 1.2° with an average of 1.0°.

5.2.1.7. Subaqueous Dune Field

The subaqueous dune field comprises three distinct fields containing dunes of different sizes, forms and orientations. Combined, the dune fields cover the third smallest area on Gifford Guyot with a combined area of 18 km² or 1.5% of the total guyot area (Table 5.4; Fig. 5.20). The largest dune field comprises E-W oriented, 1-5 m high, sinuous-crested dunes that cover an area 5.6 km long by 2.6 km wide. Dune wavelengths in this field range between 150 m and 300 m. The steepest (lee) side of each dune is located on the northern face with slopes from 3.5° to 4.9° (Fig. 5.27). Stoss faces to the south range in slope from 1.5° to 2.2°. The medium-sized dune field comprises SE-NW oriented, 1-4 m high, sinuous-crested dunes that cover an area of 3.8 km long and 1.8 km wide. Dune wavelengths range from 90 m to 350 m. The northwest lee slopes range from 1.5° to 3.1° and the southeast stoss slopes range from 0.5° to 1.9°. The smallest dune field comprises NNE-SSW oriented, 0.3-2.0 m high sinuous-crested dunes that cover an area of 1.7 km long and 1.0 km wide. Dune wavelengths range from 150 m to 210 m. Both the lee and stoss faces have slopes between 2.0° and 3.6°.

5.2.1.8. Valley

Valley features cover the second smallest area on Gifford Guyot with a combined area of 13.5 km² or 1.1% of the total area (Table 5.4; Fig. 5.20). They occur as broad depressions on the flanks that generally extend from the plateau down to the base of the guyot. The longitudinal profiles of the valleys display a decrease in overall slope with depth. Slopes at the head of the valley features are typically between 24° and 27° while at the base of the guyot the slopes range between 5° and 12°. Three large valleys were identified on Gifford Guyot (Fig. 5.28).

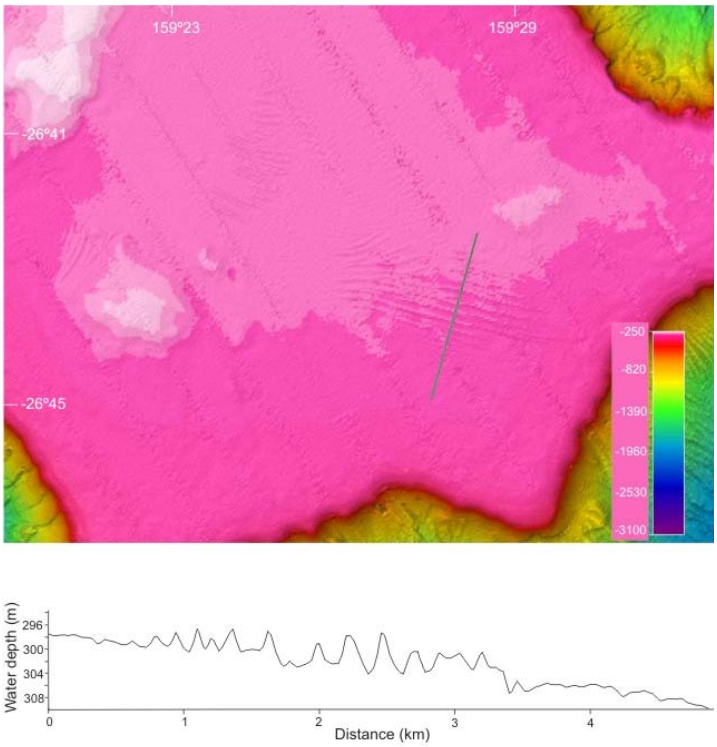

Figure 5.27. Oblique multi-beam (swath) sonar bathymetry image showing an example of the subaqueous dune field. The sinuous-crested dunes are relatively symmetrical in cross-section. Samples from the dunes reveal them to be composed of partially-cemented carbonate sand and gravel, and thus probably inactive.

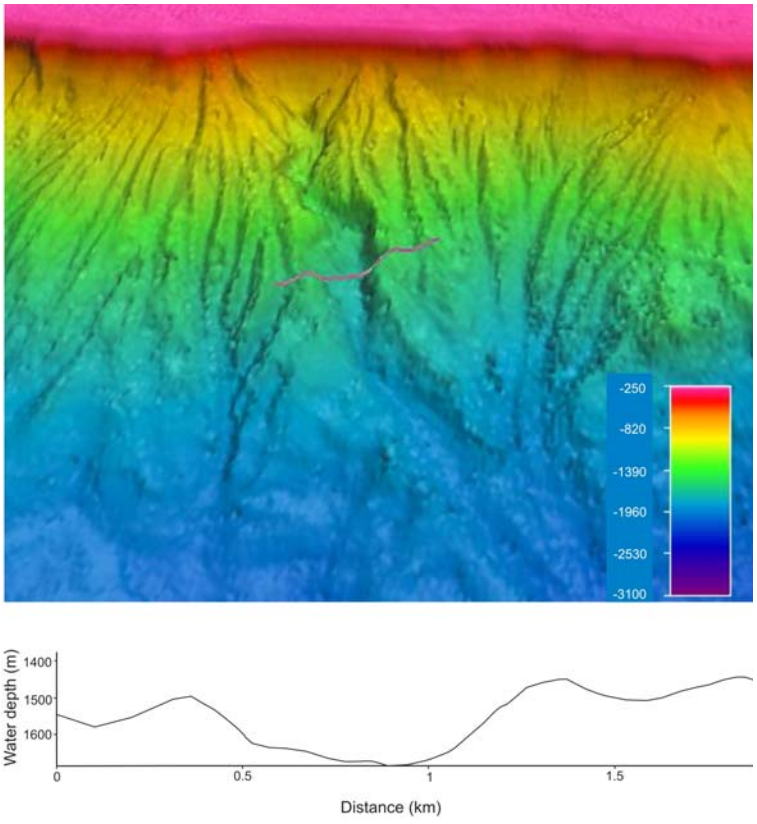

Figure 5.28. Oblique multi-beam (swath) sonar bathymetry image of a valley feature on the northeastern flank of Gifford guyot. They occur as broad depressions on the flanks that generally extend from the plateau down to the base of the guyot.

The largest occurs on the northeast margin and is 8.9 km long, 1.0 km wide, and up to 250 m deep. The largest valley is located on the northwest margin and is 5.9 km long, 1.2 km wide, and up to 160 m deep.

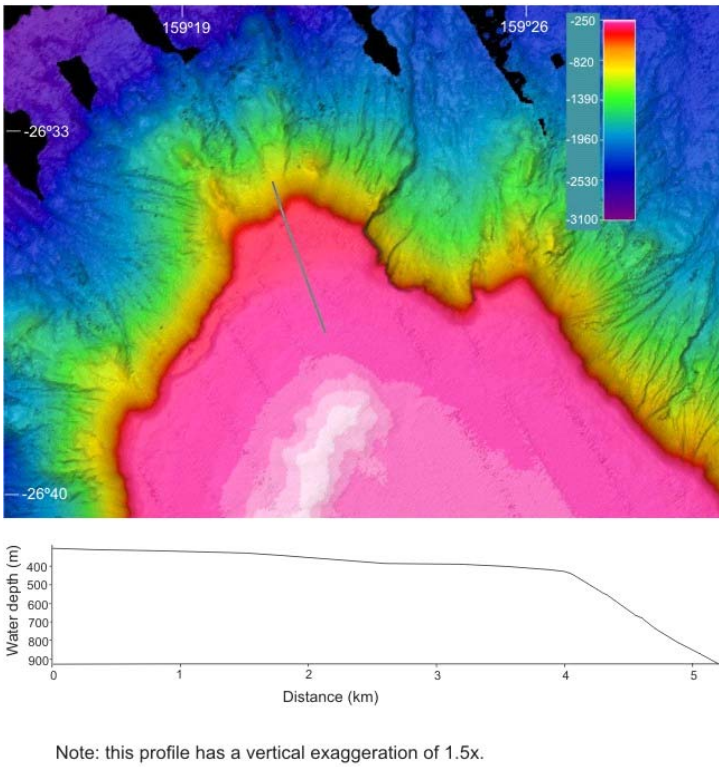

Figure 5.29. Multi-beam (swath) sonar bathymetry image showing an example of a terrace feature. They consist of sub-horizontal surfaces at slightly deeper water depths on the margins of the guyot plateau.

5.2.1.9. Terrace

Two terrace features were identified on Gifford Guyot, and with 9.8 km² these features cover the smallest area (Fig. 5.20; Table 5.4). The largest terrace consists of a sub-horizontal surface between 380 m and 395 m water depth on the northwest margin of the guyot (Fig. 5.29). A second very small terrace also occurs at similar depths on the eastern margin. Surface slopes on the terraces range from 1.2° to 3.1°. Beyond the terrace, the upper flanks of the seamount have slopes of >20°.

5.2.2. Slope

An analysis of slope on Gifford Guyot reveals a negative correlation between seabed slope and the area covered (Fig. 5.30; Table 5.5). The dominant surface slope is between 0–2.8° with the highest slopes between 47° and 78° occupying only 2.6 km² or 0.13% of the total area. The distribution of slope classes also closely matches the distribution of geomorphic feature classes, with each class having a discrete range of slope values (Table 5.4). Plateau slopes are all within the range 0–2.8°, and spurs are within the ranges of 11.6–16.6° and 29.5–35.9° (yellow and light blue ranges, respectively). Spurs are characterised by steeper slopes than adjacent debris slopes. The slump scar features are also well characterised with the steepest slopes recorded of 47.3–78.2° (dark blue). The relatively steep side walls of the valleys are also evident, ranging from 24.9–35.9° (light blue). The outwash fan geomorphic features display much lower slope values, similar to the plateau, and are in the range 11.7–35.9° to less than 7.1° at the base of the guyot. The seabed surrounding the guyot, especially to the north of Gifford Guyot, is relatively flat with slopes of less than 2.8°.

5.2.3. Plan Curvature

An analysis of the plan curvature of Gifford Guyot helps reveal the rugose nature of the seabed and clearly defines the valleys, fans and slump scars on the flanks (Fig. 5.31). These

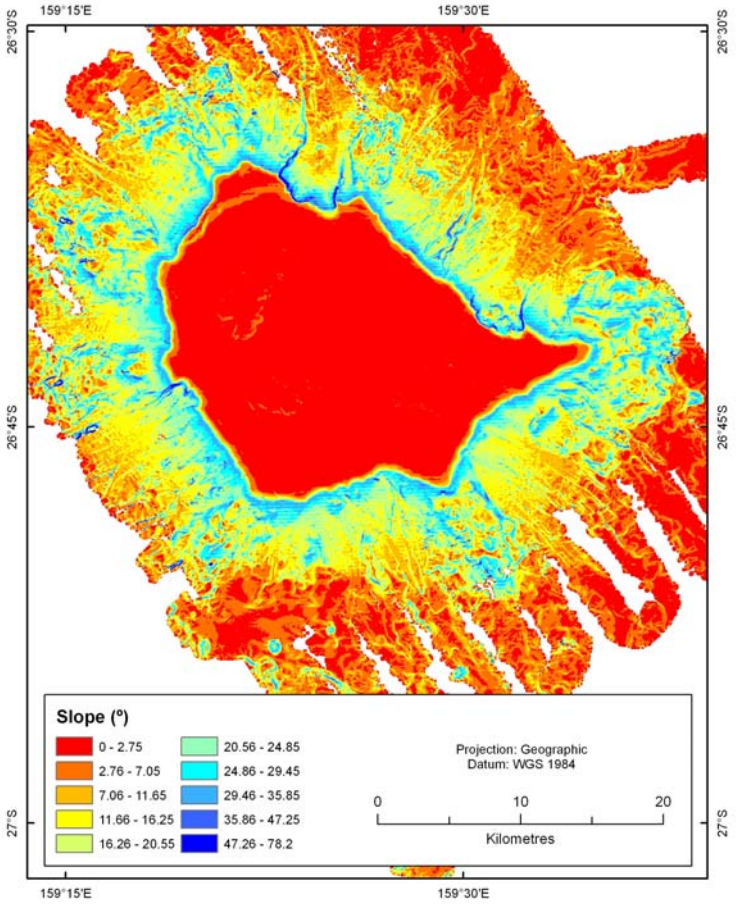

Figure 5.30. Map showing distribution of seabed slope for study area B over Gifford Guyot. The distribution of slope classes closely matches the distribution of geomorphic features, with each class having a discrete range of slope values.

Table 5.5. Slope classes for Gifford Guyot.

Slope class (°)	Area (km^2)	Area (%)
0–2.8	730.6	37.1
2.9–7.1	366.9	18.6
7.1–11.7	234.3	11.9
11.7–16.3	202.6	10.3
16.3–20.6	161.9	8.2
20.6–24.9	123.5	6.3
24.9–29.5	90.3	4.6
29.5–35.9	48.2	2.5
35.9–47.3	8.5	0.4
47.3–78.2	2.6	0.1

features are characterised by the light blue colours while the convex features of ridges, debris slopes and spurs are characterised by the purple colours. Features of low relief (and thus curvature) like the plateaus and terraces are characterised by the dark blue colours. The interfingered nature of the debris slope features is apparent with the intersection of multiple convex ridge features on all flanks. The majority of these features also extend from a single ridge feature that extends from the plateau edge, thus forming a "splayed" pattern. Plan curvature also highlights differences between debris slope and spur features, with the spurs displaying a less distinct pattern of valleys and ridges.

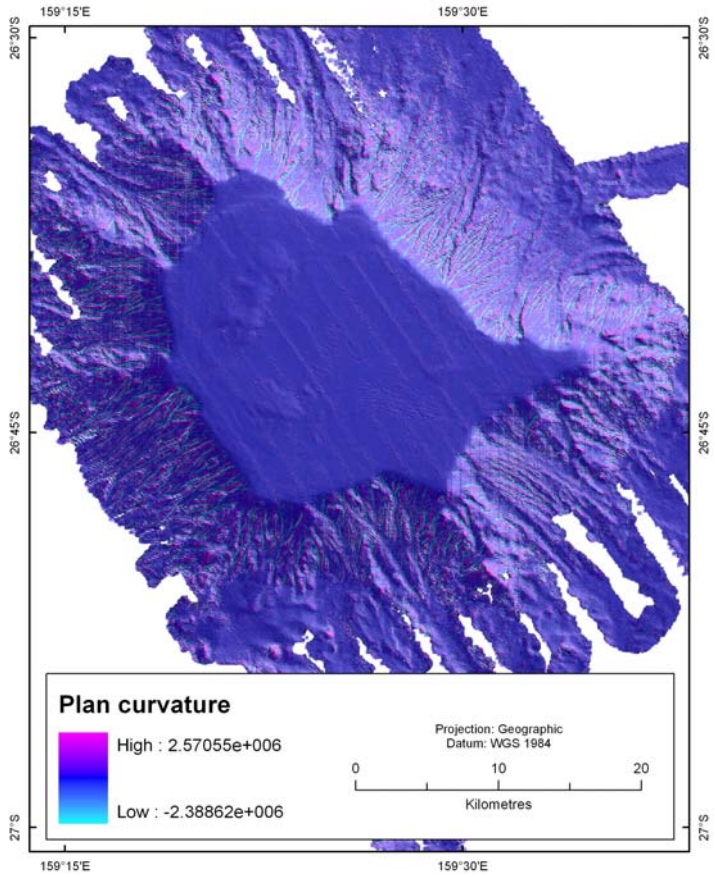

Figure 5.31. Map showing the plan curvature of the seabed for study area B over Gifford Guyot. Concave features like valleys and slump scars are characterised by the light blue colours, while the convex features of ridges, debris slopes and spurs are characterised by the purple colours. Features of low relief (and thus curvature) such as the plateaus and terraces are characterised by the dark blue colours.

5.2.4. Hypsometric Analysis

Hypsometric analyses were carried out for the entire Gifford Guyot and for each of the geomorphic features (Fig. 5.32a). The hypsometric curve for the overall geomorphology of the guyot is dominated by a prominent peak (9.2%) encompassing water depths of between 300 m and 375 m corresponding to the extensive plateau, ridge and subaqueous dune features. A second peak (2.9%) occurs between 2,000 m and 2,800 m, which covers the largest surface area (52.8%). This peak corresponds with spur, debris slope and outwash fan features. Water depths between 500 m and 2,000 m (particularly 500-1,000 m; 5.2%) are not characterised by peaks in the hypsometric curve, and consequently these depths are characterised by the highest slopes and smallest areas. A small step in the curve is evident at water depths between 375 m and 400 m which probably represent the terrace features.

5.2.4.2. Geomorphic Feature Comparisons

Comparison of the hypsometric curves for six of the individual geomorphic features on Gifford Guyot reveals that features on the flanks display very similar curves, except for the submarine fan features (Fig. 5.24). This is because these features all extend from the plateau to the base of the guyot. They are also predominantly erosional with lower surface area values at shallower depths (<1,500 m). The prominent peak at <500 m water depth corresponds to the plateau, ridge and subaqueous dune features which are not considered on this graph.

Comparison of the hypsometric curves for the plateau, ridge, subaqueous dune and terrace features (Fig. 5.32b) reveal that the first three peak at similar water depths (300 m).

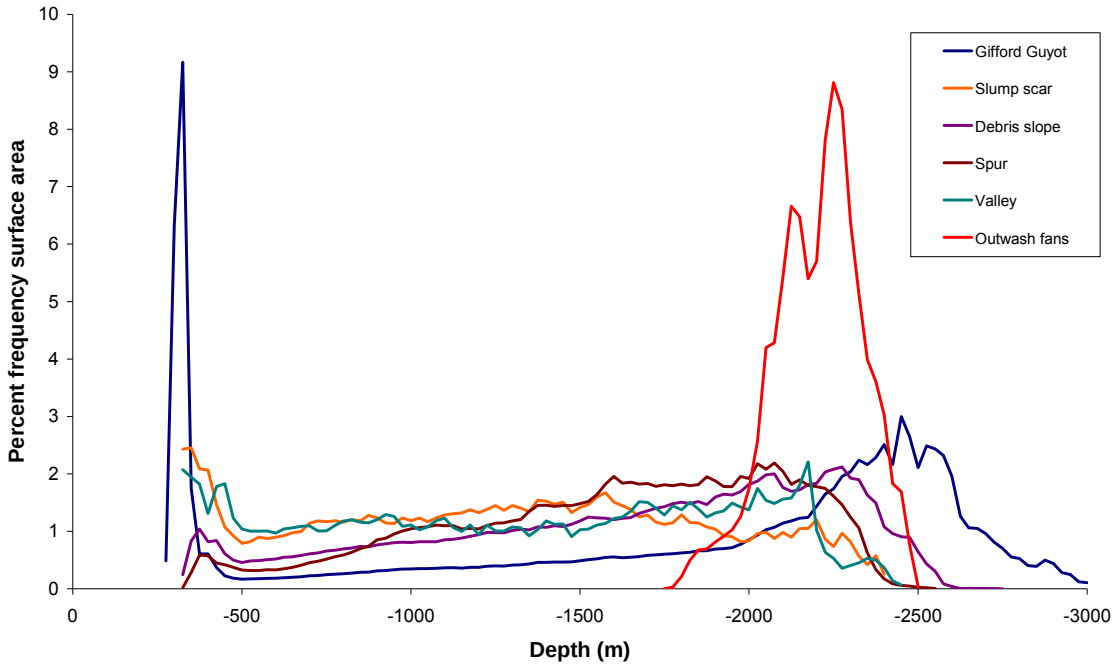

(a)

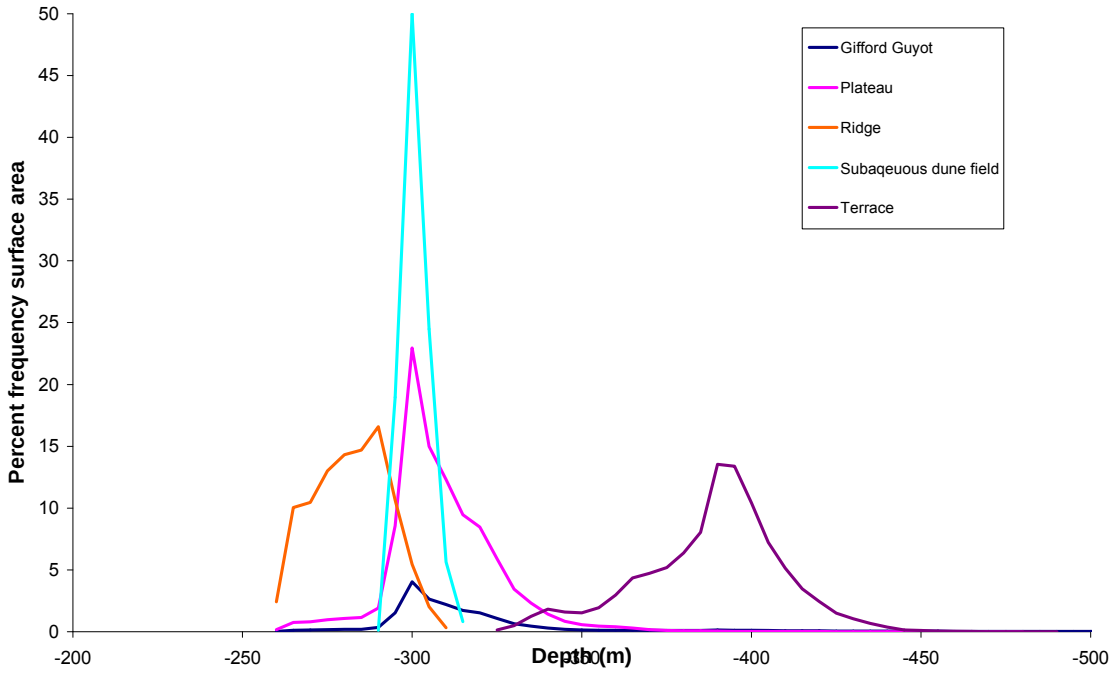

(b)

Figure 5.32. Hypsometric curves for geomorphic features on (a) the flanks and (b) summit of Gifford Guyot. The overall curve for the guyot is also shown for reference. Apart from the extensive flat-topped summit on the general curve for the guyot, other prominent peaks correspond with spur, debris slope and outwash fan features on the flanks and subaqueous dunes and terrace features on the summit.

An increase in the surface area at 300 m water depth corresponds to a decrease in the size of the feature (i.e., the dune fields are the smallest feature compared to the plateau but have the largest percent surface area at this depth). The hypsometric curve for the ridge features peaks at shallow water depths due to their greater height (up to 30 m) above the plateau surface. Conversely, the hypsometric curve for the terrace features peaks at a deeper water depth (390 m), but overlaps the plateau curve illustrating its position on the margins of the plateau. The curve for the subaqueous dune field should be treated with caution as it contains only six data points.

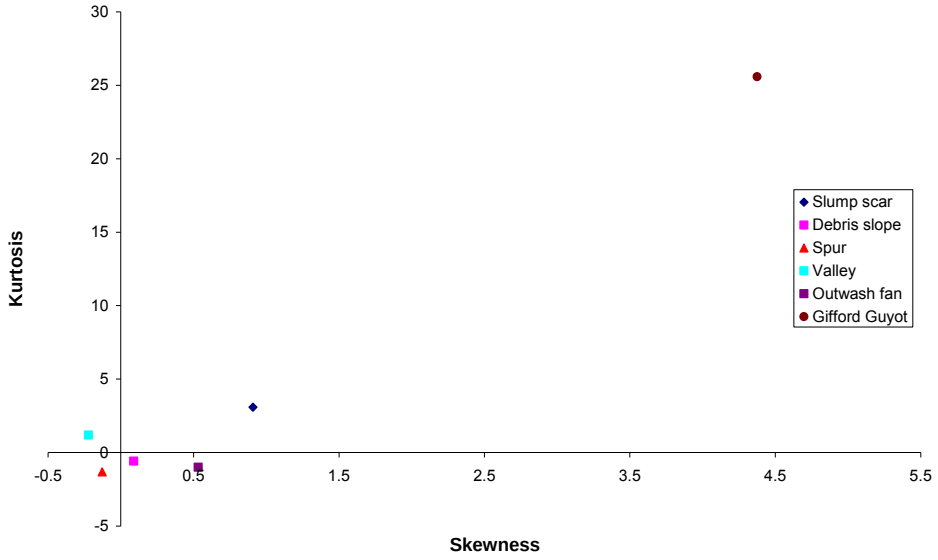

(a)

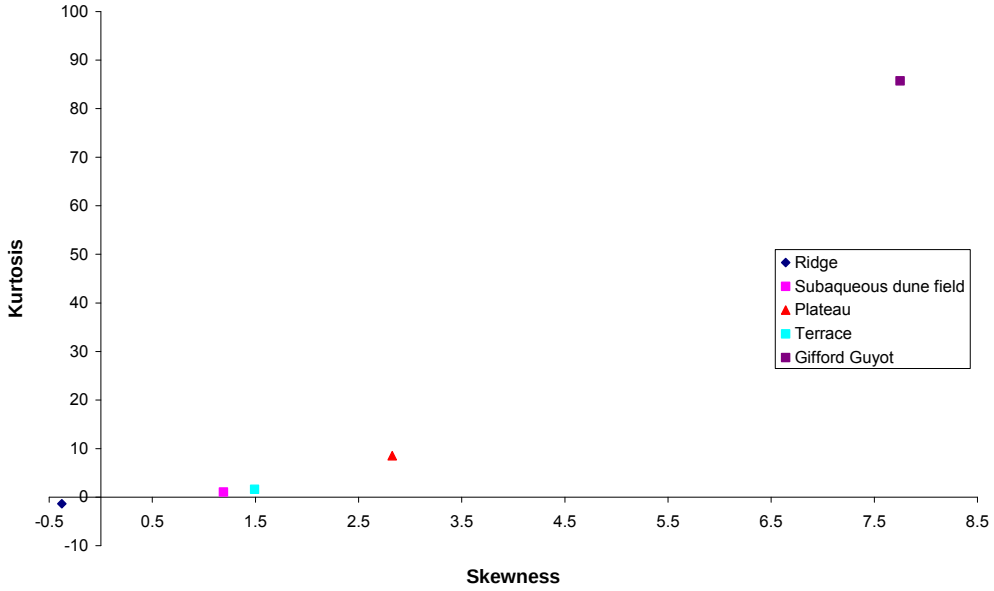

(b)

Figure 5.33. Graphs showing relationship between kurtosis and skewness for geomorphic features on (a) the flanks and (b) summit of Gifford Guyot. The curves show a dominance of deeper water depths for all features on the guyot. The extensive summit of the guyot contributes to the leptokurtic curve for the whole seamount.

Table 5.6. Results of an analysis of skewness and kurtosis for Gifford Guyot and geomorphic features.

Feature	Skewness	Kurtosis
Debris slope	0.09	-0.59
Plateau	2.83	8.52
Spur	-0.13	-1.31
Submarine fan	0.53	-0.99
Slump scar	0.91	3.09
Ridge	-0.38	-1.36
Subaqueous dune field	1.19	1.06
Valley	-0.22	1.19
Terrace	1.49	1.60
Gifford Guyot	4.38	25.59

NB: Skewness: 0.1 to -0.1 = near normal (symmetric) distribution, >0.1 = right skewed, <-0.1 = left skewed. Kurtosis: positive = leptokurtic, negative = platykurtic.

Table 5.7. Area of stable and unstable habitats on Gifford Guyot as defined by geomorphic features.

Environment	Feature(s)	Area (%)
Stable	Plateau Submarine fan	39.9
Unstable	Debris slope Valley Slump Scar	37.3
Mixed	Ridge Terrace Spur	22.8

An analysis of skewness and kurtosis reveals that the hypsometric curves for Gifford Guyot and five of the geomorphic features (subaqueous dune field, plateau, terrace, slump scar, outwash fan) are strongly right skewed and leptokurtic (excessively peaked) (Figs. 5.33a-b; Table 5.6). These curves show a dominance of deeper water depths. The extensive summit of the guyot contributes to the leptokurtic curve. The curve for the debris slope feature is relatively symmetrical and platykurtic (deficiently peaked). The characteristics of this curve are a result of the debris slopes occupying a very wide range of water depths. Curves for two features (spur, valley) are left skewed and the curve for the ridge geomorphic feature is strongly left skewed.

5.2.5. Habitat Stability

Geomorphic features on Gifford Guyot can be broadly divided into two main types: erosional and depositional. Although the timing of this erosion or deposition is unknown, this broad categorisation of features allows us to tentatively define habitat types on the guyot in terms of stability. Habitat stability provides a coarse measure of how likely the habitat is to change, with erosional features relatively unstable and depositional features relatively stable.

Unstable habitats (i.e., erosional features) are likely to be debris slope, valley, and slump scar features. Plateau and submarine fan features are stable features. The subaqueous dune field has been defined as stable as their appearance, sample and video data suggest that they are no longer active. Ridge, terrace and spur features are most likely a mix of both stable and unstable habitats. Interestingly, the relative abundance (by per cent area) of stable and unstable habitats on Gifford Guyot is similar, with slightly less mixed environments (Table 5.7).

Intuitively, stable habitats offer conditions that may result in better developed ecosystems and habitats. Unstable habitats provide conditions where it is more difficult for organisms to establish and the ecosystems are likely characterised by a different suite of organisms adapted to rapid changes.

6. Sedimentology

This chapter presents findings from the textural and compositional analyses of seabed sediments sampled from study area A over the Capel and Faust basins and study area B over Gifford Guyot.

6.1. SEDIMENTOLOGY

A total of 23 samples were collected over the Capel and Faust basins and 10 samples from the summit and sides of Gifford Guyot. Two additional samples were collected during transit to the survey area at sites of basement outcrop on the LHR. Sedimentology of the surface sediment was derived from benthic sled, grab, boxcore and piston core samples (Tables 3.4-3.7).

For study area A, 17 samples are classified as sandy mud with the other six samples classed as muddy sand (Table 6.1). Mean grain size ranges from 9 to 47 μm (moment mean), equating to medium to very coarse silt. All samples are very poorly sorted and have grain size distributions that are trimodal (19 samples), bimodal (3 samples) or polymodal (1 sample) (see Appendix G). Bulk calcium carbonate content ranges from 88 to 94 percent, with calcareous material including foraminifers and other nannofossils that have formed stiff, dewatered deposits.

The 23 samples from study area A represent a range of geomorphic features, including ridges, peaks, holes, a plain and a valley (Table 6.1). Within this sample set, the slightly coarser grained sediments (muddy sands) occur on peaks, within a valley, on small ridges and holes. However, this is not a consistent pattern as other peaks, ridges and holes are characterised by sandy mud. Overall, there is no clear relationship between sediment type and geomorphic setting within the Capel and Faust basins survey region.

The seven sediment samples from the summit of Gifford Guyot range from muddy sand to gravelly sand, with sand the dominant grain size class (Table 6.2). Mean grain size ranges from 213 μm (fine sand) to 615 μm (coarse sand). All the summit samples are poorly to very poorly sorted, but the majority (6 samples) have a unimodal grain size distribution (see Appendix G). In contrast, the three samples collected from the sides of Gifford Guyot are muddy sand to sandy mud, with mean grain size of 24 to 40 μm (i.e., coarse to very coarse silt). These samples are very poorly sorted and have trimodal distributions. Bulk carbonate content ranges from 89 to 96 percent, with the three samples from the sides of the seamount having the slightly lower values (i.e., 89-91%). Compositionally, the sand fraction of all Gifford Guyot samples includes foraminifers, bryozoans, shell fragments and sponge spicules, plus fragments of limestone in one sample (station 36) from the summit.

Additional qualitative information on the properties of seabed sediments in the survey area is available from photographs taken with underwater towed video at each sample station. Representative photographs of geomorphic features are shown in Figure 6.1. These images reveal that volcanic peaks, some small ridges and holes are characterised by rocky outcrops, boulders, cobbles and discontinuous sediment cover (Figs. 6.1a-j). In contrast, sediment cover is continuous and generally smooth across plains, valleys, larger ridges, holes and slumps (Figs. 6.1k-u). Many images in these areas also show burrows and feeding/crawling trails, providing evidence that the surface sediments are unconsolidated (e.g., Figs. 6.1r,t,u), with induration of pelagic ooze noted at only one site (Fig. 6.1v). Evidence for physical disturbance of the seabed is also limited, with ripples and shallow scour pits only observed on the floor of some holes (Fig. 6.1w) and around some rocky outcrops on peaks (Fig. 6.1j). Seabed photos do not capture the polygonal crack network that

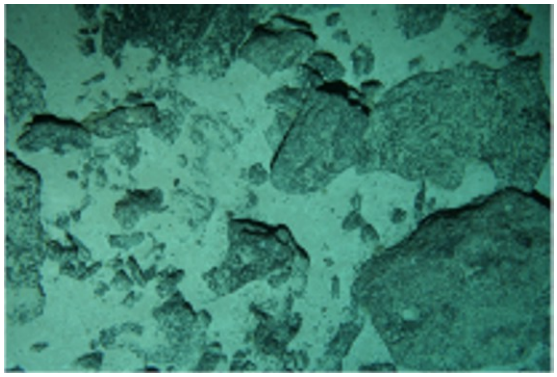

(a) Basalt cobbles and gravel with pelagic ooze on the peak at station 5 (frame 041)

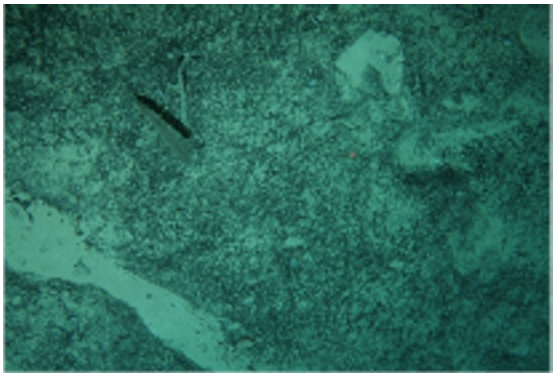

(b) Basalt outcrop on the peak at station 5 (frame 056)

(c) Basalt cobbles and gravel with pelagic ooze on the peak at station 17 (frame 010)

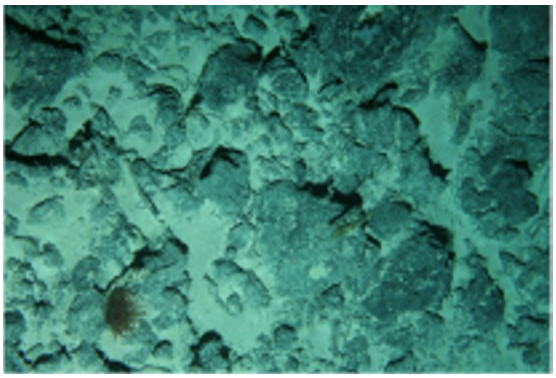

(d) Basalt cobbles and gravel with pelagic ooze on the peak at station 19 (frame 038)

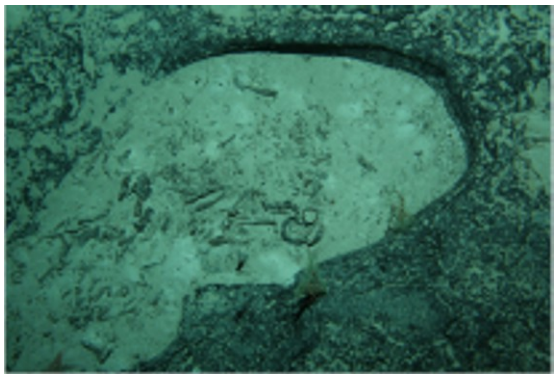

(e) Basalt outcrop and coral debris on the peak at station 32 (frame 086)

(f) Basalt cobbles and gravel with pelagic ooze on the small ridge at station 30 (frame 012)

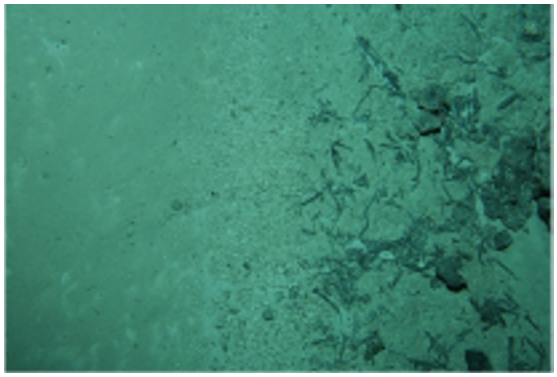

(g) Coral debris and manganese nodules on the small ridge at station 30 (frame 246)

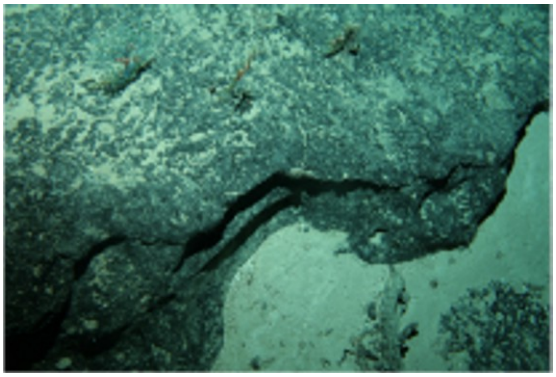

(h) Basalt outcrop and pelagic ooze on the small ridge at station 33 (frame 062)

Figure 6.1. Representative seabed photographs for geomorphic features in study area A over the Capel and Faust basins survey region. Station numbers are indicated. Photos are not to scale but most are taken about 1 m above the bed.

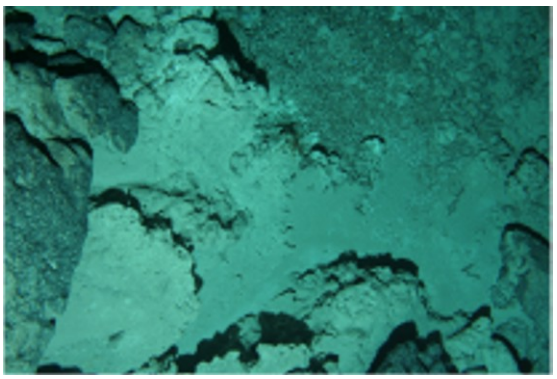

(i) Manganese concretions in the hole at station 20 (frame 130)

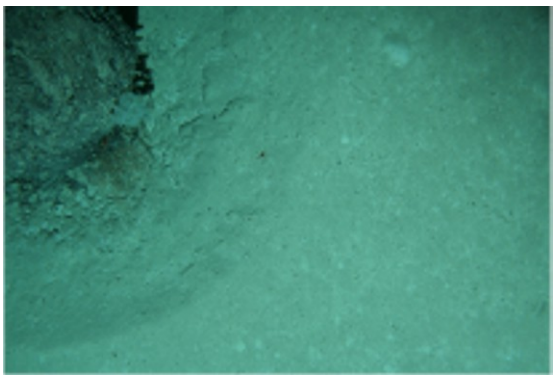

(j) Rocky substrate and localised scour in pelagic ooze in the hole at station 20 (frame 136)

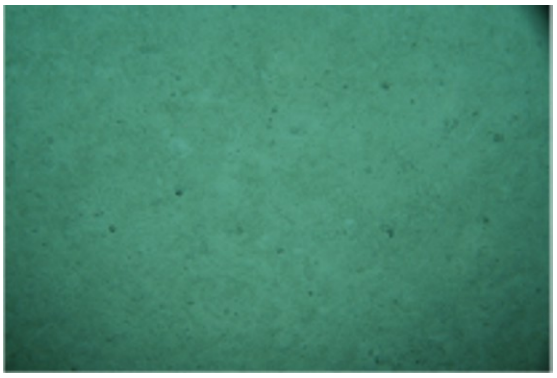

(k) Smooth pelagic ooze on the plain at station 43 (frame 008)

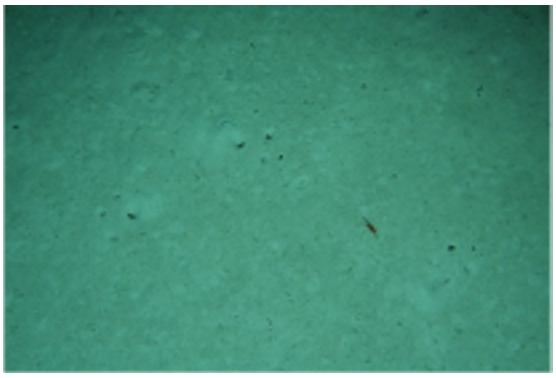

(l) Smooth pelagic ooze & burrows on the floor of the valley at station 9 (frame 026)

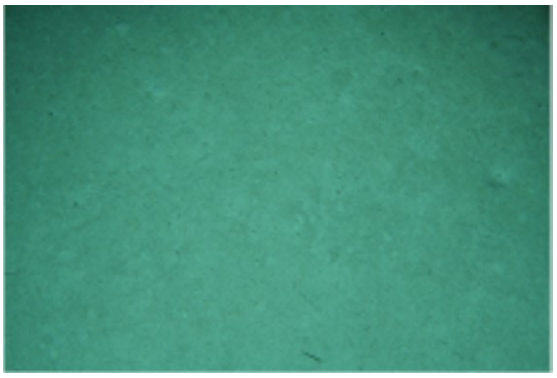

(m) Smooth pelagic ooze on the valley floor at station 10 (frame 025)

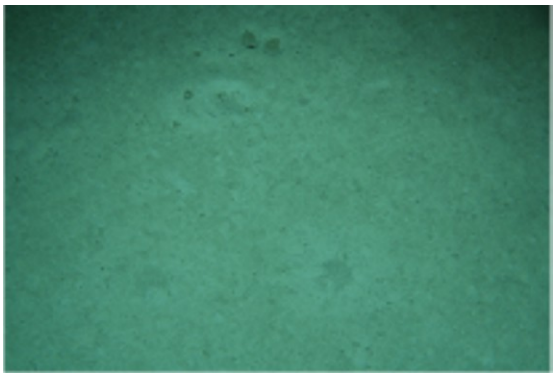

(n) Smooth pelagic ooze on the crest of the ridge at station 21 (frame 117)

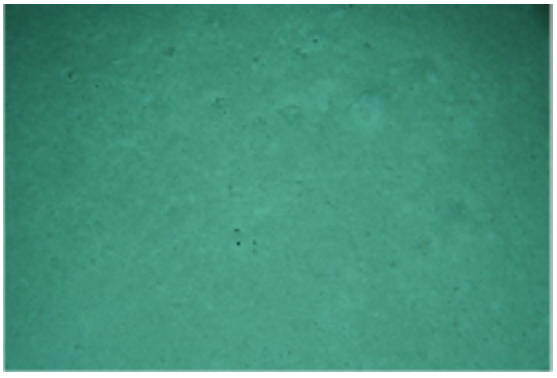

(o) Smooth pelagic ooze on the flank of the ridge at station 27 (frame 026)

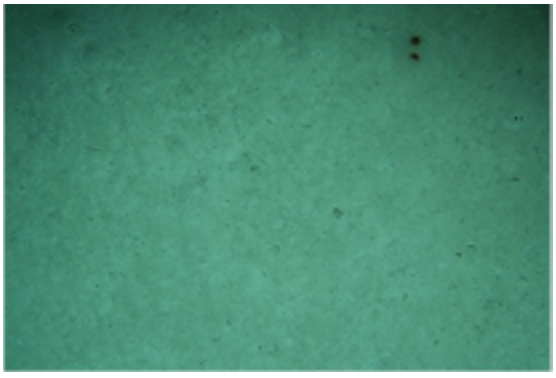

(p) Smooth pelagic ooze on the crest of a small ridge crest at station 12 (frame 023)

characterises the plain in the central to western part of the area. However, photos taken at several stations on the plain suggest that fluid escape is an active process in the formation of the cracks, evident as localised plumes of sediment-laden fluid rising from centimetre-sized vents in the seafloor (Fig. 6.1x).

Table 6.1. Summary statistics describing sediment samples collected from study area A over Capel and Faust basins. (Note: the two samples from LHR are from outside the main survey area).

Sample ID	Geomorphic Setting	Gravel (%)	Sand (%)	Mud (%)	Textural Classification	Mean Grain Size (μm)	Mud Fraction $CaCO_3$ (%)	Sand Fraction $CaCO_3$ (%)	Bulk $CaCO_3$ (%)
TAN0713/01DR01	Lord Howe Rise	3	86	11	Muddy sand	141	93.5	97.5	94.5
TAN0713/02DR02	Lord Howe Rise	0	71	29	Muddy sand	72	91.0	98.0	91.8
TAN0713/04BC01	Ridge crest	0	30	70	Sandy mud	14	91.6	95.7	90.7
TAN0713/06DR04	Valley	0	54	46	Muddy sand	28	94.4	96.9	92.5
TAN0713/08DR05	Ridge flank	0	27	73	Sandy mud	10	95.5	98.2	94.3
TAN0713/13BC02	Ridge crest	0	50	50	Sandy mud	20	96.6	96.9	91.8
TAN0713/14BS03	Ridge crest	1	40	59	Sandy mud	13	91.7	96.8	91.5
TAN0713/15BS04	Ridge flank	0	28	72	Sandy mud	10	94.8	0.0	90.7
TAN0713/16BC03	Hole	0	58	42	Muddy sand	22	97.8	97.2	91.7
TAN0713/18BC04	Hole	0	34	66	Sandy mud	16	86.9	95.6	94.3
TAN0713/20DR08	Ridge	0	66	33	Muddy sand	21	95.1	97.0	91.3
TAN0713/21BC05	Ridge crest	0	26	74	Sandy mud	13	93.9	96.8	92.6
TAN0713/22BS05	Ridge crest	0	27	73	Sandy mud	10	95.1	98.5	92.4
TAN0713/23BC06	Ridge crest	0	30	70	Sandy mud	13	95.1	97.7	91.8
TAN0713/24BC07	Ridge crest	0	37	63	Sandy mud	24	95.7	97.7	90.9
TAN0713/25GR01	Ridge flank	0	44	56	Sandy mud	18	95.7	94.1	92.4
TAN0713/26BC08	Ridge flank	0	28	72	Sandy mud	11	93.6	94.9	90.4
TAN0713/27BC09	Ridge flank	0	28	72	Sandy mud	11	95.3	94.6	91.5
TAN0713/29BC10	Plain	0	28	72	Sandy mud	9	87.1	96.9	88.5
TAN0713/30BC11	Small ridge	0	75	25	Muddy sand	47	90.8	97.1	92.3
TAN0713/30DR09	Small ridge	0	53	47	Muddy sand	14	90.8	96.4	90.6
TAN0713/31BC12	Peak	0	36	64	Sandy mud	16	79.6	97.0	90.9
TAN0713/32DR10	Peak	0	43	57	Sandy mud	20	92.3	98.0	91.7
TAN0713/33DR11	Peak	0	62	37	Muddy sand	40	92.1	97.0	91.8
TAN0713/42BS11	Plain	0	34	66	Sandy mud	14	90.9	98.1	89.9

Table 6.2. Summary statistics describing sediment samples collected from study area B over Gifford Guyot (seamount).

Sample ID	Geomorphic Setting	Gravel (%)	Sand (%)	Mud (%)	Textural Classification	Mean Grain Size (μm)	Mud Fraction $CaCO_3$ (%)	Sand Fraction $CaCO_3$ (%)	Bulk $CaCO_3$ (%)
TAN0713/34BS07	Seamount summit	5	94	1	Sand	359	I/S	98.5	96.4
TAN0713/34GR02	Seamount summit	14	84	3	Muddy sand	321	I/S	98.8	94.4
TAN0713/35GR03	Seamount summit	2	97	2	Sand	245	I/S	98.9	96.3
TAN0713/35BS08	Seamount summit	3	96	1	Sand	357	I/S	97.4	96.0
TAN0713/36DR12	Seamount summit	31	65	4	Gravelly sand	216	92.0	97.8	95.4
TAN0713/37BS09	Seamount summit	5	87	9	Muddy sand	213	89.0	96.2	93.7
TAN0713/38BC13	Seamount flank	0	49	51	Sandy mud	24	88.6	98.2	89.8
TAN0713/39BC14	Seamount flank	0	51	49	Muddy sand	32	90.7	98.4	89.1
TAN0713/40BS10	Seamount summit	10	90	0	Gravelly Sand	615	I/S	99.0	96.4
TAN0713/41BC15	Seamount flank	0	55	45	Muddy sand	40	90.5	96.4	90.7

I/S = insufficient sample for analysis.

7. Geochemistry

This chapter presents preliminary findings from geochemical analyses of seabed sediments sampled from study areas A and B. Further work is being undertaken to improve understanding of the geochemical systems of the Capel and Faust basins and to establish links with geomorphic, hydrodynamic and biological systems.

7.1. BACKGROUND

The overarching aims of the geochemistry component were to characterise seabed sediments in the vicinity of the Capel and Faust basins from a geochemical/biogeochemical perspective, and to explore the potential of geochemical surrogates for benthic biodiversity. The choice of methods and suite of parameters measured had to be constrained to fit in with the deep-sea petroleum exploration focus of the survey. As such, benthic chambers deployed on the seafloor, which are the state-of-the-art technology for measuring nutrient and carbon dioxide efflux from bottom sediments, could not be accommodated on the present survey and an alternative methodology was adopted.

The surrogacy problem was addressed from the perspective of the availability of carbon and limiting factors (nutrients and trace elements). The philosophy behind this comes from a study of grassland ecosystems by Harpole and Tilman (2007). Their results show that high nutrient abundance increases the productivity of a few species but causes an overall reduction in species richness. The reduction in species numbers occurs because an abundance of nutrients makes ecosystems more homogeneous. This reduces the number of niches and results in a few dominant species. Studies reviewed in Harpole and Tilman (2007) reached similar conclusions.

Carbon reactivity (quality, freshness) was assessed using core incubations and the Chlorin Index method developed by Schubert *et al*. (2005). Core incubation experiments measure the rates at which organic matter breaks down in the sediment to form dissolved CO_2 and nutrients over time. Carbon freshness and degradability are known to be coupled. Although it is assumed that the benthic flux is dominated by the most labile carbon phases, strictly speaking the benthic flux may also include a small component of more refractory phases (see the multiG model of Berner, 1980). The Chlorin Index is the ratio of the fluorescence intensity of a sediment sample extracted in acetone and subject to HCl treatment to that of the original sediment extract. It indicates the ratio of chlorophyll (and its degradation products) that could still be chemically transformed to phaeophytin to those that are chemically inert. The method was chosen because it compares well with sulphate reduction rates and degradation indices based on amino acid composition, and it is analytically straightforward (Schubert *et al*., 2005). Trace element ratios and the stoichiometry of metabolites in core incubation experiments are also used to deduce redox conditions, which are known to have a bearing on marine species composition and diversity.

Several extraction methods are used to characterise the metal concentrations of marine sediments, including: total HF digestion, partial extractions in dilute acids, and sequential extractions with multiple stages. In this case, the 1 M HCl extraction method developed by Snape *et al*. (2004) was used because it attacks the key labile phases (i.e., sorbed species and those found in association with Fe-Mn oxides, amorphous sulphides, labile organic matter and carbonates), which are most likely to influence biota. Extraction over 4 hours confers greater sensitivity in the differentiation of low levels of contamination from natural background levels (Snape *et al*., 2004). A sequential extraction scheme will be used to divide sediment P into its various fractions; at the time of writing this had not been completed.

Table 7.1. The different types of analyses conducted on the surface and shallow sub-surface sediment samples.

Study Area	Station	Sample	Bulk chem.	Porosity + bulk density	DOC	Sedimentology	Biomarkers	Incubation
Area A	02	DR02	Y	N	N	N	N	
	04	BC01	N	Y	Y	N	N	V+C
	06	DR04	Y	N	N	N	N	
	08	DR05	Y	N	N	N	N	
	14	BS03	Y	Y	Y	N	N	V
	15	BS04	N	N	N	Y	N	
	13	BC02	Y	Y	Y	N	N	V+C
	15	BC03	Y	Y	N	Y	N	V
	18	BC04	Y	Y	Y	N	N	V+C
	20	DR08	Y	Y	Y	N	N	V
	21	BC05	Y	Y	Y	N	N	V+C
	22	BS05	Y	Y	Y	N	N	V
	23	BC06	Y	Y	Y	N	N	V+C
	24	BC07	Y	Y	Y	N	N	V
	25	GR01	Y	Y	Y	N	N	V
	26	BC08	Y	Y	Y	N	N	V+C
	27	BC09	Y	Y	Y	N	N	V+C
	29	BC10	Y	Y	Y	Y	N	V+C
	30	BC11	Y	Y	Y	Y	N	V
	31	BC12	Y	Y	Y	N	N	V+C
	32	DR10	Y	N	N	N	Y	
Area B	33	DR11	Y	N	N	N	Y	
	34	BS07	Y	N	N	N	Y	
	35	GR03	Y	N	N	N	Y	
	36	DR12	Y	N	N	N	Y	
	37	BS09	Y	N	N	N	Y	
	38	BC13	Y	Y	Y	N	Y	V+C
	39	BC14	Y	Y	Y	N	Y	V+C

V = vial; C = core.

7.2. SAMPLE PROCESSING AND ANALYSIS

Surface and shallow (<0.20 mbsf) sub-surface sediments were sub-sampled for bulk sediment chemistry, porosity and bulk density, DOC, sedimentology, biomarkers, and vial and core incubations. The number and combination of analyses undertake were subject to the amount of sediment recovered (Table 7.1).

7.2.1. Porosity and Bulk Sediment Density

Three samples of wet sediment for porosity and bulk density analysis were collected from each boxcore by pushing a syringe into the undisturbed sediment surface to a depth of 0.02 m. The sediments were then ejected into pre-weighed 20 ml plastic vials and frozen for transport to Geoscience Australia. In the laboratory, the samples were weighed, freeze-dried, and then weighed again. Porosity was determined by dividing the volume of water (sample wet weight minus dry weight) by the volume of sample. Wet bulk density was determined by dividing the weight of the wet sample by the volume of the wet sample. Dry bulk density

was determined by dividing the weight of the dry sample by the volume of the dry sample. Volumes were corrected for seawater density in all cases.

7.2.2. TCO_2, Dissolved Oxygen and Nutrient Fluxes

7.2.2.1. Vial Incubations

Samples for vial incubations were collected from the range of different sample types (boxcore, pipe dredge, sled and grab; Table 7.1). Samples were obtained by completely filling six 85 ml Oakridge centrifuge tubes with bulk sediment. Immediately after collection, three of the sub-samples were placed in the core incubation unit and were incubated in the dark for 3-5 days at 3-4° C prior to sampling. The other three samples were centrifuged at 7,000 rpm for 5 minutes. Pore waters from each Oakridge vial were syringe-filtered (0.45 μM) into separate 3 ml Labco Exetainers. The samples were stored in the refrigerator prior to analysis. The samples were then analysed for dissolved inorganic carbon (DIC) using the equipment and procedures described above. Residual sediment was retained in the Oakridge vials and stored in the refrigerator. Sediments from the time = 0 vials were analysed for chemistry and mineralogy, dilute HCl extractable metals, and chlorin pigments.

7.2.2.2. Core Incubations Experiments

One sediment core designated for incubation was collected from each of the boxcores. The sediment cores (and overlying water) were collected by hand-pushing 84 mm diameter PVC tubes into the top of the boxcore sample. Once in the sediment, the core liners were sealed at the bottom with plastic plugs fitted with o-rings. Sediment depths of 0.12–0.21 m and water column heights of 60–95 mm were obtained in the core barrels. Gas-tight lids were used to seal the top of each core barrel. The lids were fitted on the underside with magnetic stirrers that were rotated by a second magnet on top of the lid driven by a small motor. The core incubations proceeded in darkness and at in-situ temperatures (3–4° C) for 3–5 days. The cores were allowed to equilibrate for 4–6 hours prior to initial sampling.

The dissolved oxygen concentrations of the overlying water were measured at approximately 4 hourly intervals using a HACH HQ40D metre and LDO Intellical probes. A single sample for nutrients (SiO_4^{2-}, NO_2^-, NO_3^-, NH_4^+ and PO_4^{3-}) and triplicate samples for di-nitrogen gas (N_2) and DIC were collected at the beginning (t_0) and end (t_1) of the incubations. The DIC samples were filtered through 0.45 μM disposable filters into 3 ml gas-tight containers (Labco Exetainer's), and stored in the refrigerator. Samples for N_2 analysis were collected in 12 ml Labco Exetainers. The lids of the Exetainers were stored in seawater prior to use. The sample containers were stored upside-down in plastic jars filled with seawater in the refrigerator. Water for dissolved nutrient analyses was syringe filtered through 0.45 μm filters into clean environmental grade HDPE bottles.

DIC was analysed with a AS-C3 DIC analyser (Apollo SciTech), which includes an infrared-based CO_2 detector (LiCor 7000). Certified seawater was used as a standard (A.G. Dickson, UC San Diego). The precision of the measurements was 0.1% and differences of 2 μmol l^{-1} were detectable on a background of 2,000 μmol l^{-1}. N_2 was measured using a Membrane Inlet Mass Spectrometer as described by Kana *et al*. (1994) with the following modifications. Gases were detected with a Balzers QMS422 quadrupole mass spectrometer and a water bath (±0.01° C) was used to stabilize sample temperature in the water line upstream of the membrane.

Analyses for FRP, NO_x , NO_3, and NH_3 were performed simultaneously using an automated LACHAT 8000QC flow injection system using methodology based on: a) ascorbic

acid reduction of phosphomolybdate for FRP (Standard Methods 2005–4500-P G, p. 4-156 to 4-157); b) cadmium reduction of nitrate to nitrite by diazotizing the nitrite with sulfanilamide and coupling with N-(1-naphthyl)ethylenediamine dihydrochloride for NO_x (Standard Methods 2005–4500-NO_3 I, p. 4-127 to 4-129); and c) production of the indophenol blue colour complex for NH_3 (Standard Methods 2005–4500-NH_3 H, p. 4-116 to 4-117). The frozen silica samples were left to equilibrate at ambient temperature for 3 days prior to analysis. Silica was analysed using an automated LACHAT 8000QC flow injection system. This is based on an automated procedure whereby the silica species reacts with molybdate at 37° C and pH 1.2 to form a yellow silicomolybdate complex. This complex is subsequently reduced with stannous chloride to form a heteropoly blue complex which is measured spectrophotometrically at 820 nm (Standard Methods 2005–4500-SiO_2 F).

7.2.3. Bulk Sediment Chemistry

7.2.3.1. Major and Element Oxides and Traces

Major and minor element concentrations were determined by x-ray fluorescence (XRF) using a modified version of Norris and Hutton's (1969) method, whereby no heavy absorber was added to the flux. The instrument used was a Philips PW2404 4 kW sequential spectrometer calibrated using a range of USGS and SARM (S. African Ref. Material) international standards. Approximately 1 g of ground sediment was combined with flux material and 0.5 ml of 20% $LiNO_3$ added. The mixture was then heated to 400° C for 10 minutes, followed by 1,100° C for a further 10 minutes, during which time a tablet of ammonium iodide was added. The resulting melt was then poured into moulds, cooled, and introduced to the XRF. Using this instrument and approach, detection limits for the element oxides were better than 0.006% (Table 7.2). The accuracy of the method was assessed by analysing a sample of MESS-3 standard reference material (Table 7.2).

7.2.3.2. Carbon and Nitrogen Isotopes (and Concentrations)

Sediments were analysed for $\delta^{15}N$, $\delta^{13}C$ and Total Nitrogen% (TN%) using a Thermo Finnigan Flash EA series 1112 interfaced to a Thermo Finnigan Conflo (II)I. The isotopic measurements were carried out on a Finnigan Mat 252 using ISODAT NT software. The Flash EA was operated using EAGER software. The oxidation furnace of the Flash EA was packed with copper oxide and silvered cobaltous oxide and operated at 900° C. The reduction furnace was packed with pure copper and operated at 600° C. Combustion products were separated on a packed GC column run isothermally at 40° C. Carbon and nitrogen analyses were carried out separately to improve reproducibility and accuracy. All analyses were carried out in duplicate or triplicate.

For carbon analysis, approximately 200 mg of ground dry (bulk) sediment was loaded into baked glass vials. Then 6% HCl was added, drop-wise, to the vials and was allowed to react with the sediment until effervescing stopped (at least 15 minutes). The samples were then dried for 1–2 hours in an oven at 100° C to drive off the acid. The acid addition and drying procedures were repeated a second time. The acidified sediments were then weighed into tin foil cups and placed in the auto-sampler along with a series of blanks and standards used for isotope correction. Standards ANU Sucrose and TO_2 were used along with caffeine for isotopic calibration. Water was removed from the gas stream using a 6 to 18 mesh Magnesium Perchlorate water trap.

For the nitrogen analysis, approximately 50 mg of ground dry sediment was loaded into tin foil cups. The mud grain size fraction (<63 μm) was used in this analysis because the

Table 7.2. Detection limits and accuracies of XRF analyses.

Analysis	Detection Limit (%)	Accuracy (%)
Al_2O_3	0.001	2.3
SiO_2	0.006	5.5
CaO	0.002	9.4
MgO	0.004	5.4
Fe_2O_3	0.002	4.8
TiO_2	0.002	1.8
Na_2O_3	0.004	10.8
K_2O	0.002	0.8
MnO	0.001	0.04
SO_3	0.001	N/A
As		5.6
Co		2.7
Cr	1.9	2.9
Cu	0.8	5.6
Ni	1.3	8.3
P		1.5
Sc	1.6	
Sr		0.05
V	2.8	7.8
Zn	0.5	6.3

TN% contents of the bulk samples were too low. The cups were placed in the auto-sampler along with a series of blanks and standards used for isotope correction and TN% calculation. International standards IAEA N1 and IAEA N2 were used along with caffeine. The caffeine was used as a secondary standard (it has been previously calibrated against international standards) and also to calculate TN%. Carbon dioxide was removed in all nitrogen analysis by passing the gas stream from the GC through a trap of Carbosorb AS Self Indicating Granules (BDH Prod # 331634T). Water was removed from the gas stream using a 6 to 18 mesh Magnesium Perchlorate water trap.

7.2.4. Dilute HCl Extractable Elements

HCl metal digests of sediment and MESS-3 standards were undertaken following the protocol of Snape *et al*. (2004). Prior to use, all glassware, sample tubes and bottles were cleaned in acid (10% Suprapur grade HCl) and Milli-Q water. Dilute acid extractions were prepared by mixing 20 ml of 1 M HCl and 1 g freeze-dried sediment in Sarstedt 30 ml polypropylene tubes. The accuracy of the Optifix dispenser was checked before use by dispensing and weighing a known volume. The samples were then rotated on an end-over-end mixer for 4 hours at room temperature. Following mixing, the samples were centrifuged at 2,500 rpm for 10 minutes. The samples were then filtered through 0.45 µm filters (Satorius, nylon medium) using a single use Terumo 50 ml syringe. The syringe and filter combination were rinsed/flushed with 2 x 2 ml aliquots of the extractant. The remaining solution was dispensed into the 30 ml HDPE Nalgene bottles sample bottles that had been pre-rinsed with ~3 ml of extractant. A sample blank (20 ml of 1 M HCl) and MESS-3 standard were the first and last two samples in the sample batch. Two samples were subject triplicate determination.

The HCl extracts were analysed by quadrupole ICP-MS at the University of Canberra. The ICP-MS was optimized before analysis, as follows: the plasma current was set to1,200 watts; the running vacuum was <2.00 x 10-5 Torr; the neb flow was set to 0.9 ml min^{-1} (oxides and doubly charged <2.5%); and the lens voltage set to 8.0 volts. Dual detector voltages were optimised to give maximum counts across the mass range. (All major interfering elements/compounds, i.e. Cl on V, Cr, As, Se, were checked and corrected for using the "Recommended practice for inductively coupled plasma spectrometry (ICP-MS)" Standards Australia standard, Appendix A as a guide). All major isotopes of the elements of interest (and potential interfering elements) were analysed by ICP-MS to assist with these corrections.

7.2.5. Chlorin Index

Chlorins and the chlorin indices were determined on surface sediments following the method of Schubert *et al*. (2005). Sediments were freeze-dried, homogenized and sub-sampled (40–50 mg). The sub-samples were extracted three times in 20 ml of 90% acetone by sonification (10 minutes) in clean glass vials that were heated to 450° C for 12 hours prior to use. After each extraction, the vials were centrifuged at 4,300 rpm for 5-10 minutes, and the supernatant was transferred to a new vial. Samples were kept in the dark and cooled with ice throughout the procedure to prevent the decomposition of the chlorins. Sediment extracts were measured using a fluorometer after extraction (Turner Designs 10-AU Fluorometer). The emission wavelength was 671 nm and the excitation wavelength was 428 nm. Chlorophyll-*a* was transformed to Phaeophytin-*a* by acidification with five drops of 30% hydrochloric acid. The Chlorin Index (CI) was calculated from the ratio of the chlorin concentrations of the acidified to non-acidified extracts. All samples were analysed in triplicate. The precision of the method, based on the triplicate samples was usually better than 5%.

7.3. RESULTS AND DISCUSSION

Porosity of sediment samples ranged from 60.3–80.4%, and had an average value of 73.9% (Table 7.3). These porosity values are comparable to those found on the deep western margin of Australia in carbonate sediments (Heap *et al*., 2008). Most dry bulk density values fell into a range that encompasses the average value for deep-sea calcareous oozes (e.g., 2.66; Burdige, 2006), calcite (e.g., 2.71) and aragonite (e.g., 2.95).

7.3.1. Major Element and Trace Element Relationships

Se and Mo concentrations were below the limits of analytic detection in all the samples from the study region (Appendix H). These elements may thus constitute limiting factors to the benthic ecosystems of the deep-sea in Eastern Australia. Se is an essential element for many marine phytoplankton species (Harrison *et al*., 1988), and is known to protect the membranes of metazoans from peroxidation damage (Elendt, 1990). By comparison, Mo is believed to play a fundamental role in the biogeochemical processes including N_2 fixation, denitrification, and nitrification (SCOR Working Group, 2007). The HCl-soluble Co, Cu, Zn and Ni fractions in these carbonate sediments were lower than those of river particulates from 8 large rivers representing 19% of the global sediment flux (Appendix H; Poulton & Raiswell, 2000), while Mn concentrations were considerably higher. With the exception of

Table 7.3. Porosity and wet and dry bulk densities of sediment samples.

Study Area	Station	Sample ID	Porosity (%)	Wet bulk density (g cm^{-3})	Dry bulk density (g cm^{-3})
Area A	04	BC01A1.1a	69.6 ± 3.0	1.3 ± 0.03	2.1 ± 0.2
	13	BC02A1.1a	71.8 ± 3.2	1.4 ± 0.06	2.7 ± 0.5
	18	BC04A1.1a	76.4 ± 0.9	1.4 ± 0.02	3.1 ± 0.2
	21	BC05A1.1a	75.2 ± 1.4	1.4 ± 0.02	2.9 ± 0.2
	23	BC06A1.1a	77.3 ± 2.8	1.4 ± 0.09	3.2 ± 0.7
	24	BC07A1.1a	73.5 ± 3.1	1.4 ± 0.08	2.6 ± 0.5
	25	GR01A1.1b	69.5 ± 1.7	1.4 ± 0.06	2.3 ± 0.3
	26	BC08A1.1a	76.1 ± 0.9	1.4 ± 0.01	2.9 ± 0.1
	27	BC09A1.1a	80.4 ± 2.4	1.5 ± 0.03	3.8 ± 0.5
	29	BC10_A1.1a	75.2 ± 4.1	1.4 ± 0.08	2.9 ± 0.7
	30	BC11_A1.1a	60.3 ± 3.0	1.4 ± 0.05	2.1 ± 0.2
	31	BC12_A1.1a	72.3 ± 5.8	1.5 ± 0.10	2.50 ± 0.6
Area B	38	BC13_A1.1a	73.8 ± 3.4	1.4 ± 0.04	2.8 ± 0.4
	39	BC14_A1.1a	79.3 ± 13.7	1.5 ± 0.30	1.7
	41	BC15_A1.1a	77.4 ± 11.2	1.6 ± 0.20	1.8

Mn, the concentrations of most trace elements are also lower in deep-sea carbonate oozes than nearshore mud and averages for shales (Burdige, 2006).

MESS-3 is a well-known and defined reference material comprising uncontaminated sediment from the Beaufort Sea. Townsend *et al*. (2007) applied the dilute HCl extraction protocol to MESS-3, and analysed the extracts using an ELEMENT 1 magnetic sector ICP-MS. The average extraction efficiencies of our study (based on the MESS-3 standard) were 21%, 48%, 25%, 16%, 37%, 27%, 22%, and 65% for Fe, Mn, Co, Ni, Cu, Zn, As, and Cd, respectively, and compare well with the Townsend *et al*. (2007) data (Table 12.1). The average potentially bio-available fraction for each metal was, in decreasing order: Ni (69.6%), Cu (46.1%), Co (42.5%), Mn (21.8%), and Fe (9.3%). Fe (22.6%) showed the lowest variation of the elements for which there were complete data sets (Table 12.1), while and Cu (78.3%) and Ni (>100%) showed the highest variation. All extractable Zn and some Ni concentrations were higher than the "total" concentration determined by XRF. This is likely due to the large percentage error in the XRF analyses (Appendix H).

Ge, Co, Ni and Mn analyses vary systematically with the Chlorin Index (CI; Fig. 7.1). The potentially bio-available concentrations of Ge, Co and Ni decrease with increasing CI and thus with the diminishing reactivity of the organic matter. This result is consistent with a wide range of studies that have shown that sinking biogenic particles are the major source of metals to the open ocean and that aerobic oxidation plays an important role in the release of metals associated with organic carrier phases (Burdige, 2006). In addition, oxic conditions in sediments can minimise the benthic flux of Mn that is continually scavenged by seawater, thus retaining this element in the sediment (Fig. 7.1d). Samples from stations 14, 18, 20, 30, 38, and 39 represent a conspicuous group of outliers. These sites, which for the most part are associated with volcanic outcrops, have anomalously high concentrations of Ge, Co and Ni, and lower concentrations of Mn. Potential explanations for theses anomalous results include: fluid escape from cold seeps, the admixture of volcanic rock debris in the sediment, or factors related to the mode of organic matter degradation or extent of bioturbation. The stoichiometry of the major element oxide signatures (Si, K, Ti and Fe versus Fe; Fig. 7.2) implies that continental dust (and not volcanic rock) is the major form of lithogenic material

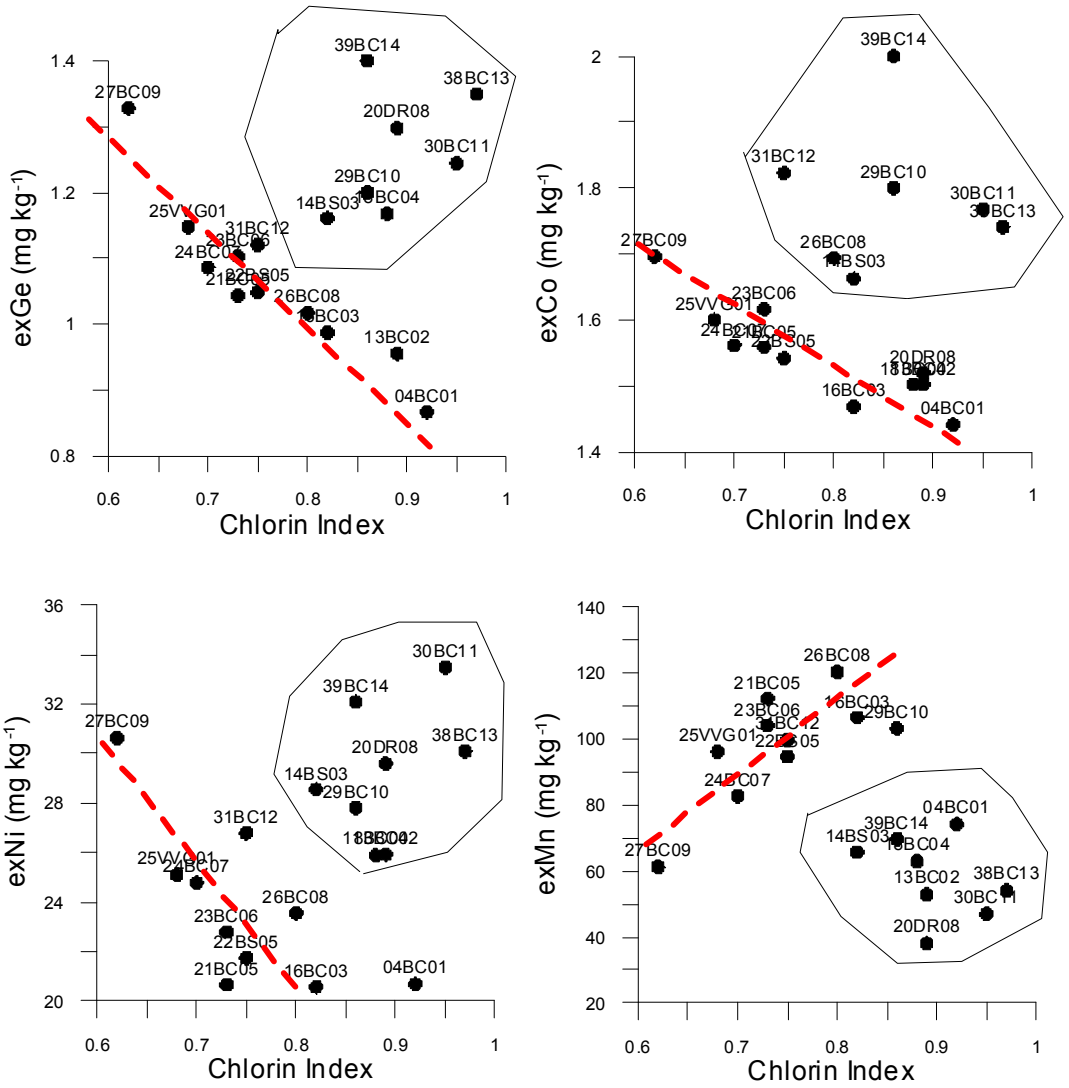

Figure 7.1. Graphs showing potentially bio-available Ge, Co, Ni and Mn versus the chlorin index. Red dashed line is hand-drawn to highlight trend.

in these deep sea sediments. Moreover, the inverse correlation between most of the Al concentrations and latitude (Fig. 7.2e) is consistent with the observed decrease in Holocene quartz concentrations from ~30° latitude toward the equator (McTainsh, 1989).

7.3.2. Organic Matter Degradation

Organic matter has distinct properties that depend on its origin. One characteristic is the relative concentration of the isotope C-13 to the most common isotope C-12. Another characteristic is the ratio of Total Organic Carbon (TOC) to Total Nitrogen (TN). The C^{13}:C^{12} ($\delta^{13}C$) and TOC:TN ratios indicate that phytoplankton is the major source of organic matter to the sediment (Fig. 7.3a). Marine phytoplankton generally has $\delta^{13}C$ values ranging from -17 to -22, and TOC:TN ratios of between 5 and 10(Burdige, 2006). Concentrations of TOC in the sediment range from 0.12 to 0.35% and this is consistent with the global TOC map produced by Seiter *et al*. (2004). The amount of carbon (and nutrients) recycled back to the ocean by benthic processes is closely related to the availability of TOC (Fig. 7.3b). A linear regression equation of TCO_2 flux=194.2*%TOC described most of the data (i.e., excluding samples 18 & 29).

Oxygen uptake follows a predictable pattern over time (Fig. 7.4a) producing a significant correlation for all stations between the start (t=0) and finish (t=1) of the

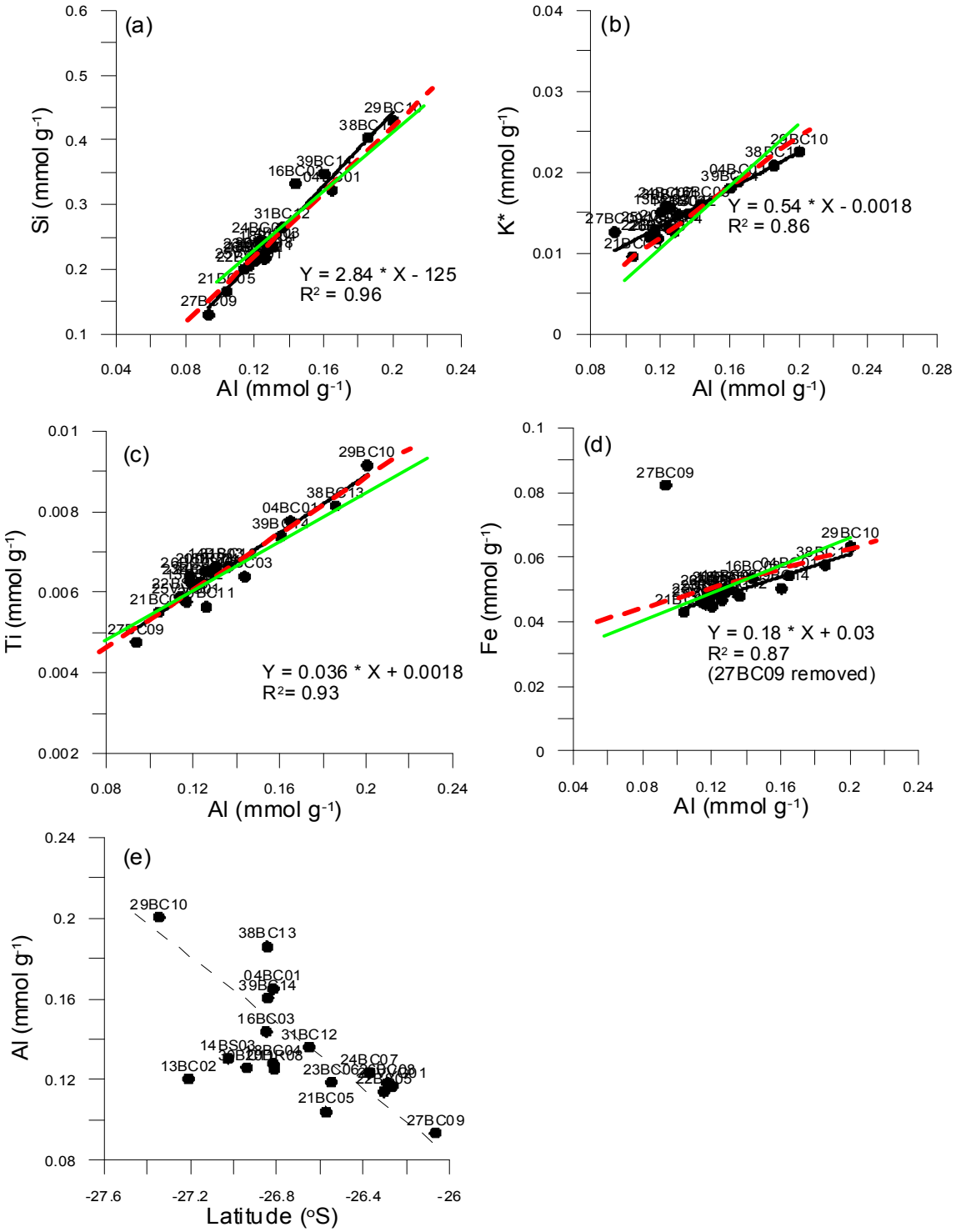

Figure 7.2. Graphs of Si, K, Ti and Fe versus Al and Al versus latitude. Note that K concentrations were corrected for K from the seawater assemblage using the Cl concentrations from the XRF trace (hence the use of K*). The red dashed lines show the stoichiometry of elements of Australian dust that had blown across the Tasman Sea and formed deposits in New Zealand (reviewed in McTainsh, 1989). The green solid line is the stoichiometry of elements for the upper continental crust. The Ti versus Al stoichiometry comes from the top 2 cm of sediment cores (NGC99 and NGC100) taken from the Tasman Sea (Kawahat, 2002).

incubations (Fig. 7.4b). The slope of the regression of this significant regression line was close to 1 signifying that it makes little difference which oxygen flux determination was used in the plot demonstrating the stoichiometry of the metabolites. Oxygen uptake based on the slopes in Figure 7.4a was thus used for subsequent analysis and reporting (Fig. 7.5a).

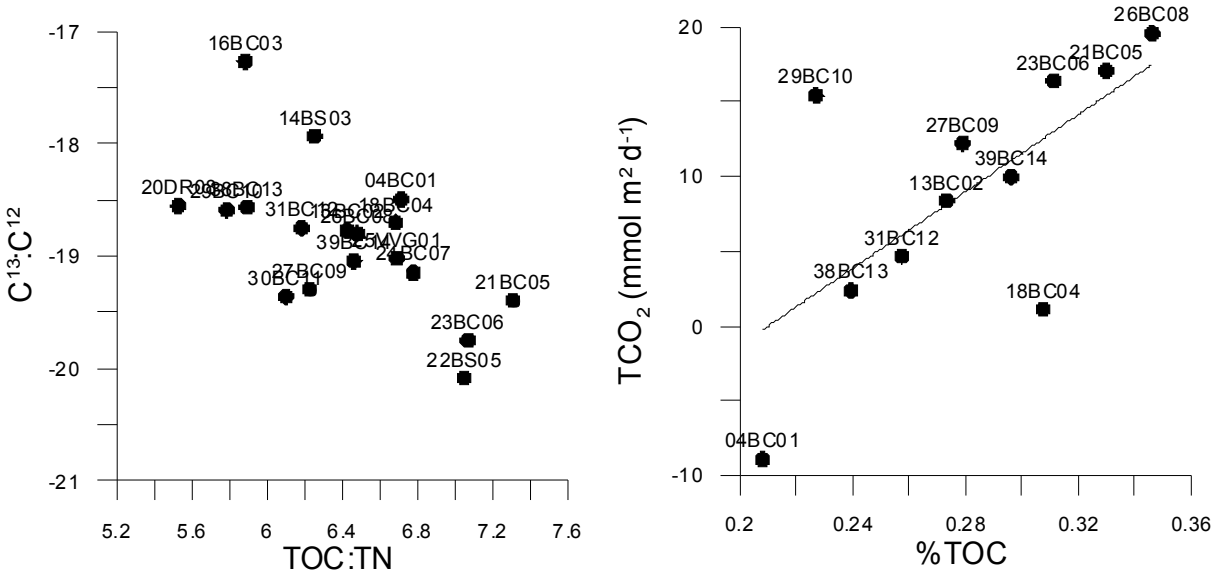

Figure 7.3. (a) $\delta^{13}C$ versus TOC:TN ratio; and (b) TCO_2 flux versus %TOC.

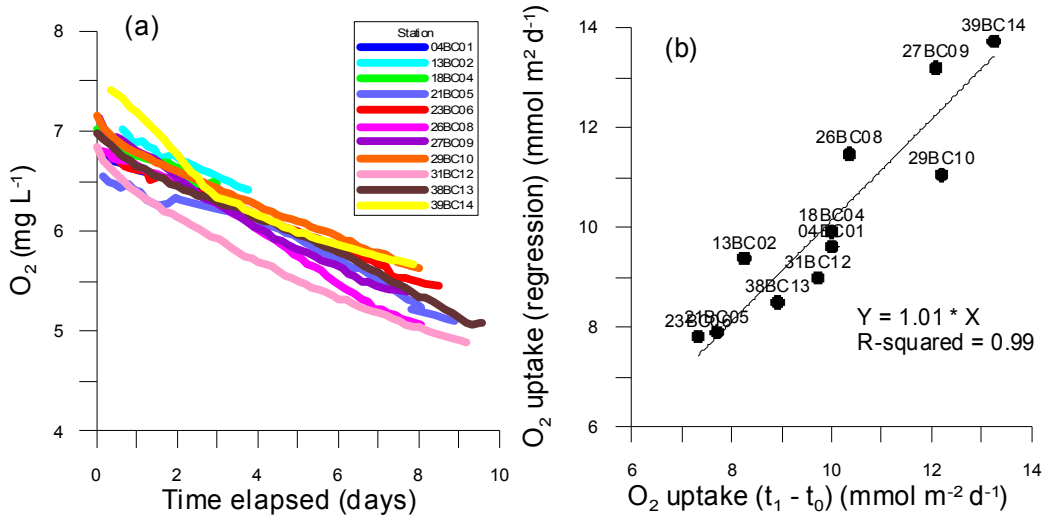

Figure 7.4. (a) The decline in oxygen consumption over time at the different sites. (b) A comparison of oxygen flux calculations based on regression of the slopes in Fig. 4a and based on the difference in concentrations between the start and finish of the incubations.

The stoichiometry of the metabolites from the core incubation experiments (Fig. 7.5) shows that the dissolved inorganic nitrogen concentrations (DIN: NO_X + NH_4) of several of the incubations were higher than those expected assuming that phytoplankton is the major source of the organic matter breaking down in the sediment (Fig. 7.5a). However, with the exception of stations 4 and 18, all of the core incubations had negative net N_2 fluxes, which implies that nitrogen gas was taken up by the sediment. When this negative N_2-N flux is added to the DIN, the total inorganic nitrogen (TIN) analyses cluster around the Redfield lines, which represent the average stoichiometry of these elements in marine phytoplankton (Fig. 7.5b). The negative net N_2 fluxes may provide evidence for the input of nitrogen from nitrogen fixation that is in addition to that derived from the breakdown of organic matter. However, the net uptake of N_2/Ar that is in fact due to N-fixation is the subject of considerable debate in the literature. The stoichiometry between PO_4 and TCO_2 and TIN is also generally in support of a phytoplankton being an important source for the organic matter in the sediment (Fig. 7.5c, d). Oxygen uptake by the sediment is plotted against the TCO_2 flux in Figure 7.5f. Core incubations from stations 21, 23, 29, 30, 27, and 26, had Oxygen:CO_2 flux ratios that were less than 1.3 (hashed line; Fig. 7.5f). This is the relationship

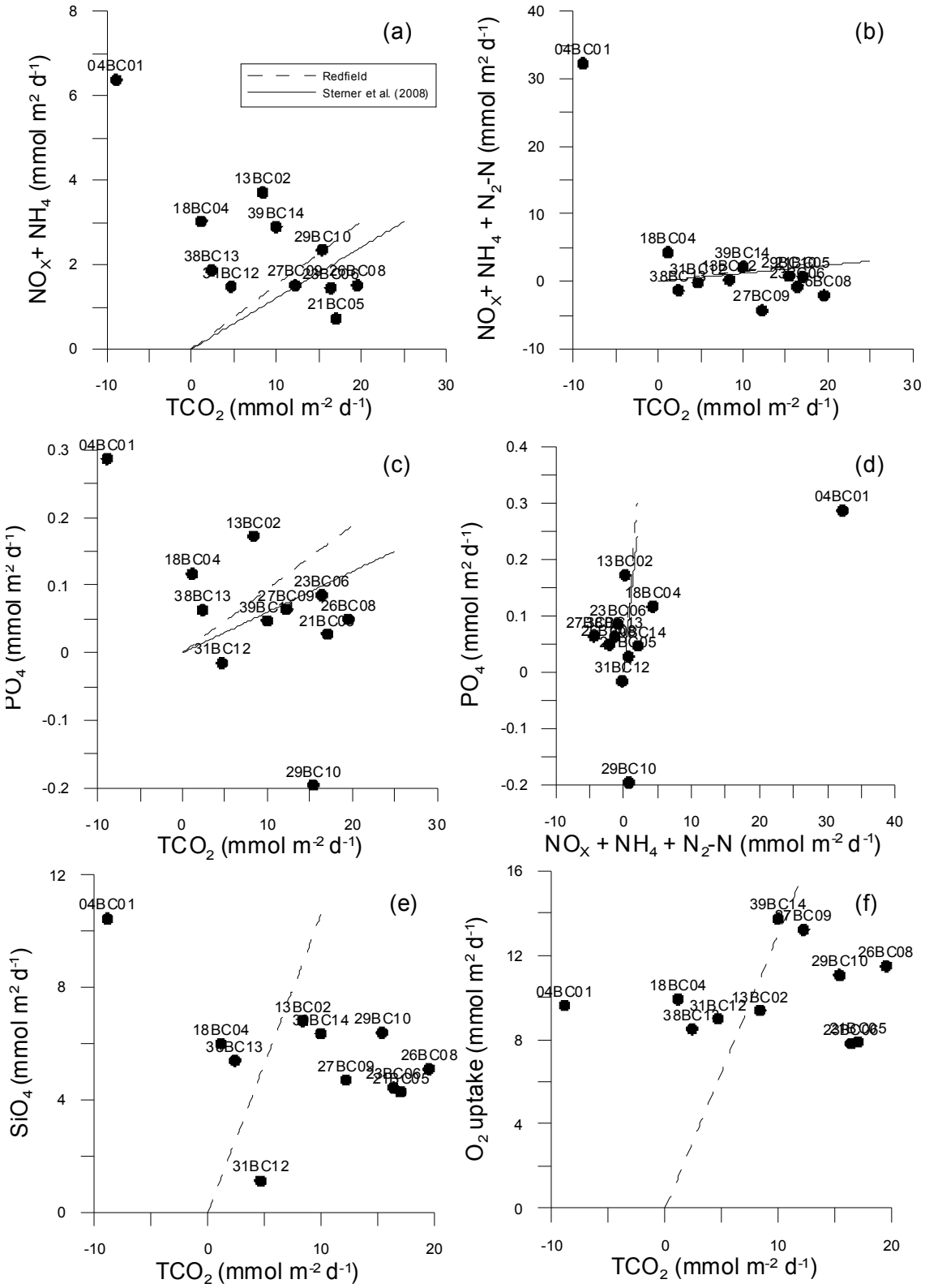

Figure 7.5. Plots showing the stoichiometry of metabolites measured in the core incubation experiments. The dashed line in (a-e) is the Redfield stoichiometry. The solid line in (a-d) is a new calculation of C:N:P ratios from Sterner *et al*. (2008). The dashed line in (f) pertains to the oxygen:CO_2 ratio of 1.3 (aerobic respiration with complete nitrification).

expected if there is sufficient O_2 in the sediment to break down all the organic matter (i.e., aerobic respiration with complete nitrification) and implies that non-oxic processes (Mn, Fe or sulphate reduction) account for a proportion of organic matter degradation in the deep-sea.

7.4. SUMMARY

Seabed sediments from the Capel and Faust basins and Gifford Guyot regions had Se and Mo concentrations that were below the limits of analytic detection used in this study. These elements may thus constitute limiting factors to benthic organisms (e.g., Se) and nitrogen-transforming biogeochemical processes (e.g., Mo). Five samples (14, 18, 20, 30, 38 & 39) had extractable trace element concentrations that were anomalous for the reactivity of organic matter, as determined by the chlorin index. Most of these samples were found in the vicinity of volcanic outcrops, including Gifford Guyot. Potential explanations for these results include fluid escape from cold seeps, the admixture of volcanic rock debris in the sediment, or factors related to manganese nodule formation and the mode of organic matter degradation (i.e., redox state).

Not surprisingly, terrestrial dust is the major form of lithogenic matter in the seabed sediments from both study regions. Interestingly, these dust concentrations varied roughly with latitude. An explanation for this latitudinal trend is not clear at present, other than natural variability.

The amount of carbon and nutrients recycled back to the ocean by benthic processes is closely related to the availability of organic matter that can be degraded by micro-organisms. The carbon isotopes and stoichiometry of metabolites in the core incubation experiments suggest that phytoplankton was the main source of organic matter that was breaking down in the sediments.

TOC concentrations in the seabed sediments were consistent with those proposed by Seiter *et al*. (2004) for the region. With the exception of two samples, bulk TOC concentrations and the benthic TCO_2 flux showed strong correlations. More work is needed to determine the relative roles of vertical versus lateral transport of particles in determining this gradient.

Negative N_2 fluxes and DIN concentrations in excess of the Redfield ratio provide evidence for N-fixation. It is not currently known whether these rates are real or merely are an artefact of the experimental design. Overall, the seabed sediments display relatively uniform geochemical properties across the two main study areas; seabed sediments from Gifford Guyot (e.g., 38BC13 & 39BC14) were similar in geochemical character as sediments from the Capel and Faust basins. This is probably the result of marine pelagic material being the dominant constituent of the sediments and the remoteness of the region from large and frequent terrigenous sediment sources.

8. Benthic Ecology

This chapter presents a description of the benthic ecology of the Capel and Faust basins and Gifford Guyot survey regions. Benthic assemblages were characterised from 44 stations: 36 stations from the Capel and Faust basins survey region and 8 from Gifford Guyot (Table 3.1). Seabed characterisations describing substrata, relief, bedform structure, and the presence of biota were recorded from 39 video-transects collected at representative sites across the survey area which, in combination, covered approximately 64 linear km of the seabed. Descriptions and taxonomic identifications of the biota found on (*cf.* epifaunal) and in (*cf.* infaunal) the sediments of the survey area were recorded from epifaunal (11 epibenthic sled and 13 dredges) and infaunal sampling gear (15 boxcores and 3 grabs), collected from 36 representative stations across the survey area.

8.1. BACKGROUND

The benthic ecology of deep-sea frontier regions of Australia has rarely been examined. On the eastern margin, two surveys have been undertaken that overlap the present study region. In 1989, the Australian Museum undertook a survey to the Lord Howe Rise and adjacent seamounts on the RV *Franklin* to collect and describe benthic invertebrates. During the survey, 49 stations (34 dredges or benthic sleds and 15 beam trawls) were sampled, with 7 stations sampled from the Capel and Faust basins survey region (3 benthic sleds and 4 beam-trawls) and 5 stations (3 benthic sleds and 2 beam-trawls) sampled from Gifford Guyot (Table 8.1). A brief description of each sample was recorded (Lowry, 1989), but samples were never fully processed or identified. In 2003, a multi-national survey (including: NIWA, NZ; CSIRO, Australia; and IFremer, France) was undertaken on RV *Tangaroa* to describe seamount assemblages of the Norfolk Ridge and Lord Howe Rise in the Tasman Sea (Williams *et al*., 2006). While no sampling was undertaken within Areas A and B of the present survey, seamounts both north and south of Gifford Guyot were surveyed and provide a broader biological setting for the region.

8.2. SAMPLE PROCESSING AND ANALYSIS

To characterise the bio-physical composition and structure of the seabed at each station we first ran a towed-video transects. Then, depending on the type of seabed, a range of sampling gear was deployed to collect biota.

8.2.1 Towed-video Transects and Seabed Characterisations

To characterise the composition and structure of the seabed high-resolution video footage and still images of the seabed were collected using NIWA's Deep Tow Imaging System (DTIS; Tables 3.2a & 3.2b). Seabed characterisations were made in two ways. First, during Leg 1 of the survey, video footage was simply recorded to mini DV tape for post-processing. Second, on Leg 2, seabed characterisations were made in real-time using the three-tiered characterisation scheme of substratum composition, bedform-relief, and biota presence described in Anderson *et al*. (2008).

Real-time characterisations were recorded approximately every 30 seconds along each camera-transect, or more frequently across transition zones (see Anderson *et al*., 2008). A 15-second moving window (i.e., 5 seconds prior to and 10 seconds following a GPS fix) was used to evaluate and characterise the seabed for each data entry point. Substrata composition (i.e., rock, boulders [>25.5 cm diameter], cobbles [6.5-25.5 cm diameter), sand and mud] was

Table 8.1. Samples collected from previous research surveys within the survey region. Samples were collected in 1989 on the RV *Franklin* (survey FR0589) by the Australian Museum during a survey to the LHR and adjacent seamounts to collect benthic invertebrates.

Study Area	Survey	Station	Latitude	Longitude	Depth (m)	Gear type
Area A	FR0589	29	-27.5673	161.5728	1,500	Benthic sled
	FR0589	30	-27.5990	161.6580	1,500	Beam-trawl
	FR0589	31	-27.6633	161.7717	1,423	Beam-trawl
	FR0589	32	-27.1995	160.6300	1,960	Beam-trawl
	FR0589	33	-27.2223	160.7235	1,989	Benthic sled
	FR0589	34	-26.8610	159.8178	2,500	Benthic sled
	FR0589	35	-26.8595	159.8120	2,500	Beam-trawl
Area B	FR0589	36	-26.6908	159.4450	292	Benthic sled
	FR0589	37	-26.7068	159.4670	294	Benthic sled
	FR0589	38	-26.7232	159.4757	295	Beam-trawl
	FR0589	39	-26.7378	159.4822	306	Beam-trawl
	FR0589	40	-26.7545	159.5098	315-360	Benthic sled

categorised by primary (>50% cover) and secondary (>20% cover) percent-cover following the earlier protocol of Stein *et al*. (1992) and Yoklavich *et al*. (2000). For example, if the seabed comprised >50% mud and >20% sand (i.e. sandy mud) the substratum composition was classified as 'mud-sand' (MS). Alternatively, if the seabed comprised >70% mud it was classified as 'mud-mud' (MM). Bedform-relief was defined as either soft-sediment 'bedform' such as hummocky, sediment ripples, or sediment waves, or by the vertical 'relief' of consolidated sediments. Relief classes ranged from flat (0 m), low (<1 m), moderate (1-3 m), to high relief (>3 m), or rock walls (high-relief with >80° incline). Relief was qualitative with visual assessment of the seabed aided by the depth and altitude readings of the sled. Benthic composition was described by recording the presence of benthic macro-organisms identified to groups (e.g. starfish and brittlestar), class (e.g. featherstars & anemones), or broad ecological categories (e.g. fish) (Appendix I).

For each data entry, observations were entered in 'GNav Real-time GIS Tracker' software (© Gerry Hatcher, 2002) using a 142-key Cherry programmable keyboard (© 2008 Cherry GmbH: http://www.cherry.de/english/products/keypads.htm). Seabed data entry took 3-12 seconds, and required a two-person team (i.e. observer and data-enterer) using a rotation of three people. Ship navigation (UTC date, time, latitude, and longitude) was captured for each data entry location and also was logged continuously (1-2 second fixes) to provide navigational tracks. To enable data checking and validation of real-time characterisations, mini DV video tapes were backed up to digital hard drives. Data were then processed at sea using a SAS (Statistic Analysis System, SAS Institute Inc., 2001) macro-program that parsed the variable-length text file, checked and cleaned syntax and format errors, and exported the file to a MS-Access database (TAN0713_video.mdb) file (see Anderson *et al*., 2008 for detailed methods).

Post-processing of Leg 1 video was undertaken using the same characterisation method but was undertaken in the laboratory post-survey. As no navigation was associated with the tapes, post-survey characterisations were recorded every 30 seconds of tape-time (e.g., for tape-time 00:00:30 the area of seabed described was 00:00:25 to 00:00:40) along each camera-transect. All video characterisations were entered and stored in the MS-Access database: TAN0713_video.mdb.

8.2.2 Epifaunal and Infaunal Collections

Epibenthic organisms were collected from 13 rock dredges (Table 3.3) and 11 epibenthic sleds (Table 3.6). Infaunal organisms were collected from three Smith-McIntyre grabs (Table 3.4) and 15 boxcores (Table 3.5).

Upon completion of the survey, all epifaunal and infaunal samples were transported to Geoscience Australia and held in Quarantine Approved Premises. At the time of writing, all preserved specimens (i.e. those preserved in ethanol and formalin, including all infaunal samples) had been released from quarantine. However, frozen specimens (mostly sponges from epifaunal samples) had not. Quarantine-released specimens were transferred to specialists for taxonomic identification. Echinoderms and polychaetes were sent to the Museum of Victoria, molluscs were sent to the Australian Museum, while other species are currently stored at Geoscience Australia pending delivery to taxonomic specialists.

8.2.2.1. Epifaunal Collections

All epifaunal specimens collected from dredges and epibenthic sleds were carefully removed, sorted into taxonomically similar groups, photographed and then preserved, based on CSIRO and Museum of Victoria requirements, in 70% ethanol (most specimens), 4% formalin (polychaete worms), or frozen (sponges) (Appendix I). Specimens were then transferred to 20 litre containers for storage and transport, where taxonomically similar groups were stored together (e.g., cnidarians, echinoderms, crustaceans, molluscs).

8.2.2.2 Infaunal Collections

Boxcores:— Most infaunal animals are found in the upper 0.02-0.05 m of benthic sediments (Hines & Comtois, 1985; Blake, 1994), while few animals are found in sediment depths greater than 0.05 metres below seafloor (mbsf). Animals found in sediment depth greater than 0.05 mbsf are usually large-bodied that can withstand the increased sediment pressure of those depths (Hines & Comtois, 1985). In this study, sediments were vertically stratified into two vertical components comprising surface sediments (≤0.05 mbsf) and bottom sediments (>0.05 mbsf). Surface and bottom sediments were separated using a large knife and placed into separate containers for elutriating. Once removed, each vertical section was separately elutriated, passed through a 500 μm sieve, transferred to a labelled (*barcoded*) container, and preserved in 70% ethanol, with the exception of macro-organisms which were removed, photographed, and preserved using the preservation requirements listed in (Appendix I: Table 12.3).

Several inconsistencies occurred during the processing of boxcore samples on Leg 1 compared to Leg 2 of the survey. For the first few stations on Leg 1 (BC01–BC03), the entire vertical depth was elutriated with no vertical separation undertaken. In subsequent samples collected during Leg 1 (BC04–BC09), surface sediments only were elutriated while bottom sediment were visually inspected and sorted by hand (i.e., tubes and burrows were followed to find the deeper larger organisms). In contrast, Leg 2 samples were vertically stratified and elutriated separately. Unfortunately, sampling locations were spatially confounded by survey leg with samples collected on Leg1 covering the Faust Basin and samples collected on Leg 2 covering both the Capel Basin and Gifford Guyot. Consequently, a full comparison between locations and depths is not possible.

Elutriated samples from boxcores collected during the survey comprised large quantities of foraminiferal ooze. As a result, large volumes of elutriate ranging from 2–4 litres were collected for most stations, and following transportation to Geoscience Australia, these samples required further sub-sampling in the laboratory prior to sorting.

In the laboratory, surface and bottom sediments (*cf.* elutriate material) were split 2-4 times (25%, 12.5%, or 6.25% of sample retained) by using either a Folsom plankton splitter (McEwen *et al.* 1954) or a newly designed wet sediment Crook splitter in which a wash bottle and/or an optional vibrating motor moves a sample down an incline where it is funnelled into a small opening and split into two equal sub-samples (Fig. 8.1). As most organisms are found in the upper 0.05 m of benthic sediments (Hines & Comtois, 1985; Blake, 1994) greater effort was given to sorting surface sediments, while sorting of bottom sediments focused on finding and removing larger more robust organisms. Surface sediments were carefully sorted under a dissecting microscope. In contrast, bottom sediments were spread in a thin layer within a shallow container and carefully sorted using forceps, removing any animals visible to the naked eye. There is evidence that the presence of smaller animals in bottom layers may be linked to sediment geochemistry (Witte, 2000) so we also examined two tablespoons of elutriate from bottom sediments under a dissecting microscope (60x magnification) to identify any abundant smaller animals, particularly species indicative of cold seeps.

All organisms were recorded and identified to highest taxonomic resolution, photographed, and preserved as part of a voucher collection. Specimens that could not be identified in the laboratory were sent to specialists for identification. Pteropods and foraminifers were not recorded as we were unable to differentiate recently living versus remnant shells.

Summary Indices:— Taxa collected from surface and bottom sediments were combined for each boxcore to determine overall species richness, abundance of target organisms, and taxonomic groups present. Three diversity indices were recorded: 1) species richness, 2) presence of taxonomic groups, and 3) abundance of target species. Species richness was calculated conservatively. Worm cases, urchin spines, and ostracods were each counted as single taxa, although an underestimate of actual species numbers contained in the sample is likely. Several organisms were unable to be identified to phyla but were included in species richness calculations. Coral rubble and shell fragments were not included in species richness as these remains because it was not possible to determine whether these remains represented recently dead organisms or had died long ago. Diversity indices included both macrofauna removed in the field and microfauna removed during post-processing.

Standardization of species richness and abundance across samples was not possible because initial sample size was not recorded. Penetration depth could have been used as a proxy, but this was considered insufficient due to differences between vertical strata sampling in Legs 1 and 2 and the uneven surfaces of some boxcore samples. Instead, it was assumed that foraminifera density was constant across sites. Since elutriated material was composed almost entirely of foraminifera, the volume of elutriated material was used as a proxy for initial sample size. Species richness and abundance were therefore standardised according to volume of elutriate and the number of times the sample was split, dividing species richness or abundance by the amount of elutriated sample examined under the microscope. A linear relationship between elutriate amount and number of species/organisms found (slope = 1) was assumed.

Grabs:— To examine the biology, a single push-core subsampler (79 mm inside diameter PVC pipe) was pushed into the sediment to a depth of 0.20 m. This sub-sample was then removed, elutriated, passed through a 500 μm sieve, transferred to a labelled (*barcoded*) container, and preserved in 70% ethanol, with the exception of macro-organisms which were removed, photographed, and preserved using the preservation requirements listed in Appendix I. At the time of writing this report, grab samples had not been sorted.

Figure 8.1. Crook wet sediment splitter used to evenly divide (split) boxcore elutriate during post-processing of infauna.

8.3. RESULTS

8.3.1. Towed-video Transects and Seabed Characterisations

This study provides the first direct observations of the Capel and Faust basins and Gifford Guyot survey regions. Over 32 hours of seabed video footage and 6,229 still photographs were acquired during the survey, in which an estimated 64 line-km of the seabed was surveyed. Select images are contained in Appendix J. By location, 18.5 hours of video and 3,520 stills covering the Faust Basin, 9.75 hours of video and 1,927 still photos covering the Capel Basin; and 4.5 hours of video and 782 stills from Gifford Guyot were recovered. The duration of each camera-transect varied from 22-62 minutes depending on logistical time available at each site, given other gear deployment. Video footage from select stations is contained in Appendix K.

A total of 3,413 seabed characterisations were recorded from 39 video-transects of the possible 42 undertaken during the survey. Of these 1,301 seabed characterisations were recorded in real-time from 16 camera-transects run during Leg 2 (Capel Basin and Gifford Guyot), while an additional 2,235 seabed characterisations were recorded by post-processing video footage from 23 camera-transects run during Leg 1 (Faust Basin). Three camera-transects were not characterised due to the camera being out of focus (CAM01), lack of visibility due to turbidity (CAM19), and a bait-bag being attached to the DTIS (CAM26).

For the entire survey region, the substrata was dominated by homogeneous soft-sediments that comprised 78% of the seabed, while 13% was hard substrata, with the remaining 9% comprised of mixed habitats of gravels or boulders. Mud (74% of all locations), sand (9%) and rock (17%) were the most common primary substratum types (i.e., >50% of each location) recorded during the survey, while boulders (0.09%) and cobbles (0.03%) were extremely rare. Recording secondary substratum type provided information on fine-scale (~10 m) heterogeneity. The dominant mud soft-sediments, for example, were characterised by secondary sands (MS 68%), while homogeneous mud was rare (MM 5%). Similarly, while homogeneous rocky areas were occasionally recorded (RR 12%), outcrops containing boulders or cobbles were rare (RB 0.55%, BR 0.03%, BB 0.03%, MC 0.12%, CS 0.03). Importantly, although Gifford Guyot is a complex seamount and would be expected to have a very different physical environment to that of the Capel and Faust basins survey region, major habitat similarities were present. The Capel and Faust basins survey region (Figs. 8.2-8.5) and Gifford Guyot (Figs. 8.6-8.8) were both characterised by homogeneous

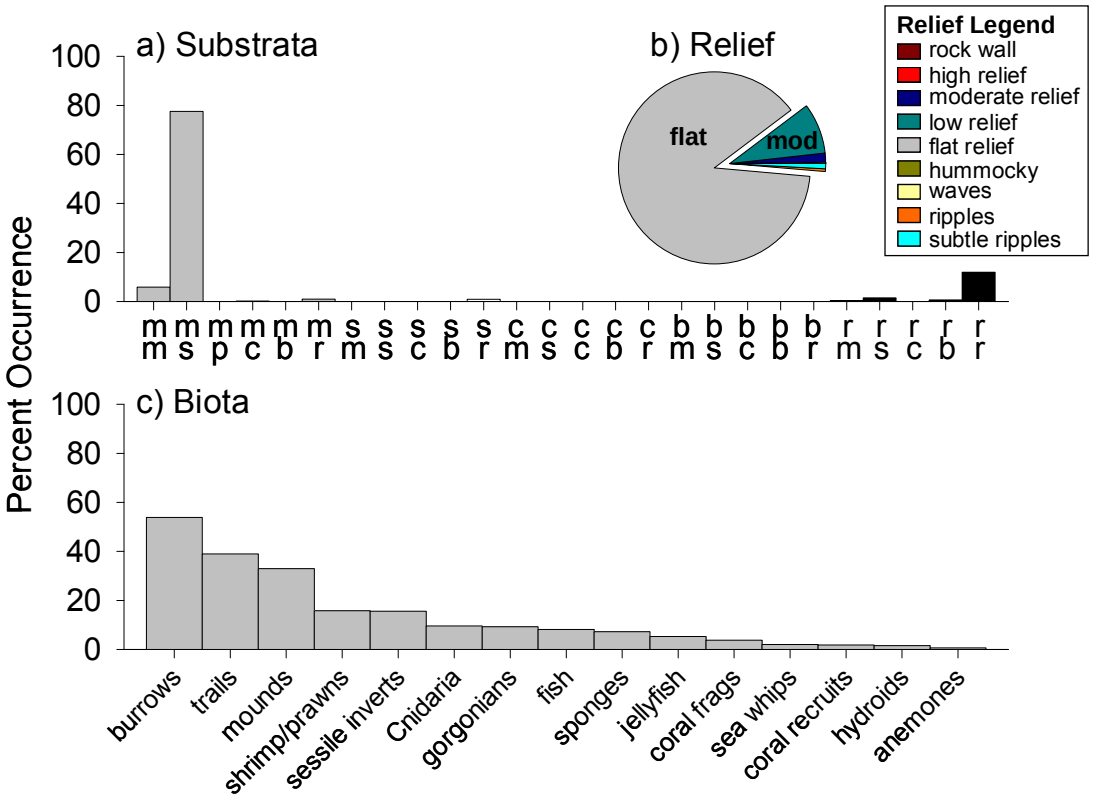

Figure 8.2 Seabed characterisations for study area A over the Capel and Faust basins based on towed-video observations. Percent occurrence of: (a) primary and secondary substrata (m=mud (grey), s=sand (white), p=pebbles, c=cobbles (dark grey), b=boulders (dark grey), r=rock (black)), primary=top line, secondary=2nd line; (b) relief types; and (c) biota types.

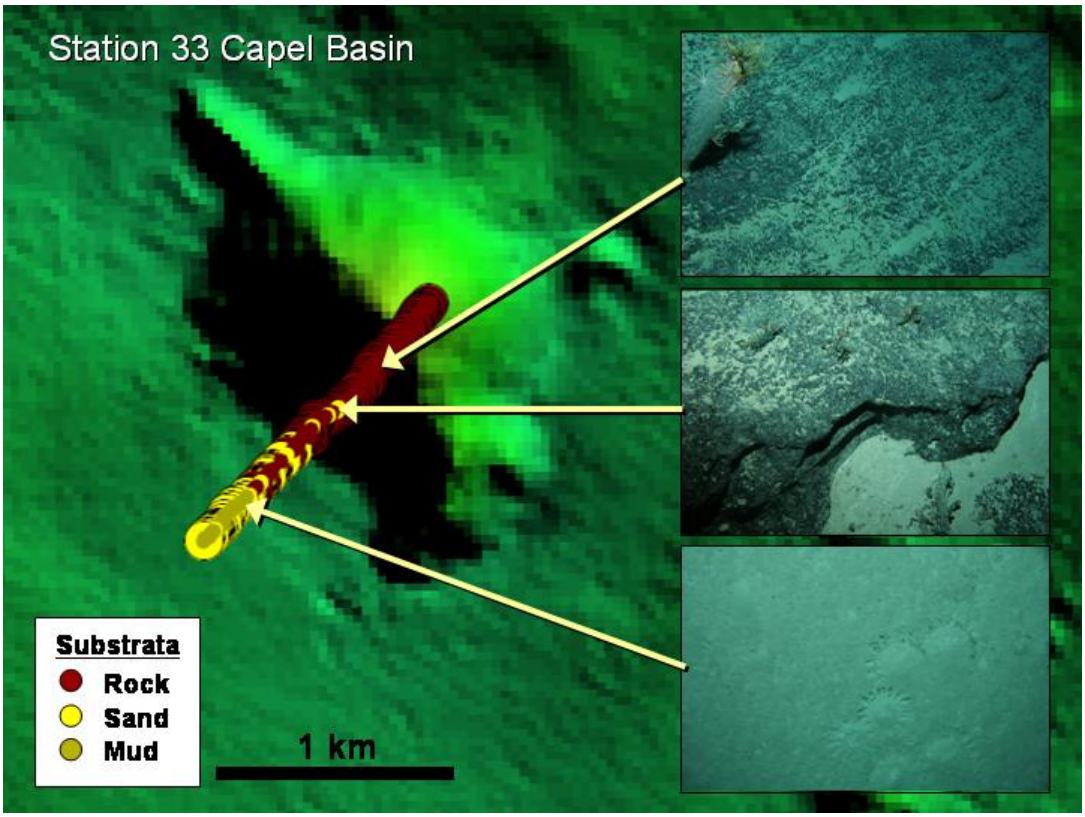

Figure 8.3. Multi-beam sonar bathymetry image of a volcanic cone protruding 250 m above the surrounding seabed, overlayed with a single video-transect (station 33 cam31) depicting 1° and 2° substratum characterisations, and co-located still images of the seabed.

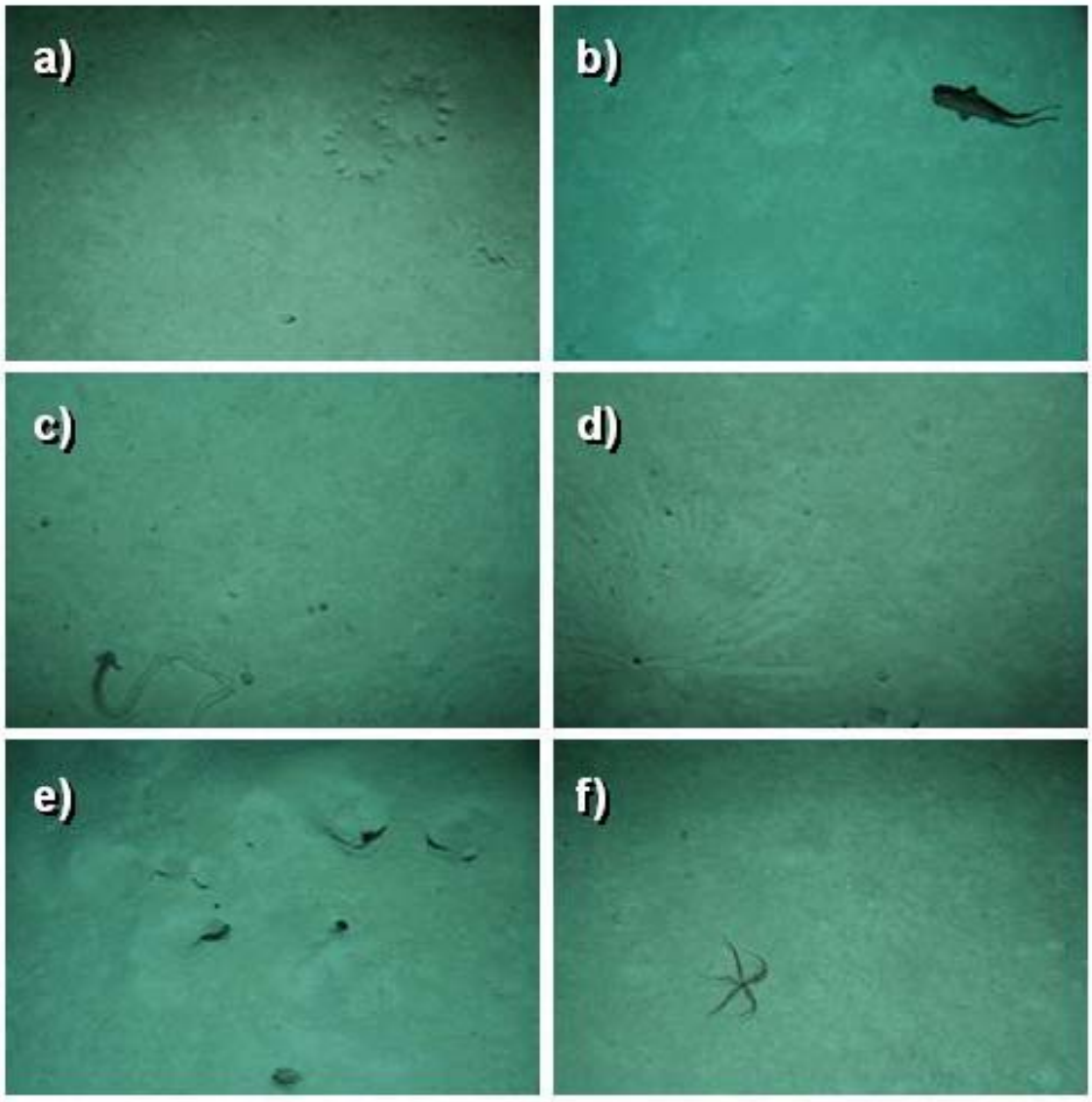

Figure 8.4. Still colour photographs of soft sediment habitats from study area A over the Capel and Faust basins. (a) Station 16 (1,421 m): – bioturbated sediments with cookie-cutter patterns, (b) Station 20 (1,301 m): – bioturbated sediments with deep-sea shark, (c) Station 29 (1,940 m): – bioturbated sediments with acorn worm and trail, (d) Station 31 (1,516 m): – bioturbated sediments with polychaete worm tracks, (e) Station 25 (1,483 m) – bioturbated sediments showing burrows, (f) Station 16 (1,421 m): – bioturbated sediments with crinoid (featherstar).

soft-sediments (13% vs. 12% respectively) with low amounts of outcropping (13% vs. 12% respectively) of mostly flat (88% vs. 68% respectively) or low relief (9% vs. 16% respectively), with rare occurrence of moderate relief (2% vs. 1%). However, differences in outcrop composition were recorded with volcanic substrata in the basins (Fig. 8.5) and calcareous conglomerate on Gifford Guyot (Figs. 8.7 & 8.8).

The Capel and Faust basins and Gifford Guyot survey regions were also both characterised by relatively depauperate fauna, however some specific differences were apparent. Initial examination of the data identified that the Capel and Faust basins survey region was characterised by a high occurrence of large bioturbation signs (e.g., acorn worms, spaghetti tracks, and large mounds and burrows), but these were rare or absent on the sediment-starved summit and upper sections of Gifford Guyot. Bioturbators require sediment to move through, and therefore this pattern of higher occurrences with depth may simply reflect greater sediment deposition with depth. However, stations surveyed in the basins ranged in depth from 1,296 m to 2,198 m, nearly 1,000 m depth change. Initial exploration of these data suggests that there may also be an association of large bioturbators

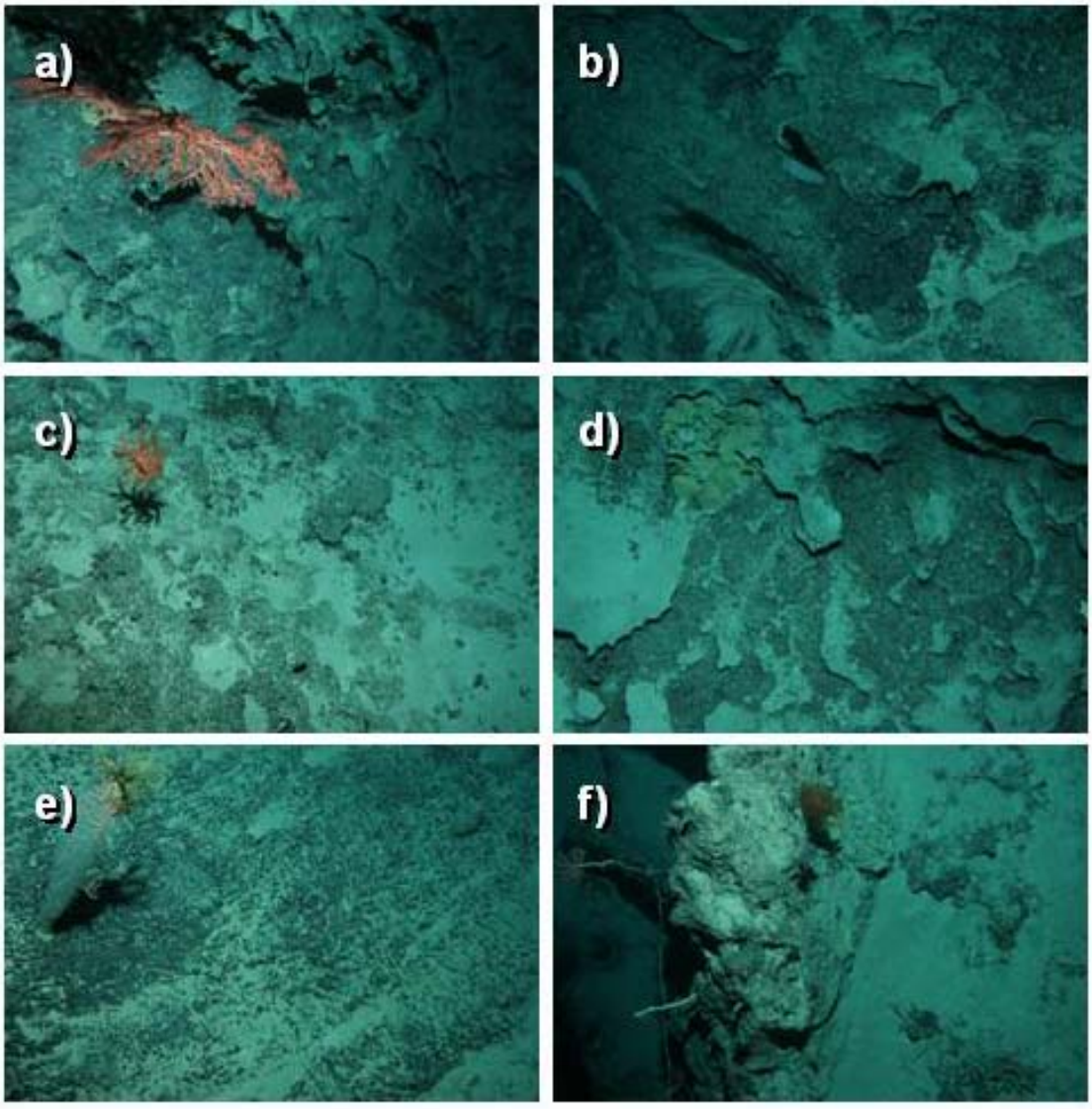

Figure 8.5. Still colour photographs of rocky outcrop habitats from study area A over the Capel and Faust basins. (a) Station 19 (1,380 m): – volcanic outcropping with ophiuroids entwined in a red gorgonian, (b) Station 17 (977 m): – volcanic outcropping black-coral and glass sponge, (c) Station 17 (977 m): – volcanic outcropping with orange starfish, (d) Station 17 (977 m): – volcanic outcropping with encrusting yellow sponge, (e) Station 33 (1,351 m): – volcanic outcropping with crinoids and ophiuroids on glass sponge, (f) Station 30 (1,566 m) –outcropping with corals, gorgonians, and other invertebrates.

with depth. For example, acorn worms (Hemicordata), a common bioturbator in the region (Fig. 8.4c), were found at depths of 2,000 m or greater in the Capel and Faust basins survey region and were also present on the deep slope region (2,198 m) of Gifford Guyot, suggesting that some combination of sediment type and depth may be important to these bioturbating taxa. In contrast to these deep fauna, the summit and upper slopes of Gifford Guyot were comparatively shallow (248-414 m respectively) and supported a variety of taxa, such as Ascidians (e.g., Fig. 8.8d) and rock-associated fishes (e.g., Figs. 8.8a, b, f) that were not observed in the deeper basin habitats.

8.3.1.1. Area A: Lord Howe Rise – Marginal Plateau

At total of 2,963 seabed characterisations were recorded for the Capel and Faust basins survey region (793 and 2,235 respectively). Substrata in this region was dominated by homogeneous soft-sediments that comprised 84% of the seabed surveyed, while 12% was volcanic outcrops, with the remaining 4% comprising a range of mixed habitats with gravels

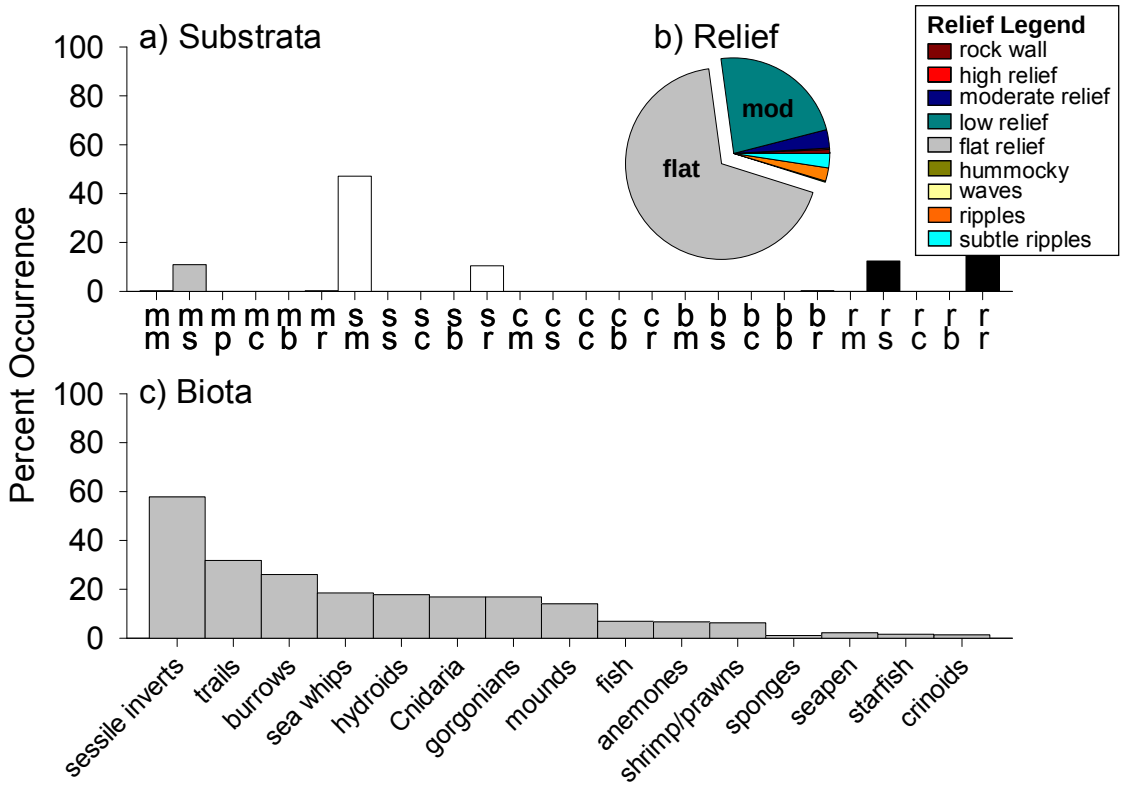

Figure 8.6. Seabed characterisations for study area B over Gifford Guyot based on towed-video observations. Percent occurrence of: (a) primary and secondary substrata (m=mud (grey), s=sand (white), p=pebbles, c=cobbles (dark grey), b=boulders (dark grey), r=rock (black), primary=top line, secondary=2nd line; (b) relief types; and (c) biota types.

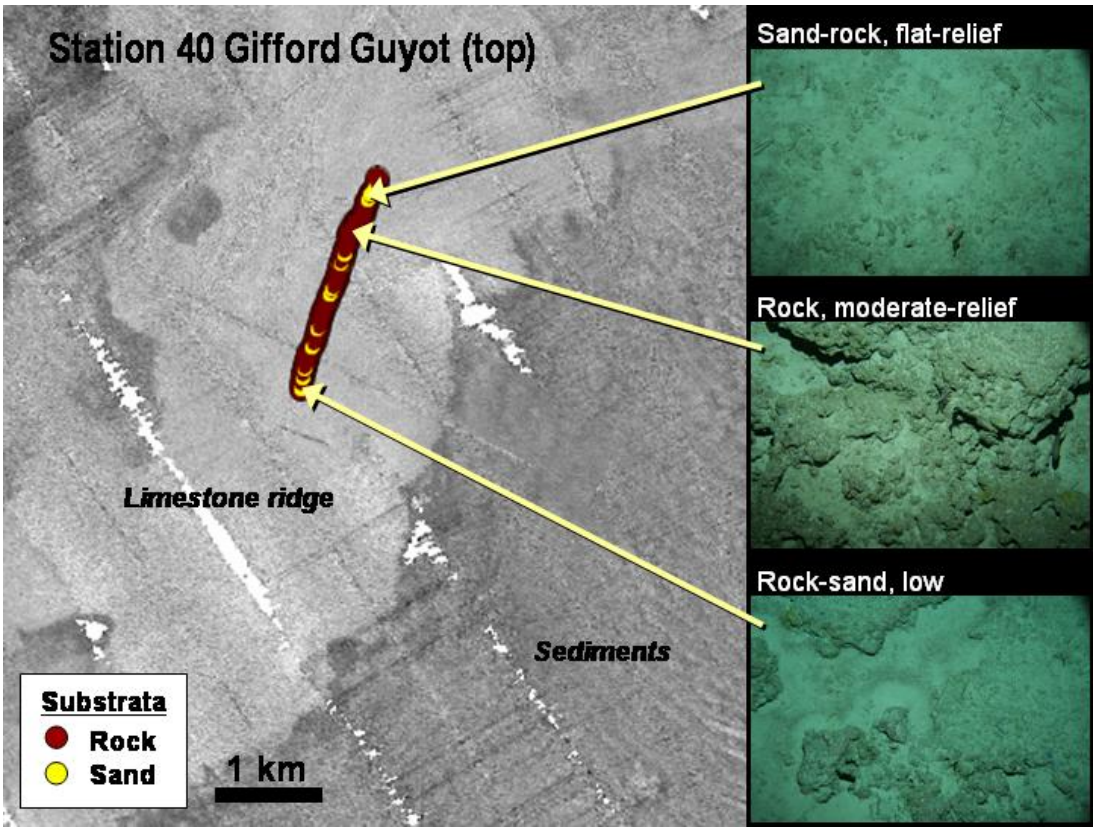

Figure 8.7. Multi-beam sonar backscatter of the northern limestone ridge on the summit of the Gifford Guyot, protruding 10-30 m above the surrounding seabed (lighter areas = higher backscatter intensities that depict limestone outcropping, while darker areas = lower backscatter intensities depict a veneer of soft-sediments), overlayed with a single video-transect (station 40CAM37) depicting primary and secondary substratum characterisations, and co-located still images of the seabed.

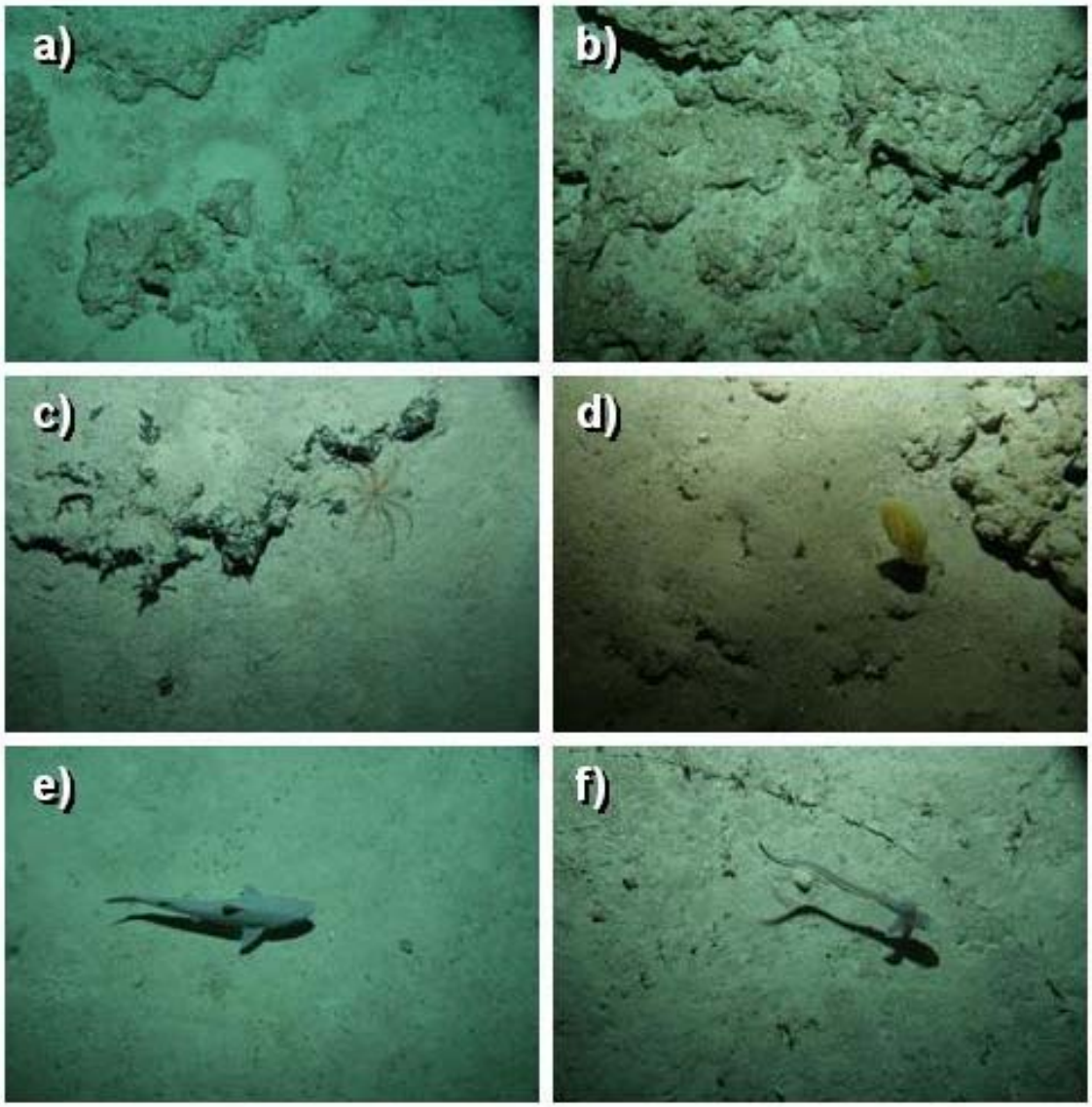

Figure 8.8. Still colour photographs of benthic habitats from the flanks and summit of Gifford Guyot. (a) Station 40 (248 m; summit): – low-relief limestone ridge with small gorgonians, sponges, and *Parapercis* fish, (b) Station 40 (248 m; summit) – moderate-relief limestone ridge with sponges, gorgonian, and small fish, (c) Station 37 (414 m; upper slope) – mixed sediment veneer and calcareous-conglomerate outcropping with crinoid, (d) Station 34 (288 m; summit) – mixed sediment veneer and limestone outcropping with yellow ascidian (sea squirt), (e) Station 34 (288 m; summit) – sediment veneer over consolidated bedform with shark, (f) Station 37 (414 m; upper slope) – sediment veneer over consolidated bedform with a halosaur fish.

or boulders (Figs. 8.2-8.5). Seabed relief was mostly flat (88% of basin locations) with rare occurrences of bedforms (1%) (Fig. 8.4). Volcanic outcrops, although bathymetrically distinct in the multibeam images, were at fine-scales characterised by low, moderate, or flat relief (54%, 33%, 13% of all hard substrata, respectively). Low and moderate relief habitats accounted for an overall 9% and 2% of all basin habitats (Fig. 8.5). Basin habitats were relatively depauperate of biota. Bioturbation marks (e.g., burrows [53%], tracks [38%], mounds [n=32%]) were the most common signs of life (61% of all basin locations had bioturbation marks) (Fig. 8.4). Sessile organisms, such as corals and gorgonians, occurred sparsely (i.e., 1-3 individuals in 15 s of video footage) at 8% of all basin locations (Fig. 8.5) but were rarely recorded as very dense fields (0.02% at a single station; CAM05). Motile species including shrimp and prawns (15%), fishes (8%), and jellyfish (5%) were also regularly recorded in basin environments, but were sparsely distributed and were never abundant.

8.3.1.2. Area B: Gifford Guyot - Seamount

A total of 450 characterisations from six video transects were recorded for Gifford Guyot. Substrata on the seamount were dominated by homogeneous soft-sediments that comprised 58% of the seabed surveyed, while 23% comprised a range of mixed rock and sand habitats and 19% comprised homogeneous rock outcrops (Figs. 8.6-8.8). Seabed relief was generally flat (68% of all locations; 93% of homogeneous soft-sediments) with rare occurrences of ripples (4%) and sandwaves (<1%). Homogeneous rocky outcrops (19% of all locations) were characterised by low relief (83%), with rarer occurrences of moderate and flat relief (7%, 6% respectively) (Figs. 8.7 & 8.8b). Rock walls (2%) with low and moderate relief outcropping habitats accounted for an overall 9% and 2% of all habitats surveyed. Mixed habitats were characterised by flat or low relief (54% and 32% respectively), with rarer occurrences of moderate relief (8%), and sand ripples (4%) (Figs. 8.8a, c, d).

Like the Capel and Faust basins survey region, habitats on Gifford Guyot were also relatively depauperate of biota. However, they appeared to have higher occurrences of sessile invertebrates but lower occurrences of bioturbation, particularly on the summit. Unknown sessile invertebrates were the most common signs of life (58%) on Gifford Guyot. Bioturbation marks (e.g., tracks [31%], burrows [26%], mounds [n=14%]) were also common, albeit at lower densities than in the Capel and Faust basins survey region. Only 47% of all seamount locations had bioturbation marks compared to 61% in the Capel and Faust basins survey region. Like the Capel and Faust basins survey region, sessile organisms such as gorgonians (15%) and corals (3%) only occurred sparsely on the rocky outcrops of the Gifford Guyot (18% of all seamount locations; generally 1-6 individuals in 15 seconds of video footage) (Fig. 8.8). Sea whips, hydroids, and sea pens were also recorded, but were found mostly on the summit (18%, 17%, and 2%, respectively). Motile species including fishes (7%), shrimp and prawns (6%), and jellyfish (<1%) were also recorded on and down the slopes of the seamount (Figs. 8.8a, b, e, f), albeit sparsely and slightly less frequently than in the Capel and Faust basins survey region.

8.3.2. Epifaunal Collections

A wide variety of epifaunal specimens were collected during the survey. Many of these had previously been recorded from the NORFANZ 2003 survey (Williams *et al*., 2006), although no formal identifications were available. At the time of writing this report only data from echinoderms and polychaete worms had been taxonomically identified by specialists.

8.3.2.1 Echinoderms

A total of 80 echinoderm specimens and 33 species were collected during the survey and were identified to lowest taxonomic level at the Museum of Victoria, with the exception of several crinoid fragments, each assumed to be a separate species (Appendix I). Of this total, 19 species and 47 specimens were collected from the benthic sled; 16 species and 31 specimens were collected from the dredge; and one species and two specimens (*Fibularia* sp.) were collected in a Van Veen grab (Appendix I). A total of 26 species were collected from a single station, while only five species occurred at three or more stations.

Ophiuroids were the most dominant component of the echinoderm fauna (21 species). *Ophiomusium scalare* was the most widely distributed echinoderm, occurring at five stations in both the Faust Basin region (Stations 1, 5, 6,) and Gifford Guyot region (stations 35, 37), while spanning a large depth range (290-1,532 m) (Fig. 8.9; Appendix I). *Ophiopyrgus trispinosus* was the most abundant echinoderm, with 13 animals collected from four locations in the Faust Basin region (Stations 2, 8, 11, 15) (Appendix I). Station 11 contained the highest

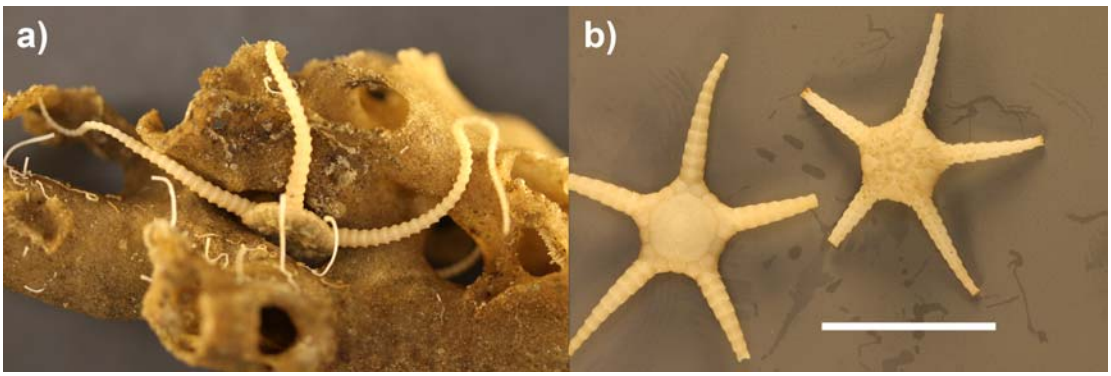

Figure 8.9. Ophiuroids found in epifaunal samples from TAN0713: (a) *Ophiomusium scalare* in sponge and (b) *Ophiopygrus trispinosus.* Scale bars are 1 cm.

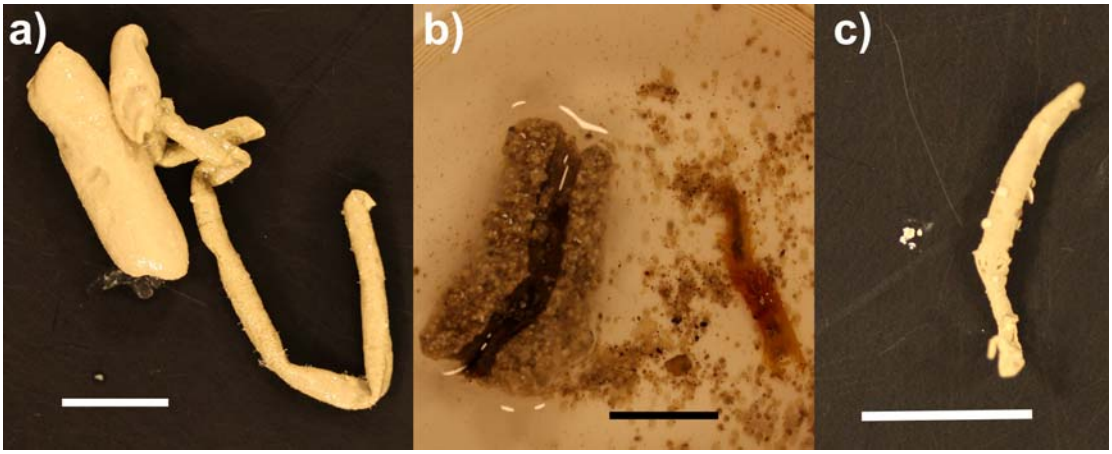

Figure 8.10. Polychaetes found in epifaunal samples from TAN0713: (a) ampharetid in tube, (b) sabellid, and (c) maldanid in tube. Scale bar is 1 cm.

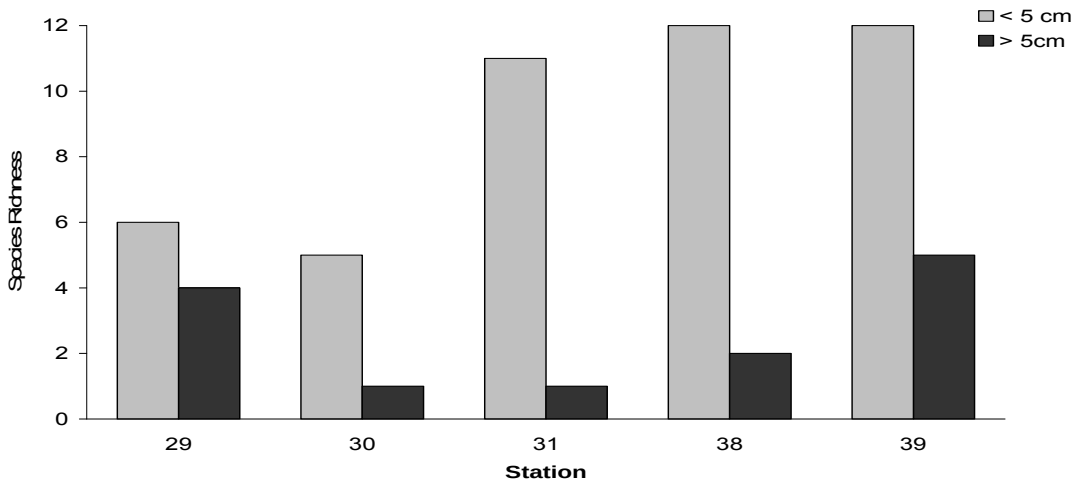

Figure 8.11. Numbers of species found in upper and lower layers of sediment from boxcores. Species richness represents raw data, and volumes of sample vary across stations and sediment layers. For upper layers, species richness was calculated by microscopically sorting a sub-sample of elutriate (see Appendix I for volumes). For bottom layers, species richness was calculated by visually sorting the entire elutriate sample and microscopically sorting two tablespoons.

number of echinoderms (15 animals of four species), and Stations 01 and 35 had the highest species richness (6 species each). Echinoderm assemblages overall were not significantly different between the Capel and Faust basins and Gifford Guyot survey regions (ANOSIM, R = -0.063, p = 0.877).

8.3.2.2 Polychaetes and Other Worms

A total of 34 worm specimens (26 specimens from the Capel and Faust basins survey region, and 8 specimens from Gifford Guyot) were collected during the survey and were identified to phylum (non-polychaetes) or family (polychaetes) at the Museum of Victoria (Appendix I). Worms were represented by four phyla (Phorinida, Nemertea, Polychaeta, Sipuncula). 15 specimens were collected from the benthic sled; 12 specimens were collected from the dredge; and 7 specimens were collected from boxcores (Appendix I).

Polychaetes (Fig. 8.10) were the most dominant component (16 families and 23 specimens) (Appendix I). All polychaetes were represented by single specimens, with the exception of the ampharetids at Station 11. Ampharetids, sabellids, and aldanids were the most widely distributed polychaete families, occurring at two sites each (Appendix I). Ampharetids were the most abundant family, with five animals collected from two locations (Stations 11 & 15).

8.3.3. Infaunal Collections

A total of 15 boxcore stations were processed: 9 stations from the Faust Basin region (Study Area A - Leg 1), 3 stations from the Capel Basin (Study Area A - Leg 2), and 3 stations from the Gifford Guyot (Study Area B - Leg 2). Sediments from all three regions mostly comprised foraminiferal ooze of pelagic origin. All regions were depauperate of living infauna (Appendix I). Bottom sediments were more depauperate than top layers, with no abundant taxa recorded. A comparison of top and bottom layers at stations in which bottom and top layers were elutriated separately, revealed lower species richness in bottom layers than top (Fig. 8.11), although these results should be interpreted cautiously due to differences in post-processing methods. No cold-seep indicator species were identified.

8.3.3.1. Taxonomic Groups

A total of 8 taxonomic groups were recorded from the boxcore samples: molluscs, echinoderms (sea urchin spines), crustaceans, brachiopods, bryozoans, cnidarians, sponges, and worms (worm casings, polychaetes, and other worms) (Fig. 8.12; Appendix I). Station 13 (Faust Basin) had the most taxonomic groups (7 out of 8 taxa). All taxonomic groups were found at multiple stations, with the exceptions of brachiopods which were only found at Station 13 and bryozoans which were only found at Station 39. We also recorded an unidentified biological structure in the form of a crenulated yellow ribbon. These yellow ribbons were recorded at stations 29 and 31 and Gifford Guyot (Stations 38 & 39) (Fig. 8.13). These yellow ribbons appeared to be biological but were similar in appearance to hard plastic and might be the remnant of a reproductive encapsulating structure.

8.3.3.2. Species/taxa Abundances

Four taxa (ostracods combined, bivalve sp. 1, gastropod sp. 1, and scaphopods combined) were present in high enough abundances and occurred at multiple sites to warrant further examination (see Fig. 8.14). Scaphopods were most abundant at Station 13, while bivalve sp. 1 and gastropod sp. 1 were most abundant at stations 39 and 41. Ostracods were most abundant at stations 31 and 38. All four taxa were absent at station 26 (Appendix I).

8.3.3.3. Species/taxa Richness

The number of species/taxa varied between 3-25 species per station (Appendix I), but this likely reflects different sample amounts. Standardised species richness values indicate that station 38 at 2,423 m depth had the highest numbers of species, and station 29 at 1,935 m

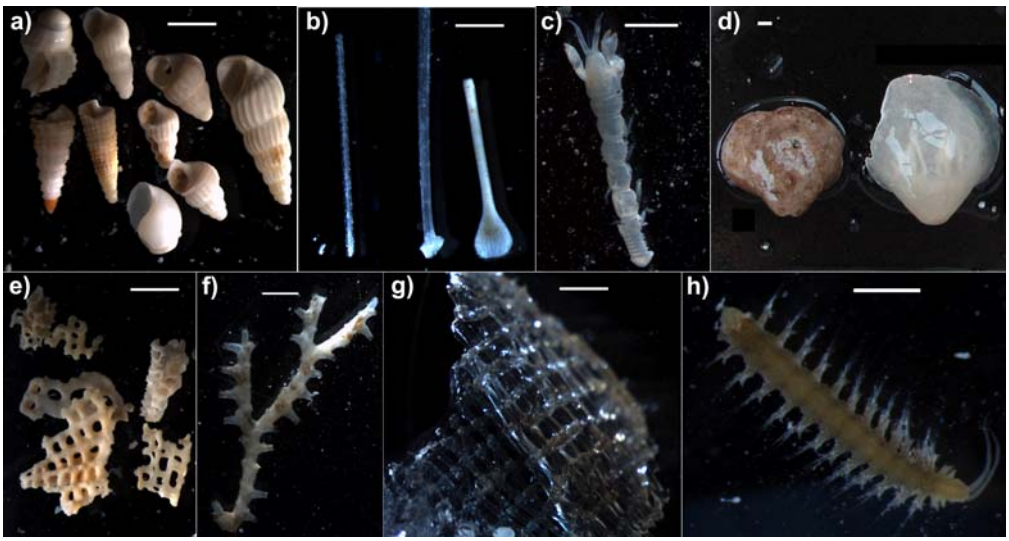

Figure 8.12. Representatives of taxonomic groups found in boxcore samples: (a) gastropods, (b) urchin spines, (c) tanaid crustacean, (d) brachiopods, (e) bryozoan fragments, (f) cnidarian, (g) glass sponge, and (h) polychaete fragment. Scales = 1 mm.

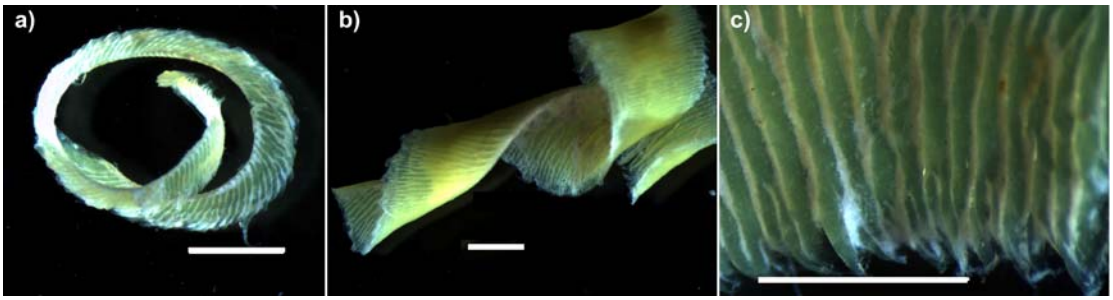

Figure 8.13. Unidentified biogenic structure found in boxcore samples from four stations including: (a-b) study area A (Capel and Faust basins), and (c) study study area B (Gifford Guyot). Scales = 1mm.

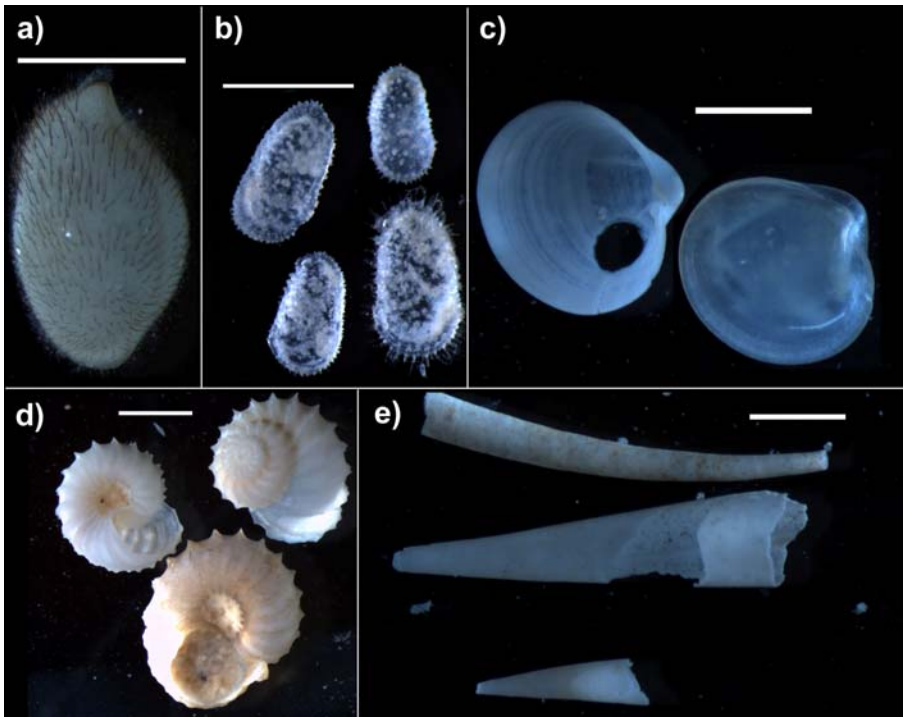

Figure 8.14. Photographs of four abundant species/taxa found in boxcores samples: (a-b) ostracods, (c) bivalve sp. 1, (d) gastropod sp. 1, and (e) scaphopods. Scales = 1 mm.

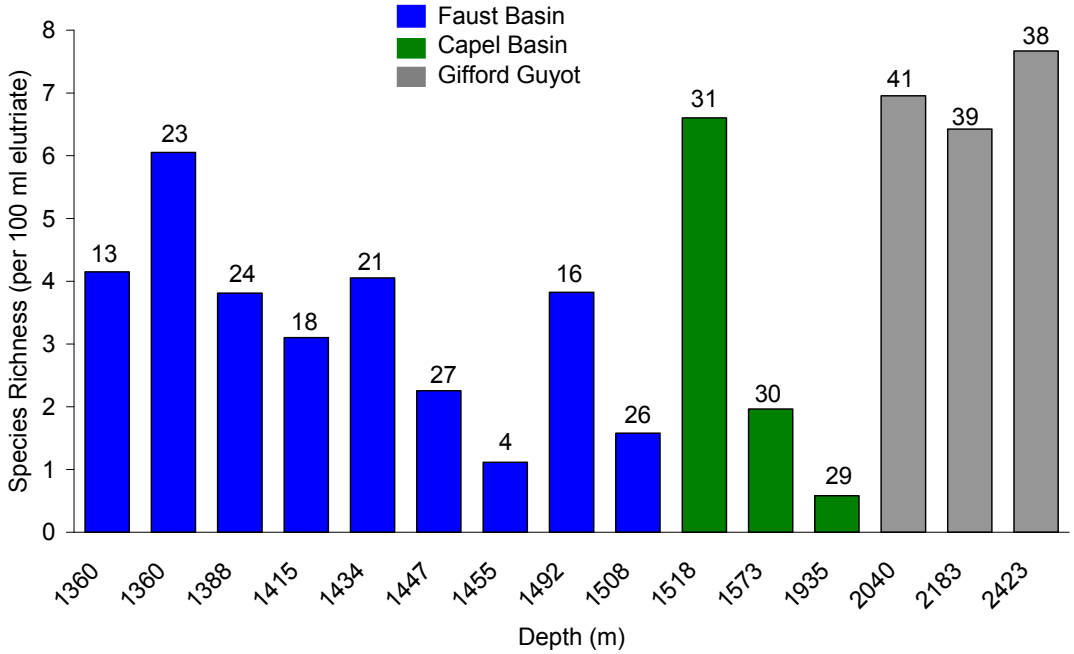

Figure 8.15. Species richness of infauna by station. Species richness calculated as a standardised measure of species number per 10 ml of elutriate. Station numbers are listed above each histogram bar.

depth had the lowest. We compared species richness across the Capel and Faust basins and Gifford Guyot survey regions and found that species richness was significantly different across regions (unbalanced ANOVA, df = 2, F = 5.2503, p = 0.023). Gifford Guyot had significantly higher species richness than the Capel and Faust basins survey region (Tukeys HSD, $\alpha = 0.05$) (Fig. 8.15). Since the three deepest sites occurred at Gifford Guyot (Fig. 8.15), it is difficult to determine whether high species richness here is related to depth or other factors associated with seamounts.

8.4. SUMMARY

Surprisingly, both sediment plains and the numerous rocky outcrops in both study areas (Capel and Faust basins and Gifford Guyot) supported lower numbers and densities of organisms than would be expected from deep sea basins and seamounts. Previous studies have identified that soft-sediment plains in the deep sea can support high species diversity, although abundance of animals may be low (Gage, 1996; Cronin & Raymo, 1997; Levin *et al*., 2001). Similarly, seamounts throughout the world have been identified as diversity hotspots that support a wealth of distinct marine life, including habitat-forming invertebrates, such as matrix-forming corals, which provide refugia for a variety of other fauna (Koslow & Gowlett-Holmes, 1998; Pitcher, 2007). It is unclear why sessile invertebrates and motile species were not abundant in this region.

Seamounts are known to vary in community structure and levels of biodiversity (e.g. Cronin & Raymo, 1997; Koslow & Gowlett-Holmes, 1998; Stone *et al*., 2004) and may reflect a range of biogeographic, oceanographic, temperature and depth patterns, as well as fishing intensity (Stocks, 2004; Pitcher, 2007). At the time of writing, epifaunal collections from Gifford Guyot had not been fully identified or enumerated, however, comparisons with surrounding seamounts surveyed during the NORFANZ 2003 survey (Williams *et al*., 2006) are planned, once specimens have been taxonomically identified.

Rocky substrata in this study had surprisingly few attached or associated organisms and almost no dense habitat-forming sessile invertebrates. In coastal environments, rocky habitats are a limited resource with organisms covering all available rock surfaces (Bertness

et al., 2001). Rocky habitats in deep sea environments are also known to support dense assemblages of suspension feeders, such as corals and sponges (e.g., Rodgers, 1994). In this study, however, organisms were only sparsely recorded throughout the survey, while large areas of rock remained uncolonised. Infaunal and epifaunal specimen collections were also low in diversity and abundance. While differences in sampling methodologies used between studies may explain some of the observed community differences, low occurrences of organisms recorded in the towed-video observations of both Area A and Area B suggest some factor(s) may be limiting diversity in this region.

Environmental factors, such as nutrients, oxygen, organic content, and trace element levels, can all influence faunal diversity and abundance (Levin *et al*., 2001). For example, low nutrients can limit the number and assortment of species that can co-occur in a region, while dysoxia (oxygen-limited and energy-depleted regions) may reduce diversity and abundance to depauperate levels (Cronin & Raymo, 1997; Levin, 2003). Interestingly, organic-rich sediments increase biochemical oxygen consumption, leading to dysoxic or even anoxic environments that can be reworked by deposit feeders, but support few other species (Jacobs & Lindberg, 1998). Geochemical analyses of the sediment samples collected from the Capel and Faust basins and Gifford Guyot survey regions are currently being undertaken and may shed some light on whether any of these factors are limiting on the east Australian margin.

9. Basin Geology

9.1. ROCK DREDGE SAMPLING

Dredging was undertaken at 13 sites during the survey to recover rock samples from both pre-rift basement and post-rift rocks of the Capel and Faust basins (Table 3.3). Dredge targets were selected pre-survey based on interpretation of GA302 survey seismic data, and using shipboard assessment of multibeam bathymetry data being acquired during the survey. The extensive cover of Neogene bathyal sediments throughout the study areas and the generally low seabed gradients reduced the number of suitable dredge targets.

Several previous marine surveys to the LHR successfully recovered continental rocks. Most recently, during the 2006 AUSFAIR survey, significant quantities of volcanic and volcaniclastic rocks were collected from the eastern flanks of the Lord Howe Platform (Colwell *et al*., 2006; Purvis & Pontifex, 2006). Preliminary ages on the zircons in the volcanic rocks indicate that these rocks correlate with syn-rift megasequences in the Capel and Faust basins, and as such, do not represent the pre-rift basement. Samples that unequivocally represent the basement have only been recovered previously from the Dampier Ridge (McDougall *et al*., 1994) and the Challenger Plateau (Tulloch *et al*., 1991), but not from the LHR itself. Therefore, one of the main objectives of the dredge sampling during the present survey was to recover rock samples in order to confirm the existence of East Gondwanan basement beneath the northern LHR. Two potential targets for basement rocks were identified and dredged, both of these on transit lines near the southeastern corner of study area A (Fig. 9.1).

The second objective of the dredge sampling was to collect samples of post-rift volcanic rocks within the survey area. These samples were to be analysed after the survey to characterise their petrology and geochemistry, to determine their age, and to identify their genetic relationship (or otherwise) to the previously identified hotspot volcanism within the LHR region. Sampling took place at 11 sites over the two study areas (Fig. 9.1).

Dredging at the majority of sampling sites resulted in the recovery of in situ rock material in varying quantities. The two pre-rift basement sampling sites predominantly yielded ferromanganese crust (Fig. 9.2). Underwater camera footage indicated that the rock outcrops are extensively encrusted with this material. At site 01DR01, small fragments of acid to intermediate (rhyolite?) volcanic rocks (Fig. 9.3) and a phosphatised whale bone (Fig. 9.4) were also recovered. The volcanic rocks superficially resemble those sampled during the AUSFAIR survey in the eastern Lord Howe Platform, and show signs of oxidation (iron oxide staining) indicating extrusion within a subaerial or shallow subaqueous environment. The rocks are probably of syn-rift age and are unlikely to represent the pre-rift basement.

The relatively young volcanic edifices exposed at the seabed (e.g., 05DR03) generally yielded large hauls of vesicular and scoriaceous mafic volcanics (Fig. 9.5), volcaniclastic breccia and sandstones (Fig. 9.6), and peperites. The rocks have a fresh appearance, although widespread clay and zeolites(?) infilling the vesicles of the volcanics indicate some alteration.

Smaller quantities of volcanic rocks accompanied by ferromanganese crust were recovered from the volcanic edifices that are partially draped by bathyal sediments (e.g. 08DR05, 33DR11). The poorer recovery is attributable to the widespread induration of the rock surfaces by the ferromanganese crust. Subsurface stratigraphic relationships observed in GA302 seismic data indicate that these volcanic edifices are older than those fully exposed

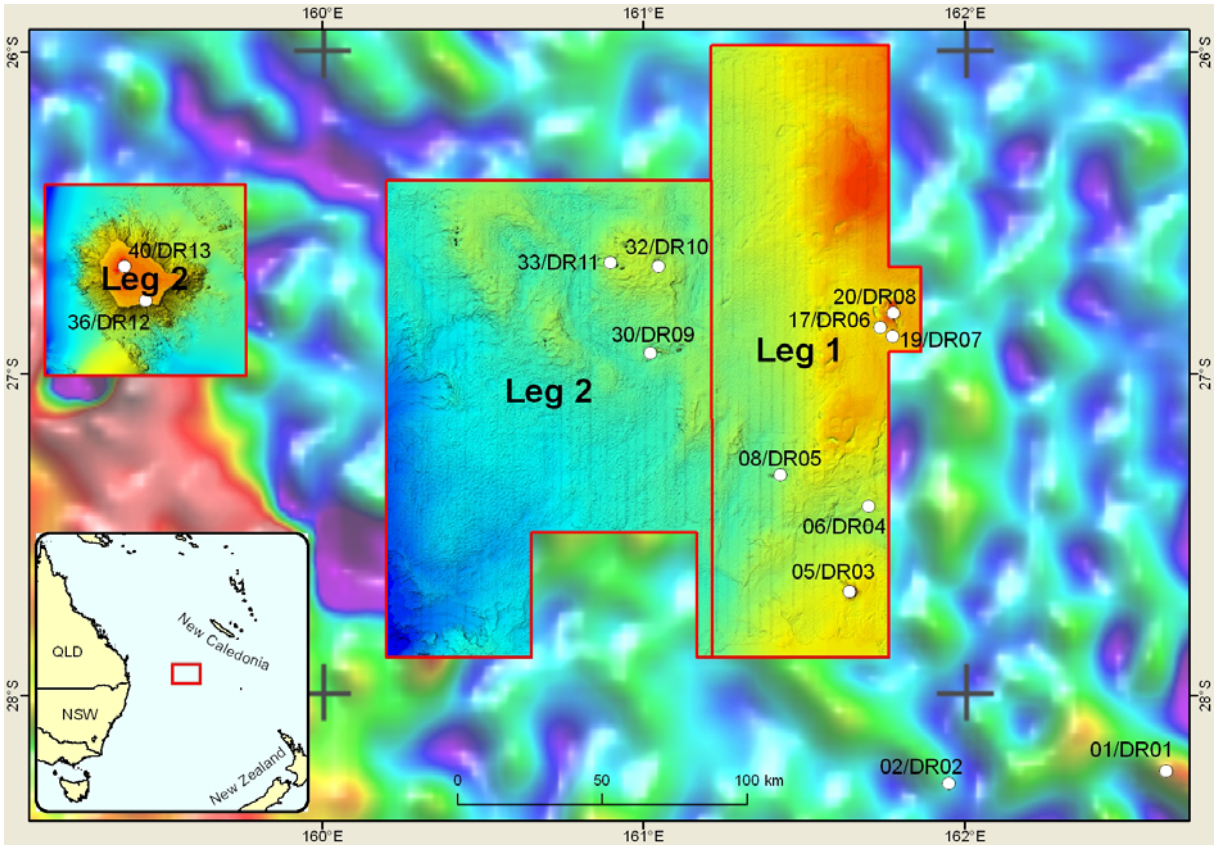

Figure 9.1. Map showing location of rock dredges recovered in study area A over the Capel and Faust basins. Two rock dredges were also collected in study area B over Gifford Guyot. Leg 1 and 2 refer to the survey legs (Chapter 1).

Figure 9.2. Photograph showing examples of ferromanganese crusts contained in rock dredge 01DR01.

at the seabed. The apparent absence of ferromanganese crust from the younger edifices suggests that the degree of encrustation is, at least in part, a function of time elapsed since the extrusion of the volcanic rocks.

Figure 9.3. Photograph showing an acid to intermediate volcanic rock (rhyolite) recovered from study area A over the Cape and Faust basins.

Figure 9.4. Photograph of a phosphatised whale bone recovered in 01DR01 from study area A over the Capel and Faust basins.

At some of the dredge sites associated with volcanic edifices and associated igneous intrusions (08DR05, 20DR08, 30DR09), samples of indurated calcareous sediments were also recovered (Fig. 9.7). These sediments are similar in appearance to the widespread unconsolidated seabed sediments of the area, but are semi-lithified. They may be a product of cementation resulting from hydrothermal activity or contact metamorphism associated with the comparatively recent volcanic activity.

Figure 9.5. Photograph of vesicular and scoriaceous mafic volcanics recovered in 05DR03 from study area A over the Capel and Faust basins.

Figure 9.6. Photograph of volcaniclastic breccia and sandstones recovered in 05DR03 from study area A over the Capel and Faust basins.

The two dredge sites from study area B (36DR12, 40DR13) yielded samples of calcarenite, coralline limestone and some mafic volcanics. They indicate that the platform of the Gifford Guyot has been extensively mantled by partially lithified calcareous sediments of terrestrial to shallow marine origin since the initial extrusion of the volcanic rocks, and that the guyot has subsided since the deposition of the sediments.

In summary, dredging operations of the present survey were successful in recovering samples of Cenozoic post-rift volcanic rocks for further analysis. However, no rock samples providing unequivocal evidence for the existence of the pre-rift East Gondwanan basement

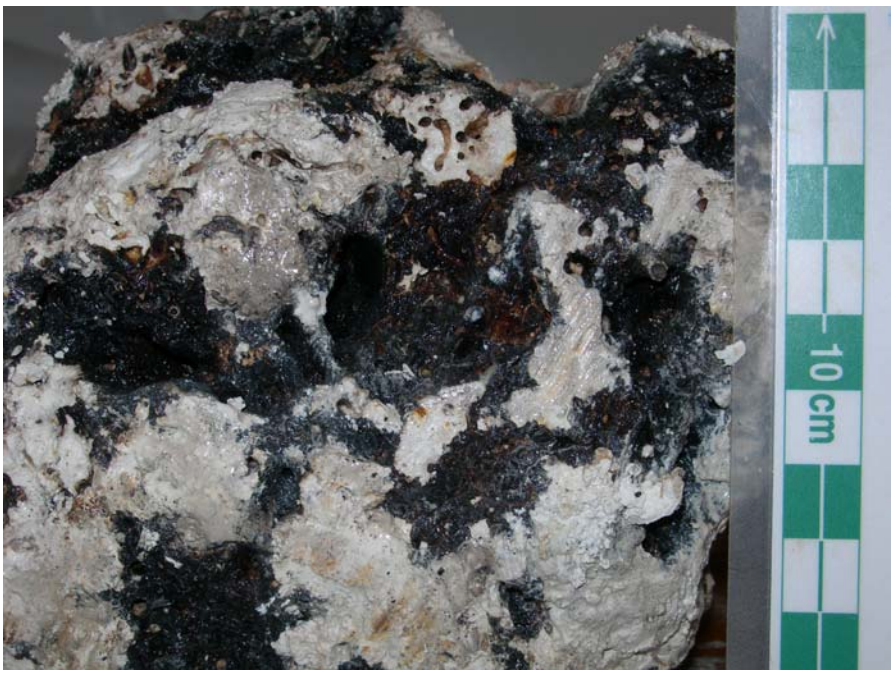

Figure 9.7. Photograph of indurated calcareous sediments from study area A over the Capel and Faust basins.

beneath the northern LHR were collected. The paucity of rock outcrops and the encasing of the existing outcrops by ferromanganese crust indicate that basement rock samples would be extremely difficult to recover through dredging alone in study area A over the Capel and Faust basins.

9.2. PETROLEUM POTENTIAL

Paucity of data, especially from wells, does not allow a detailed assessment of the petroleum potential of the Capel and Faust basins. Some insights may, however, be gained from analogue studies of nearby basins that share a common tectonostratigraphic history.

Regional reconstructions place the Capel and Faust basins adjacent to the Clarence-Moreton Basin in eastern Australia, prior to the opening of the Tasman Sea (Gaina *et al*., 1998; Norvick *et al*., 2001, 2008). The Clarence-Moreton Basin contains several potential source rocks including the oil-prone Jurassic Marburg Formation and Walloon Coal Measures and the gas-prone Triassic Ipswich Coal Measures (Willis, 1985; O'Brien *et al*., 1994; Stewart & Alder, 1995). The 'layered' pre-rift basement observed on seismic data in the Capel Basin may represent the offshore extension of these units. The Murihiku terrane, which possibly underlies the Faust Basin, also contains Jurassic coal measures as shown at Wakanui-1 in the offshore Northland Basin in New Zealand (Uruski & Stagpoole, 2004), and thus may also have source rock potential. The 'coaly' seismic character seen in parts of the Syn-rift 1 megasequence (Fig. 12.1) suggests that they may be correlatives of the gas-prone Aptian–Albian coal measures in the Otway (Edwards *et al*., 1999; Boreham *et al*., 2004) and Maryborough (Lipski, 2001) basins.

The Syn-rift 2 megasequence associated with the Capel and Faust basins (Figs. 12.1 & 12.2) may contain the equivalents of the oil- and/or gas-prone Upper Cretaceous source rocks in the Gippsland (Emperor and Golden Beach subgroups), offshore Taranaki (Rakopi Formation), Great South and Canterbury basins (Killops *et al*. 1997; Uruski *et al*., 2003; Lipski 2004; Norvick *et a*l., 2008). However, their depth of burial may be insufficient in many areas for maturity to be attained.

Potential reservoir rocks may include fluvial, lacustrine and deltaic facies in the Syn-rift 1 to Syn-rift 2 sections, and/or deltaic, shoreline, shelf and turbidite facies in the Syn-rift 2

to Lower Sag sections. The fine-grained bathyal sediments in the Lower to Upper Sag sections would provide a thick regional seal (Figs. 12.1 & 12.2). The majority of traps within the region are fault-related or stratigraphic, although occasional anticlinal traps associated with compressional reactivation are also observed.

The greatest risk in terms of the petroleum prospectivity of the Capel and Faust basins is posed by the uncertainty regarding the presence of source rocks. However, if source rocks are present within the pre-rift to Syn-rift 1 sections, the larger depocentres of the basins are likely to have attained sufficient depth for oil and/or gas generation. Isolated measurements taken previously in the LHR region indicate average to above-average (57–100 m Wm^{-2}) heat flow (Grim, 1969; Burns *et al*., 1973; Morin & von Herzen, 1986; Colwell *et al*., 2006). The high fault densities and evidence for widespread fluid movement (probably hydrothermal) encountered in some areas indicate that the seal integrity may have been compromised in parts. Finally, syn- and post-rift igneous activity may have implications for source rock distribution and maturity as well as for reservoir quality.

9.3. DISCUSSION AND SUMMARY

The newly acquired gravity data confirms the existence of several large fault-bounded grabens and half-grabens, as initially revealed by seismic and filtered satellite gravity data (Kroh et al., 2007). There are apparent linkages between the occurrence of seabed features mapped by multibeam sonar and the subsurface geological structure seen in seismic data, which suggests that faulting and fluid migration (whether through syneresis or hydrothermal activity) have been active until Recent. This may have implications for seal integrity.

Dredge samples collected during the survey do not include any rocks likely to represent the pre-rift basement or the syn-rift depositional sequence. Thus, questions regarding the nature of the pre-rift basement underlying the Capel and Faust basins, and the existence of potential petroleum source rocks, remain unresolved. The one small rock sample (TAN0713/01DR01_D1) recovered during dredging may be derived from silicic volcanism accompanying or immediately preceding the Cretaceous rifting in the LHR region. If so, it is presumably analogous to the latite and trachyte recovered from the eastern flank of the Lord Howe Platform during the AUSFAIR MD-153 survey in 2006 (Colwell *et al*., 2006), and the Cenomanian (c. 94 Ma) rhyolite recovered from DSDP hole 207 (Burns *et al*., 1973; van der Lingen, 1973; McDougall & van der Lingen, 1974). It may indicate that silicic volcanic rocks form an important component of the early syn-rift sequence within the basin.

The predominance of mafic volcanic and volcaniclastic rocks in the dredge samples and the seabed volcanic features apparent in the multibeam bathymetry data indicate widespread post-rift volcanism in the Capel–Faust Basins. Magnetic data acquired during the survey and the existing seismic data indicate that large post-rift intrusive bodies also occur in the subsurface of the survey area. Stratigraphic relationships observed in the GA302 seismic data indicate an Oligocene to Recent age. Such volcanic activity may have implications for the thermal history and source rock maturation within the basin, by providing a late stage heat pulse. Associated hydrothermal activity may have implications for seal integrity and reservoir rock porosity and permeability. Preliminary results of the head-space gas analysis of sediment core samples indicate that there are no direct indications of hydrocarbon within the sub-bottom sediments (G. Logan, pers. comm., 2008). However, the shallow depth of the samples (generally less than 4 m below seabed) is insufficient for an unequivocal determination of the presence, or otherwise, of hydrocarbons at depth within the basins.

10. References

Anderson, T.J., Cochrane, G.R., Roberts, D.A., Chezar, H., and Hatcher, G., (2008), A rapid method to characterize seabed habitats and associated macro-organisms. *In*: Todd, B.J., and Greene, H.G. (Eds.), *Mapping the Seafloor for Habitat Characterization: Geological Association of Canada*, Special Paper 47, p.71-79. Geological Society of Canada, Ottawa.

Auzende, J-M., Beneton, G., Dickens, G., Exon, N., François, C., Hodway, D., Juffroy, F., Lafoy, Y., Leroy, A., van de Beuque, S., and Voutay, O., 2000. Mise en evidence de diapirs mésozoïques sur la bordure orientale de la ride de Lord Howe (sud-oest Pacifique): campagne ZoNéCo 5. C.R. Academie de Science Paris. *Sciences de la Terre et des Planètes* **330**, 209–215.

Beggs, J.M., 1993. Depositional and tectonic history of the Great South Basin. *In*: Balance, P.F. (Ed.), *South Pacific sedimentary basins: Sedimentary basins of the world 2*, 365–373. Elsevier.

Bernardel, G., Alcock, M., Petkovic, P., Thomas, S., and Levinson, M., 2000. *Seafloor mapping of the South-east Region and adjacent and southern Macquarie Ridge.* Australian Geological Survey organisation Record **2000/46**. 75p.

Bernecker, T. and Partridge, A.D., 2001. Emperor and Golden Beach Sub-groups: the onset of Late Cretaceous sedimentation in the Gippsland Basin. *In*: Hill, K.C. and Bernecker, T., (Eds.), *Eastern Australasian Basins Symposium; a refocused energy perspective for the future*. Petroleum Exploration Society of Australia Special Publication, p.391–402.

Berner, R.A. 1980. *Early diagenesis: A theoretical Approach*. Princeton University Press, Princeton. 241p.

Bertness, M.D., Gaines, S.D., and Hay, M.E., 2001. *Marine Community Ecology*. Sinauer Associates, Inc., Massachusetts. 550p.

Best, A.I. and Gunn, D.E., 1999. Calibration of marine sediment core loggers for quantitative acoustic impedance studies. *Marine Geology* **160**, 137-146.

Blake, J.A., 1994. Vertical distribution of benthic infauna in continental slope sediments off Cape Lookout, North Carolina. *Deep Sea Research Part II: Topical Studies in Oceanography* 41, 919-927

Blevin, J.E., 2001. Hydrocarbon prospectivity of Australia's remote frontier areas in offshore east and southeast Australia — examples from the basins of Lord Howe rise. *In*: Hill, K.C. and Bernecker, T., (Eds.), *Eastern Australasian Basins Symposium; a refocused energy perspective for the future*. Petroleum Exploration Society of Australia Special Publication, p.25–35.

Boreham, C.J., Hope, J.M., Jackson, P., Davenport, R., Earl, K.L., Edwards, D.S., Logan, G.A., and Krassay, A.A., 2004. Gas-oil-source correlations in the Otway Basin, southern Australia. *In*: Boult, P.J., Johns, D.R., and Lang, S.C., (Eds.), *Eastern Australasian Basins Symposium II*, Petroleum Exploration Society of Australia Special Publication, p. 603–627.

Brothers, R.N. and Lille, A.R., 1988. Regional geology of New Caledonia. *In*: Nairn, A.E.M., Stehli, F.G., and Uyeda, S., (Eds.), *The Pacific Ocean: The ocean basins and margins*, p. 325–374. Plenum Press, New York.

Bryan, S.E., Constantine, A.E., Stephens, C.J., Ewart, A., Schon, R.W., and Parianos, J., 1997. Early Cretaceous volcano-sedimentary successions along the eastern Australian continental margin: implications for the breakup of eastern Gondwana. *Earth and Planetary Science Letters* **153**, 85–102.

Bryan, S.E., Ewart, A., Stephens, C.J., Parianos, J., and Downes, P.J., 2000. The Whitsunday volcanic province, central Queensland, Australia: lithological and stratigraphic investigations of a silicic-dominated large igneous province. *Journal of Volcanology and Geothermal Research* **99**, 55–78.

Burdige, D.J., 2006. *Geochemistry of marine sediments*. Princeton University Press. 609p.

Burns, R.E., Andrews, J.E., et al., 1973. *Initial Reports of the Deep Sea Drilling Project*, Volume **21**. U.S. Govt. Printing Office, Washington.

Colwell, J., Foucher, J.-P., Logan, G., and Balut, Y., 2006. *Programme AUSFAIR (Australia–Fairway basin bathymetry and sampling survey) Cruise Report*. Les rapports de campagnes à la mer, MD 153/AUSFAIR–ZoNéCo 12 and VT 82/GAB on board RV *Marion Dufresne*, Partie 2. Institut Polaire Français Paul Emile Victor, Plouzané, France, Réf : OCE/2006/05. 144pp.

Cook, R. A., Sutherland, R., and Zhu, H., 1999. *Cretaceous–Cenozoic geology and petroleum systems of the Great South Basin, New Zealand*. Institute of Geological and Nuclear Sciences Monograph 21.

Crawford, A.J., Mèffre, S., and Symonds, P.A., 2003. 120 to 0 Ma tectonic evolution of the southwest Pacific and analogous geological evolution of the 600 to 220 Ma Tasman Fold Belt System. *In*: Hillis, R.R. and Müller, R.D., (Eds.), *Evolution and dynamics of the Australian Plate*. Geological Society of Australia Special Publication **22** and Geological Society of America Special Publication **372**, 383–403.

Cronin, T.M. and M.E. Raymo, 1997. Orbital forcing of deep-sea benthic species diversity. *Nature* **385**, 624-627.

Damuth, J.E., 1980. Use of high-frequency echograms in the study of near-bottom sedimentation processes in the deep-sea: a review. *Marine Geology* **38**, 51–75.

Damuth, J.E., 1975. Echo character of the western equatorial Atlantic floor and its relationship to the dispersal and distribution of terrigenous sediments. *Marine Geology* **18,** 17–45.

Edwards, D.S., Struckmeyer, H.I.M., Bradshaw, M.T., and Skinner, J.E., 1999. Geochemical characteristics of Australia's southern margin petroleum systems. *APPEA Journal* **39**, 297–321.

Elendt, B.-P., 1990. Selenium deficiency in crustacean. *Protoplasma* **154**, 25-33.

Ellis, P.L., 1968. *Geology of the Maryborough 1:250,000 sheet area*. Geological Survey of Queensland Report 26.

Etheridge, M.A., Branson, J.C. and Stuart-Smith, P.G., 1985. The Bass, Gippsland and Otway basins, southeast Australia: a breached rift system formed by continental extension. *In*: Beaumont, C. and Tankard, A.J., (Eds.), *Sedimentary basins and basin forming mechanisms*, Canadian Society of Petroleum Geologists Memoir **12**, 147–162.

Etheridge, M., McQueen, H., and Lambeck, K., 1991. The role of intraplate stress in Tertiary (and Mesozoic) deformation of the Australian continent and its margins: a key factor in petroleum trap formation. *Exploration Geophysics* **22**, 123–128.

Etheridge, M.A., Symonds, P.A., and Lister, G.S., 1989. Application of the detachment model to reconstruction of conjugate passive margins. *In*: Tankard, A.J. and Balkwill, H.R., (Eds.), *Extensional tectonics and stratigraphy of the North Atlantic margins*. American Association of Petroleum Geologists Memoir **46**, 23–40.

Exon, N.F., Lafoy, Y., Hill, P.J., Dickens, G.R., and Pecher, I., 2007. Geology and petroleum potential of the Fairway Basin in the Tasman Sea. *Australian Journal of Earth Sciences* **54**, 629–645.

Exon, N.F., Quilty, P.G., Lafoy, Y., Crawford, A.J., and Auzende, J.-M., 2004. Miocene volcanic seamounts on northern Lord Howe Rise: lithology, age and origin. *Australian Journal of Earth Sciences* **51**, 291–300.

Foreman, M.G.G., 1977. *Manual for tidal heights analysis and prediction*. Pacific Marine Science Report 77-10, Institute of Ocean Sciences, Patricia Bay, Sidney, BC, 97 pp.

Gaina, C., Müller, D.R., Royer, J.-Y., Stock, J., Hardebeck, J., and Symonds, P., 1998. The tectonic history of the Tasman Sea: a puzzle with 13 pieces. *Journal of Geophysical Research* **103(B6)**, 12,413–12,433.

Gage, J.D., 1996. Why are there so many species in deep-sea sediments? *Journal of Experimental Marine Biology and Ecology* **200**, 257-286.

Game, P.M., 1970. Petrology of Lord Howe Island, Part 1: the younger volcanics. *Bulletin of the British Museum (Natural History) Mineralogy* **2**, 223–284.

Gavrilov, A.N., Duncan, A.J., McCauley, R.D., Parnum, I.M., Penrose, J.D., Siwabessy, P.J.W., Woods, A.J., & Tseng, Y-T., 2005. Characterization of the Seafloor in Australia's Coastal Zone using acoustic techniques. *Proceedings of the International Conference "Underwater Acoustic Measurements: Technologies & Results"*, Crete, Greece.

Gray J.S., 2002. Species richness of marine soft sediments. *Marine Ecology Progress Series* **244**, 285-297

Grim, P.J., 1969. Heatflow measurements in the Tasman Sea. *Journal of Geophysical Research* **74**, 3,933-3,934.

Hammerstad, E., 2000. Backscattering and seabed image reflectivity. EM Technical Note Kongsberg Horton Norway 6pp.

Harpole, W.S. and Tilman, D., 2007. Grassland species loss resulting from reduced niche dimension. *Nature* **446**, 791-793.

Harrington, H.J., 1983. Correlation of the Permian and Triassic Gympie terrane of Queensland with the Brook Street and Maitai terranes of New Zealand. *Permian geology of Queensland*. Proceedings of the Symposium on the Permian Geology of Queensland, Brisbane 14–16 July 1982, Geological Society Australia, Queensland Division, 431-436.

Harrington, H.J., 1987. Geological units common to eastern Australia and New Zealand. *Proceedings of the Pacific Rim Congress 1987*, p.801-804. The Australasian Institute of Mining and Metallurgy, Melbourne.

Harrington, H.J., 1998. The basement geology of Lord Howe Rise and Norfolk Ridge predicted by projections from Australia, New Zealand and New Caledonia. Pacific Exploration Technology Abstracts p. 33-36. South Pacific Commission, Suva.

Harrington, H.J., 1999. Submerged and detached portions of the New England and Lachlan foldbelts east of the Tasman Sea. Specialist Group in Tectonics and Structural Geology, Field Conference Abstracts, p.96-98. Halls Gap, Victoria.

Harrison, P.J., Yu, P. W., Thompson, P. A., Price, N.M., and Phillips, D.J., 1986. Survey of selenium requirements in marine phytoplankton. *Marine Ecology Progress Series* **47**, 89-96.

Hashimoto, T., Rollet, N., Earl, K., and Bernardel, G., 2008a. Capel and Faust basins — new information from the offshore frontier between Australia, New Zealand and New Caledonia. 2008 New Zealand Petroleum Conference Proceedings.

Hashimoto, T., Rollet, N., Higgins, K., Bernardel, G., and Hackney, R., 2008b. Capel and Faust basins: Preliminary assessment of an offshore deepwater frontier region. *In*: Blevin, J.E., Bradshaw, B.E., and Uruski, C. (Eds.), *Eastern Australasian Basins Symposium III*. Petroleum Exploration Society of Australia Special Publication, 311–316.

Hayes, D.E. and Ringis, J., 1973. Seafloor spreading in the Tasman Sea. *Nature* **243**, 454–458.

Heap, A., Edwards, D., Fountain, L., Spinnocia, M., Hughes, M., Mathews, E., Griffin, J., Borissova, I., Blevin, J., Mitchell, C., and Krassay, A., 2008. *Geoscience Australia Survey SS08/2005 Post-survey Report: Geomorphology, Sedimentology and Stratigraphy of Submarine Canyons on the SW Australian Slope (RV* Southern Surveyor *September – October 2005)*. Geoscience Australia Record 2008/16. 138p.

Herzer, R.H., Chaproniere, G.C.H., Edwards, A.R., Hollis, C.J., Pelletier, B., Raine, J.I., Scott, G.H., Stagpoole, V., Strong, C.P., Symonds, P., Wilson, G.J., and Zhu, H., 1997. Seismic stratigraphy and structural history of the Reinga Basin and its margins, southern Norfolk Ridge system. *New Zealand Journal of Geology and Geophysics* **40**, 425–451.

Herzer, R.H., Sykes, R., Killops, S.D., Funnell, R.H., Burggraf, D.R., Townend, J., Raine, J.I., and Wilson, G.J., 1999. Cretaceous carbonaceous rocks from the Norfolk Ridge system, Southwest Pacific: implications for regional petroleum potential. *New Zealand Journal of Geology and Geophysics* **42**, 57–73.

Hill, P.J., 1994. *Geology and geophysics of the offshore Maryborough, Capricorn and northern Tasman Basins: results of AGSO Survey 91*. AGSO Record **1994/1**.

Hines, A.H. and Comtois, K.L., 1985. Vertical distribution of infauna in sediments of a subestuary of central Chesapeake Bay. *Estuaries* **8**, 296-304.

Jacobs, D.K. and Lindberg, D.R., 1998. *Oxygen and evolutionary patterns in the sea: onshore/offshore trends and recent recruitment of deep-sea faunas*. Proceedings of the National Academy of Sciences USA 95, 9,396–9,401.

Jongsma, D. and Mutter, J.C., 1978. Non-axial breaching of a rift valley: evidence from the Lord Howe Rise and the Southeastern Australian margin. *Earth and Planetary Science Letters* **39**, 226–234.

Johnson, D.P., 2004. *The Geology of Australia*. Cambridge University Press, Cambridge. 276p.

Kamp, P.J.J., 1986. The mid-Cenozoic Challenger Rift System of western New Zealand and its implications for the age of Alpine fault inception. *Geological Society of America Bulletin* **97**, 255–281.

Kana, T.M., Darkangelo, C., Hunt, M.D., Oldham, J.B., Bennett, G.E., and Cornwell, J.C. 1994. Membrane inlet mass spectrometer for rapid high-precision determination of N_2, O_2, and Ar in environmental samples. *Analytical Chemistry* **66**, 4,166-4,170.

Kawahata, H., 2002. Shifts in oceanic and atmospheric boundaries in the Tasman Sea (Southwest Pacific) during the Late Pleistocene: evidence from organic carbon and lithogenic fluxes. *Paleogeography, Palaeoclimatology, Palaeoecology* **277**, 1-25.

Kennett, J.P. and von der Borch, C.C., 1986. *Southwest Pacific Cenozoic paleoceanography*. *In*: Initial Reports of the Deep Sea Drilling Project, Volume **90**, p. 1493-1517. U.S. Govt. Printing Office, Washington.

Killops, S.D., Cook, R.A., Sykes, R., and Boudou, J.P., 1997. Petroleum potential and oil-source correlation in the Great South and Canterbury Basins. *New Zealand Journal of Geology and Geophysics* **40**, 405–423.

King, P.R. and Thrasher, G.P., 1997. *Cretaceous–Cenozoic geology and petroleum systems of the Taranaki Basin, New Zealand*. Institute of Geological and Nuclear Sciences Monograph **13**.

Koslow, J.A. and Gowlett-Holmes, K., 1998. *The seamount fauna off southern Tasmania: Benthic communities, their conservation and impacts of trawling*. Final Report to Environment Australia and the Fisheries Research and Development Corporation. FRDC project 95/058.

Kroh, F., Morse, M.P. and Hashimoto, T., 2007. *New data on the Capel and Faust basins. Preview,* **130**, 22–24.

Lacoste, L.J.B., 1973. Cross-correlation method for evaluating and correcting shipboard gravity data. *Geophysics* **38**, 701-709; DOI:10.1190/1.1440369.

Lafoy, Y., Brodien, I., Vially, R., and Exon, N.F., 2005. Structure of the basin and ridge system west of New Caledonia (Southwest Pacific); a synthesis. *Marine Geophysical Researches* **26**, 37–50.

Launay, J., Dupont, J., Lapouille, A., Ravenne, C., and de Brion, C.E., 1977. Seismic traverses across the northern Lord Howe Rise and comparison with the southern part (South-west Pacific). *Symposium on International Geodynamics in Southwest Pacific*, p.155–163. Noumea, 27 August–2 September 1976, Editions Technip, Paris.

Levin, L.A., Etter, R.J., Rex, M.A., Gooday, A.J., Smith, C.R., Pineda, J., Stuart, C.T., Hessler, R.R, and Pawson, D. 2001. Environmental influences on regional deep-sea species diversity. *Annual Review of Ecology and Systematics* **32**, 51-93.

Lipski, P., 2001. Geology and hydrocarbon potential of the Jurassic–Cretaceous Maryborough Basin. *In*: Hill, K.C. and Bernecker, T., (Eds.), *Eastern Australasian Basins Symposium; a refocussed energy perspective for the future*. Petroleum Exploration Society of Australia Special Publication, 263-268.

Lipski, P., 2004. Evidence for an oil play fairway on the inner shelf of the Great South Basin. 2004 New Zealand Petroleum Conference Proceedings.

Lowry, J., 1989. *Research Summary Cruise FR5/89: Survey of the Benthic Invertebrates from the*

Lord Howe Rise and Seamounts close to the Coast of NSW. CSIRO Division of Oceanography, Hobart. 11p.

McDougall, I. and Duncan, R.A., 1988. Age progressive volcanism in the Tasmantid Seamounts. *Earth and Planetary Science Letters* **89**, 207–220.

McDougall, I. and van der Lingen, G.J., 1974. Age of rhyolites on the Lord Howe Rise and the evolution of the southwest Pacific Ocean. *Earth and Planetary Science Letters* **21**, 117-126.

McDougall, I., Embleton, B.J.J., and Stone, D.B., 1981. Origin and evolution of Lord Howe Island, Southwest Pacific. *Journal of the Geological Society of Australia* **28**, 155-176.

McDougall, I., Maboko, M.A.H., Symonds, P.A., McCulloch, M.T., Williams, I.S., and Kudrass, H.R., 1994. Dampier Ridge, Tasman Sea, as a stranded continental fragment. *Australian Journal of Earth Sciences* **41**, 395-406.

McEwen, G.F., Johnson, M.W., and Folsom, T.R., 1954. A statistical analysis of the performance of the Folsom plankton sample splitter, based upon test observations. *Meterology and Atmospheric Physics* 7, 502-537.

McTainsh, G.H., 1989. Quaternary dust processes and sediments in the Australian region. *Quaternary Science Reviews* **8**, 235-253.

Middleton, D., 1999. New physical-statistical methods and models for clutter and reverberation: the KA-distribution and related probability structures. *IEEE Journal of Oceanic Engineering* **24**(3), 261-284.

Morin, R.H. and von Herzen, R.P., 1986. Geothermal measurements at Deep Sea Drilling Project Site 587. *In*: Kennett, J.P. and the Shipboard Party (Eds.), *Initial reports of the Deep Sea Drilling Project 90*, p.1,317-1,324. U.S. Government Printing Office, Washington D.C.

Mortimer, N., 2004. New Zealand's geological foundations. *Gondwana Research* **7**, 261-272.

Mortimer, N., Hauff, F., and Calvert, T., 2008. Continuation of the New England Orogen, Australia, beneath the Queensland Plateau and Lord Howe Rise. *Australian Journal of Earth Sciences* **55**, 195-209.

Mortimer, N., Herzer, R.H., Gans, P.B., Parkinson, D.L., and Seward, D., 1998. Basement geology from Three Kings Ridge to West Norfolk Ridge, southwest Pacific Ocean: evidence from petrology, geochemistry and isotope dating of dredge samples. *Marine Geology* **148**, 135-162.

Nelson, C.S., Briggs, R.M., and Kamp, P.J.J., 1986. Nature and significance of volcanogenic deposits at the Eocene/Oligocene boundary, hole 593, Challenger Plateau, Tasman Sea. *In*: Kennett, J.P. and the Shipboard Party, (Eds.), *Initial reports of the Deep Sea Drilling Project 90*, p.1,175-1,188. U.S. Government Printing Office, Washington D.C.

Nilsson, C.S. and Cresswell, G.R., 1981. The formation and evolution of East Australian Current warm-core eddies. *Progress in Oceanography* **9**, 133-183.

Norvick, M.S., Smith, M.A., and Power, M.R., 2001. The plate tectonic evolution of eastern Australasia guided by the stratigraphy of the Gippsland Basin. *In*: Hill, K.C., and Bernecker, T., (Eds.), *Eastern Australasian Basins Symposium; a refocussed energy perspective for the future*, p.15-24. Petroleum Exploration Society of Australia Special Publication.

Norvick, M.S., Langford, R.P., Hashimoto, T., Rollet, N., Higgins, K.L., and Morse, M.P., 2008. New insights into the evolution of the Lord Howe Rise (Capel and Faust basins), offshore eastern Australia, from terrane and geophysical data analysis. *In*: Blevin, J.E., Bradshaw, B.E., and Uruski, C., (Eds.), *Eastern Australasian Basins Symposium III*, p. 291-310. Petroleum Exploration Society of Australia Special Publication.

O'Brien, P.E., Powell, T.G., and Wells, A.T., 1994. Petroleum potential of the Clarence–Moreton Basin. *In*: Wells, A.T. and O'Brien, P.E., (Eds.), *Geology and petroleum potential of the Clarenc–Moreton Basin, New South Wales and Queensland*. AGSO Bulletin **241**, 277-290.

Paris, J.P., 1981. Géologie de la Nouvelle-Calédonie. *Bureau des Recherches Géologiques et Minières Memoire* **113**, 279 pp.

Paris, J.P. and Lille, R., 1977. New Caledonia: evolution from Permian to Miocene mapping data and hypotheses about geotectonics. *Symposium on International Geodynamics in Southwest Pacific*, p. 195–208. Noumea, 27 August–2 September 1976, Editions Technip, Paris.

Partridge, A.D., 2001. Revised stratigraphy of the Sherbrook Group, Otway Basin. *In*: Hill, K.C. and Bernecker, T., (Eds.), *Eastern Australasian Basins Symposium; a refocused energy perspective for the future*, p.455-464. Petroleum Exploration Society of Australia Special Publication.

Pawlowicz, R., Beardsley, B., and Lentz, S., 2002. Classical tidal harmonic analysis including error estimates in Matlab using T_TIDE. *Computers & Geosciences* **28**, 929-937.

Perkin R.G., and Lewis, E.L., 1980. The Practical Salinity Scale 1978: Fitting the data. *IEEE Journal of Oceanic Engineering* **X**, 9-16

Pickard, G.L., and Emery, W.J., 1982. *Descriptive Physical Oceanography: An Introduction*. 4th edition, Pergamon Press, Oxford, 249 pp.

Pitcher, T.J., 2007. *Seamount: Ecology, Fisheries and Conservation*. Fish and Aquatic Resources Series, Vol. 12, Oxford Press. 527p.

Pugh, D., 2004. *Changing Sea Levels: Effects of Tides, Weather and Climate*. Cambridge University Press, Cambridge, 265 pp.

Purvis, A.C. and Pontifex, I.R., 2006. *Mineralogical report no. 8881*. Prepared for Geoscience Australia by Pontifex and Associates Pty. Ltd., Kent Town, South Australia, 29 June 2006 (unpublished).

Robinson, S.G., 1990. Applications for whole-core magnetic susceptibility measurements of deep-sea sediments: Leg 115 Results. *In*: Duncan, R.A., Backman, J., Peterson, L.C., *et al*. (Eds.), ODP, *Scientific Results, Ocean Drilling Program Leg 115*, pp.737-771. Texas A&M University, College Station.

Rodgers, A.D., 1994. The biology of seamounts. *Advances in Marine Biology* **30**, 305-354.

Roeser, H. and the Shipboard Party, 1985. *Geophysical, geological and geochemical studies on Lord Howe Rise*. Bundesanstalt für Geowissenschaften und Rohstoffe Report, Cruise SO36.

Schellart, W.P., Lister, G.S., and Toy, V.G., 2006. A Late Cretaceous and Cenozoic reconstruction of the Southwest Pacific region: tectonics controlled by subduction and slab rollback processes. *Earth-Science Reviews* **76**, 191-233.

Schubert, C.J., Niggemann, J., Klockgether, G., and Ferdelman, T.G., 2005. Chlorin Index: A new parameter for organic matter freshness in sediments. *Geochemistry, Geophysics & Geosystems* **6**, 1-12.

SCOR Working Group, 2007. GEOTRACES – An international study of the global marine biogeochemical cycles of trace elements and their isotopes. *Chemie der Erde* **67**, 85-131.

Sdrolias, M., Müller, D., and Gaina, C., 2001. Plate tectonic evolution of eastern Australian marginal ocean basins. *In*: Hill, K.C. and Bernecker, T., (Eds.), *Eastern Australasian Basins Symposium; a refocused energy perspective for the future*, p.227-237. Petroleum Exploration Society of Australia Special Publication.

Seiter, K., Hensen, C., and Zabel, M., 2005. Benthic carbon mineralisation on a global scale. *Global Biogeochemical Cycles* **19**, 1-26.

Siwabessy, P.J.W., Gavrilov, A.N., Duncan, A.J., & Parnum, I.M., 2006. Analysis of statistics of backscatter strength from different seafloor habitats. *Acoustics 2006*, Australian Acoustic Association, Christchurch, New Zealand, 507-514.

Snape, I., Scouller, R.C., Stark, S.C., Stark, J., Riddle, M.J., and Gore, D.B., 2004. Characterisation of the dilute HCl extraction method for the identification of metal contamination in Antartic marine sediment. *Chemosphere* **57**, 491-504.

Shor, G.G., Kirk, H.K., and Menard, H.W., 1971. Crustal Structure of the Melanesian Area. *Journal of Geophysical Research* **76**, 2,562-2,586.

Slater, R.A. and Goodwin, R.H., 1973. Tasman Sea guyots. *Marine Geology* **14**, 81–99.

Stagg, H.M.J., Alcock, M., Borissova, I., and Moore, A.M.G., 2002. *Geological framework of the southern Lord Howe Rise and adjacent areas*. Geoscience Australia, Record **2002/25**.

Stagg, H.M.J., Borissova, I., Alcock, M., and Moore, A.M.G., 1999. Tectonic provinces of the Lord Howe Rise; Law of the Sea study has implications for frontier hydrocarbons. *AGSO Research Newsletter* **31**, 31-32.

Sterner, R.W., Andersen, T., Elsner, J.J., Hessen, D.O., Hood, J.M., McCauley, E., and Urabe, J., 2008. Scale dependent carbon:nitrogen:phosphorus seston stoichiometry in marine and freshwaters. *Limnology and Oceanography* **53**, 1,169-1,180.

Stewart, J.R. and Alder, J.D., 1995. New South Wales Petroleum Potential. *New South Wales Department of Mineral Resources Coal and Petroleum Geology Branch Bulletin* **1**.

Stocks, K., 2004. Seamount invertebrates: composition and vulnerability to fishing. *Ín:* Morato, T. and Pauly, D. (Eds.), *Seamounts: Biodiversity and Fisheries*. Fisheries Centre Research Report, Vol 12 (5), pp.17-24. University of British Columbia, Vancouver.

Stone, S.S., Madin, L.P., Stocks, K., Hovermale, G., Hoagland, P., Schumacher, M., Etnoyer, P., Sotka, C., and Tausig, H., 2004. Seamount Biodiversity, exploitation and conservation. *In:* Glover, L.K., Earle, S.A., and Kelleher, G., (Eds.), *Defying Ocean's End: An Agenda for Action*, pp.43-70. Island Press, USA

Symonds, P.A., Colwell, J.B., Struckmeier, H.I.M., Willcox, J.B., and Hill, P.J., 1996. Mesozoic rift basin development off eastern Australia. *Geological Society of Australia Extended Abstracts* **43**, 528–542.

Talukdar, K.K., Tyce, R.C., & Clay, C.S., 1995, Interpretation of Sea Beam backscatter data collected at the Laurentian fan off Nova Scotia using acoustic backscatter theory. *The Journal of the Acoustical Society of America* **97**(3), 1545-1558.

Townsend, A.T., Palmer, A.S., Stark, S.C., Samson, C., Scouller, R.C., and Snape, I., 2007. Trace metal characterisation of marine sediment reference materials MESS-3 and PAC-2 in dilute HCl extracts. *Marine Pollution Bulletin* **54**, 226-246.

Tulloch, A., Beggs, M., Kula, J., Spell, T., and Mortimer, N., 2006. Cordillera Zealandica, the Sisters Shear Zone and their influence on the early development of the Great South Basin. *2006 New Zealand Petroleum Conference Proceedings*.

Tulloch, A., Kimbrough, D.L., and Wood, R.A., 1991. Carboniferous granite basement dredged from a site on the southwest margin of the Challenger Plateau, Tasman Sea. *New Zealand Journal of Geology and Geophysics* **34**, 121-126.

Uruski, C.I. and Stagpoole, V., 2004. *Wakanui-1, independent well summary*. New Zealand Crown Minerals open-file Petroleum Report 3053, Ministry of Commerce, Wellington.

Uruski, C., Baillie, P., and Stagpoole, V., 2003. Development of the Taranaki Basin and comparisons with the Gippsland Basin: implications for deepwater exploration. *APPEA Journal* **43**, 185–196.

Van de Beuque, S., Stagg, H.M.J., Sayers, J., Willcox, J.B., and Symonds, P.A., 2003. *Geological framework of the northern Lord Howe Rise and adjacent areas*. Geoscience Australia, Record **2003/01**.

Van der Lingen, G.J., 1973. The Lord Howe Rise rhyolites. *In*: Burns, R.E and the Shipboard Party, (Eds.), *Initial reports of the Deep Sea Drilling Project 21*, p.523–539. U.S. Government Printing Office, Washington D.C.

Veevers, J.J., 2000. *Billion-year earth history of Australia and neighbours in Gondwanaland*. GEMOC Press, Macquarie University, Sydney.

Von Herzen, R.P., 1973. Geothermal measurements, Leg 21. *In*: Burns, R.E and the Shipboard Party, (Eds.), *Initial reports of the Deep Sea Drilling Project 21*, p. 443–457. U.S. Government Printing Office, Washington D.C.

Walters, R.A., Goring, D.G., Bell, R.G., 2001. Ocean tides around New Zealand. *New Zealand Journal of Marine and Freshwater Research* **35**, 567-579.

Willcox, J.B. and Sayers, J., 2001. Gower Basin, Lord Howe Rise. *In*: Hill, K.C. and Bernecker, T., (Eds.), *Eastern Australasian Basins Symposium; a refocussed energy perspective for the future*, p.189-200. PESA Special Publication.

Willcox, J.B. and Sayers, J., 2002. *Geological framework of the central Lord Howe Rise (Gower Basin) region*. Geoscience Australia Record **2002/11**.

Willcox, J.B., Sayers, J., Stagg, H.M.J., and van de Beuque, S., 2001. Geological framework of the Lord Howe Rise and adjacent oceanic basins. *In*: Hill, K.C. and Bernecker, T., (Eds.), *Eastern Australasian Basins Symposium; a refocussed energy perspective for the future*, p.211–225. PESA Special Publication.

Williams, A., Gowlett-Holmes, K., and Althaus, F., 2006. *Biodiversity survey of the seamounts and slopes of the Norfolk Ridge and Lord Howe Rise (NORFANZ)*. Final Report to the National Oceans Office, April 2005. CSIRO Marine Research, Hobart, Tasmania.

Witte, U., 2000. Vertical distribution of metazoan macrofauna within the sediment at four sites with contrasting food supply in the deep Arabian Sea. *Deep Sea Research Part II: Topical Studies in Oceanography* **14**, 2,979-2,997.

Willis, I.L., 1985. *Clarence–Moreton Basin, New South Wales, Petroleum Data Package*. Geological Survey of New South Wales Report **1985/010**.

Zhu, H. and Symonds, P.A., 1994. Seismic interpretation, gravity modelling and petroleum potential of the southern Lord Howe Rise region. 1994 New Zealand Petroleum Conference Proceedings.

11. Acknowledgements

We thank the masters and crews of Leg 1 and Leg 2 on the RV *Tangaroa* for their professional conduct throughout the survey. We gratefully acknowledge Fred Smits from NIWA for his co-ordination and logistical support. Technical support for the survey was ably provided by Kevin Mackay, Niki Davey, Steve George, Arne Pallentin, Matt Walkington, Rob Stewart and Stephen Robbins (NIWA), and Cameron Buchanan, Michele Spinnocia, Andrew Hislop, Craig Wintle, John Jaycock, Gareth Crook, Ray De Graaf, Stan Hancock, Franz Villagran, and Mathew Carey (Geoscience Australia). Maggie Tran, Janice Trafford, Kylia Wall, Liz Webber and Jenny Andersen (Geoscience Australia) are thanked for their assistance with processing of samples in the laboratory. We also thank the students and staff from the University of the Sea program who participated in the survey. Biological sampling and technical advice was provided by Dr Roland Pitcher, Dr Ted Wassenberg, Dr Doug Chetwynd, and Mr Ian McLeod (CSIRO, Cleveland), and Dr Alan Williams and Dr Karen Gowlett-Holmes (CSIRO, Hobart). We are indebted to Dr Matt McArthur (Geoscience Australia), Dr Robin Wilson, Dr Gary Poore, Dr Tim O'Hara, and Dr Mark. Norman (Museum of Victoria), Dr Jim Lowry and Dr Mark McGrouther (Australian Museum), Dr Chris Battershill and Dr Carsten Wolff (AIMS), Dr W. Richard Webber and Bruce Marshall (Te Papa Museum, NZ), and Dr Malcolm Francis (NIWA, NZ), for taxonomic identifications. The original report benefited from the review of Dr Heike Struckmeyer of Geoscience Australia.

12. Appendices

12.1. APPENDIX A – REGIONAL GEOLOGY

12.1.1. Structure

The Capel and Faust basins are located in the northern part of the LHR, a large stranded continental fragment that extends 1,600 km from the eastern Coral Sea near New Caledonia to the Bellona Trough (Fig. 1.1). The area is located in the vicinity of the former eastern Gondwana margin, which experienced plate convergence throughout much of the Palaeozoic and Mesozoic (Gaina *et al*., 1998; Sdrolias *et al*., 2001; Veevers, 2000; Crawford *et al*., 2003; Schellart *et al*., 2006). The current structural configuration of the region was attained largely as a result of oblique extension during the Early Cretaceous to Eocene, that culminated with the opening of the Tasman Sea and produced a mosaic of continental fragments, rifts and small oceanic basins in the back-arc region of the margin (Hayes & Ringis, 1973; Gaina *et al*., 1998; Sdrolias *et al*., 2001; Norvick *et al*., 2001, 2008; Crawford *et al*., 2003). The LHR is the largest of the continental fragments with an estimated crustal thickness of 14–34 km (Shor *et al*., 1971; Zhu and Symonds, 1994). The rifting of the LHR from eastern Australia is believed to have been strongly asymmetric, with the Lord Howe Rise being conceptualised as the 'lower plate' margin composed of extended continental crust (Jongsma & Mutter, 1978; Etheridge *et al*., 1989). The rise is flanked to the east and west by sag basins (e.g., Middleton, Fairway and New Caledonia; Auzende *et al*. 2000; Lafoy *et al*. 2005; Exon *et al*. 2007; Norvick *et al*., 2008) and smaller continental fragments (e.g., Dampier Ridge; McDougall *et al*., 1994). Some of these sag basins may be underlain by transitional or oceanic crust (Shor *et al*., 1971; Gaina *et al*., 1998; Lafoy *et al*., 2005; Norvick *et al*., 2008).

The Lord Howe Rise exhibits a NNW–SSE to N–S trend and may be subdivided into three major structural zones (Stagg *et al*., 1999, 2002; Willcox *et al*., 2001; Van de Beuque *et al*., 2003; Fig. 12.1). The LHR Platform (Stagg *et al*., 1999, 2002; Van de Beuque *et al*., 2003) is an eastern zone of extensive basement highs 100–200 km wide, in water depths of 1,000–1,300 m. Crustal thicknesses of 29–34 km (Shor *et al*., 1971; Zhu & Symonds, 1994) and the poor development of rift depocentres indicate that little crustal thinning took place here during rifting (Van de Beuque *et al*., 2003). It is draped by a thin (0–0.5 ms TWT) cover of mostly Cenozoic bathyal sediments.

The Central Rift Province (Stagg et al., 1999, 2002; Van de Beuque *et a*l., 2003) lies to the west of the LHR Platform in water depths of 1,300–1,700 m (Fig. 12.2). It includes the Faust Basin in the northern LHR and the Moore Basin in the southerly LHR. It comprises a series of basement highs and comparatively small, rift depocentres with sediment thicknesses of up to 3.0-3.5 s TWT. The sedimentary succession within the depocentres is likely to be dominated by Lower and Upper Cretaceous syn-rift clastics and volcanics, which are overlain by a Campanian–Recent sag sequence grading upward from non-marine or marginal marine clastics to bathyal carbonates (Willcox & Sayers, 2002; Van de Beuque *et al*., 2003; Norvick *et al*, 2008).

The rift depocentres are larger and deeper further westward in the Western Rift Province (Stagg *et al*., 1999, 2002; Van de Beuque *et al*., 2003; Fig. 12.2), which includes the Capel Basin in the north and the Monowai Basin in the south. In the central part of the LHR, the Central and Western Rifts merge to form the Gower Basin (Stagg *et al*., 1999; Willcox & Sayers, 2002; Colwell *et al*., 2006). Individual depocentres attain planform dimensions of up to 150 km by 40 km and are filled with sediments up to 4.0–4.5 s TWT thick. This general

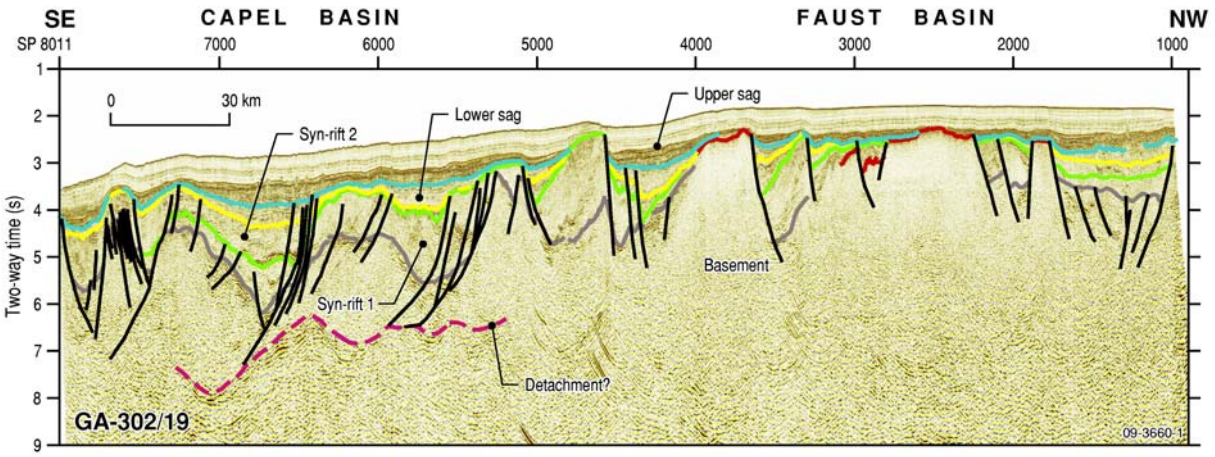

Figure 12.1. Seismic profile along GA-302 Line 019 in the northern LHR showing the contrasting rift basin development between the Western Rift Province (Capel Basin) and the Central Rift Province (Faust Basin).

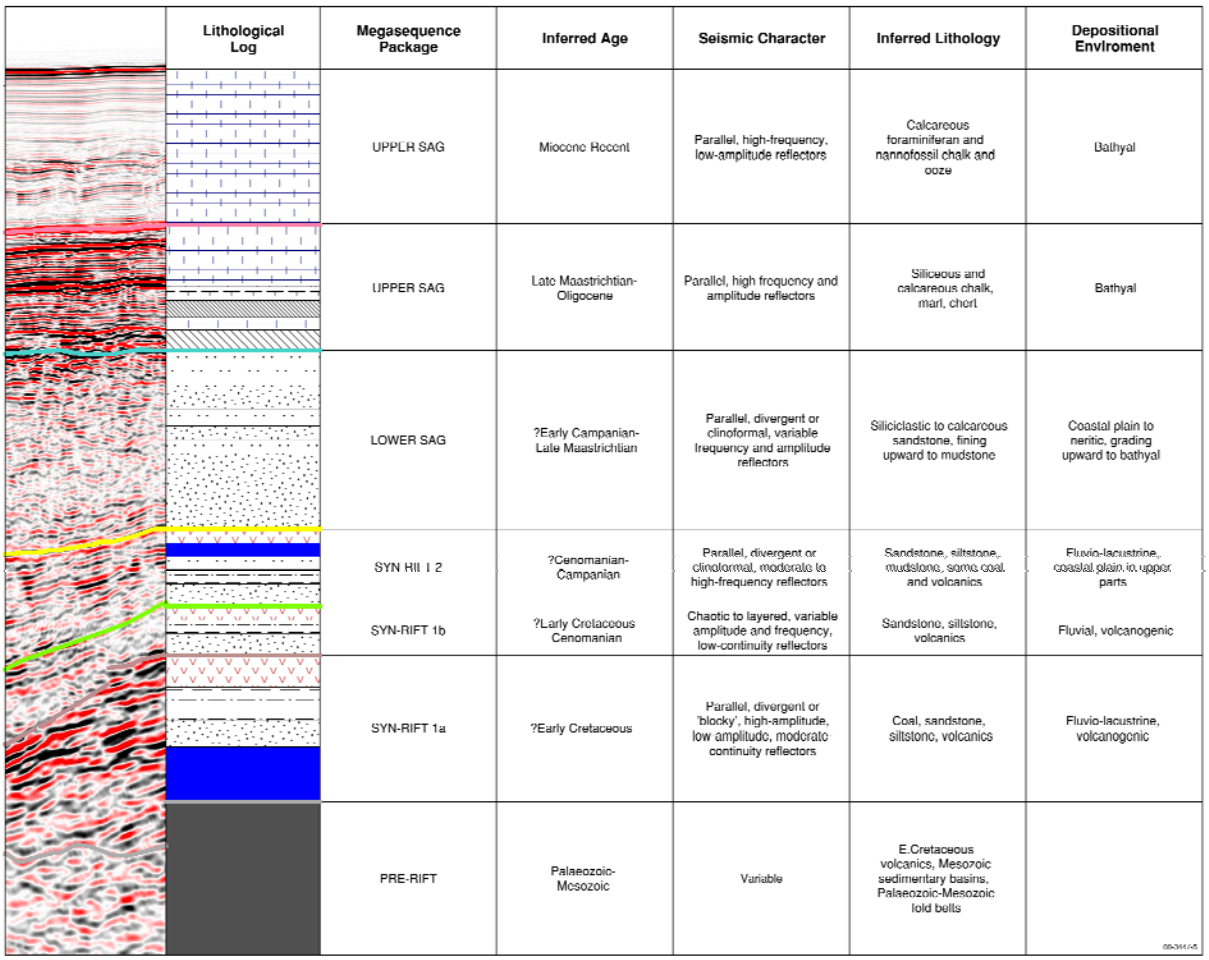

Figure 12.2. Main megasequence packages in the Capel and Faust basins, identified through seismic interpretation. Ages and lithologies of the megasequences are inferred from regional tectonic reconstructions and analogue basin studies.

westward increase in the degree of rift development reflects that of crustal thinning from the LHR Platform through to the Middleton Basin; crustal thicknesses are estimated to be 20 km or less in the Central and Western Rift Provinces (Shor *et al*., 1971; Zhu & Symonds, 1994).

12.1.2. Stratigraphy and Geologic Evolution

The GA302 seismic data, in conjunction with filtered satellite and shipboard gravity data, reveal the presence of over 10 major rift depocentres in the Capel and Faust basins, separated

by basement highs. The gravity data suggest that the depocentres are aligned along a dominant N–S to NW–SE structural trend. The depocentres are comparatively small, isolated, and bounded by easterly and westerly dipping faults in the Faust Basin, whereas they are larger, deeper, and bounded by lower-angle westerly dipping faults in the Capel Basin. The differences in rift development between the Capel and Faust basins may reflect the control placed on crustal thinning by heterogeneities in the composition and rheology of the basement. Preliminary interpretation of the seismic data has revealed a heterogeneous pre-rift basement, at least two syn-rift megasequences, and two post-rift sag megasequences (Norvick *et al*., 2008; Hashimoto *et al*., 2008a, b).

The pre-rift basement defines the boundaries to the rift depocentres and the intervening structural highs. On the basis of previous dredge sampling in the region and tectonostratigraphic reconstructions, the northern LHR is likely to be underlain by the offshore continuations of the Devonian–Triassic New England Orogen and the Upper Triassic–Lower Cretaceous sedimentary basins (especially the Clarence-Moreton, Nambour and Maryborough) of eastern Australia, the Triassic–Upper Jurassic Murihiku and Maitai terranes of New Zealand, and the Teremba terrane of New Caledonia (Harrington, 1983, 1987, 1998, 1999; Norvick *et al*., 2001, 2008; Mortimer, 2004; Mortimer *et al*., 2008). The pre-rift basement to the Capel and Faust basins imaged by seismic data may be subdivided according to its seismic character into 'opaque', 'layered' and 'volcanic' facies (Hashimoto *et al*., 2008a). The 'opaque' facies is characterised by weak internal reflections and may represent the deformed and variable lithologies of the New England Orogen, or it may simply be a consequence of acoustic masking by an indurated layer at the upper contact. The 'layered' facies features discontinuous, parallel, high-amplitude and low-frequency reflectors that are possibly indicative of coal-bearing sedimentary rocks; it may represent fragments of the Mesozoic eastern Australian basins or stratified sediments of the Maitai, Murihiku or Teremba terranes (Mortimer, 2004; Norvick *et al*., 2008). It is also possible that these sediments represent the oldest syn-rift sediments at the base of the rift depocentres. The 'volcanic' facies is characterised by high-amplitude, discontinuous, contorted or chaotic reflections generally overlying 'opaque' basement facies. It may represent the product of magmatism emplaced prior to or during the initial phases of rifting and may therefore correlate in part with the initial stages of the Syn-rift 1 megasequence.

The Syn-rift 1 megasequence package was deposited during the first major phase of rifting. Tectonic reconstructions and analogies with eastern Australian and offshore New Zealand basins suggest that this megasequence is the correlative of the widespread volcanic, volcaniclastic, sedimentary and intrusive rocks associated with extension and magmatism along the entire eastern Gondwana margin during the Lower Cretaceous to Cenomanian (Ellis, 1968; Hill, 1994; Symonds *et al*., 1996; Bryan *et al*., 1997, 2000; Veevers, 2000; Norvick *et al*., 2001, 2008; Tulloch *et al*., 2006). In the Capel and Faust basins, the highly variable seismic character of the Syn-rift 1 package indicates a heterogenous composition that may include volcanic flows, intrusives, volcaniclastics and fluvio-lacustrine sediments. High-amplitude, low-frequency reflectors suggestive of coal are commonly observed in the lower part of the Syn-rift 1 megasequence in the Capel Basin; these may alternatively be interpreted as being part of a pre-rift 'layered' basement. Dredge samples recovered from the eastern LHR Platform during the AUSFAIR survey include trachyte, latite and volcaniclastic conglomerate and sandstone (Colwell *et al*., 2006; Purvis & Pontifex, 2006). Preliminary results of zircon dating of the volcanic samples suggest an Upper Cretaceous age. Therefore, some of these rocks may, together with the Cenomanian rhyolite intersected at the DSDP 207 drill hole in the southern LHR (van der Lingen, 1973; McDougall & van der Lingen, 1974), represent this megasequence package. The Syn-rift 1 megasequence attains maximum

thickness in the western Faust and eastern Capel basins and exhibits growth into easterly and westerly dipping faults, suggesting that the area was proximal to the main locus of this rift phase.

The second phase of rifting in the area is represented by the Syn-rift 2 megasequence. It is interpreted as a fluvio-lacustrine to coastal plain clastic-dominated package with some volcanic and intrusive rocks. It is possibly equivalent to the Cenomanian–Eocene syn-rift clastics in other eastern and southern Australian offshore basins such as the Capricorn, Gippsland, Bass and Otway basins (Hill, 1994; Bernecker & Partridge, 2001; Blevin, 2001; Norvick *et al*., 2001, Partridge, 2001; Willcox & Sayers, 2001; Willcox *et al*., 2001), and basins of the NZ and western Pacific regions, Reinga Basin and West Norfolk Ridge (Herzer et al., 1997, 1999; Mortimer *et al*., 1998), Taranaki Basin (King & Thrasher, 1996; Norvick *et al*., 2001), Great South Basin (Beggs, 1993; Cook *et al*., 1999), and onshore New Caledonia (Paris & Lille, 1977; Paris, 1981; Brothers & Lille, 1988). In the Capel and Faust basins, the megasequence is inferred to have been deposited during the Cenomanian–Campanian (Norvick *et al*., 2008). The megasequence thickens to the west and is thin or absent in part of the Faust Basin. The continuous, moderate to high-frequency reflectors commonly exhibit growth into westward-dipping faults. This geometry suggests that the locus of rifting lay to the west of the Capel and Faust basins during this time, and that the main driver was the extension in the Tasman Sea and Middleton basins (Gaina *et al*., 1998; Sdrolias *et al*., 2001; Norvick *et al*., 2001).

The syn-rift megasequences are overlain by sediments deposited during the post-rift thermal sag phase. The Lower Sag megasequence is inferred to comprise shallow marine to bathyal siliciclastic to carbonate sediments deposited during the Campanian–Maastrichtian (Norvick *et al*., 2001, Willcox & Sayers, 2001). The Upper Sag megasequence is dominated by Late Maastrichtian–Recent bathyal carbonates, including siliceous to calcareous chalk, marl and chert of Late Maastrichtian–Oligocene age, and foraminiferan and nannofossil chalk and ooze of Miocene–Recent age (Andrews, 1973; Norvick *et al*., 2008).

Localised inversion and anticlinal structuring is observed within the syn-rift and sag sequences, suggesting that the LHR region has been affected by compressional or transpressional stresses during the post-rift phase. An Eocene tectonic event, associated with a regional unconformity, fault reactivation, inversion and gentle folding, has been described previously from the LHR region (Willcox & Sayers, 2002; Van de Beuque, 2003), Capricorn Basin (Hill, 1994) and Gippsland Basin (Etheridge *et al*., 1985, 1991), which has been ascribed to the major global reorganisation in plate motions at c. 43 Ma (Etheridge *et al*., 1991; Veevers, 2000; Willcox & Sayers, 2002). Seismic data indicate areas of seafloor slumping that coincide with basement-involved faults at depth. This suggests ongoing neotectonic activity in the region, possibly associated with distal stresses originating from plate boundaries or fracture zones (Hashimoto *et al*., 2008a; Norvick *et al*., 2008).

Post-rift volcanism in the LHR region appears to have been concentrated during the Oligocene–Miocene (Stagg *et al*., 2002; Van de Beuque, 2003). Ages of volcanic centres along the Tasmantid seamount chain, and in onshore eastern Australia, decrease progressively to the south. This suggests that the igneous activity was associated with hotspots beneath the northward-moving Australian Plate (Vogt & Connolly, 1971; Wellman & McDougall, 1974; McDougall & Duncan, 1988). Smaller, apparently randomly-distributed volcanic centres of Miocene age may also be attributable to hotspot activity in areas of comparatively thick continental crust (Exon et al., 2004). In the southern LHR and Challenger Plateau, widespread volcanism also took place during the Eocene–Oligocene (Stagg *et al*., 2002), in association with extension in western New Zealand (Kamp, 1986; Nelson *et al*., 1986; Veevers, 2000).

12.2. APPENDIX B – SURVEY LEADER'S LOG

Geoscience Australia Survey TAN0713 – Eastern Australia
07/10/2007 – 22/11/2007
Survey Leaders Log
RV *Tangaroa*
Peter Harris (Leg 1) and Andrew Heap (Leg 2)

Leg 1.

Tuesday 07 October: RV *Tangaroa* sailed from Wellington at 0400 hrs UTC. Wind was storm force most of the day, 50 knots gusting to 70 knots, which delayed taking on fuel and which made most of us seasick when we got into Cook Strait that evening. There was some improvement on the 8th October but most people stayed in their bunks.

Thursday 09 October: The weather is much moderated and people are up and around. All data acquisition is going according to plan: gravity, magnetics, multi-beam sonar and sub-bottom data have been collected since departure and all systems are functioning well. Position at 2115 hrs UTC is -36° 55', 170° 20', speed 10.5 knots. We are on a direct course to station "Basement 1". Our ETA for station 1 is 2200 hrs UTC (10/10/07).

Friday 10 October: RV *Tangaroa* is in transit NNW making good speed at 11 knots. Position at 2015 hrs UTC is: -33° 22', 167° 03'. Our revised ETA for Station 1 is now 1500 hrs UTC. Seas are much calmer, winds are 15 to 25 knots and conditions are OK for sampling work at present. The team are in good spirits and looking forward to starting work soon. One issue is that IT did not provide sufficient passwords to allow computers brought from GA to be networked on the ship. This means we have several computers here that we can't use (including the Chief Scientists) and there are only two machines for sending e-mail on a ship with 40 crew. Ian Atkinson is in contact with people at IT but if it could be impressed upon them that we need those access codes to do our job it might help. Otherwise all systems are operating and all is well.

Saturday 11 October: RV *Tangaroa* still steaming north this past 24 hrs. Seas are moderate and wind is 10-15 knots. Ship's position at 2000 hrs UTC (10/10/07): -29° 49', 163° 56'. We are now mapping in Australia's extended continental shelf region east of Lord Howe and expect to start swath mapping around station "Basement 1" this afternoon. All underway equipment is functioning well and the team's spirits are high. Yesterday we enjoyed hearing presentations from the University of the Sea students on their projects (all are post-gradute students). Meanwhile GA staff are preparing for station work later today, learning to operate NIWA software for the underwater camera etc. Advised that IT have now provided sufficient passwords to network GA computers on the ship.

Sunday 12 October: RV *Tangaroa* is presently on station working at Station Basement 2. Position at 2200 hrs UTC (11/10/07) was -28° 16.7', 161° 56.8'. Wind is 10 knots and seas are <2 m. Yesterday, we completed mapping around station Basement 1 and completed a camera, dredge and CTD. The target feature is volcanic as sampled by manganese encrusted volcanic rocks and pumice in the dredge. Some thick growths of deep sea

corals were also seen in the video and sampled in the dredge. We are going for the record of "most people in a small room to observe underwater video operations in action"; last night we had around 15 enthusiastic observers. Today, after completion of Station 2 we will transit up to Area A and start multi-beam mapping. All is going well and people are in good spirits. As for networking the GA computers on the ship, it seems that IT have installed multiple items of security software that we are unable to circumvent in spite of having admin passwords, so we have not been successful on that front. This has been inconvenient for the team and created extra work for us (e.g., copy files onto external disks and carry from one machine to next to copy files, etc.). In future, greater cooperation with IT will be needed.

Monday 13 October: RV *Tangaroa* swath mapping Area A. Position at 2330 hrs UTC (12/10/07)is -26° 55', 161° 39'. Seas are 3 m and wind 20 knots. Yesterday, we completed camera and dredge operations at Station 2 (Basement 2 on the plan). The dredge brought back a small sample of manganese crusts and pumice along with bamboo corals and echinoderms. A sharks tooth was sieved from the calcareous sandy mud in the pipe dredge. Overall the story from Stations 1 and 2 is one of extremely slow sedimentation in the Holocene, with possible current winnowing as indicated by the presence of ripple marks observed in the video data. We have completed a CTD at Station 3 in Area A to calibrate the sound velocity and have finished 3 lines in Area A. We are working towards completing mapping of this section by early on 17th October but have reduced the line spacing to 3.2 km on account of the lower than expected swath range; this is reduced we suspect by the soft bottom sediments which provide only a poor bottom reflection. The team is in good spirits and all equipment is functioning well.

Tuesday 14 October: RV *Tangaroa* swath mapping Area A. Position at 2300 hrs UTC (13/10/07) is -27° 07', 161° 31'E. Seas are 3-4 m and wind 20 knots. Multi-beam sonar mapping is revealing the morphology of the northern Lord Howe Rise, a mostly subdued topography, probably affected by the ~500 m thick drape of Miocene-Pleistocene sediments reported by previous workers in the area. Features mapped so far include a large 3 km diameter, 400 m high volcano, a sea valley trending E-W across the area and isolated rocky outcrops with scoured moats around their bases.

Wednesday 15 October: RV *Tangaroa* swath mapping Area A. Position at 2200 hrs UTC (14/10/07) is -27° 09', 161° 23'E. Seas are 2-3 m and wind 13 knots. We have completed 11 lines of swath and are presently on Line 12. Latest revised completion time for mapping Area A is late PM on 16th October, after which we will start station work. Most people are over their seasickness now and are in good spirits. All data collection is going well.

Thursday 16 October: RV *Tangaroa* mapping Area A. Position at 2130 hrs UTC -27° 31', 161° 15'. Wind is 7 knots and seas 2.5 m. Sea temperature is 21° C. All personnel are looking forward to commencement of sampling today. Weather conditions are excellent: sunny and calm with light winds. The near-complete multi-beam map of Area A is very interesting and poses several interesting science questions. We have mapped two significant areas of rocky seabed that we have added to our list of dredge targets. These look superficially to be volcanics, based on comparison with the main volcano (Site V1). Another interesting feature is the appearance of mass wasting in the surface

morphology of the western margin of the ooze layer that drapes the upper section of the main N-S trending ridge. We have selected slump scarps and scours along that surface as sampling sites. In all we have selected 10 possible sites for stations over the next 2.5 days. Meanwhile the students have finished a very thorough analysis of the underwater camera data from Station 1. They have counted 70 different species of benthic fauna and analysed their distribution in relation to substrate type. They are all very keen and give a fresh and positive tone to our work.

Friday 17 October: RV *Tangaroa* sampling Area A. Position at 2230 UTC (16/10/07) is -27° 19', 161° 27'. Wind is 14 knots and seas are 2-3 m. After completion of multi-beam mapping at 0300 hrs UTC, we have completed work at 5 stations. The first was a seep site (Station 5) where we collected a 3.6 m piston core, box core and camera. There was very sparse biota in the camera, abundant burrows and mounds. The piston core contained stiff white nannofossil clay. In the box core the surface sediments were a cohesive, oxygenated nannofossil ooze which yielded a single polycheate worm in the sieve. We experienced camera and winch problems and work was stopped for 1 hour while repairs were underway. The camera failed on two occasions requiring repairs and causing loss of some data. The next station was the volcano (Station 6) where we collected a good haul in the rock dredge of various volcanic rocks, including some massive basalts we believe will be suitable for radiometric dating. The camera tow revealed abundant hard corals and a volcanic, boulder-strewn, highly rugose seascape. During the night two other volcanic outcrops were dredged, both yielding manganese crusts and the dredge brought up abundant hard corals and other animals. A benthic sled was towed over the 5th site of the night, returning sparse biota and sediment samples. A second 1-hour winch failure occurred at 1800 hrs UTC. For the latter three sites the NIWA camera operator (Stephen George) was asleep after having been awake for 20 hrs. A second NIWA technician (Nicola Davey) is being trained up to operate the camera so we will be able to have support for 24 hrs, but NIWA had only sent 1 trained camera operator and 1 CTD operator, which has caused some operational difficulties. Hence we will have to retrace our steps today to conduct camera operations over the sites dredged during the night when we had no operator. All in all we have had a very productive 24 hrs and the team are working hard and are in good spirits.

Saturday 18 October: RV *Tangaroa* continues sampling Area A, Lord Howe Rise. Position at 2345 UTC (17/10/07) is -27° 11', 161° 18'. Wind is 24 knots from the S and seas are 3 m. The sampling program continues successfully with the completion of seven stations in Area A so far. Completed operations in Area A include: three dredges, five bottom cameras, two benthic sleds, two piston cores and one box core. A 4.2 m piston core was obtained at a potential seep site (FS4) and samples taken for gas analysis. The site appears to be a hard ground in the seismic line that traverses the site and it has a comparatively rough character in the multi-beam data; our attempt to collect a box core was not successful at the site. We will resume multi-beam mapping operations at 1400 hrs UTC today in Area B. All personnel are well and equipment is functioning properly. A minor issue is that the e-mail system on the ship has problems and people are frustrated by being unable to send or receive mail. NIWA technical staff are investigating.

Sunday 19 October: RV *Tangaroa* is mapping Area B. Position at 0000 hrs UTC is -26° 54', 161° 41'. Wind is 25 knots from the SE and seas 4-5 m. Last night we completed station

work in Area B. Stations were occupied in a seafloor depression and on a flat area of seabed in the north of the mapped area. Box core, camera and benthic sled operations were completed yielding good sample recovery. However, worsening sea conditions hampered operations. Sampling work was completed by 0000 hrs UTC and swath mapping of Area B commenced at 0115 hrs UTC. Rough seas have caused some discomfort to the team, but in spite of this nine stations were completed in Area A in the allotted 60 hours. Swath mapping Area B will continue for the next four days.

Monday 20 October: RV *Tangaroa* continues swath mapping Area B. Position at 0000 hrs UTC is -26° 32', 161° 33'. Wind is easterly at 24 knots and seas 3m. Swath mapping is revealing the northern sector of our survey area to be largely low relief undulating seafloor with isolated rocky outcrops of possible volcanic origin. All equipment is functioning well and seas are gradually moderating as the wind is veering into the east. We are presently on the 7th line in Area B and expect it will require another three days to complete mapping the area. Meanwhile analysis of the seabed samples and video data is continuing on board. One interesting discovery was distinct, linear (clearly anthropogenic) marks seen by the underwater camera in the SW section of Area A. The opinion of the ships officers is that the marks are not trawl marks due to the shape of three parallel furrows, and it is speculated that they were caused by a cable laying ship. Since the longevity of any disturbance in this deep ocean environment is uncertain, the age of the marks is unknown.

Tuesday 21 October: RV *Tangaroa* continues swath mapping Area B. Position at 2300 hrs UTC (20/10/07) is -26° 30', 161° 26'. Wind is easterly at 23 knots and seas 3 m. Mapping continues to reveal the character of the seafloor in Area B as a low relief, undulating plateau. Interesting features include depressions, apparent slump scarps and occasional rocky outcrops. Closer inspection of these geomorphic features in seismic section shows that many are associated with subsurface basement topography, faults and volcanism. This survey will thus contribute to the general interpretation of subtle geomorphic features apparent in deep sea multi-beam sonar imagery. We expect to complete mapping work of Area B in around 48 hours time. All equipment is functioning well and people are in good spirits, apart from cases of persistent seasickness among two of the students.

Wednesday 22 October: RV *Tangaroa* continues swath mapping Area B. Position at 2230 hrs UTC (21/10/07) is -26° 15', 161° 18'. Wind is easterly at 23 knots and seas 3 m. The seafloor morphology continues as a low relief undulating plain, with some evidence for mass wasting and subsidence locally. The team are eager to start station work this evening as we will start the last swath line for this area at around 0200 UTC. The seas have reduced enough today that those suffering from seasickness have mostly recovered. All equipment is functioning and personnel are in good spirits.

Thursday 24 October: RV *Tangaroa* is sampling Area B. Position at 2300 hrs UTC (22/10/07) is -26° 19', 161° 42'. Wind is 10 knots from the E and seas 2 m. In the 24 hrs since yesterday we have completed another four stations which included two rock dredges on volcanic outcrops. Some samples of weathered basalt have been recovered. We did some fill-in swath mapping in the SE corner of Area B to complete the image of volcanics in that region. A volcanic ring-complex has been revealed, containing at least two other small cones. The benthos of the volcanic area is rich in corals and sessile

fauna seen in underwater video. A mystery is the several areas where large pieces of dead coral debris cover the seabed and where there is minimal live coral cover having only small live coral branches at present. We made radio contact yesterday with the French cable laying vessel "Ile de Re" which is carrying out cable-repair work in our area. Our mapping and sampling work brought us to within 1-mile of the ship and it is now clear that the elongate grooves we had seen earlier in seabed photos were indeed related to cable-laying operations. Frederick Saint-Cast spoke with the French captain on behalf of GA and we provided coordinates of volcanic peaks in the area that were of great interest to him. The captain of "Ile de Re" offered to share their swath data with GA and e-mail addresses have been exchanged.

Friday 25 October: RV *Tangaroa* is sampling Area B. Position at 2300 hrs UTC is -26° 17', 161° 20'. Wind is 17 knots from the E and seas 3 m. Good progress is being made with the sampling work and we are on schedule to complete 12 stations in Area B by our deadline at 1400 hrs UTC. We have completed four stations in the past 24 hours. These have been in mostly low relief areas characterised by muddy, bioturbated seafloor. Yesterday, three hours after a benthic sled operation was completed, we deployed the camera and found the bottom obscured by turbidity up to 0.5 km distance from the sled track line. The camera operation was completed by moving the ship 1 mile away from the benthic sled track, but our inadvertent experiment shows how disturbance of the bottom by sled or dredge operations causes a significant turbidity event over a broad area in such deep sea environments. Camera operations must always be carried our before any sled or dredge operations. All equipment is functioning and good quality data are being collected. The team are all getting excited about arriving at Lord Howe Island this weekend and spirits are high.

Leg 2.

Sunday 28 October: RV *Tangaroa* departed Lord Howe Island at 0300 hrs UTC after a successful crew change and re-supply. Scientific crew completed safety inductions before sailing. The ADCP was deployed without hitch at the northern site in 52 m water depth at 05:29 hrs UTC at -31° 24.000; 159° 04.870. We then deployed the gravity meter and proceeded to steam to Area C on a course west of, and parallel to, the Leg 1 transit to Lord Howe Island. Winds are 25 knots from 037° seas are 2-3 m. Most of the scientific crew are finding their sea legs.

Monday 29 October: RV *Tangaroa* continues to transit to Area C. Position at 0000 hrs UTC is -28° 55', 160° 32'. Wind is 22 knots from the NE and seas 2 m. Good progress is being made transiting back to the study area and the ship is now making 10 knots, after an uncomfortable night in moderate seas and 30+ knot winds where the ship was making only 8-9 knots. The multi-beam sonar shows the seabed to be mostly gently undulating with little surface relief. We have been getting up to 3.2 km wide coverage on the swath. The sub-bottom profiler has been giving intermittent coverage and little sub-bottom penetration. All staff are up and about and feeling much better. Winds and sea have eased considerably. An emergency drill was held at 0000 hrs UTC. All scientific crew participated ably in the drill.

Tuesday 30 October: RV *Tangaroa* continues to swath map Area C. Position at 0000 hrs UTC is -27° 08.273, 161° 08.873. Wind is 14 knots from 055°, seas are slight (1.5 m) from the

NE. Each of the 107 km long lines are taking about 6 hours to complete at an average of 10 knots. Turns are slow at 20-30 minutes to allow the gravity meter to settle down after making the turn. We have completed three lines in the last 20 hours. The outer beams on the multi-beam sonar are noisy and data are limited. Michele is doing a great job of "cleaning" these data. A concern is that there appears to be a persistent gap in the data on the port side, where it would appear that one of the multi-beam receivers is not receiving data, causing an artefact. This "gap" is not constant but is more common than is not. We are presently keeping a watch on this and Michele is presently able to "clean up" this section. Today, the students gave presentations on their research and backgrounds. All scientific crew appear to be mostly over their seasickness and spirits are high.

Wednesday 31 October: RV *Tangaroa* continues to swath map Area C. Position at 0000 hrs UTC is -27° 27.124, 161° 03.191. Wind is 18 knots from 077°, seas are slight (1.5 m) from the NE. Good progress continues to be made mapping Area C. The seabed is mostly undulating and hummocky, although a 200 m high (bedrock?) ridge occurs in the central eastern region. The ridge appears moated, indicating that currents are active around the structure. The sub-bottom profile continues to give minimal penetration of the seabed. We noticed during the night that the multi-beam gives better coverage when the seabed has more relief and we believe that the noisy outer beams are due to intermittent sound return from a relatively hard, compact muddy seabed. Apart from one or two cases of persistent sea sickness, all crew are in good spirits.

Thursday 01 November: RV *Tangaroa* continues to swath map Area C. Position at 0000 hrs UTC is -27° 14.136, 160° 55.877. Wind is 15 knots from 094°, seas are slight (1.5 m) from the NE. Good progress is being made in mapping Area C. The seabed continues to be hummocky and undulating although several cones (volcanic?) have been recorded in the north. These are potential sampling stations and one of them was identified as a target for dredging. All of the scientific crew are now over their seasickness and are settling in to enjoy the survey. We are all looking forward to completing the mapping and get sampling. We believe that we will begin sampling of Area C sometime on Saturday before transiting to Gifford Guyot. The weather is expected to remain fine and calm until Sunday. Preparations for the naming of the camera ceremony and Melbourne Cup day continue.

Friday 02 November: RV *Tangaroa* continues to swath map Area C. Position at 0000 hrs UTC is -27° 03.448, 160° 49.047. Wind is 11.5 knots from 080°, seas are slight (1.5 m) from the NE. We are now building up a nice picture of the western flank of the Lord Howe Rise. The area is characterized by a circular rise in the north that is punctuated by 4 volcanic cones up to 200 m high. Correlating with the seismic sections, the rise appears to be pelagic sediments draped over a sub-surface volcanic high with incipient volcanoes protruding from the surface above the seabed. The hummocky seabed, and the extents of broad, gentle rises and hollows, appear to also be related to polygonal faulting, with the faults extending into the subsurface on the seismic lines. A shallow, sinuous channel on the seabed on the eastern margin of the circular rise appears to be current swept, and probably formed from currents being deflected around the rise. Scientific crew were instructed in sampling techniques and protocols in preparation for beginning sampling of Area C which will occur after 1300 hrs UTC. We have selected five sites for sampling. The weather is forecast to remain fine and calm for the next

couple of days. The winning entry for the "Name-the-camera-competition" was *Brittlestar Gallactica* by Mary Mulcahy of UTS. All equipment is functioning well and the crew are in good spirits.

Saturday 03 November: RV *Tangaroa* continues to sample Area C. Position at 0000 hrs UTC is -27° 20.662, 160° 52.212. Wind is 7.3 knots from 051°, seas are slight (1.5 m) from the NE. Air temperature is 24° C. In the 24 hours since yesterday, we have completed two camera stations, a CTD, a box core, a piston core, and a rock dredge. The first camera station showed sandy and muddy substrate, with flat relief and low diversity. The second camera station was on a (bedrock?) ridge, and this station was characterised by moderate relief and moderate diversity. The CTD was taken in the deepest region (2000 m) in the SW of the study area. The piston core showed up to 3.4 m of pelagic sandy mud. A dredge collected on the ridge returned pumice, manganese nodules, coarse sandstone, and nannofossil sandy mud. All equipment is functioning well and the crew are in good spirits.

Sunday 04 November: RV *Tangaroa* continues to sample Area C. Position at 0000 hrs UTC is -26° 39.585, 160° 58.469. Wind is 11 knots from 354°, seas are slight (1.5 m) from the NE. Air temperature is 24° C. In the past 24 hours, we have completed three camera stations, a box core, a CTD, two dredges, and a benthic sled. The CTD was collected on the shallowest part (1500 m) in the north of the region. The camera stations were taken on an area of soft substrate, and two volcanic cones. The camera on the soft substrate showed a flat seabed comprised of foraminiferal ooze, with numerous burrows and trails. The box core from this station showed the seabed to be composed of foraminiferal fine sandy clay. Both the camera stations on the volcanic cones showed moderate relief with moderate biodiversity. Pillow basalts and manganese crusts were abundant, interspersed with foraminiferal muddy sand. The two dredges from these sites contained fragments of basalt, manganese crust, heavily bored (black stained) limestone, pumice and foraminiferal muddy sand. The benthic sled returned empty because the weak link broke and the net was inside out. From the net we recovered a squat lobster, shrimp, golden coral, and a salp. In each case, we were held fast to the seabed, but finally freed the gear with some expert manoeuvring of the ship by the crew. We completed sampling of Area C at 07:00 UTC and commenced swath mapping the E-W magnetic and gravity field tie line in the north of the area on our way to Area D. We expect to get to Area D by 16:00 UTC. All equipment is functioning well and the crew are in good spirits.

Monday 05 November: RV *Tangaroa* continues to swath map Area D. Position at 0000 hrs UTC is -26° 39.243, 159° 33.826. Wind is 12 knots from 318°, seas are slight (1.5 m) from the NE. Air temperature is 24° C. Mapping of Gifford Guyot has revealed spectacular steep slopes and what appear to be lava flows around the flanks, and the existence of several parasitic cones. Good progress is being made in covering the larger of the two seamounts that make up Gifford Guyot. There are numerous sites for possible camera, dredge and sled sampling. To our knowledge this will be most complete bathymetric mapping of a seamount on the northeastern Australian margin that has been undertaken. We are looking forward to the next few days where a clearer picture of the full extent and morphology and seabed environments of the seamount become apparent. All equipment is functioning well and the crew are in good spirits.

Tuesday 06 November: RV *Tangaroa* continues to swath map Area D. Position at 0000 hrs UTC is -26° 55.018, 159° 26.394. Wind is 23 knots from 198°, seas are 2 m) from the S. An amazing picture is beginning to emerge of Gifford Guyot. We have almost completed mapping the seamount, and will spend the next 9-12 hours filling in gaps on the 300 m deep flat top, and then we will begin sampling the different environments. The flanks of the seamount are precipitous with slopes of up to 45°, with numerous debris (and lava?) flows, slides, slumps, canyons, and fans. The flat top contains a series of subaqueous dunes, up to 6 m high and 200 m wavelength. A total of eight possible sampling locations have been proposed, including: field of subaqueous dunes, the flat top, submarine canyon, submarine fan, and the surrounding deep-seabed. Once mapped Gifford Guyot will be the most detailed dataset for a seamount in Australia, and the first time any seamount of this size has been mapped to such resolution. Scientific and ship's crew all participated in the Melbourne Cup celebrations at lunch today, with a special cake baked for the occasion. All equipment is working well and staff are in excellent spirits.

Wednesday 07 November: RV *Tangaroa* continues to sample Area D. Position at 0000 hrs UTC is -26° 43.252, 159° 25.701. Wind is 8 knots from 219°, seas are slight (1.0 m) from the SW. In the last 24 hours, we have completed mapping the stunning flat-topped Gifford Guyot and completed five stations. Station one on the dunes, showed them to be partly cemented and composed of weakly cemented calcrete. The grains are principally composed of foraminifera tests. The site was also characterised by moderate biota. Stations on the southern rim showed moderate diversity and rocky reefs. The rock dredge collected basalts, limestones (containing corals), calcrete and pelagic carbonate slightly muddy sand. The rocks also contained numerous organisms and the dredge also included a fish. The fan site was characterised by carbonate (foraminiferal) muddy sand. The benthic sled also contained numerous organisms, and basalt (pillow lava) in a conglomerate matrix and limestones. The site at the base of the fan was characterised by unconsolidated carbonate (foraminiferal) muddy sand. Unfortunately, we lost communications with the camera halfway through the run; the technicians are working on fixing the problem. We completed a box core at the site.

Thursday 08 November: RV *Tangaroa* continues to sample Area D. Position at 0000 hrs UTC is -26° 34.623, 159° 24.606. Wind is 9.5 knots from 057°, seas are slight (1.0 m) from the SW. In the last 24 hours we have completed three stations on the top and southern and north-eastern flanks of Gifford Guyot. A dredge on a ridge located at on the northern part of the flat top contained live coral (solitary). The problem with the camera is a faulty chip that relays the altimeter and depth data to the winch driver. However, given the significance of this shallow (250 m) ridge, we completed a camera at this site with the winch driver flying by eye. The ridge is characterised by rocky reef interspersed with coarse carbonate sand and moderate biota, including fish, gorgonians, brittlestars, urchins, sharks, and rays. A benthic sled was run over the crest of the ridge and returned weakly-cemented, porous calcrete. Grains in the calcrete were mostly composed of bryozoans, foraminifers, and molluscs fragments. No corals was sampled or seen in the video. After our fun and excitement of the many different environments at the seamount, we are now transiting back Area E to finish mapping the Capel and Faust basins and sample the stations prioritized by the petroleum program. This break of several days will allow all to catch up on processing of samples. All crew are in good spirits.

Friday 09 November: RV *Tangaroa* continues to swath map Area C. Position at 0000 hrs UTC is -26° 31.615, 160° 42.331. Wind is 20 knots from 060°, seas are moderate (2.0 m) from the SW. In the last 24 hours, we have transited back to Area C and completed the last three lines to complete mapping of the area. The western flank of the Lord Howe Rise is characterised by mostly hummocky seabed (polygonal faulting) and gentle relief. On the transit across several shallow depressions that contained transparent fill were imaged on the far western slopes. The swath data are noisier with the increase in sea state and wind. Apart from this, all equipment is working well and the crew are in good spirits.

Saturday 10 November: RV *Tangaroa* continues to swath map Area E. Position at 0000 hrs UTC is -27° 51. 309, 160° 36.739. Wind is 32.5 knots from 127°, seas are moderate (2-3 m) from the SW. Fine and sunny. We expect these conditions to last for the next 24 hours. In the last 24 hours, we have completed the last of the lines in Area C and one of the longer lines in Area E. The seabed is hummocky (polygonal faulting) and the volcanic rise seen the north of Area C continues west into Area E. Some staff continue to feel the effects of the rougher conditions and have spent more time in their bunks today. Tara gave a talk to the scientific and ship's crew at 0100 UTC about her work on the Kermadec Islands, which was well attended. The swath and sub-bottom profiler data continue to be noisy due to the rougher conditions. Apart from this, all equipment is working well and the crew are in good spirits.

Sunday 11 November: RV *Tangaroa* continues to swath map Area E. Position at 0000 hrs UTC is -27° 00.944, 160° 33.547. Wind is 20.3 knots from 124°, seas are moderate (2.0 m) from the SE. We are making good progress in swath mapping Area E. The seabed continues to be hummocky and displays polygonal faulting. We will commence sampling the first of three stations about 1600 UTC today. These sites are potential seep sites and will be the target of cameras and piston cores. All equipment is working well and crew are in good spirits.

Monday 12 November: RV *Tangaroa* continues to sample Area E. Position at 0000 hrs UTC is -27° 26.921, 160° 42.768. Wind is 22.3 knots from 151°, seas are moderate (2.0 m) from the SE. In the last 24 hours we have occupied three stations in the south of Area E that were prioritised as potential seep sites. We collected three cameras, three piston cores and a benthic sled from these sites. The underwater video showed each of the sites to be characterised by relatively flat bottom of pelagic carbonate sediments, with many burrows, tracks and infauna. All of the piston cores returned over 3 m of sediment, and they were sub-sampled for geochemical analysis. The benthic sled recovered. We lost our first piece of equipment at the second site, with the piston corer not returning from the depths, and we bent all the barrels due to the drifting of the ship. This is the first time we've ever lost the corer and not the weight. Fortunately, there was a spare bomb and plenty of barrels so we were able to continue. We also had communication problems with the camera, but the NIWA technicians worked valiantly and fixed the problem in time for the deployment. We will finish sampling at approximately 1300 UTC and re-commence swath mapping of Area E. All equipment working well and staff in good spirits.

Tuesday 13 November: RV *Tangaroa* continues to swath map Area E. Position at 0000 hrs UTC is -27° 47.757, 160° 25.910. Wind is 9.8 knots from 111°, seas are slight (1.0 m) from the SE. Fine and sunny. We continue to make good progress mapping Area E. The seabed continues to be hummocky, however a roughly circular 100 m-deep depression characterised by slump features is beginning to emerge in the far south of the area. A photo competition is being run with many entries on the table so far. All equipment working well and staff in good spirits.

Wednesday 14 November: RV *Tangaroa* continues to swath map Area E. Position at 0000 hrs UTC is -27° 26.341, 160° 23.453. Wind is 9.5 knots from 122°, seas are slight (1.0 m) from the SE. An interesting picture of the western flank of Lord Howe Rise is emerging. We have mapped a linear series of six (volcanic?) cones up to 150 m high in the north of the area. The 100 m deep depression in the south of the area has now broadened out to a flat, shallow valley in water depths of 2500 m. The eastern part of the depression is characterised by numerous circular slump features with relatively steep slopes (>20°). The remainder of the seabed continues to be characterised by the ubiquitous hummocky bottom and polygonal faulting. A survey photo was taken with all scientific and ship's crew participating. All equipment working well and staff in good spirits.

Thursday 15 November: RV *Tangaroa* continues to swath map Area E. Position at 0000 hrs UTC is -26° 49.658, 160° 21.341. Wind is 11.2 knots from 131°, seas are slight (1.0 m) from the SE. We are now swath mapping the lower sections of the western Lord Howe Rise. The seabed continues to be hummocky with polygonal faulting, which the students are seeing on the seabed video as irregular depressions in the pelagic sediments. No new features have been revealed, but we hope that new features may appear in the last few lines. All equipment working well and staff in good spirits.

Friday 16 November: RV *Tangaroa* continues to swath map Area E. Position at 0000 hrs UTC is -27° 06.232, 160° 16.220. Wind is 20.5 knots from 101°, seas are slight (1.0 m) from the SE. We completed swath mapping of Area E at approximately 1900 UTC and commenced sampling of two stations. The swath revealed the western flank of Lord Howe Rise to be characterised by a gently westward-dipping hummocky seafloor. Structures on the seabed were characterised by polygonal faulting, probably caused by dewatering of the upper few meters of the seabed sediment. We will continue sampling until beginning the transit to Wellington, New Zealand at approximately 0900 hrs UTC.

Saturday 17 November: RV *Tangaroa* continues to sample Area E. Position at 0000 hrs UTC is -27° 06.565, 160° 24.317. Wind is 17.2 knots from 111°, seas are slight (1.0 m) from the SE. We have completed two cameras and three piston cores and one benthic sled. The piston cores recovered 2.3 m, 2.95 m and 3.35 m of pelagic ooze. The cameras showed the seabed to be characterised by carbonate sandy mud with abundant infauna, but only moderate to low benthic fauna. We are still having problems with the communication cable to the camera and the NIWA technicians have used equipment from the CTD to try to rectify the problem. This means that we are unable to do anymore CTD's. Once we completed sampling, we finished off the last survey line, and then began the transit to Wellington at approximately 0930 hrs UTC.

Sunday 18 November: RV *Tangaroa* continues to transit to Wellington. Position at 0000 hrs UTC is -29° 08.534, 162° 26.895. Wind is 12.4 knots from 133°, seas are slight (1.0 m) from the SE. The survey has been a great success, mapping approximately 95% of the total area planned. A significant achievement included mapping Gifford Guyot. This amazing 2,000 m-high feature is the first seamount to be mapped in such detail on the Australian margin. The margins of the guyot are characterised by enormous slump scarps, slides, aprons and fans. On the 300 m deep surface are sinuous-crested, partly-cemented sandwaves up to 6 m high and several km long. We also discovered 10 new volcanic cones up to 150 m high on the Lord Howe Rise, including a linear series of 6 six cones on the western flank. The seabed over the Capel and Faust basins was mostly characterised by polygonal faulting, presumably from de-watering of the upper few metres of pelagic sediments, which we believe we captured in a camera tow (29CAM27). Other significant features included large circular slumps and current-eroded channels. Sediment and rocks recovered included: basalts (from the volcanic cones and guyot), manganese crusts, porous limestone, partly-cemented calcrete, and unconsolidated foraminiferal muddy sand and sandy mud. The biota observed and recovered was diverse, with moderate diversity on the rocky seabeds and abundant infauna in the unconsolidated sediments. Notable organisms include: sharks, crinoids, anemones, holothurians, squat lobsters, several species of fish, shrimps and crabs, as well as numerous brittlestars, hard corals and worms. We believe that many of these are new species. In the study area, we mapped 25,800 km^2 of seabed and collected 10,900 line-km of sub-bottom profiler, magnetic and gravity data (not including transits). The survey occupied 46 stations that returned: 42 camera tows (40 hours video + several thousand still images), 7 CTD's (to 2,200 m water depth), 15 Box Cores, 14 Piston Cores, 11 Benthic Sleds, 13 Rock Dredges, and 3 Grabs. Again, we have discovered completely new features of Australia's margin.

Monday 19 November: RV *Tangaroa* continues to transit to Wellington. Position at 0000 hrs UTC is -32° 01.260, 165° 45.763. Wind is 21 knots from 064°, seas are moderate (1-2 m) from the SW. We continue to make good progress to Wellington and have now passed over the eastern margin of the Lord Howe Rise, which was characterised by rugged seabed and slumps. The students have completed compiling the 1 minute snippets of the video stations. The FES crew continue to pack up the equipment and samples. The winners of the photograph competition were announced at a ceremony at 1300 hrs (LT) this afternoon, with a great selection to choose from.

Tuesday 20 November: RV *Tangaroa* continues to transit to Wellington. Position at 0000 hrs UTC is -35° 17.542, 168° 47.365. Wind is 16 knots from 115°, seas are slight (1.0 m) from the SE. Fine weather has allowed us to make good progress towards Wellington and the technicians have packed up all the gear and samples in good time. We are currently checking through the databases to ensure all has been allocated and accounted for. We have found some inconsistencies between Leg1 and Leg 2 descriptions and sampling protocols which will need to be fixed after we arrive in Canberra. We continue to collect multi-beam, sub-bottom and gravity and magnetics data. The seabed is becoming more variable closer to NZ with numerous knolls and valleys being detected. All equipment working well and staff are in good spirits.

Wednesday 21 November: RV *Tangaroa* continues to transit to Wellington. Position at 0000 hrs UTC is -38° 31.503, 171° 52.967. Wind is 1.8 knots from 210°, seas are slight (1.0 m)

from the SW. The multibeam data shows that we are now coming up the continental slope of west coast of NZ. Spectacular meandering canyons were imaged on the multibeam data from 1,500-800 m water depth, with the lower canyon channels infilled with sediment and the upper regions eroded. The shelf break appears hard on the sub-bottom profiles. We lost multibeam data for approximately 40 minutes this morning due to an unknown fault where the system had to be shut down. It is now working properly. All packing has been completed and final presentations, and thank you speeches, and trivia night are scheduled for this evening. All equipment working and staff are in good spirits.

Thursday 22 November: RV *Tangaroa* arrived in Wellington, New Zealand at 1905 hrs UTC (21/11/2007). Vessel position is -41° 16.148, 174° 47.232. Wind is 13.9 knots from 040°. Currently, we are tied alongside Burnham Wharf in Wellington Harbour at the end of a most successful survey. Yesterday about 1700 hrs (LT) we got our first glimpse of land with the impressive snow-covered Mt Taranaki (2,510 m) looming large on the horizon, and the flares and structures of the offshore oil rigs of the Maui gas field clearly visible. We have been accompanied by albatross most of the last 12 hours, and earlier were passed by a large pod of Sie whales. Last night, Heap summarised the science outcomes of the survey, and we held the RV *Tangaroa* trivia night organised by the University of the Sea students. It was a resounding success with the winners suitably adorned with sashes and crowns made by the students. The skipper, Roger, played guitar and sand an apt song entitled "The Ship With No Beer" to the tunes of that perennial Aussie folk song. The one thing that makes a survey is the people. Everyone on board: crew, technicians and scientists alike, are some of the best I've had the pleasure to sail with. A thoroughly enjoyable and successful survey.

12.3. APPENDIX C – MULTIBEAM SONAR STATISTICS

A report detailing the summary statistics for the multi-beam sonar data collected during the survey is provided as a pdf on the data DVD. The report contains details about data acquisition, processing and display, as well as statistics on the quality of the data collected for each of the raw multi-beam files. Summary information for the sound velocity profiles used to correct the multi-beam data are also provided.

12.4. APPENDIX D – GRAVITY & MAGNETICS SET-UP

12.4.1. Vessel Off-set Diagram

Job	Client	Vessel	Location
27529	NIWA / GEOSCIENCE AUSTRALIA	RV *Tangaroa*	CAPEL-FAUST
Technician	**Gravity Meter No.**	**Magnetometer**	**Mag Tow Distance**
DONALD CHILDERS	UltraSys S-65	Sea Spy	210 m

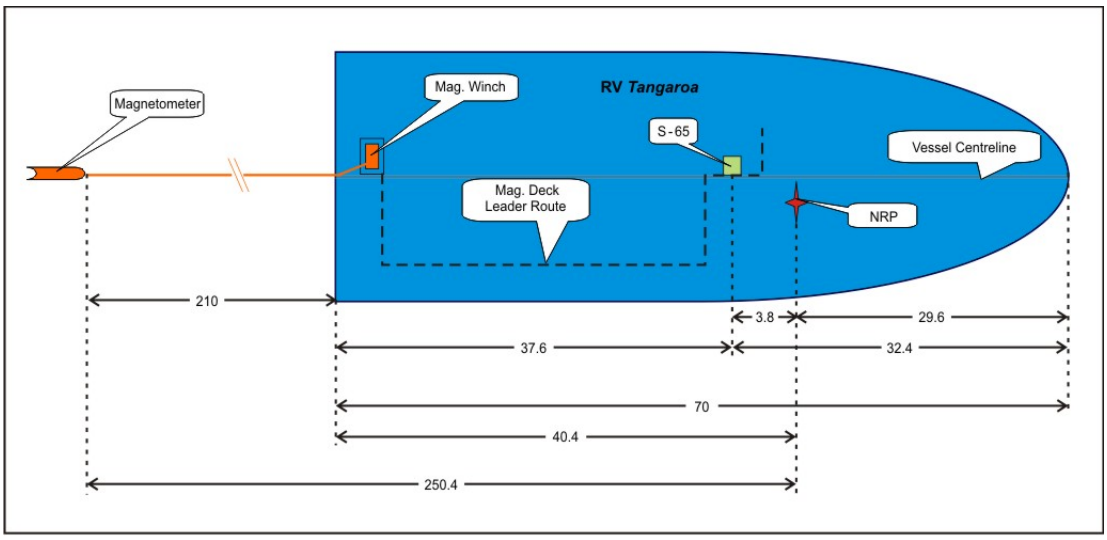

12.4.2. Ultrasys In-port Checks

Job	27529		NIWA / Geoscience Australia
Date	6 OCTOBER 2007	**Client Ref #**	
Julian Day	279	**Vessel**	R/V *Tangaroa*
Time (UTC)	16:00	**Survey Area**	Capel-Faust
Technician	Donald Childers	**Latitude (D°.M)**	-41°.3114435
Still Reading #	01	**Longitude (D°.M)**	174°.811760
Gravity Meter #	S-65	**Lat & Long Source**	FURUNO GPS
Acquisition Version	2.01	**Data File Name(s)**	200727916 & 17.zip
Platform Period (min)	4	**Zip Disk#**	01
Port Information			
Dock to Water (m)	3.6		6.0
Meter to Dock (m)	6.2	**Meter to Water (m)**	-2.6
Average Gravity	1911.5	**Average ST**	1911.5

Gravity System Measurements

Cross Gyro Orientation	OK	**Cross Bubble Level**	OK
Long Gyro Orientation	OK	**Long Bubble Level**	OK
	Beam Zero: (0.0 ± 20.0 mV)	**Beam Gain: (9000 ± 20.0 mV)**	
Prior to adjustment	215.0 mV	8592 mV	
After adjustment	4.0 mV	9002 mV	

K-Check	**Gravity**	**Spring Tension**	**TC (± 1.5 mGals of 30)**
+30 mGal	1911.6	1941.6	-30.0
-30 mGal	1910.4	1881.8	+30.3

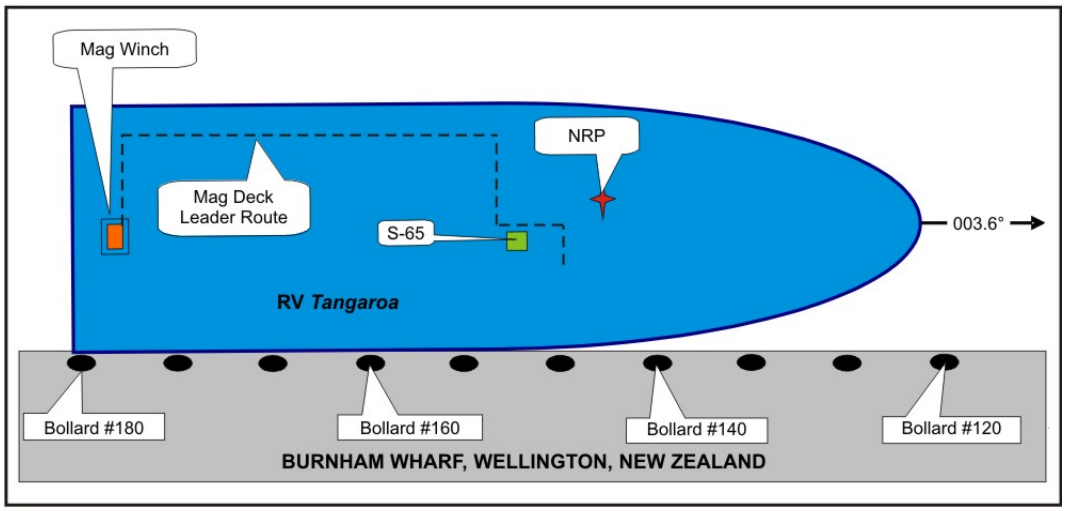

12.4.3. Free-air Corrections

Job No.:	27529	**Client:**	NIWA / Geoscience Australia
Still Reading No.	01	**Client Ref No.:**	
Meter No.	S-65	**Vessel:**	R/V *Tangaroa*
Date:	6 OCTOBER 2007	**Port:**	BURNHAM WHARF, WELLINGTON, NEW ZEALAND
Julian Day:	279	**Latitude (D°.M)**	-41°.3114435
Time (UTC):	16:00	**Longitude (D°.M)**	174°.811760
Technician(s):	Donald Childers	**Lat & Long Source:**	FURUNO GPS
Dock to Water(m):		3.6	
Water Depth (m):		6.0	
Gravity meter is below the water (m):		2.6	
Gravity meter is below the dock(m):		6.2	

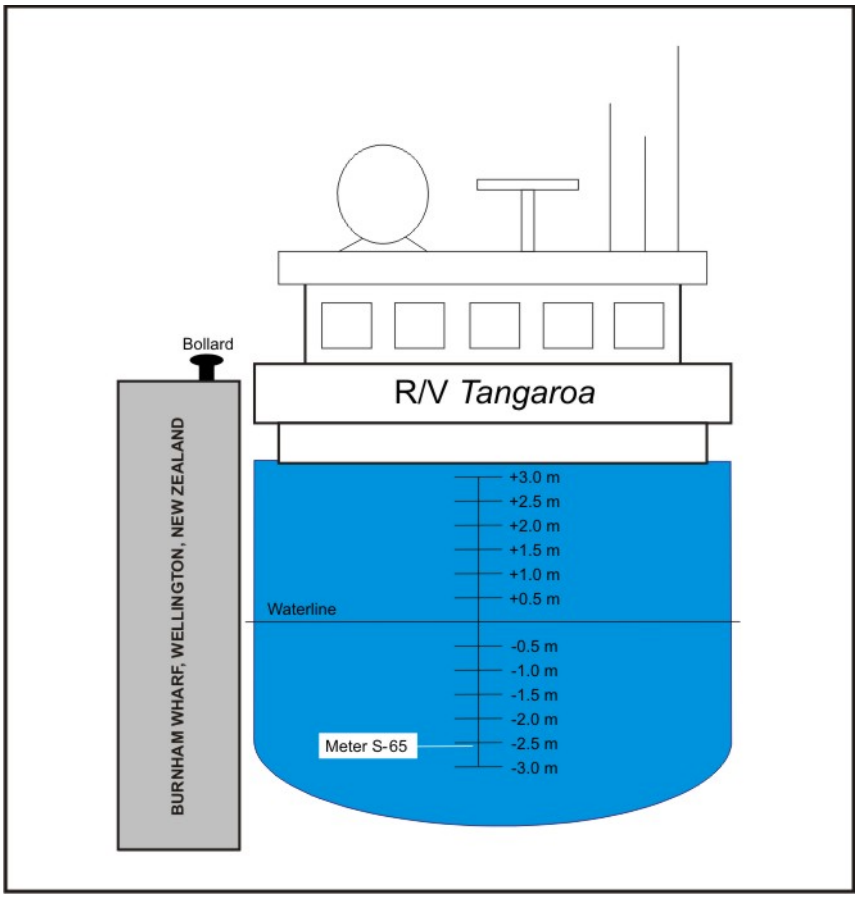

12.4.4. Gravity and Magnetic Monitors

Three stations were operated during this survey[1], to measure the magnetic diurnal variation. Two stations were located on Norfolk Island and one at Ashby, NSW, at approximately the same latitude as the Norfolk Island stations. The purpose of deploying three stations in this way was to gain an understanding of the differences in the diurnal variations across an island and across the ocean.

12.4.4.1. Norfolk Island Station 1

This was the primary station and operated during 7th October–2nd December 2007. The station was located near the Bureau of Meteorology's building at -29.03833°, 167.94167°.

[1] Survey Id 2436 is also used internally by Geoscience Australia for navigation, bathymetry and potential field data.

The magnetometer was a Scintrex ENVI Total Field proton precession magnetometer with quoted absolute accuracy of ±1 nT set to a reading period of 2 s and a cycle time of 15 s. The console was housed in a plastic box along with 12V lead-acid battery and associated wiring. Data were transmitted to the laptop via a bluetooth connection. The sensor was on a pole 2 m off the ground and oriented according to the cardinal markings on the sensor head (Figure 12.3).

The plastic box was housed in a tent for weather protection, while the sensor was located just outside the tent. Power was supplied to the battery to keep it charged via a waterproof battery charger connected to an external power supply. The data acquisition software used was TWedge 1.2 (TEC-IT Datenverarbeitung GmbH) running Windows XP on a laptop computer housed in the Bureau of Meteorology building. Date and time on the instruments was set to UTC using the time standard using the Bureau of Meteorology monitors and transferred manually. Hence, there is at least a 1 s error in the time. Field data for the station can be located in MMS[2] as CD0213.

12.4.4.2. Norfolk Island Station 2

This was the secondary station and operated from 11th October – 18th November 2007. This station was located at Steele Point on the eastern side of the island on the property '*Melaleuka*'. The station location was approximately -29.0376°, 167.9886° in soft earth on a gentle slope. This instrument comprised a 3-component device built by Geoscience Australia. As this instrument was subject to temperature fluctuations it was buried 1 m into the soil to minimise temperature fluctuations. The instrument was set up using purpose-built communication software. The instrument was water-proof sealed inside a hard cylindrical case, which was then enclosed inside heavy duty plastic bags before placement in the ground. Data were recorded onto internal flash memory and power was supplied by two 12V sealed lead-acid batteries.

12.4.4.3. Ashby, NSW

This station was located at Yamba, NSW north coast and operated during 25th October – 9th December 2007. The station was located on the property at 12 Murrayville Rd at approximately -29.4025°, 153.2114°. The magnetometer was a Scintrex ENVI total field instrument identical to the primary station on Norfolk Island and the same setup was used. An example of data from the Ashby station is compared to the Norfolk Island stations in Figure 12.4.

12.4.4.4. Data Processing and Further Work

The Norfolk Island Station 1 data (the station that covered the entire temporal extent of the survey) will be used by the contractor in post-processing to remove the diurnal component from the magnetic field readings. This is expected to reduce the mis-ties and mis-levels to which daily variations in the field are contributing factors, and allow production of a better grid at the highly detailed level of the survey line spacing. The similarity of the two Norfolk Island traces provides an additional level of confidence that there is little influence of peculiarities of the location near the Norfolk Island airport. The differences between the

[2] MMS is an acronym for Media Management System accessed via the Unix main menu under GA Applications. The system manages tape, CD and DVD media for archiving intermediate processed data, projects at their completion, and so forth. The media are kept in a central, secure storage close to or in the computer room. It is not used for field or final processed data. The computer room operator should be contacted if uncertain how to operate MMS.

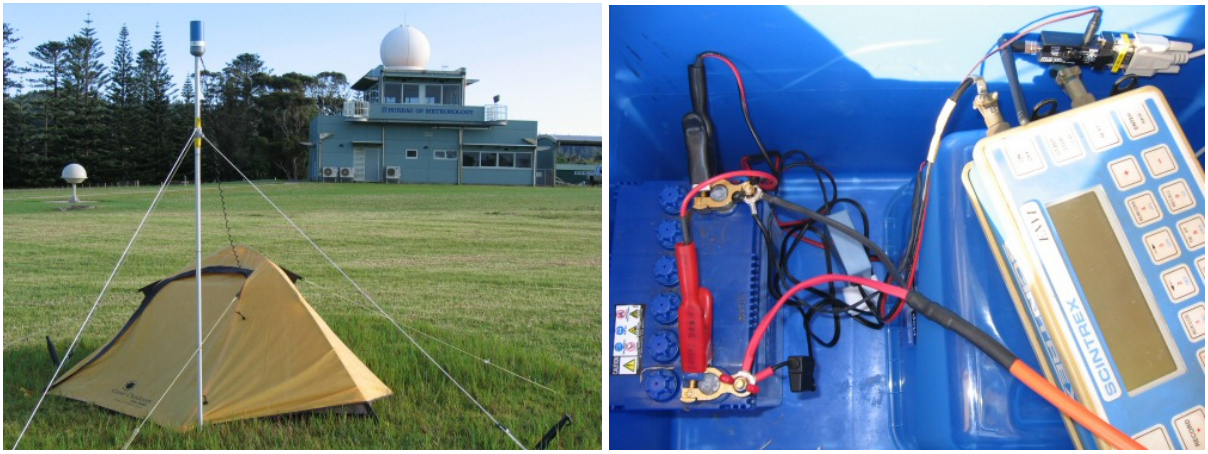

Figure 12.3. Magnetometer station 1 (left) with Bureau of Meteorology building in background. Connections to magnetometer (right) inside the plastic box located in the tent.

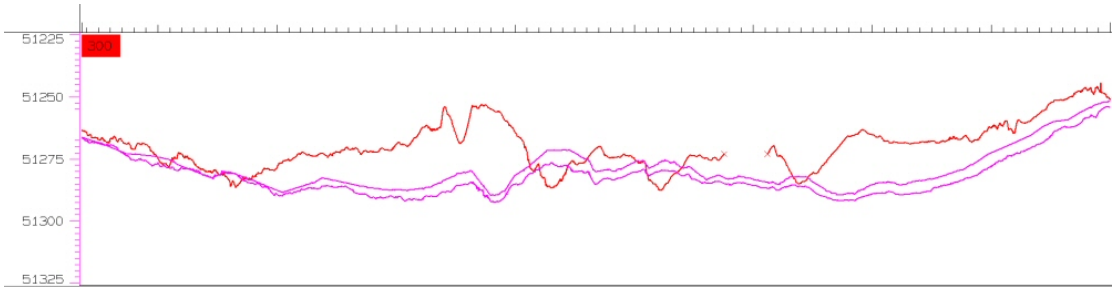

Figure 12.4. Example of data: the Ashby station (red) is compared to the two Norfolk Island stations for day 300. The Ashby station has been offset by -3065 nT to achieve the comparison.

Ashby and Norfolk Island stations (see Figure 12.4), and between these and a station at Charters Towers (QLD) will be the subject of further study to learn about the best locations to deploy diurnal monitor stations in future survey work.

12.5. APPENDIX E – FINAL FUGRO REPORT

This appendix contains the final report by Fugro Robertson Inc. of the gravity and magnetics data collected on the survey as a pdf on the accompanying data DVD. It contains detailed descriptions of data acquisition and processing, and preliminary results.

12.6. APPENDIX F – SUB-BOTTOM PROFILER IMAGES

This appendix contains a document (.pdf) containing images of select sections of the sub-bottom profiles. Images are screen captures from the sub-bottom profiler software that show representative seabed characterisations or relevant features or sub-bottom sedimentary architectures.

12.7. APPENDIX G – SEABED TEXTURE

Data in this appendix are based on sieve analysis and carbonate bomb analysis, and are thus expressed as weight percents. Grainsize distributions for all of the sub-surface samples are expressed as volume percentages measured from the Malvern™ Mastersizer-2000 laser particle size analyser and can be found on the accompanying data DVD. Grainsize distribution graphs and associated data from the Malvern are contained on the data DVD in pdf format. The filenames follow the convention: 7-digit Lab Number, GA Survey Number, Station Number, Operation Type, and Operation Number (e.g., 1952610 TAN0713/29BC10).

12.8. APPENDIX H – GEOCHEMISTRY RESULTS

Table 12.1. Potentially bio-available concentrations of Ge and trace elements which are either micronutrients (*e.g.* Fe, Co, Zn, Se), which play an important role in biogeochemical processes (*e.g.* Fe, Mn, Se, Zn, Cd, Cu, Ni). The concentrations of metals extracted by 1M HCl as a proportion of the total concentrations of each metal (based on XRF) are also shown.

Study Area	Sample ID	exFe mg kg^{-1} (%)	exCo mg kg^{-1} (%)	exGe mg kg^{-1}	exSe mg kg^{-1}	exMo mg kg^{-1}	exCd mg kg^{-1}	exMn mg kg^{-1} (%)	exCu mg kg^{-1} (%)	exZn mg kg^{-1}	exNi mg kg^{-1} (%)	exPb mg kg^{-1}	exAs mg kg^{-1} (%)
Area A	04BC01	330.2 (10.9)	1.4 (24)	0.9	<0.2	<0.2	0.4	74.2 (19.1)	10.9 (54.6)	10.2	20.7 (67.7)	1.7	<0.2
	13BC02	2.7 (0.1)	1.5 (75.1)	1.0	<0.2	<0.2	0.4	52.9 (15.9)	2.2 (15)	9.5	25.9 (50.1)	0.2	<0.2
	14BS03	<0.2	1.7 (27.7)	1.2	<0.2	<0.2	0.6	65.7 (16.3)	2.7 (20.8)	12.2	28.6 (45.5)	0.1	<0.2
	16BC03	389.8 (13.1)	1.5 (21)	1.0	<0.2	<0.2	0.3	106.6 (33.6)	8.0 (88.5)	8.1	20.6 (53.5)	1.2	<0.2
	18BC04	3.1 (0.1)	1.5 (30)	1.2	<0.2	<0.2	0.5	63 (14.5)	3.5 (24.9)	9.7	25.9 (85)	0.2	<0.2
	20DR08	1.2 (0.04)	1.5 (50.6)	1.3	<0.2	<0.2	0.4	38.1 (8.5)	1.7 (10.2)	8.6	29.6 (77.7)	0.1	<0.2
	21BC05	541.4 (22.6)	1.6 (39)	1.0	<0.2	<0.2	0.4	112.3 (28.4)	10.2 (59.8)	8.9	20.7 (101.7)	1.8	0.3 (5.5)
	22BS05	521.7 (20.2)	1.5 (38.5)	1.0	<0.2	<0.2	0.4	94.7 (23.5)	9.5 (30.5)	9.7	21.7 (96.6))	1.9	0.6 (10)
	23BC06	514.3 (19.4)	1.6 (32.3)	1.1	<0.2	<0.2	0.4	104.1 (25.4)	9.5 (43.1)	8.0	22.8 (70.2)	1.9	<0.2
	24BC07	266.0 (9.8)	1.6 (78.1)	1.1	<0.2	<0.2	0.4	82.7 (21.4)	9.9 (61.7)	9.2	24.8 (68.6)	1.7	<0.2
	25GR01	225.3 (8.9)	1.6 (40)	1.1	<0.2	<0.2	0.4	96.2 (24.8)	9.7 (74.6)	9.3	25.1 (39.8)	1.5	<0.2
	26BC08	225.3 (21.4)	1.7 (42.3)	1.0	<0.2	<0.2	0.3	120.4 (27.8)	10.8 (59.9)	8.8	23.6 (80.7)	2.0	<0.2
	27BC09	10.4 (0.2)	1.7 (28.3)	1.3	<0.2	<0.2	0.4	61.3 (20.8)	3.3 (32.9)	10.3	30.6 (65.3)	0.3	0.5 (5.9)

Study Area	Sample ID	exFe mg kg^{-1}	exCo mg kg^{-1}	exGe mg kg^{-1}	exSe mg kg^{-1}	exMo mg kg^{-1}	exCd mg kg^{-1}	exMn mg kg^{-1}	exCu mg kg^{-1}	exZn mg kg^{-1}	exNi mg kg^{-1}	exPb mg kg^{-1}	exAs mg kg^{-1}
	29BC10	580.3 (21.4)	1.7 (42.3)	1.0	<0.2	<0.2	0.3	120.4 (27.8)	10.8 (59.9)	8.8	23.6 (80.7)	2.0	<0.2
	30BC11	7.2 (0.3)	1.8 (58.9)	1.2	<0.2	<0.2	0.4	46.9 (16.4)	2.2 (15.7)	8.1	33.5 (158.3)	0.2	<0.2
	31BC12	486.4 (18.2)	1.8 (60.8)	1.1	<0.2	<0.2	0.3	99.8 (27.4)	9.4 (77.9)	8.8	26.8 (41.1)	1.6	<0.2
Area B	38BC13	15.0 (0.5)	1.7 (58)	1.3	<0.2	<0.2	0.3	54.1 (17.5)	7.8 (30)	8.2	30.1 (39.9)	0.7	<0.2
	39BC14	265.5 (3.9)	2.0 (31.1)	1.4	<0.2	<0.2	0.3	69.7 (25)	9.8 (68.4)	8.5	32.1 (54.2)	1.4	<0.2
Extraction efficiency (%)		19-23	23-28	N/A	N/A	N/A	58-73	47-50	34-40	25-30	15-18	N/A	21-23
XRF error on Mess-3 (%)		4.8	2.7	N/A	N/A	N/A	N/A	0	5.6	6.3	8.3	N/A	5.7
River particles			29 ± 2.6					19 ± 1.1	67 ± 1.6	46 ± 4.1	43 ± 1.5		

12.9. APPENDIX I – BENTHIC BIOTA

This appendix contains summary details of the seabed video characterisations undertaken and the benthic biota sampled during the survey. Benthic biota samples have been distributed to relevant taxonomic experts for formal identification and archival. Elutriate and some samples have been archived at Geoscience Australia.

Table 12.2. Seabed characterisation scheme: substratum, bedform-relief, and biota types and definition used to characterise the seabed.

	Type	Definition
Substratum	Rock	Exposed Bedrock
	Boulders	Boulders (>0.25 m loose material)
	Cobble	Cobbles (>0.065 m and <0.25 m)
	Sand	Sand (lighter colour, grains visible to naked eye)
	Mud	Mud (darker colour than sand, grains not visible)
	Pebbles	Pebbles (<0.065 m)
Bedform	Sediment waves	Wave-like bedform in sediment
	Sediment ripples	Ripple-like bedform in sediment
	Hummocky	Irregular bedform, >50% of surface-area
Relief	Flat relief	<1 m substratum relief
	Low relief	1-3 m substratum relief
	Moderate relief	>3 m substratum relief
	High relief	>60% substratum relief/complexity (visual line-chain method)
	Rock wall	Vertical wall with a slope angle >80^{o} (visual line-chain method)
Biota	Cnidaria	Cnidaria
	Hard corals	Cnidaria: Anthozoa: Scleractinia – live hard corals
	Hard corals – fragments	Cnidaria: Anthozoa: Scleractinia – dead coral fragments
	Christmas Tree corals	Cnidaria: Anthozoa: Antipathria (e.g. black corals)
	Soft coral	Cnidaria: Anthozoa: Alcyonacea
	Gorgonian – fan	Cnidaria: Anthozoa: Gorgonacea – fan shaped
	Gorgonian – other	Cnidaria: Anthozoa: Gorgonacea
	Gorgonian – whips	Cnidaria: Anthozoa: Gorgonacea – whip shaped
	Hydroids	Cnidaria: Hydrozoa
	Hydroids a, b	Cnidaria: Hydrozoa (spA, sp B, or other)
	Sea pens	Cnidaria: Anthozoa: Pennatulacea
	Anemones	Cnidaria: Anthozoa: Actiniaria
	Jellyfish	Cnidaria: Scyphozoa
	Sponges – 3D	Porifera: 3-dimensional forms (*e.g. vase sponges*)
	Sponges – encrusting	Porifera: encrusting forms
	Glass sponge	Porifera: Hexactinellida
	Echinoderms	Echinodermata
	Starfish (seastars)	Echinodermata: Asteroidea
	Brittlestars – on sed.	Echinodermata: Ophiuroidea – directly on the seabed
	Brittlestars – on Cnid.	Echinodermata: Ophiuroidea – on Cnidarian species
	Stalked featherstars	Echinodermata: Crinoidea –attachment by stalks to the seabed
	Featherstars – on sed.	Echinodermata: Crinoidea – directly on the seabed
	Featherstars – on Cnid.	Echinodermata: Crinoidea – on Cnidarian species
	Sea urchins	Echinodermata: Echinoidea

	Type	Definition
	Sea cucumbers	Echinodermata: Holothuroidea
	Crustacea	Arthropoda: Crustacea
	Lobster	Arthropoda: Crustacea: Malacostraca – all lobster
	Spider crabs	Arthropoda: Crustacea:Malacostraca: Brachyura: Majidae
	Crabs	Arthropoda: Crustacea: Malacostraca: Brachyura
	Shrimps/prawns	Arthropoda: Crustacea: Malacostraca – shrimp/prawn
	Tubeworms	Annelida: Polychaeta
	Acorn worm	Hemichordata: Enteropneusta
	Mollusc	Mollusca
	Gastropod	Mollusca: Gastropoda (marine snails and slugs)
	Octopus	Mollusca: Cephalopoda: Octopoda
	Fish	Chordata: Osteichthyes (*e.g.* eels, ratfish, hagfish, cod, sharks)
	Shark	Chordata: Chondrichthyes
	Ray	Chordata: Chondrichthyes
	Motile invertebrates	Unknown motile invertebrates, such as fishes, jellyfish, etc.
	Sessile invertebrates	Unknown invertebrates attached the seabed
Lebensspuren	Tacks*	Tracks visible on the surface of the sediments
	Burrows	Holes that penetrate the surface sediments
	Mounds	Mounds of sediment
	Shell	Shell remains (*e.g. middens*)
	Pits	A depression in the surface sediments ≤10 wide
	Craters	A depression in the surface sediments >10 wide
Additional	Manganese nodules	Irregular black-brown concretions of manganese
	Trash	Any form of human waste
	Unknown	Substratum was visible, but not well enough to discern organism
	Undefined	Seabed not visible

Table 12.3. Fixation and preservation methods used for marine taxa collected during the survey. A = absolute ethanol; F = 4% Formalin; C = Freezer; J = absolute ethanol in small jar, S = store dry.

Taxa Class	Preservation
ANNELIDA: Polychaeta (segmented worms)	F
ASCIDIA: TUNICATA (sea squirts)	F
BIOLOGICAL CONGLOMERATES (+sponges)	C
BIOLOGICAL CONGLOMERATES (no sponges)	A
BRACHIOPODA: (brachiopods)	A
BRYOZOA: (bryozoans)	C
CNIDARIA: (anemones)	F
CNIDARIA: (gorgonians)	A
CNIDARIA: (hydroids)	A
CNIDARIA: (jellyfish)	F
CNIDARIA: (sea pens)	A
CNIDARIA: (soft corals)	A
CNIDARIA: (unknown)	A
CNIDARIA: coral fragments	A
CNIDARIA: Scleractinia (live stony corals)	A

Taxa Class	Preservation
CRUSTACEA (unknown)	A
CRUSTACEA: (non-decapods)	A
CRUSTACEA: Cirripedia (barnacles)	A
CRUSTACEA: Decapoda (lobsters shrimp)	A
CRUSTACEA: Galathaid (squat lobsters)	A
ECHINODERMATA (unknown)	A
ECHINODERMATA: Asteroidea (starfish)	A
ECHINODERMATA: Crinoidea (featherstars)	A
ECHINODERMATA: Crinoidea entwined on cnidarian	A
ECHINODERMATA: Echinoidea (urchins)	A
ECHINODERMATA: Holothuroidea (sea cucumbers)	A
ECHINODERMATA: Ophiuroidea (brittle+basket stars)	A
ECHINODERMATA: Ophiuroidea entwined on cnidarian	A
FISH	F
FORAMINIFERA	A
MISCELLANEOUS - ETHANOL	A
MISCELLANEOUS - FORMALIN	F
MISCELLANEOUS - FREEZER	C
MOLLUSCA (unknown)	A
MOLLUSCA: Bivalve	A
MOLLUSCA: Cephalopoda (octopus squid)	A
MOLLUSCA: Gastropoda	A
MOLLUSCA: Opisthobranchia Nudibranchia (slugs)	A
MOLLUSCA: Polyplacophora (chitons)	A
MOLLUSCA: Pteropods (sea butterflies)	A
MOLLUSCA: Scaphopoda (tusk shells)	A
NEMERTEANS (ribbon worms)	F
PLANTS (marine)	C
PORIFERA: (glass sponges)	C
PORIFERA: (sponges)	C
PYCNOGONIDA (sea spiders)	A
RUBBLE – SUBSTRATE	S
SEDIMENT ANIMALS 1 mm SIEVED	A
SEDIMENT ANIMALS 500 μm SIEVED	A
SEDIMENT ANIMALS 500 μm SIEVED - Boxcore btm >0.05 m	A
SEDIMENT ANIMALS 500 μm SIEVED - Boxcore top 0.05 m	A
SEDIMENT ANIMALS 500 μm SIEVED - Pipe-Dredge Sample	A
SIPUNCULA:	F
SUPERNATANT ANIMALS 500 μm SIEVED	A
WORM unknown	F

Table 12.4. Biological data from infaunal boxcores: a) Taxonomic groups present, b) Abundance of target groups, c) Species richness. Taxonomic groups present are indicated with an 'X'; groups absent are indicated with a '-'. Italicised text represents samples within a station that had multiple elutriate samples (13, 29, 30, and 41). Standardised values are per 100 ml. Stations 04 and 13 include elutriate from the entire vertical section of the boxcore. Stations 23 and above include only the top layers. Vertical stratification of Stations 16, 18, and 21 are unknown.

A)

Study Area	Station[1]	Brachiopods	Bryozoan	Cnidarian	Crustaceans	Molluscs	Porifera	Urchins	Worms	Total Groups
Area A	04BC01	-	-	-	X	X	X	-	X	3
	13BC02	X	-	X	X	X	X	X	X	7
	16BC03	-	-	X	-	X	X	X	X	5
	18BC04	-	-	X	X	X	X	X	X	6
	21BC05	-	-	X	X	X		X	X	5
	23BC06	-	-	X	X	X		-	X	3
	24BC07	-	-	-	X	X	X	-	X	4
	26BC08	-	-	-		-	-	X	X	2
	27BC09	-	-	-		X	-	X	X	3
	29BC10	-	-	-	X	X	-	X	X	4
	30BC11	-	-	-	X	X	-	X	X	4
	31BC12	-	-	-	X	X	X	-	X	4
Area B	38BC13	-	-	-	X	X	X	X	X	5
	39BC14	-	X	-	-	X	-	X	X	3
	41BC15	-	-	-	X	X	X	X	X	5
	41BC15	-	-	-	X	X	X	X	X	5

[1] *Stations 13, 29, 30, and 41 had multiple elutriate samples. Data on taxonomic groups was combined to obtain overall station presence.*

B)

			Scaphopods		Gastropod sp. G		Ostracods		White clams	
Study Area	Station *Sample ID*	Elutriate volume (ml)	Raw	Standardised[2]	Raw	Standardised[2]	Raw	Standardised[2]	Raw	Standardised[2]
Area A	04BC01	53.88	1	1.86	0	0	1	1.86	0	0
	13BC02			450.03		5.05		3.00		5.78
	59115	65.67	0	0	0	0	3	4.57	2	3.05
	59116	14.69	0	0	1	6.81	1	6.81	2	13.62

Study Area	Station *Sample ID*	Elutriate volume (ml)	Scaphopods Raw	Scaphopods Standardised[2]	Gastropod sp. G Raw	Gastropod sp. G Standardised[2]	Ostracods Raw	Ostracods Standardised[2]	White clams Raw	White clams Standardised[2]
	59117	29.30	8	27.31	2	6.83	1	3.41	6	20.48
	59121	35.36	0	0	1	2.83	0	0	2	5.66
	59120	35.46	6	16.92	1	2.82	0	0	0	0
	59118	29.30	4	13.65	2	6.83	0	0	1	3.41
	59119	21.71	3	13.82	0	0	2	9.21	0	0
	59113	7	247	3528.57	1	14.29	0	0	0	0
	16BC03	34	5	14.71	0	0	0	0	0	0
	18BC04	32.24	4	12.41	0	0	1	3.10	0	0
	21BC05	37	5	13.51	1	2.70	1	2.70	0	0
	23BC06	18.17	4	22.01	0	0	0	0	1	5.50
	24BC07	21	10	47.62	0	0	2	9.52	0	0
	26BC08	38	0	0	0	0	0	0	0	0
	27BC09	22.19	4	18.03	0	0	0	0	0	0
	29BC10			0		0		3.78		0
	59186	235	0	0	0	0	1	0.43	0	0
	059184 & 059185	42	0	0	0	0	3	7.14	0	0
	30BC11			0		0		7.08		0
	59188	21.21	0	0	0	0	1	4.72	0	0
	59189	14.69	0	0	0	0	1	9.44	0	0
	31BC12	16.66	0	0.00	0	0	4	24.02	1	6.00
Area B	38BC13	15.64	9	57.53	0	0	3	19.18	0	0
	39BC14	18.68	10	53.54	3	16.06	0	0	2	10.71
	41BC15			159.15		6.61		6.61		13.67
	59356	14.63	26	177.68	1	6.83	1	6.83	4	27.34
	59355	15.64	22	140.63	1	6.39	1	6.39	0	0

[2] *Abundance was standardised by dividing the raw data by the elutriate volume and multiplying by 100ml. Stations 13, 29, 30, and 41 had multiple elutriate samples. For these stations, the overall standardised value for that station was calculated by taking the mean standardised value for the samples within that station.*

C)

Study Area	Station ***Sample ID***	Elutriate volume (ml)	Species Richness Raw[1]	Species Richness Standardised[2]
Area A	04BC01	53.88	6	1.1137
	13BC02		25	4.1491
	59115	65.67	10	1.5227
	59116	14.69	9	6.1277
	59117	29.30	10	3.4133
	59121	35.36	7	1.9794
	59120	35.46	8	2.2563
	59118	29.30	7	2.3893
	59119	21.71	9	2.6471
	59113	7	9	12.8571
	16BC03	34	13	3.8235
	18BC04	32.24	10	3.1019
	21BC05	37	15	4.0541
	23BC06	18.17	11	6.0531
	24BC07	21	8	3.8095
	26BC08	38	6	1.5789
	27BC09	22.19	5	2.2535
	29BC10		6	0.5825
	59186	235	4	0.9524
	059184 & 059185	42	5	0.2128
	30BC11		5	1.9644
	59188	21.21	4	1.8862
	59189	14.69	3	2.0426
	31BC12	16.66	11	6.6044
Area B	38BC13	15.64	12	7.6705
	39BC14	18.68	12	6.4246
	41BC15		12	6.9547
	59356	14.63	11	7.5172
	59355	15.64	10	6.3921

[1] Stations 13, 29, 30, and 41 had multiple elutriate samples. For these stations, species richness was calculated by counting the number of distinct species across all samples.

[2] Species richness was standardised by dividing the raw data by the elutriate volume and multiplying by 100 ml.

Table 12.5. Echinodermata (e.g. sea-urchins, brittlestars, crinoids) collected from the TAN0713 survey. All specimens were identified by Dr Tim O'Hara and are lodged at the Museum of Victoria.

Study Area	Class Family	Taxa	Station number	Start Lat.	Start Long.	Depth (m)	Museum Reg. number	No. of specimens
	Asteroidea							
Area A	Astropectinidae	*Plutonaster*	02DR02	-28.2764	161.9492	1,570	F159691	1
Area A	Goniasteridae	*Circeaster arandae*	06DR04	-27.4137	161.7004	1,532	F159690	1
Area A	Pterasteridae	*Hymenaster*	15BS04	-26.8547	161.3333	1,624	F159689	1
Area B	Pterasteridae	*Pteraster obesus*	35BS08	-26.7355	159.4271	290	F159688	1
	Crinoidea							
Area A	Pentacrinitidae	*Endoxocrinus alternicirrus*	01DR01	-28.2385	162.6268	1,365	F159692	2
Area A		unidentified	01DR01	-28.2385	162.6268	1,365	F159694	1
Area A		unidentified	06DR04	-27.4137	161.7004	1,532	F159695	1
Area B		unidentified	37BS09	-26.8051	159.4070	902-735	F159693	1
	Echinoidea							
Area B	Fibulariidae	*Fibularia*	34SG02	-26.7346	159.4662	293	F159685	2
Area B	Laganidae	*Peronella hinemoae*	35BS08	-26.7355	159.4271	290	F159684	8
Area B	Pedinidae	*Caenopedina*	35BS08	-26.7355	159.4271	290	F159687	1
Area B		unidentified	35BS08	-26.7355	159.4271	290	F159686	1
	Ophiuroidea							
Area B	Amphiuridae	*Amphiura* sp MoV 5235	40BS10	-26.6447	159.3767	253	F159676	1
Area A	Asteroschematidae	*Asteroschema tubiferum*	06DR04	-27.4137	161.7004	1,532	F159683	1
Area A	Asteroschematidae	*Asteroschema tubiferum*	17DR06	-26.8589	161.7368	1,354	F159679	1
Area A	Asteroschematidae	*Asteroschema tubiferum*	19DR07	-26.8841	161.7762	1,400	F159682	1
Area A	Asteroschematidae	*Ophiocreas oedipus*	01DR01	-28.2385	162.6268	1,365	F159678	1
Area A	Asteroschematidae	*Ophiocreas oedipus*	05DR03	-27.6795	161.6404	1,424	F159681	1
Area A	Asteroschematidae	*Ophiocreas oedipus*	32DR10	-26.6661	161.0468	1,600	F159680	1
Area B	Hemieuryalidae	*Ophiomoeris obstricta*	40BS10	-26.6447	159.3767	253	F159675	1
Area A	Ophiacanthidae	*Ophioplinthaca*	11BS02	-27.5167	161.3819	1,572	F157379	1
Area A	Ophiacanthidae	*Ophioplinthaca plicata*	01DR01	-28.2385	162.6268	1,365	F157373	1

Study Area	Class Family	Taxa	Station number	Start Lat.	Start Long.	Depth (m)	Museum Reg. number	No. of specimens
Area A	Ophiacanthidae	*Ophioplinthaca plicata*	02DR02	-28.2764	161.9492	1,570	F159666	1
Area B	Ophiacanthidae	*Ophiopristis*	40BS10	-26.6447	159.3767	253	F159677	1
Area A	Ophiacanthidae	*Ophiurothamnus clausa*	11BS02	-27.5167	161.3819	1,572	F157378	3
Area A	Ophiactidae	*Ophiactis abyssicola*	01DR01	-28.2385	162.6268	1,365	F159669	1
Area A	Ophioleucidae	*Ophiernus vallincola*	22BS05	-26.3045	161.7020	1,300	F157374	1
Area A	Ophiuridae	*Amphiophiura trifolium*	42BS11	-27.4323	160.5381	2,110	F159672	3
Area B	Ophiuridae	*Astrophiura permira*	36DR12	-26.7832	159.4576	638-390	F159663	3
Area B	Ophiuridae	*Dictenophiura platyacantha*	34BS07	-26.7338	159.4662	290	F157381	1
Area B	Ophiuridae	*Dictenophiura platyacantha*	35BS08	-26.7355	159.4271	290	F157375	1
Area A	Ophiuridae	*Ophiomastus* sp 3 (abyssal)	32DR10	-26.6661	161.0468	1,600	F159674	1
Area A	Ophiuridae	*Ophiomusium facundum*	02DR02	-28.2764	161.9492	1,570	F159665	1
Area A	Ophiuridae	*Ophiomusium facundum*	11BS02	-27.5167	161.3819	1,572	F157380	7
Area A	Ophiuridae	*Ophiomusium facundum*	14BS03	-27.0247	161.6652	1,385	F157382	1
Area A	Ophiuridae	*Ophiomusium relictum*	06DR04	-27.4137	161.7004	1,532	F157386	1
Area A	Ophiuridae	*Ophiomusium scalare*	01DR01	-28.2385	162.6268	1,365	F159668	1
Area A	Ophiuridae	*Ophiomusium scalare*	01DR01	-28.2385	162.6268	1,365	F157372	1
Area A	Ophiuridae	*Ophiomusium scalare*	05DR03	-27.6795	161.6404	1,424	F157384	1
Area A	Ophiuridae	*Ophiomusium scalare*	06DR04	-27.4137	161.7004	1,532	F157385	2
Area B	Ophiuridae	*Ophiomusium scalare*	35BS08	-26.7355	159.4271	290	F159667	1
Area B	Ophiuridae	*Ophiomusium scalare*	37BS09	-26.8051	159.4070	902-735	F159670	1
Area A	Ophiuridae	*Ophiophycis johni*	33DR11	-26.6561	160.8975	1,632	F159662	1
Area A	Ophiuridae	*Ophiopyrgus trispinosus*	02DR02	-28.2764	161.9492	1,570	F159664	2
Area A	Ophiuridae	*Ophiopyrgus trispinosus*	08DR05	-27.3160	161.4275	1,622	F157376	2
Area A	Ophiuridae	*Ophiopyrgus trispinosus*	11BS02	-27.5167	161.3819	1,572	F157377	4
Area A	Ophiuridae	*Ophiopyrgus trispinosus*	15BS04	-26.8547	161.3333	1,624	F157383	5
Area A	Ophiuridae	*Ophiosphalma*	42BS11	-27.4323	160.5381	2,110	F159673	1
Area A	Ophiuridae	*Ophiosphalma fimbriatum*	42BS11	-27.4323	160.5381	2,110	F159671	1

Table 12.6. Polychaeta and other worms collected from the TAN0713 survey. All specimens were identified by Dr Robin Wilson and are lodged at the Museum of Victoria. Latitude and longitude represent the starting point of the sampling transect for sleds and dredge samples.

Location	Phylum: Family	Station no.	Lat.	Long.	Depth (m)	No. of specimens
Area A	Phoronida[1]	22BS05	-26.3045	161.7020	1,300	2
Area A	Phoronida[1]	32DR10	-26.6661	161.0468	1,600	2
Area B	Nemertea	35BS08	-26.7355	159.4271	290	1
Area B	Nemertea	40DR13	-26.6678	159.3856	253	1
Area A	Nemertea[1]	13BC02	-27.2045	161.5910	1,360	1
Area A	Polychaeta: Ampharetidae	11BS02	-27.5167	161.3819	1,572	4
Area A	Polychaeta: Ampharetidae	15BS04	-26.8547	161.3333	1,624	1
Area A	Polychaeta: Flabelligeridae	26BC08	-26.2889	161.3423	1,508	1
Area A	Polychaeta: Goniadidae	30BC11	-26.9393	161.0258	1,573	1
Area B	Polychaeta: Hesionidae	36DR12	-26.7832	159.4576	638	1
Area A	Polychaeta: Nereididae	23BC06	-26.5475	161.6024	1,360	1
Area A	Polychaeta: Onuphidae	11BS02	-27.5167	161.3819	1,572	1
Area A	Polychaeta: Orbiniidae	18BC04	-26.8171	161.7245	1,415	1
Area B	Polychaeta: Phyllodocidae	35BS08	-26.7355	159.4271	290	1
Area B	Polychaeta: Polynoidae	40DR13	-26.6677	159.3856	253	1
Area A	Polychaeta: Sabellariidae	05DR03	-27.6795	161.6404	1,424	1
Area A	Polychaeta: Sabellidae	02DR02	-28.2764	161.9491	1,570	1
Area A	Polychaeta: Sabellidae	08DR05	-27.3160	161.4257	1,622	1
Area B	Polychaeta: Serpulidae	40BS10	-26.6447	159.3767	253	1
Area A	Polychaeta: Sigalionidae	23BC06	-26.5475	161.6024	1,360	1
Area B	Polychaeta: Syllidae	35BS08	-26.7355	159.4271	290	1
Area B	Polychaeta: Terebellidae: Polycirrinae	34BS07	-26.7338	159.4662	290	1
Area A	Polychaeta:aldanidae	08DR05	-27.3159	161.4257	1,622	1
Area A	Polychaeta:aldanidae	02DR02	28.2764	161.949	1,570	1
Area A	Polychaete (posterior fragment- unidentifiable)	13BC02	-27.2045	161.5910	1,360	1
Area A	Sipuncula	02DR02	-28.2764	161.9492	1,570	1
Area A	Sipuncula	05DR03	-27.6795	161.6404	1,424	1

Location	Phylum: Family	Station no.	Lat.	Long.	Depth (m)	No. of specimens
Area A	Sipuncula	15BS04	-26.8547	161.3333	1,624	1
Area A	Sipuncula	22BS05	-26.3045	161.7020	1,300	1

[1] *Tentative identification only*.

12.10. APPENDIX J – DIGITAL STILL IMAGES

This appendix contains select digital still photographs taken during the survey. All still images in this appendix were selected to give representative assessments of the seabed environments and biota. The images are catalogued by station, faunal type, and substrate type for quick reference. Filenames follow the following convention: *Station number_operation number_ photograph number* (e.g., stn29_cam27_0050).

12.11. APPENDIX K – UNDERWATER VIDEO FOOTAGE

Video snippets (1-minute video clips) have been made from select stations that highlight representative habitat and biota from the study areas. The transects were chosen to represent a range of depths and locations. The red lasers are 20 cm apart. All video is in .avi format. The Cinepak codec is required for viewing. This codec comes with all Windows platforms above Windows 95. The appropriate version of the code can be downloaded from www.probo.com/cinepak.htm. The filenames follow the format: *Station number, Operation number*.

Instructions for Data DVD

Geoscience Australia Survey TAN0713, Post-survey Report:
Seabed Environments of the Capel and Faust basins and Gifford Guyot, Eastern Australia – post survey report by Andrew D. Heap, Michael Hughes, Tara Anderson, Scott Nichol, James Daniell, Rachel Przeslawski, Danielle Payne, Lynda Radke, Riko Hashimoto, and Shipboard Party.

The DVD contains the above-titled report as: Record2009_22.pdf.

View this .pdf document using Adobe Acrobat Reader (click Adobe.txt for information on readers).

Double click on **Record2009_22.pdf** to launch the document.

Directories on data DVD
Appendices Directory:
with sub-directories of Appendix C, Appendix E, Appendix F, Appendix G, Appendix J, and Appendix K.